



HAL
open science

Tetraamido- (TAML) and tetraaza- (cyclam) metallo-complexes as mild catalysts for the sustainable oxidation of alcohols

Zhan Zhang

► **To cite this version:**

Zhan Zhang. Tetraamido- (TAML) and tetraaza- (cyclam) metallo-complexes as mild catalysts for the sustainable oxidation of alcohols. Organic chemistry. Université de Lyon, 2018. English. NNT : 2018LYSE1312 . tel-02343622

HAL Id: tel-02343622

<https://theses.hal.science/tel-02343622>

Submitted on 3 Nov 2019

HAL is a multi-disciplinary open access archive for the deposit and dissemination of scientific research documents, whether they are published or not. The documents may come from teaching and research institutions in France or abroad, or from public or private research centers.

L'archive ouverte pluridisciplinaire **HAL**, est destinée au dépôt et à la diffusion de documents scientifiques de niveau recherche, publiés ou non, émanant des établissements d'enseignement et de recherche français ou étrangers, des laboratoires publics ou privés.



N°d'ordre NNT : 2018LYSE1312

THESE de DOCTORAT DE L'UNIVERSITE DE LYON

opérée au sein de
l'Université Claude Bernard Lyon 1

Ecole Doctorale N° 206
Chimie, Procédés, Environnement

Spécialité de doctorat : Chimie
Discipline : Chimie organique

Soutenue publiquement le 20/12/2018, par :
Zhan Zhang

Tetraamido- (TAML) and tetraaza- (cyclam) metallo-complexes as mild catalysts for the sustainable oxidation of alcohols

Devant le jury composé de :

Mme Blondin, Genevieve	Directeur de Recherches CNRS ; CEA Grenoble	Rapporteur
Mme Draye, Micheline	Professeur, Univ. Savoie-Mt Blanc	Rapporteur
M. Bucher, Christophe M. Duguet, Nicolas	Directeur de Recherches, CNRS ; ENS Lyon Maître de Conférences, Univ. Claude Bernard Lyon 1	Examineur Examineur
M. Siri, Olivier	Directeur de Recherches CNRS ; Univ. Aix Marseille	Examineur
M. Andrioletti, Bruno	Professeur, Univ. Claude Bernard Lyon 1	Directeur de thèse

UNIVERSITE CLAUDE BERNARD - LYON 1

Président de l'Université

Président du Conseil Académique

Vice-président du Conseil d'Administration

Vice-président du Conseil Formation et Vie Universitaire

Vice-président de la Commission Recherche

Directrice Générale des Services

M. le Professeur Frédéric FLEURY

M. le Professeur Hamda BEN HADID

M. le Professeur Didier REVEL

M. le Professeur Philippe CHEVALIER

M. Fabrice VALLÉE

Mme Dominique MARCHAND

COMPOSANTES SANTE

Faculté de Médecine Lyon Est – Claude Bernard

Faculté de Médecine et de Maïeutique Lyon Sud – Charles Mérieux

Faculté d'Odontologie

Institut des Sciences Pharmaceutiques et Biologiques

Institut des Sciences et Techniques de la Réadaptation

Département de formation et Centre de Recherche en Biologie Humaine

Directeur : M. le Professeur G.RODE

Directeur : Mme la Professeure C. BURILLON

Directeur : M. le Professeur D. BOURGEOIS

Directeur : Mme la Professeure C. VINCIGUERRA

Directeur : M. X. PERROT

Directeur : Mme la Professeure A-M. SCHOTT

COMPOSANTES ET DEPARTEMENTS DE SCIENCES ET TECHNOLOGIE

Faculté des Sciences et Technologies

Département Biologie

Département Chimie Biochimie

Département GEP

Département Informatique

Département Mathématiques

Département Mécanique

Département Physique

UFR Sciences et Techniques des Activités Physiques et Sportives

Observatoire des Sciences de l'Univers de Lyon

Polytech Lyon

Ecole Supérieure de Chimie Physique Electronique

Institut Universitaire de Technologie de Lyon 1

Ecole Supérieure du Professorat et de l'Education

Institut de Science Financière et d'Assurances

Directeur : M. F. DE MARCHI

Directeur : M. le Professeur F. THEVENARD

Directeur : Mme C. FELIX

Directeur : M. Hassan HAMMOURI

Directeur : M. le Professeur S. AKKOUCHE

Directeur : M. le Professeur G. TOMANOV

Directeur : M. le Professeur H. BEN HADID

Directeur : M. le Professeur J-C PLENET

Directeur : M. Y. VANPOULLE

Directeur : M. B. GUIDERDONI

Directeur : M. le Professeur E.PERRIN

Directeur : M. G. PIGNAULT

Directeur : M. le Professeur C. VITON

Directeur : M. le Professeur A. MOUGNIOTTE

Directeur : M. N. LEBOISNE

Acknowledgments

First, I would like to specially thank the members of the committee who accepted to evaluate my work. Your insightful comments and encouragement incite me to widen my research from various perspectives.

I express my sincere gratitude to my PhD supervisor: Bruno ANDRIOLETTI, who gave me the opportunity to work in this interesting field of science. Thanks to your motivation and great help, I came here in Lyon for my totally new and colorful life and scientific work. With numerous useful suggestions and kind encouragement, I overcame different difficulties, together with gaining much more knowledge and experiences, during processing my projects. I appreciate for all of your help.

I also want to thank all the collaborators who have contributed to this work: Dr. Christophe BUCHER, Dr. Lhoussain KHROUZ, Dr. Carine MICHEL and my former advisor Prof. Guochuan Yin from China, who gave me great help in my projects. All of you were so patient to me and help me figure out all the problems I met. I really learnt a lot from you. I want to thank you again for all your kindly support.

I would like to thank all the previous and current colleagues in our team, who built a positive and entertaining atmosphere in the laboratory and whose intelligence always encourage me to work harder to catch up with them. When I just came to France, life was so difficult here, I couldn't even go out. With your help, I could go to the parties, bars, matches and go shopping. I learnt to wait without anxiety because I know this was France that I really need patience. Moreover, you taught me French, which is interesting and make my life easier in France. I will bring back this romantic language and always keep in mind.

I would also thank all the members of the ICBMS for the entire information and friendly

atmosphere during my research. The equipment facilities as well as the convenient network resources offered by the institute, who provide advanced and efficient tools, thus contributing to the high quality data for my work.

I thank all my family members, my parents and my brother, who encouraged and supported me spiritually during all these years, especially those moments when I was having hard time and homesick. And I would like to greatly thank my husband Xingjie MA (who I just married with this year) for always being my side, listening to any complains and cook good Chinese food for me.

I would like to thank my friends I met in France. You make my life here so colorful and interesting. We are like a big family to be each other's support. I thank all the kind people I met these years in France. With your encouragement and interesting sometimes even unexpected feedbacks for the hard points I met as well as the good memories in mind. I will appreciate for life-long time.

Résumé

Depuis la nuit des temps, la Nature utilise des enzymes à base de fer ou de manganèse pour réaliser des réactions d'oxydation catalytique hautement efficaces et sélectives. En s'inspirant de la Nature, selon une approche le plus souvent biomimétique, de nombreux complexes moléculaires ont été synthétisés. Parmi ceux-ci, il a été prouvé que les complexes de type Fe(TAML) imitaient très efficacement les enzymes, notamment la peroxydase.^{1,2} De nombreux complexes de Fe(TAML) ont été décrits au cours des dernières années. Comme les ligands du TAML sont parmi les plus résistants à l'oxydation, des complexes de Fer à l'état d'oxydation élevé ont été isolés et caractérisés. Ainsi en présence de peroxyde d'hydrogène, les complexes Fe(TAML) sont utilisés pour oxyder une large gamme de substrats et présentent une activité élevée similaire à celles des peroxydases.

Notre groupe a étudié l'utilisation du complexe Fe(TAML-Me₂) pour l'oxydation de liaisons C-H benzyliques en présence de DIAB ou TBHP. Afin de rendre l'oxydation plus éco-compatible, H₂O₂ ou TBHP doivent être adoptés comme oxydants. De plus, des modifications du complexe doivent être envisagées pour le rendre encore plus stable vis-à-vis de l'oxydation ou multifonctionnel. L'un des objectifs de cette thèse était de fonctionnaliser le complexe Fe (TAML-Me₂) à différentes fins.

Sur la base du complexe le plus simple Fe(TAML-Me₂), l'une des fonctionnalisations consistait à utiliser un triazole substitué par une chaîne hexyle par le biais d'une réaction "click" entre une queue alcynylée et un azoture pour obtenir du Fe[TAML-(Me)(triazole)]. Le triazole que nous avons introduit sur la structure pourrait, en effet, influencer les propriétés physicochimiques du complexe de fer qui pourraient être utilisées en catalyse homogène. Dans le même temps, un TAML fonctionnalisé par un triazole porteur d'une queue éthoxysilylée a été préparé. Ce catalyseur devait pouvoir être greffé sur un support inorganique pour une utilisation ultérieure en catalyse

hétérogène. Enfin, un TAML fonctionnalisé à queue fluorée a été développé. Ce nouveau complexe de fer devait entre autres être soluble dans les solvants fluorés pour une utilisation potentielle en milieu biphasique. Un tel milieu est en effet susceptible de favoriser la recyclabilité du catalyseur. Quatre complexes de fer, y compris celui de référence, ont été synthétisés purifiés et évalués avec succès.

De plus, nous avons comparé les propriétés physicochimiques des complexes $\text{Fe}(\text{TAML-Me}_2)$ et $\text{Fe}[\text{TAML}-(\text{Me})(\text{triazole})]$. Nous avons constaté qu'ils présentaient des comportements différents en électrochimie dans les solvants, tels que l'acétonitrile et le DMF, mais un comportement similaire dans le méthanol. En spectroscopie UV-Vis, les deux composés ont présenté un pic d'absorbance caractéristique et un coefficient d'absorbance totalement différents dans les trois solvants de référence. A partir des analyses RPE, nous avons pu déduire que les deux composés présentaient des arrangements identiques dans l'acétonitrile, mais qu'il existe certaines différences dans le méthanol et se comportent différemment dans le DMF.

Les deux complexes $\text{Fe}(\text{TAML-Me}_2)$ et $\text{Fe}[\text{TAML}-(\text{Me})(\text{triazole})]$ ont également été utilisés dans le cadre de l'oxydation catalytique d'alcools. L'oxydation d'alcools benzyliques a été réalisée avec 1 mol% de catalyseur et du TBHP en tant qu'oxydant. Pour tous les alcools benzyliques primaires, le catalyseur de référence présente une activité plus élevée que $\text{Fe}[\text{TAML}-(\text{Me})(\text{triazole})]$ dans les mêmes conditions. Cependant, en ce qui concerne les alcools benzyliques secondaires, les deux ont présenté une activité semblable et élevée. Cette observation indique que $\text{Fe}[\text{TAML}-(\text{Me})(\text{triazole})]$ possède une activité d'oxydation plus douce que $\text{Fe}(\text{TAML-Me}_2)$. Cette observation a été corroborée par les résultats d'électrochimie.

L'autre objectif de la thèse était de développer une oxydation catalytique bénigne pour l'environnement avec un catalyseur bioinspiré, $\text{Mn}^{\text{II}}(\text{Me}_2\text{EBC})\text{Cl}_2$, qui a été gracieusement fourni par le Prof. Guochuan Yin. Le catalyseur au manganèse

$\text{Mn}^{\text{II}}(\text{Me}_2\text{EBC})\text{Cl}_2$ a été employé dans de nombreuses applications avec H_2O_2 comme oxidant.³⁻⁷

Dans ce cadre, nous avons montré que le complexe $\text{Mn}^{\text{II}}(\text{Me}_2\text{EBC})\text{Cl}_2$ pouvait catalyser l'oxydation d'une série d'alcools benzyliques et aliphatiques avec H_2O_2 à pH 3 à température ambiante. Les conversions des alcools en composés carbonylés correspondants ont atteint 98% avec une sélectivité bonne à excellente. Les diols ont également été transformés avec une efficacité et une sélectivité élevée pour les mono cétones, sans autre oxydation. De plus, plusieurs composés modèles de la lignine ont également été oxydés efficacement dans nos conditions. En particulier, la molécule modèle de β -O-4 a été convertie presque quantitativement en cétone correspondante sans clivage de la liaison C-C. Cette étude démontre ainsi que le système $\text{Mn}^{\text{II}}(\text{Me}_2\text{EBC})\text{Cl}_2/\text{H}_2\text{O}_2$ constitue une méthode prometteuse pour l'oxydation de la lignine. De plus, l'étude du mécanisme que nous avons réalisée exclut la présence de radical hydroxyle. Par ailleurs, il a été prouvé que l'espèce active était un complexe de manganèse (IV) à haute valence. Un mécanisme plausible a été proposé.

Abbreviations

ABTS	2,2'-azino-bis(3-ethylbenzothiazoline- 6-sulphonic acid)
BDE	Bond Dissociation Energy
BPA	Bisphenol A
CAN	Ceric Ammonium Nitrate
CTAB	cetyltrimethylammonium bromide
CV	Cyclic Voltammetry
cyclam	1,4,8,11-tetraazacyclotetradecane
DAIB	(Diacetoxyiodo)benzene
DCE	1,2-Dichloroethane
DCM	Dichloromethane
DFT	Density Functional Theory
DIPA	Diisopropylamine
DMF	Dimethylformamide
DMFc	Decamethylferrocene
DMSO	Dimethyl sulfoxide
EPR	Electron Paramagnetic Resonance
GC-MS	Gas Chromatography coupled Mass Spectrum
HAT	Hydrogen Abstraction Transfer
HPLC	High Performance Liquid Chromatography
HRMS	High Resolution Mass Spectroscopy
<i>m</i> CPBA	<i>m</i> -ChloroPeroxyBenzoic Acid
Me ₂ EBC	4,11-dimethyl-1,4,7,11-tetraazabicyclo[6.6.2]hexadecane
MSN	Mesoporous Silica Nanoparticles
NBS	<i>N</i> -bromosuccinimide
NMO	<i>N</i> -methyl morpholine <i>N</i> -oxide
NMR	Nuclear Magnetic Resonance

OEC	Oxygen Evolving Complex
OEP	2,3,7,8,12,13,17,18-Octaethyl-21H, 23H-porphin
OER	Oxygen Evolution Reaction
OP	organophosphorus
PCP	pentachlorophenol
PG	Pyrolytic graphite
4-PSA	4-phenylsulfonic acid
PSII	Photosystem II
TAML	TetraAmido Macrocyclic Ligand
TBAB	Tetrabutylammonium bromide
TBAP	Tetrabutylammonium perchlorate
TBAT	Tetrabutylammonium tetrafluoroborate
TBHP	<i>tert</i> -Butyl Hydrogen Peroxide
TCP	2,4,6-trichlorophenol
TEA	Triethylamine
THF	Tetrahydrofuran
TLC	Thin Layer Chromatography
TOC	Total Organic Carbon
TOF	Turnover Frequency
TPAP	Tetra- <i>n</i> -propylammonium perruthenate
UV-Vis	Ultra-Violet visible
XAS	X-ray Absorption Spectroscopy

CONTENTS

PART I. INTRODUCTION	5
1 Brief overview on catalytic oxidation	5
1.1 Introduction on catalytic oxidation	5
1.2 Catalytic oxidation of alcohols	8
1.2.1 Introduction on oxidation of alcohols	8
1.2.2 Traditional methods of oxidation.....	9
1.2.3 Bioinspired methods	13
1.3 Our approach	16
1.3.1 Fe(TAML)	16
1.3.2 [Mn(Me ₂ EBC)Cl ₂].....	18
2 State of the art on Fe(TAML)	20
2.1 Introduction on TAML	20
2.2 Introduction on Fe(TAML).....	24
2.3 Properties of Fe(TAML).....	26
2.3.1 Coordination model and structure	26
2.3.2 Solubility.....	29
2.3.3 Stability	29
2.4 High valent iron(TAML)	33
2.4.1 Preparation and properties of mono Fe ^{IV} species.....	33
2.4.2 Preparation and properties of Fe ^V species	39
2.5 Functionalization of Fe(TAML) complexes	41
2.6 Application of Fe(TAML).....	43
2.6.1 General oxidation mechanism using Fe(TAML) and a peroxide	43
2.6.2 Homogeneous catalysis application with Fe(TAML).....	44
2.6.3 Heterogeneous catalysis applications with Fe(TAML).....	50
3 State of the art on Mn(Me₂EBC)Cl₂.....	54
3.1 Introduction on cyclam.....	55
3.2 Introduction on [Mn^{II}(Me₂EBC)Cl₂]	58
3.2.1 Structure and the synthesis of [Mn ^{II} (Me ₂ EBC)Cl ₂]	58
3.2.2 Properties of [Mn ^{II} (Me ₂ EBC)Cl ₂]	59
3.3 Introduction on Mn^{III} complexes with Me₂EBC.....	60
3.4 The corresponding manganese(IV) complexes	61
3.4.1 Structure and synthesis of [Mn ^{IV} (Me ₂ EBC)(OH) ₂](PF ₆) ₂	61
3.4.2 Properties of [Mn ^{IV} (Me ₂ EBC)(OH) ₂](PF ₆) ₂	62
3.4.3 The different existing forms of the manganese(IV) complex	63
3.5 Application of [Mn^{II}(Me₂EBC)Cl₂]	69

PART II. RESULTS AND DISCUSSION ON IRON(TAML) 75

1	Synthesis of functionalized Fe(TAML) for oxidation catalysis	75
1.1	Strategies of functionalization of Fe(TAML).....	76
1.2	Synthesis of functionalized Fe(TAML).....	81
1.2.1	Functionalization of TAML on the head.....	81
1.2.2	Functionalization of TAML on the tail.....	82
2	Characterization of Fe(TAML)	93
2.1	DFT calculations.....	93
2.2	Mössbauer.....	95
2.3	Electrochemical studies.....	95
2.4	UV-Vis studies.....	103
2.5	EPR study.....	106
3	Catalytic oxidation with Fe(TAML)	110

PART III. RESULTS AND DISCUSSION ON MANGANESE COMPLEX.....115

1	Catalytic oxidation of alcohols	115
1.1	Choice of the catalyst and the oxidant.....	115
1.2	Optimization the reaction conditions.....	115
1.3	Investigation on the scope of substrates.....	120
1.4	Mechanistic study.....	123
1.5	Conclusions.....	126
2	Catalytic oxidation of olefins	127
2.1	Introduction of oxidation of olefins.....	127
2.2	Epoxidation of olefins.....	127
2.3	Mechanistic study.....	129
2.4	Conclusions.....	130
3	Catalytic oxidation of other substrates	131
3.1	Catalytic oxidation of 5-HMF.....	131
3.2	Catalytic oxidation of lignin model compounds.....	132

GENERAL CONCLUSION AND PERSPECTIVES135

EXPERIMENTAL PART143

1	General procedures	143
2	Synthetic protocols	145
2.1	Synthesis of simplest [Fe(TAML-Me ₂)]Li 7a.....	145
2.2	Synthesis of functionalized Fe(TAML).....	151

3	Catalysis procedures and results	166
3.1	Catalysis with $[\text{Mn}(\text{Me}_2\text{EBC})\text{Cl}_2]$	166
3.2	Catalysis with Fe(TAML) catalysts	167
3.3	Results for the oxidation of alcohols	168
REFERENCES		181

Part I. Introduction

1 Brief overview on catalytic oxidation

1.1 Introduction on catalytic oxidation

Oxidation plays a key role in industry. It is the second largest process after polymerization, accounting for about 30% of the total chemical production.^{1,2} For example, 10 million ton of ethylene oxide is produced from oxidation every year (**Table 1**). 5 million ton of formaldehyde is also obtained from oxidation of methanol annually (**Table 1**). It is also produced a large quantity of phthalic anhydride and maleic anhydride through oxidation every year. Oxidation reactions are commonly applied to transform petroleum-based feedstock to chemical starting materials.³ As the procedures often use polluting and harmful materials such as metal salts in stoichiometric oxidations and nitrogen oxides produced by nitric acid, green and sustainable should be taken into consideration when designing new oxidation procedures.

Table 1. Large-scale production of chemicals from oxidation.

Reagents	Product	Catalysts	Production kg/year	Reference
C ₂ H ₄ , O ₂	ethylene oxide	Ag	1*10 ¹⁰	4,5
CH ₃ OH, O ₂	formaldehyde	Iron oxide/ Mo	5*10 ⁹	6,7
<i>o</i> -xylene, O ₂	phthalic anhydride	V ₂ O ₅	2*10 ⁹	8
<i>n</i> -butane, O ₂	maleic anhydride	V ₂ O ₅	4*10 ⁸	9

Selective catalytic oxidation is crucial for the development of green and sustainable chemistry.¹ Catalytic oxidation has made impressive progress over the past years. It is particularly important in producing bulk and fine chemicals and eliminating pollution.¹⁰

Many key chemicals such as alcohols, aldehydes, carboxylic acid, ketones and epoxides are produced from catalytic oxidation. Large-scale production of ethylene oxide, acrolein, maleic anhydride and so on are also well-known examples.^{1,10} In addition, catalytic oxidation is a particular area where homogeneous catalysis has the largest contribution in industrial organic chemistry.¹¹ In the bulk production of chemicals (**Table 2**), some of largest industrial production involving catalytic oxidation in the world are considered. According to **Table 2** classified by size, most of the reported processes are homogeneous catalysis.

Table 2. Production of bulk chemicals by catalytic oxidation catalysis.^{a, 11}

Reactant	Product	Year	Output 10 ⁶ t/y	Oxidant	Process
<i>p</i> -xylene	terephthalic acid ^b	1987	10.1	O ₂	homogeneous
ethylene	ethylene oxide	1984	8.5	O ₂	heterogeneous
toluene, benzene, cyclohexane, propylene	phenol	1987	4.2 ^c	O ₂	homogeneous
methanol	formaldehyde	1984	3.9	O ₂	heterogeneous
ethylene	acetaldehyde	1986	3.0	O ₂	homogeneous
ethylene/HOAc	vinyl acetate	1986	2.6 ^c	O ₂	heterogeneous
acetaldehyde	acetic acid	1986	2.3 ^c	O ₂	homogeneous

^aEstimated world capacity, data taken from ref 11. ^bIncluded dimethyl terephthalate.

^cOnly oxidation processes considered.

Oxidation catalysis is a critical tool for the development of green and sustainable chemistry and catalysis is a key tool.^{12,13} Using a suitable catalyst is important for economical and sustainable process. Selective oxidation catalysis can improve the yield of the target products, decreasing the promotion of by products, and enhancing atom-

efficient (the first principal of green chemistry)¹⁴ and E-factors (E = amount of waste/amount of product).^{13,15} In addition, new catalytic oxidation processes that could replace old energy-inefficient or multi-step reactions, can be more environmentally friendly.¹

Oxidation catalysis is not only crucial in industry but also necessary in aerobic life. Hence, oxidation of carbohydrates and fatty acids for energy is happening constantly and these reactions are involved in the biosynthesis, metabolism and detoxification catalyzed by natural metalloenzymes.^{10,16} Enzymes containing iron and manganese metal centers are most widely involved in these reactions. Iron-based enzymes, such as, methane monooxygenase,¹⁷ catechol dioxygenase¹⁸ and lipoxygenase¹⁹ has been studied for long. The most representative iron-based enzyme is cytochrome P450. The active site of the cytochrome P450 is sketched in **Figure 1**.²⁰ These enzymes exist in most organisms, such as mammals, plants, bacteria and so on.^{21,22} Iron-based enzymes participate in the activation of dioxygen or superoxide radical and dihydrogen peroxide.^{23,24} The enzymes are either heme²² or non-heme proteins.²⁵ Heme proteins contain an iron(III) ion and a porphyrin ligand. The most important role of iron enzymes is their activation of dioxygen in the oxidation of different substrates. There are also some representative manganese-containing enzymes such as superoxide dismutase,²⁶ manganese catechol dioxygenase,²⁷ catalase,²⁸ lipoxygenase²⁹ and the most representative compound oxygen-evolving complex (OEC) of Photosystem II (PSII).^{30,31} It has been reported that the OEC consists of cubane cluster Mn_4CaO_5 (**Figure 2**), which has been characterized.^{30,32,33} One function of the OEC is the oxidation of water for oxygen releasing, which is performed by light-induced electron transfer reactions (**Figure 2**).³⁴ Manganese catalase and the oxygen-envolving complex are most frequently studied in the recent research. However, manganese enzymes have been less reported than iron enzymes as they are found in less sources.

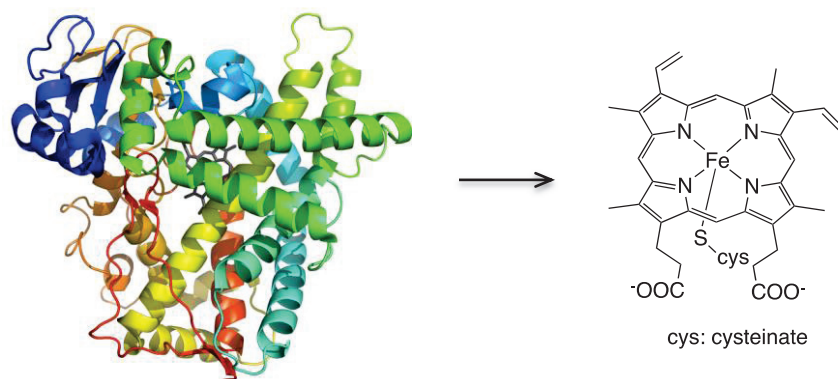


Figure 1. Cytochrome P450 and its active site.²⁰

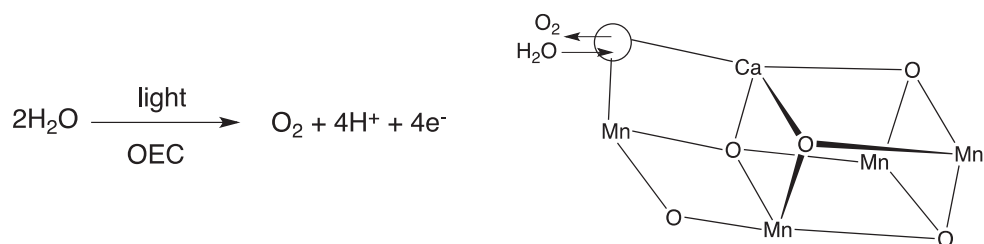


Figure 2. Structure of the Mn_4CaO_5 cluster and process of oxygen releasing.

These metalloenzymes are working in mild conditions, exhibiting specific high efficiency and selectivity for certain substrates as well as regioselectivity and stereoselectivity. They are generally benign for the environment, which satisfies the principles of green and sustainable chemistry.³⁵ These special functions and properties inspired researchers to synthesize biomimetic compounds, to imitate the features.

1.2 Catalytic oxidation of alcohols

1.2.1 Introduction on oxidation of alcohols

The oxidation of alcohols is an important transformation in organic synthesis that can be achieved by various methods, already reported in the literature,³⁶⁻³⁸ which will be

discussed later on. There has been growing demand for oxidation of alcohols for fine and specialty chemicals. The products from alcohols such as aldehydes, carboxylic acids or ketones, are key intermediates for the chemical industry.¹

1.2.2 Traditional methods of oxidation

Chromium trioxide (CrO_3) is a strong oxidizing agent, which is used in the oxidation of secondary alcohols to ketones in the presence of sulfuric acid.³⁹ The procedure involving sulfuric acid and chromium trioxide is proved to be safe, affording chromic acid. This method was first discovered by Jones. Jones's oxidation is the most frequent procedure and the beginning of the successful chromium-based oxidants.⁴⁰ It was used for oxidation of ethyl-3-hydroxypent-4-enoate (**Figure 3**), which provided a method for large scale production of an unstable ketone.⁴⁰

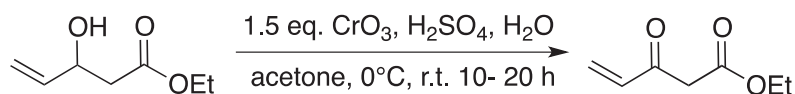


Figure 3. Jones's reagent for the oxidation of alcohol.

The catalytic oxidation of primary alcohols to aldehydes is normally difficult to achieve because aldehydes are easily transformed to the corresponding acids under oxidative conditions. Sodium dichromate was reported to oxidize a series of benzyl alcohols to the corresponding aldehydes in good yields under neutral conditions. For example, cinnamic alcohol was oxidized to cinnamaldehyde in 91% of the yield after under reflux for 3 hours (**Figure 4**).⁴¹

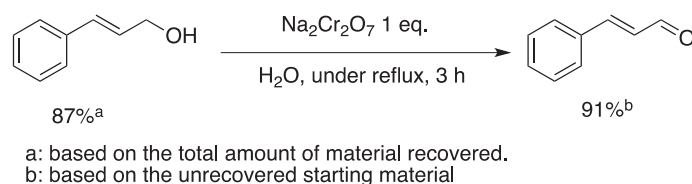


Figure 4. Oxidation of cinnamic alcohol to cinnamaldehyde with sodium dichromate.

Except for chromium-based oxidant, tetra-*n*-propylammonium per-ruthenate (TPAP reagent) (**Figure 5**) is also used as a mild oxidant for alcohols.⁴² In the oxidation of primary and secondary alcohols, 68% to 99% yield of aldehydes or ketones were isolated in 0.5 h to 1.5 h using TPAP reagent with *N*-methyl morpholine *N*-oxide (NMO) (**Figure 5**) as co-oxidant.

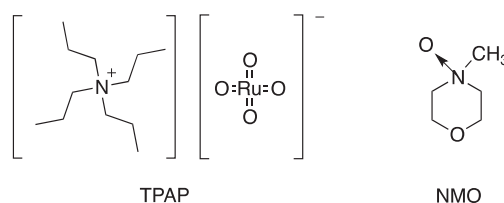
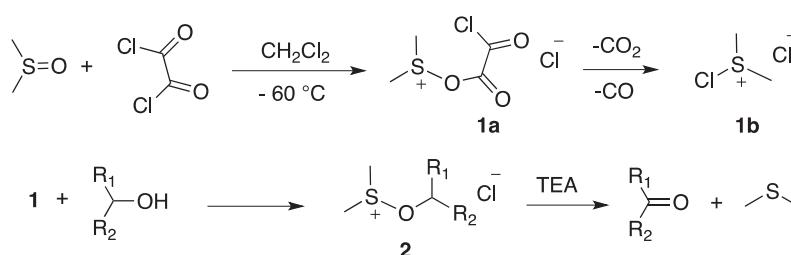


Figure 5. Structures of TPAP and NMO.

Menger *et al.* reported that a permanganate salt ($\text{NaMnO}_4 \cdot \text{H}_2\text{O}$) could transform a range of alcohols such as 2-octanol, cyclohexanol, 5 α -androstane-17 β -ol to the corresponding ketones in good yields (up to 100%) at room temperature.⁴³ As the salt is not soluble in the reaction mixture, the later reaction can be considered as a heterogeneous catalyzed reaction.

The famous Swern oxidation, avoiding the use of toxic metals such as chromium is also commonly used. This reaction allows for the preparation of aldehydes and ketones from alcohols directly, without producing acids.⁴⁴⁻⁴⁶ The Swern oxidation involves the activation of dimethyl sulfoxide (DMSO) with oxalyl chloride at low temperature (-

60°C), forming the intermediate **1** (**Scheme 1**).⁴⁷ The structure of **1** is unknown, and both **1a** and **1b** are possible. The intermediate **1** then quickly reacts with a primary or secondary alcohols to afford the alkoxyulfonium salt **2**, which can quantitatively convert to the carbonyl compounds in high yield in the presence of triethylamine (TEA) (**Scheme 1**).⁴⁴ Using this method, alcohols such as benzyl alcohol, 1-octanol and cyclohexanol are converted to the corresponding aldehydes or ketones in more than 94% yield.⁴⁴



Scheme 1. Mechanism of the Swern oxidation of secondary alcohol.⁴⁴

The Swern oxidation was also applied to heterogeneous catalysis. Tsuchiya, D. *et al.* reported that ion-supported (IS) methyl sulfoxide could also realize the Swern reaction with oxalyl chloride in the oxidation of a series of primary and secondary alcohols in dichloromethane at -70°C in good yield (**Figure 6**).⁴⁶ In addition, the reaction did not produce any unpleasant odor.

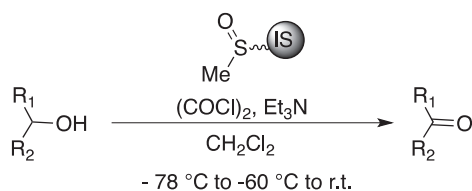


Figure 6. Oxidation of alcohols to ketones with an ion-supported methyl sulfoxide.⁴⁶

The traditional methods for oxidation transformation often use heavy metal oxides such as permanganate, dichromate, ruthenium(VIII) oxide, or use toxic reagents, such as oxalyl chloride, which produces a large amount of environment wastes. In addition, there are also lots of oxidants applied in the oxidation (**Table 3**), classified in oxygen content order. Ozone has relative high oxygen content, but it is highly noxious and requires costly equipment for its generation.¹¹ Iodosobenzene is a strong oxidant, but the oxygen content is too low. In order to meet the requirement for a sustainable and green chemistry, the new oxidizing conditions should emerge.

Table 3. Single atom oxygen donors.¹¹

Oxidant	Product	Oxygen content (weight)%
O ₂		100
H ₂ O ₂	H ₂ O	47.0 ^a
O ₃	O ₂	33.3
NaClO	NaCl	21.6
<i>t</i> -BuOOH	<i>t</i> -BuOH	17.8
PhIO	PhI	7.3

^a calculated on 100% H₂O₂.

Dioxygen, hydrogen peroxide and other peroxide are preferred (**Table 3**), for the replacement of metal and chlorine-based oxidation reactions, as they could reduce the persistent contamination to a large extent.⁴⁸ Dioxygen (cheap, safe and abundant) is used as an oxidant, mostly applied in heterogeneous catalysis, which could contribute to green and sustainable processes.^{38,49,50} Hydrogen peroxide is the most attractive oxidant due to costs, ease, and safety of operation.¹¹ In addition, hydrogen peroxide has a relatively high oxygen content, and the only product is water. It is a promising peroxide due to environmental considerations. More and more effective catalysts which could activate hydrogen peroxide in oxidation reaction have been developed.⁵¹

1.2.3 Bioinspired methods

As metalloenzymes have notably high efficiency and selectivity for some specific substrates, work at mild conditions and have been shown harmless to environment,⁵² substantial attempts have been made to develop biomimetic oxidation reactions. Generally, they contain environmentally benign metals (e.g., manganese and iron) and use mild oxidants (e.g., dioxygen and hydrogen peroxide). Furthermore, iron, copper and manganese are the most popular elements in biomimetic oxidation, as they are of great abundance, and little expensive.³⁵ These catalysts have been developed for the oxidation of non-activated carbon hydrogen bonds to more valuable products.^{53,54} In addition, the oxidation of non-activated C-H bonds in the presence of iron and manganese catalysts has been achieved by using oxidants such as alkyl hydroperoxides, dihydrogen peroxide, and dioxygen.^{10,55-57} As a result, a variety of biomimetic catalysts have been synthesized and applied for the catalytic oxidation of alcohols over the past decades.

Hence, Sekino *et al.*⁵⁸ reported that a μ -peroxo diiron(IV) complex generated *in situ* from $[\text{Fe}_2(\text{L}^{\text{Ph}_4})(\text{O}_2)(\text{Ph}_3\text{CCO}_2)]^{2+}$ **3** (**Figure 7**. $\text{L}^{\text{Ph}_4} = \text{N,N,N',N'}$ -tetrakis(1-methyl-2-phenyl-4-imidazolyl)methyl-1,3-diamino-2-propanolate) with a dinucleating ligand could catalyze the oxidation of benzyl alcohol with dioxygen. Kinetic and isotope labeling experiment suggested that the diiron(IV)-oxo species was the active oxidant for the oxidation.

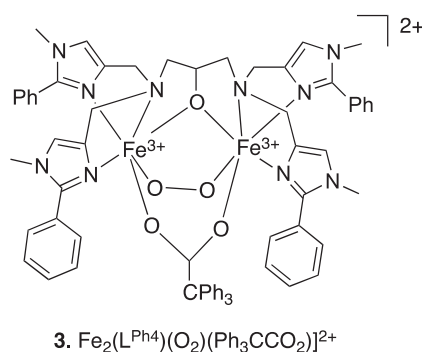


Figure 7. Structure of μ -peroxo diiron(III) complex.

Similarly, Nam *et al.* investigated the oxidation of benzyl alcohol with oxoiron(IV) complexes based on nonheme ligands such as N_4Py (**Figure 8. 4**), TPA (**Figure 8. 5**) and revealed detailed mechanistic insights.⁵⁹ It was reported that the oxidation of alcohol was conducted by the two different high-valent iron-oxo complexes of nonheme ligands generated *in situ*, separately. The proposed mechanism for the oxidation of alcohol by nonheme iron(IV)-oxo species was in **Scheme 2**. For example, cyclobutanol was oxidized to the carbon radical **6** by hydrogen abstraction, followed by an electron transfer (**Scheme 2**, pathway **A**). If the radical **6** escaped from the solvent cage, a ring-opened product formed (**Scheme 2**, pathway **B**).⁶⁰

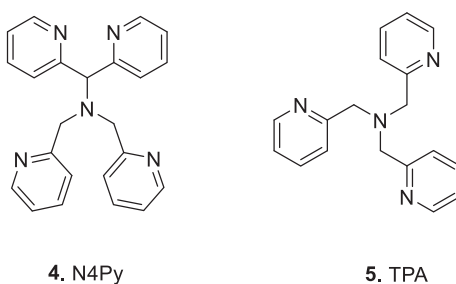
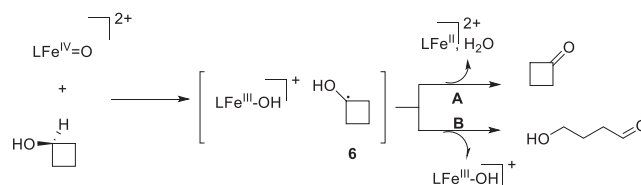
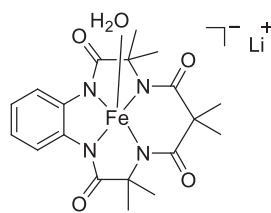


Figure 8. Structures of nonheme ligands N_4Py and TPA.



Scheme 2. Oxidation of cyclobutanol by nonheme iron(IV)-oxo complexes.

Among others, the Fe-TAML iron complex $\text{Fe}(\text{TAML-Me}_2)\text{Li}$ (**Figure 9**) was proven very efficient for the catalytic oxidation of benzyl alcohols, and for some lignin model compounds, in the presence of (diacetoxyiodo)benzene (DAIB).⁶¹ The three different linkages such as α -O-4, β -O-4 and β -1 in lignin model compounds were also oxidized by the combination of $\text{Fe}(\text{TAML-Me}_2)\text{Li}$ and DAIB in good conversion. The oxidative products contained the products from C-C bond cleavage, which provided a promising method for transformation of lignin to small aromatic molecules.



7a. $\text{Fe}(\text{TAML-Me}_2)\text{Li}$

Figure 9. Structure of $\text{Fe}(\text{TAML-Me}_2)\text{Li}$ **7a**.

With biomimetic manganese-based catalysts, Shen *et al.* reported that the complex $\text{Mn}(\text{S-PMB})(\text{CF}_3\text{SO}_3)_2$ **8** (**Figure 10**) efficiently oxidized a large range of secondary alcohols to the corresponding ketones with hydrogen peroxide in the presence of acetic acid.⁶² The turnover number in the oxidation was up to 4700. A manganese complex **9** based on the BQEN ligand (**Figure 10**), was also proven to efficiently promote the oxidation of alcohols with peracetic acid as the oxidant.⁵² The catalytic oxidation of alcohols by other non-heme complexes was also investigated.^{35,63-68} In addition,

oxidants such as dioxygen and hydrogen peroxide are in the content of sustainable chemistry.

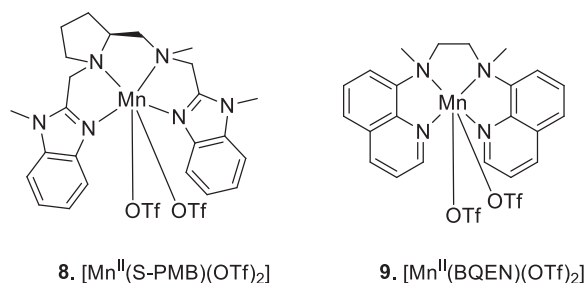
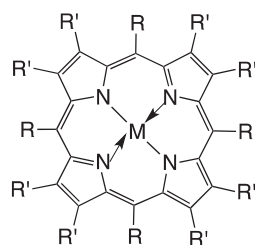


Figure 10. Structures of *cis*- $[\text{Mn}^{\text{II}}(\text{S-PMB})(\text{CF}_3\text{SO}_3)_2]$ **8**⁶⁹ and *cis*- $[\text{Mn}^{\text{II}}(\text{BQEN})(\text{CF}_3\text{SO}_3)_2]$ **9**⁵².

1.3 Our approach

1.3.1 Fe(TAML)

Our research group used to work on the catalytic oxidation with metal coordinated porphyrins complexes.⁷⁰⁻⁷² Porphyrins are cyclic molecules composed of four pyrrole units linked together by methyne bridges. These ligands can coordinate a large variety of transition metals (Fe, Mn, Zn, Ni, Co,...) (**Figure 11**). Porphyrin complexes are widely used in Nature in the active sites of enzymes for catalytic oxidation, reduction and dioxygen transport.⁷³ Synthetic porphyrin metal complexes have been widely used in catalytic oxidation,⁷⁴ such as epoxidation,⁷⁰ hydroxylation,⁷⁵ oxidation of C-H.⁷⁶



M = Fe, Mn, Zn, Ni, Co,...

Figure 11. Structure of a porphyrin complex.

The advantage of metalloporphyrins comes from their important activity (catalytic charge normally used < 1 mol%) and their stability under oxidizing conditions. These two aspects can be modified by adjusting the center metal, the functional groups R/ R', and the use of axial ligand. Besides, the metalloporphyrins are highly versatile. They have been used with a range of oxidants such as TBHP, oxygen, hydrogen peroxide, NaClO, PhIO and so on. However, the synthesis of porphyrins often turns out to be difficult and expensive (low yield and difficult purification).

Our group also worked on a trianionic ligand, the pentafluorophenyldipyrrinphenol ligand DPPH₃ **11** (**Figure 12**).⁷⁷ The dipyrinphenol ligand can be seen as a combination of porphyrin and salen cores. The corresponding [Mn^{II}(DPP)]⁻ complex **12** has also been synthesized (**Figure 12**). It has been well characterized by X-ray crystal structure, EPR, electrochemistry and DFT calculations.⁷⁷ The spectrum and theoretical data indicate that it resembles the structure of salen and corrole. The catalytic performance of MnDPP has been tested in the oxidation of cyclooctene with PhIO. It afforded the epoxide in 97% yield, but the kinetics were not sufficient as well as the stability of the catalyst.

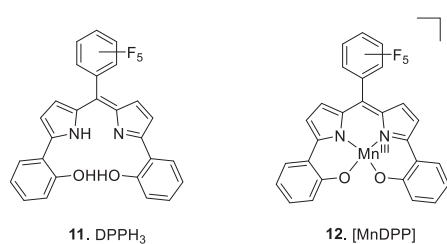


Figure 12. Structures of the DPPH₃ ligand **11** and the [Mn^{II}(DPP)]⁻ complex **12**.

The catalytic oxidation with Fe(TAML)Li has been explored in our lab only in the recent years. We used the TAML ligand, [TAML-Me₂] coordinated with iron **7a** as the catalyst. Fe(TAML) complexes have been used in a large range of applications which

will be discussed in **Part II**. In our lab, Fe(TAML)Li **7a** was evaluated for the catalytic oxidation of benzylic C-H bond with TBHP in high efficiency with high selectivity.⁷⁸ Furthermore, the iron catalyst has also been used for the efficient conversion of alcohols to aldehydes in the presence of DAIB [(diacetoxyiodo)benzene] and also for the oxidation of lignin model compounds.⁶¹ TAML is a ligand, resistant to oxidative destruction and hydrolysis. Thus, Fe(TAML)Li complexes are relatively more stable than usual catalysts. We then chose Fe(TAML) complex as our research model.

1.3.2 [Mn(Me₂EBC)Cl₂]

Before joining Prof. Andrioletti group, I used to work on the manganese complex **14** with a cross-bridged cyclam (Me₂EBC) ligand **13** (**Figure 13**) in catalytic oxidation in Prof. Guochuan Yin group.

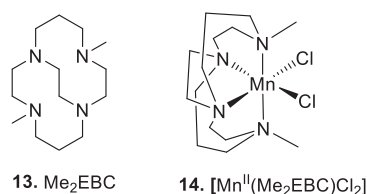


Figure 13. Structure of cross-bridged cyclam Me₂EBC **13** and the corresponding manganese(II) complexes **14**.

[Mn(Me₂EBC)Cl₂] has been well characterized and has been used for a series of applications, such as hydrogen transfer reaction, electron transfer and oxygen transfer reaction, which will be introduced in **Part III**. According to the literature, [Mn(Me₂EBC)Cl₂] can oxidize sulfides to the corresponding sulfone with H₂O₂ or PhIO in the presence or without Lewis acid.^{79,80}

In order to further explore the reactivity of the manganese catalysts in catalytic oxidation, we selected the manganese(II) complex [Mn(Me₂EBC)Cl₂], previously

provided by Prof. Guochuan Yin as our catalyst. The complex has been fully characterized by X-ray, magnetic and electrochemistry methods, which will be further discussed in **Part III**.⁸¹ In my research, I wanted to explore the oxidation of alcohols with the $[\text{Mn}(\text{Me}_2\text{EBC})\text{Cl}_2]$ and further explore its possible applications.

2 State of the art on Fe(TAML)

2.1 Introduction on TAML

To meet the requirement of green and sustainable chemistry, catalysts design should obey the rules of pollution limitation. Besides, ligands more resistant to oxidative degradation and complexes more stable toward hydrolysis should be developed. The TAML ligands incorporate the principal biochemical elements (C, H, O, N) to avoid toxicity functionalities.⁸² Moreover, the TAML design follows an oxidation-resistant design loop (**Figure 14**), which makes it practical and efficient.^{48,83} First, design a ligand thought to be oxidation resistant and make metal complex. Next, oxidize the metal complex until ligand decay occurs. After that, identify the vulnerable part of the ligand by characterization of the degradation products. Modify the weak site to make the ligand more robust. Then try again the four steps until the ligand is oxidation-resistant enough.

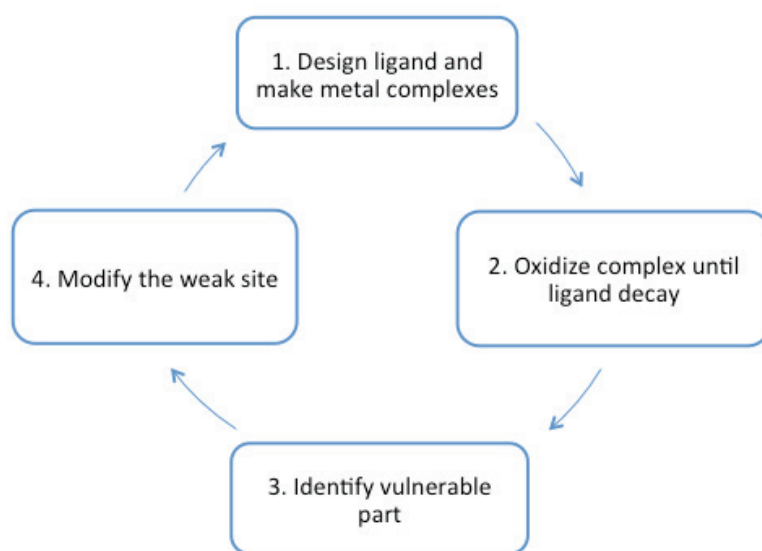


Figure 14. The TAML design loop for oxidation-resistance.⁴⁸

The TAML ligand **15** (**Figure 15**) is a TetraAmido Macrocyclic Ligand, firstly designed in 1987.⁴⁸ The TAML displays four amides, which are strong donors once deprotonated, making it suitable for coordination with metals. Moreover, the four deprotonated amides have four negative charges, which can be neutralized by metal centers in high oxidative states.⁸⁴ The combination of these features, allows to isolate stable high-valent middle and late transition-metal species in high oxidation state.

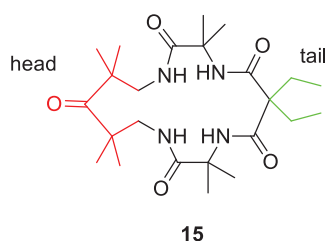


Figure 15. The structure of the first TAML **15**.⁸⁴

To make the ligand more resistant to oxidative destruction and hydrolysis, progress has been made since 1987.⁴⁸ The TAML has modifiable “head” and “tail”. Hence, it has been found that the TAML compound **16** with an aromatic ring on the “head” instead of the acyclic, the stability towards oxidative degradation can be increased (**Figure 16**). Indeed, the aromatic π system can conjugate with the metal center, and distribute the positive charge to the ligand.⁸⁵ The Collins group designed an aromatic TAML with two chlorine substituents on the ring.⁸³ Functionalization of the ligand was progressed by changing the “head” or the “tail”, which is a significant advantage of the TAML ligands compared to others. Different substituents were also appended, such as H, $-\text{NO}_3$, $-\text{Me}$ and so on. Substituents on the “head” can have different purpose, such as $\text{CH}_3(\text{CH}_2)_{10}\text{C}(\text{O})\text{NH}-$, CO_2^- , $-\text{N}-\text{CH}_3$ on the ring (**Figure 17**).^{48, 86} Complex **7b** in **Figure 17** is a micelle-forming catalyst that forms mixed micelles with dodecyltrimethylammonium bromide (DTAB). The mixed micelles can dissolve and bleach the water-insoluble dye. When the aqueous solution of the dye containing this mixed micelles treated with H_2O_2 , it can dissolve through attraction to the Stern layer

of the micelle.⁴⁸ The complex **7c** with an anionic CO₂⁻ group, improve the delocalization of the negative charge on the complex, which can decrease the rate for the catalyst to attack substrates on heterogeneous supports with negative charges.⁴⁸ Complex **7d** is similar to **7c** using positively charged groups. However, changes on the “tail” can greatly change the lifetime and the hydrolytic degradation rate of the complex.⁸⁷ For example, replacement of R = Me with R = F, a strong electron-withdrawing group, the hydrolytic stability of complex Fe(TAML-F₂) is 10¹¹-fold increased in acidic media.⁸⁶ The complexes **7e**, and **7f** have been proved to have longer lifetime than complex **7a** because of hydrogen abstraction on the tail are harder.⁴⁸ Besides, methyl was used as a “tail” instead of Et, as Et was easily oxidized on some occasion (it will be discussed later).

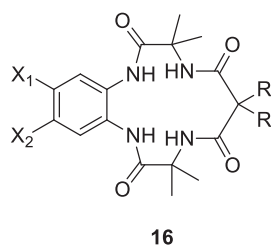


Figure 16. The general structure of TAML.

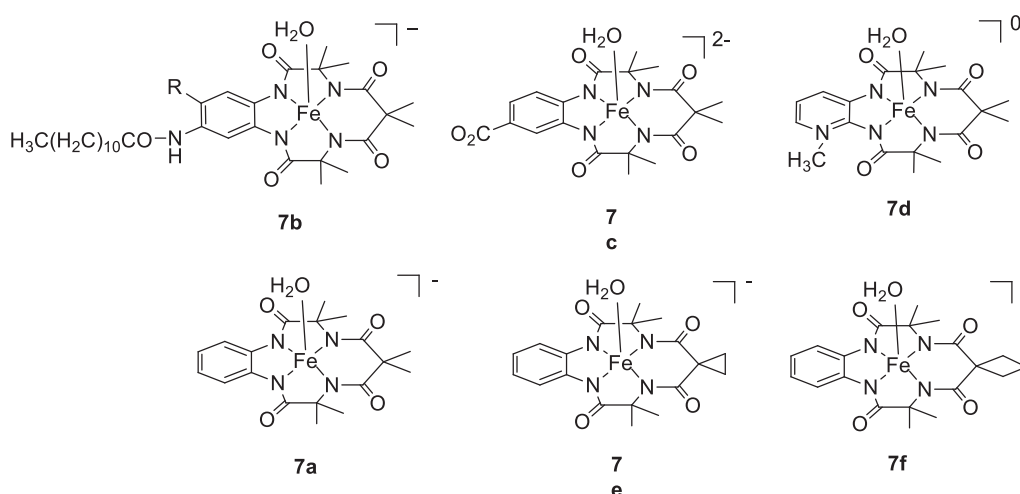
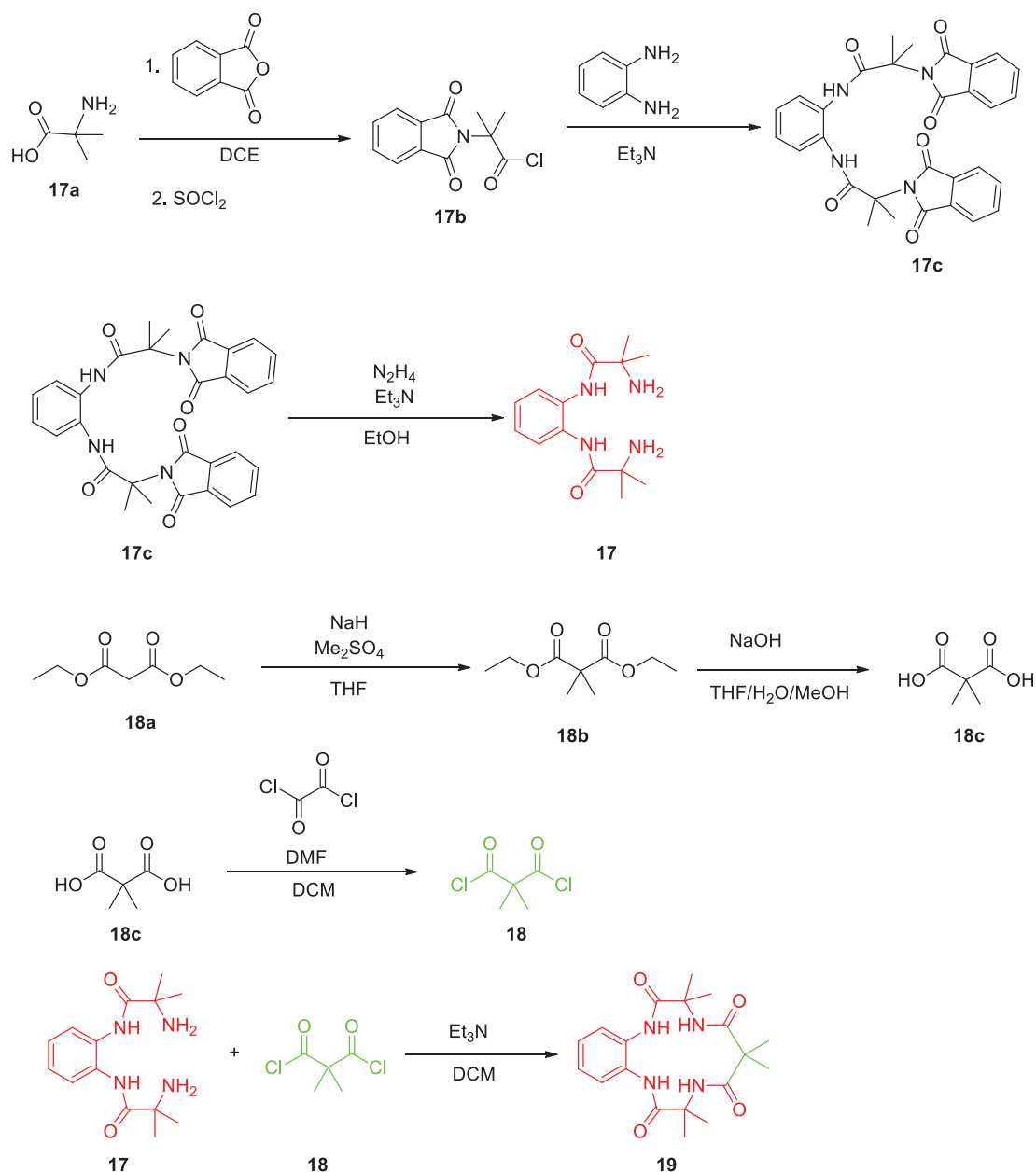


Figure 17. Different substituents on the “head” and “tail” of [Fe^{III}(TAML)] complexes.

As the TAML ligand **19** (**Scheme 3**) is the simplest ligand, it has been widely studied in the literature. The synthesis protocol for the TAML-Me₂ is shown in **Scheme 3**.⁸⁸ Firstly, the product **17** was synthesized by the protection of the amino-acid **17a**, followed by formation of the corresponding acid chloride **17b** using thionyl chloride. Next, the protected “diamide diamine” **17c** was synthesized. At last, the diamide diamine **17** was obtained by deprotection of **17c** with hydrazine. The product **18** was synthesized in 4 steps starting from diethyl malonate **18a**. **18a** was converted to **18b** by deprotonation with sodium hydride, then reacted with dimethyl sulfate. The compound **18c** was obtained by saponification of **18b**. The final dichloride product **18** is obtained by reaction of **18c** with oxalyl chloride. The TAML ligand **19** was efficiently obtained by reaction between compound **17** and 2,2-dimethylmalonyl dichloride **18**.



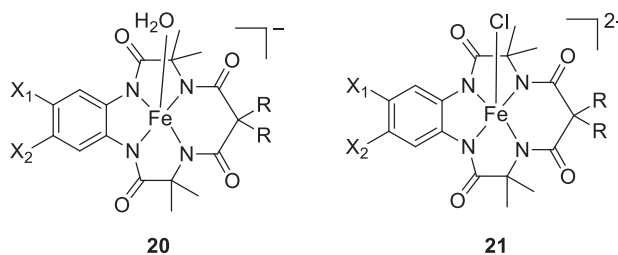
Scheme 3. Synthesis of the simplest TAML **19**.⁸⁸

2.2 Introduction on Fe(TAML)

Although a wide range of metals, such as iron, manganese, nickel, copper, cobalt and so on have been investigated,⁸⁵ iron-TAML complexes tend to be the most frequent targeted catalysts. Iron is the mostly used element in oxidation catalysis in biochemistry and it is the least toxic element for green chemistry. Besides, iron TAML can activate

green oxidants, H₂O₂ and organic peroxide such as *tert*-butyl hydroperoxide, benzoyl peroxide, cumyl hydroperoxide for the catalytic oxidation of a wide range of targeted substrates.^{48,89,90}

To make the complexes more stable and selective, different functionalizations have been done on TAML. Fe(TAML) complexes with various substituents on the aromatic ring and different tails have been investigated, as showed in **Figure 18**.⁹¹ There are two kinds of axial coordination for Fe(TAML): water or a chloride anion. Functionalization is on the aromatic ring or on the “R” part, as mentioned before. Chloride and –NO₂ instead of –H on the ring, can increase the reactivity of the Fe^{III}(TAML) complexes with oxidant.⁹² However, the purpose of modification on the “tail” is mainly to increase the stability of the complexes towards hydrolysis. The –Me group is more acid tolerant than –Et, while the fluorinated tail is the most acid-tolerant among the three.



20/21	X ₁	X ₂	R
a	H	H	Me
b	Cl	Cl	Et
c	Cl	Cl	Me
d	Cl	Cl	F
e	NO ₂	H	Me
f	NO ₂	H	F
g	H	H	F
h	MeO	MeO	Me

Figure 18. The first TAML generation investigated.⁹¹

2.3 Properties of [Fe(TAML)]

2.3.1 Coordination model and structure

Iron(III) TAMLs are five coordinated “square pyramid” species, in which Fe^{III} coordinates the four deprotonated nitrogen and an axial water molecular in the solid state (**Figure 19**, left).^{90,93} Iron in the complex is Fe(III), which is partially neutralized by four nitrogen, leaving a negative residue.⁹² Thus, the complex contains an Fe(TAML) with one negative charge and one counter-cation.⁹¹ The four nitrogen atoms are planar with short Fe-N bonds (mean 1.885 Å), while Fe(III) sits out of the plane by 0.364 Å. The axial ligand of Fe^{III} can be also chloride (**Figure 19**, right). In **21g**, the average

length of Fe-N bonds is 1.894 Å, and iron(III) is out of the plane by 0.403 Å. The Fe-Cl bond length (2.361 Å) in **21g** is longer than in FeCl₄⁻ (2.182-2.187 Å),⁹⁴ iron(III) porphyrins (2.218 Å),⁹⁵ and in 5-coordinated iron(III) complexes (average 2.235 Å).^{91,96} The elongated Fe-Cl bond is because the four deprotonated strongly σ -donating and π -donating equatorial amide nitrogen quench the Lewis acidity of axial chloride attributing destabilization. **20a** has a boat conformation and the ligand is almost in planarity of symmetry with the dimethyl groups.⁹¹ **21g** has a chair configuration and one of the F atom is almost in the ligand plane.⁸⁷ However, the other F atom (F₂) is perpendicular to the plane.

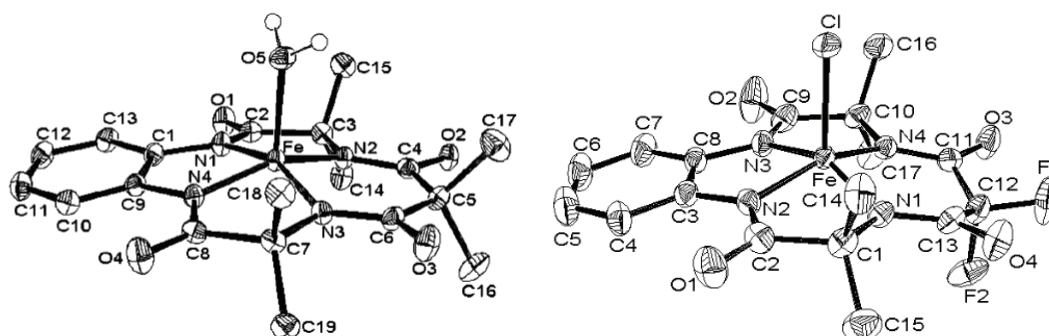


Figure 19. Crystal structures of **20a** (left) and **21g** (right), with Li⁺ as countercation.⁸⁷

In neutral water solution, Fe(TAML) complexes are six coordinated systems with two axial water molecules bound.⁹¹ Interestingly, the compound with an axial Cl ligand will be cleaved by water to form a hydro or hydroxyl species (**Figure 20**).⁹¹ The equilibrium constant K_{Cl} (0.18 M⁻¹) indicates that the coordination of Cl⁻ is negligible at [Cl]⁻ < 0.5 M.⁸⁷ Some of the Fe(TAML) compounds can also coordinate with one or two pyridine, imidazole or azide molecules in water solution upon addition of one of the solvents.^{91,97}

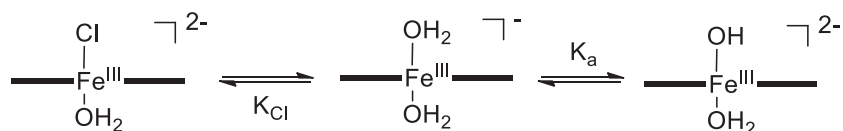


Figure 20. Fe^{III}(TAML) complex containing an axial chloride hydrolysis in water.⁸⁷

The UV-Vis spectra of an aqueous solution of **20a** upon addition of pyridine indicate the stepwise substitution of two axial water molecules by the pyridine (**Figure 21**). Imidazole with the equilibrium constants (K_L and K_{2L} : 69 and 4.7 M^{-1}) is a better ligand for Fe(TAML) compared to pyridine (K_L and K_{2L} : 4.7 and 0.42 M^{-1}). The nitrogen atom directly coordinates with iron. From the crystal structure of [(Me₂-TAML)Fe^{III}-(1-MeIm)]⁻, the imidazole plane is almost perpendicular to the plane passing through the atoms Fe₁, N₂ and N₄. (**Figure 22**).⁹⁸

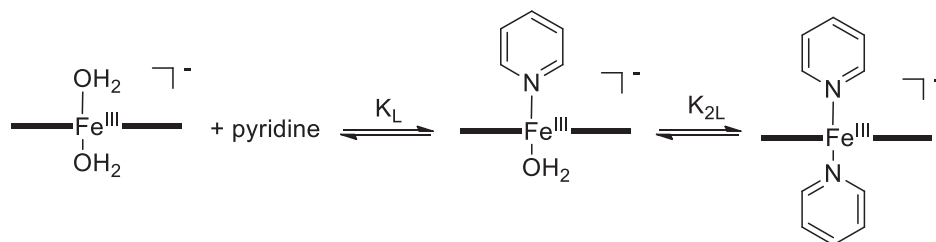


Figure 21. Stepwise substitution of two axial water molecules by pyridine.

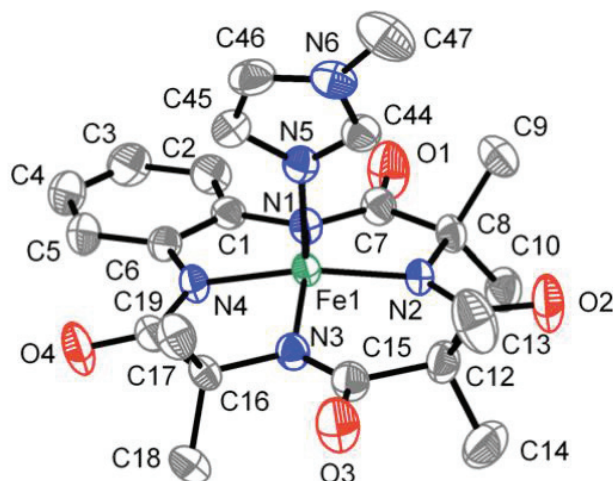


Figure 22. Crystal structure of [(Me₂-TAML)Fe^{III}-(1-MeIm)]⁻.

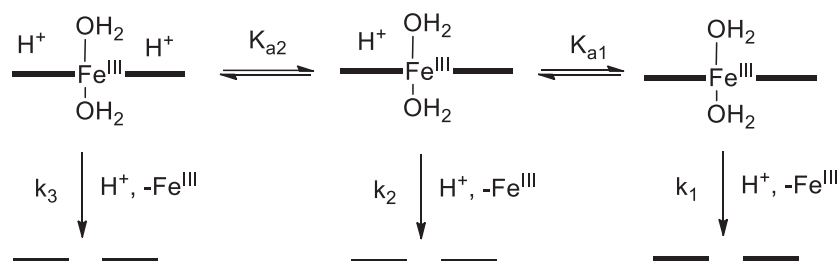
2.3.2 Solubility

The solubility of Fe^{III}(TAML) depends largely on the counterion of the complexes. When the counter cation is Li⁺ or Na⁺, the complexes are hydrophilic, and are quite soluble in protic or polar solvents such as alcohols and water. On the contrary, with a hydrophobic organic cation, like PPh₄⁺, the compound can dissolve in aprotic weakly coordinating solvents, such as dichloromethane, trimethylacetonitrile, nitrobenzene, toluene, 1,2-dichloroethane, 1,2-dichlorobenzene, α,α,α -trifluorotoluene and chloroform.^{92,99}

2.3.3 Stability

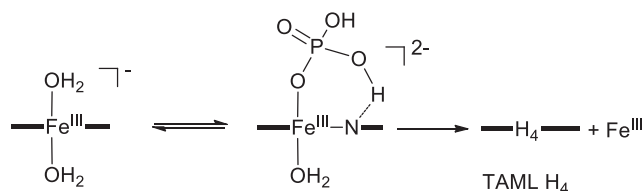
Fe(TAML) complexes are pH dependent complexes. Fe(TAML) complex **20a** is stable for months in neutral water solution, while at pH 3-4, it starts to decompose rapidly. When at pH 1, more than 95% of free TAML ligand is isolated.⁸⁷ Generally, the Fe-N bonds are hydrolyzed by specific acids or buffer agents. The H⁺-induced demetalation occurs through protonation of a nitrogen-iron bond, forming the N-H bond, as shown

in **Scheme 4**.⁸⁷ The acid induced demetalation gently depends on the substituents on the “head”, but it is dramatically influenced by the “tail”. If Me is replaced by F, the tolerance to an acid strongly improves, because F is electron withdrawing.⁸⁷ The cleavage of a single M-N bond leads to strong distortion of the ligand plane and then rapidly induces cleavage of other M-N bonds.



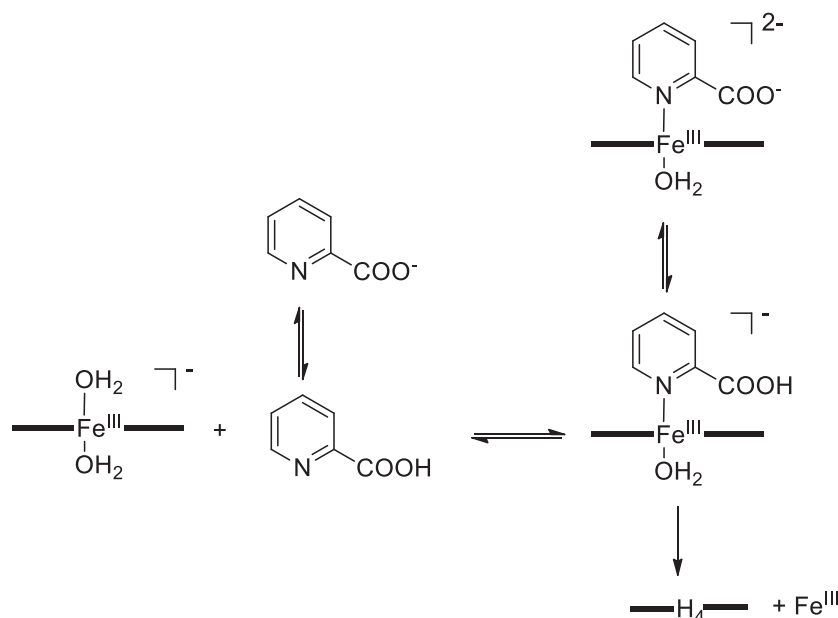
Scheme 4. Acid- induced demetalation of Fe(TAML) **7a**.⁸⁷

The Fe(TAML) complexes also tend to be catalytically demetalated by some Brønsted acid buffer solutions such as H_2PO_4^- , HSO_3^- , CH_3COOH and $\text{HO}_2\text{CCH}_2\text{CO}_2^-$ at pH 4-9.⁹⁷ The proposed mechanism for a phosphate-induced demetalation is presented in **Scheme 5**.⁹⁷ Firstly, one water molecule of Fe(III) species was substituted by H_2PO_4^- ion to produce a mono aquo complex. The amide nitrogen coordinated with Fe(III) has a strong attraction with the hydrogen in H_2PO_4^- through hydrogen bond. Hence, the amide nitrogen atoms protonate and the Fe(III) disconnects with the N-amide forming free TAML ligands and Fe(III) ion.



Scheme 5. Demetalation of Fe(TAML) by phosphate buffer.⁹⁷

The demetalation ability in a buffer solution depends largely on the structure of the acid and the acidities. Picolinic acid catalyzes the demetalation of complex **20a** according to a first order reaction.⁹⁷ Both pyridine and nicotinic acid accelerate the demetalation of **20a**. The mechanism is disclosed in **Scheme 6**. Picolinic acid binds to the axial site of iron and delivers the carboxylic proton to a Fe-N bond. It will be more difficult for the ligand where the amidato-N atoms are less basic, such as complex **7e** Fe(TAML-CH₂CH₂). It is important to understand the influence of the buffer solution, because it will allow a long-term storage of iron-TAML catalysts in solutions.



Scheme 6. Demetalation of **20a** by picolinic acid.⁹⁷

The modification of the ligand aims at improving the stability and the corresponding metal complexes towards oxidation and hydrolysis. The first ligand decomposition was evidenced when Fe(Cl₂-TAML-Et₂) **20b** was reacted with *tert*-butylhydroperoxide in acetonitrile under ambient conditions with a deep blue color formed. In these conditions, the complex was modified to an Fe^{IV}(CN) complex **22f** through one-electron oxidation (**Scheme 7**). The infrared spectrum also indicated that there was a small amount of macrocyclic complex formed, hidden in the blue solid, which turned out to be a

2.4 High valent iron(TAML)

As TAML ligand exhibits a high σ donor capacity and four negative charges, the Fe^{III} in the resting state has no oxidative power for common reductants. Hence, normally oxidative species should have higher oxidation state than Fe^{III} , such as Fe^{IV} and Fe^{V} complexes (**Figure 23**). All the high oxidation state compounds are generated from the Fe^{III} resting state.⁹² Identification and characterization of high valent iron complex are essential for understanding the mechanism of catalysis.

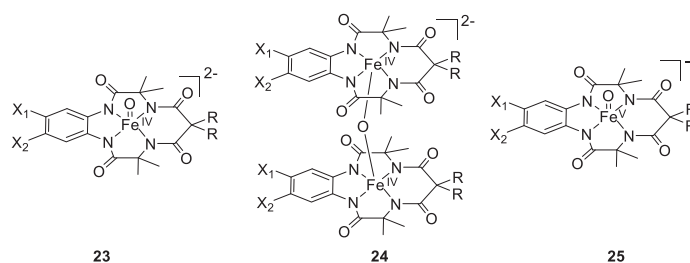


Figure 23. Three common high-valent states of Fe(TAML).

2.4.1 Preparation and properties of mono Fe^{IV} species

There are two kinds of $\text{Fe}(\text{IV})$ species: the mono $\text{Fe}^{\text{IV}}\text{O}$ and diiron(IV) μ -oxo complex. The mono $\text{Fe}^{\text{IV}}\text{O}$ complexes are best described as compounds II in cytochrome P450 (**Figure 24**).^{100,101} To obtain the compound II analogue, the $[(\text{TAML})\text{Fe}^{\text{IV}}\text{O}]^{2-}$ was produced by oxidation of $[\text{Fe}^{\text{III}}(\text{TAML})(\text{OH}_2)]^-$ with *tert*-butyl hydroperoxide (TBHP) in aqueous solution at $\text{pH} > 12$ in nearly quantitative yield (**Scheme 8**).¹⁰¹

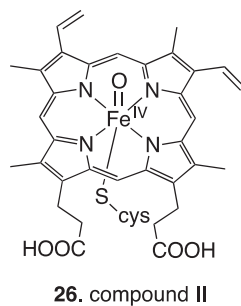
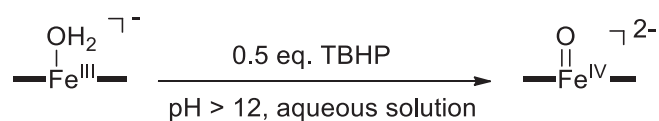


Figure 24. Structure of compound II in cytochrome P450.



Scheme 8. Formation of [(TAML)Fe^{IV}O]²⁻ species.

The Fe^{IV}O species was characterized by UV-Vis spectroscopy, Mössbauer spectroscopy, XAS (X-ray absorption spectroscopies) and DFT calculations.¹⁰¹ The UV-Vis spectrum showed that a new peak at $\lambda = 435 \text{ nm}$ formed with a red species when TBHP was added to an aqueous solution of **20a** at pH 14 (**Figure 25**).¹⁰¹ It has been demonstrated that 0.5 equiv. of oxidant per Fe^{III} afforded the highest yield for Fe^{IV}O. Mössbauer spectrum showed that the Fe^{IV}O complexes had a characteristic electronic spin of $S = 1$.

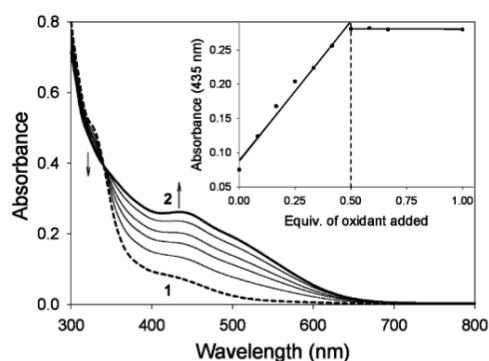
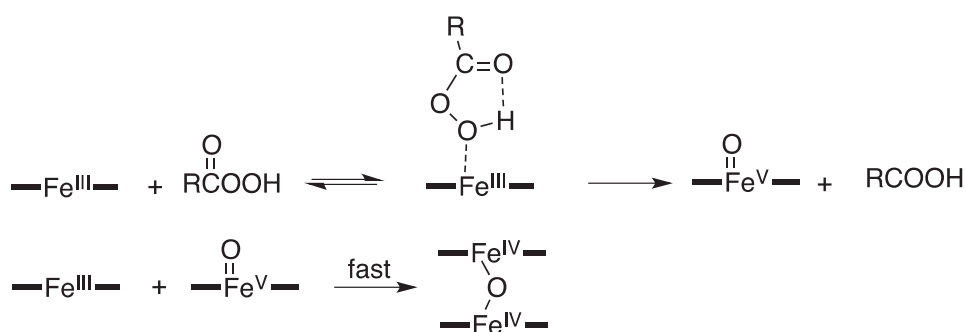


Figure 25. UV-Vis spectrum of the formation of Fe^{IV}O(TAML) complex (**2**) at pH 14 in an aqueous solution.¹⁰⁰

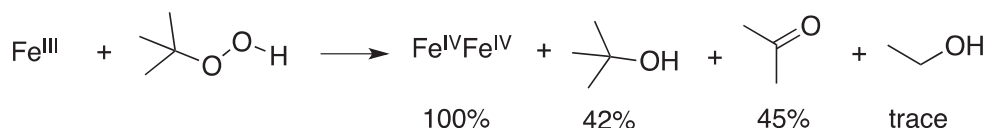
The oxo-bridged diiron(IV) could be generated not only with *m*CPBA but also with other oxidants, such as TBHP, benzoyl peroxide, *tert*-butylperoxide, and hydrogen peroxide.¹⁰² Consequently, the mechanism of the formation of the μ -oxo dimer is quite different. The formation of the $\text{Fe}^{\text{IV}}\text{OFe}^{\text{IV}}$ dimers in the presence of *m*CPBA in MeCN at $-40\text{ }^{\circ}\text{C}$ involves a heterolytic mechanism (**Scheme 9**).^{92,103} Fe^{III} ion reacts with the peroxyacid followed by the removal of the acidic proton from the coordination oxygen. The proton either goes in the solution or transfer to the carbonyl oxygen forming a postulated five-membered ring as depicted in **Scheme 9**, which is the key to drive the cleavage of the heterolytic O-O bond. The O-O bond cleavage causes the formation of $\text{Fe}^{\text{V}}\text{O}$ species, followed by a fast reaction with Fe^{III} species to afford the final $\text{Fe}^{\text{IV}}\text{OFe}^{\text{IV}}$ by comproportionation.



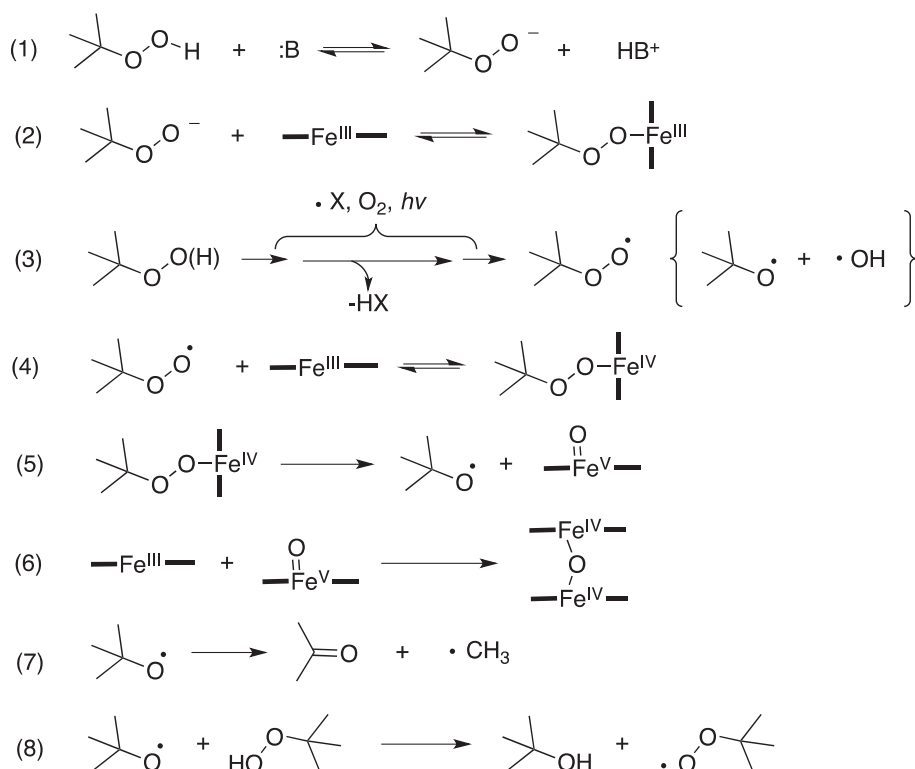
Scheme 9. Mechanism of formation of $\text{Fe}^{\text{IV}}\text{OFe}^{\text{IV}}$ in the presence of *m*CPBA.^{92,103}

In contrast, the oxidation of $\text{Fe}^{\text{III}}(\text{TAML})$ by TBHP in wet MeCN at $-40\text{ }^{\circ}\text{C}$ reaches a 100% conversion (**Equation 1**). Unlike other oxidants, it involves a free radical mechanism (**Scheme 10**).^{92,102} The rate of this reaction was affected by bases (B), light, oxygen and TEMPO.⁹² The free radicals ${}^t\text{BuOO}\cdot$ or ${}^t\text{BuO}\cdot$ and $\cdot\text{OH}$ were produced by light-induced deprotonation of TBHP in the presence of dioxygen (step 3). One potential mechanism involves the reaction of radical ${}^t\text{BuOO}\cdot$ with $\text{Fe}(\text{III})$ to produce

Fe(IV) (step 4), which then was split into Fe(V) and ^tBuO• through a homolytic O-O bond cleavage (step 5). The final oxo-bridged diiron(IV) was formed by comproportionation from Fe(V) and Fe(III) (step 6). The other products in **Equation 1** were generated through a free radical mechanism (step 7 and 8). Some bases such as amines, pyridine and imidazole could inhibit the reaction by coordination with the Fe(III) center. However, some bases can deprotonate TBHP (step 1), followed by the formation of an alkylperoxide adduct with Fe(III) complex (step 2). In this way, the final product would be also formed by heterolysis of O-O bond.

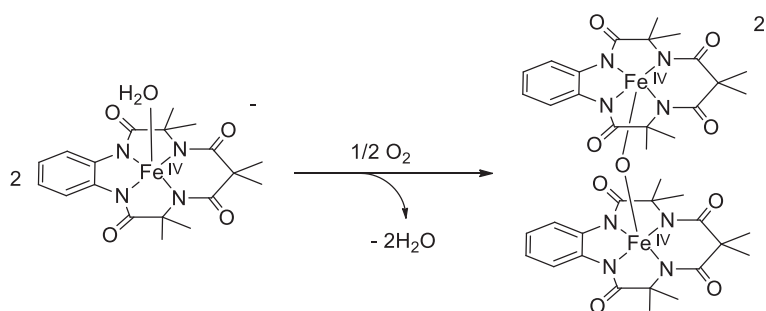


Equation 1. Conversion of Fe^{III} to Fe^{IV}Fe^{IV} by TBHP.



Scheme 10. Tentative mechanism of formation of Fe^{IV}OFe^{IV} by TBHP in wet MeCN at -40 °C.⁹²

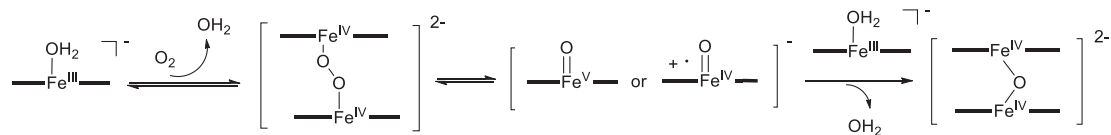
When the oxo-bridged diiron(IV) was produced as the diphosphonium salt of **20a** (or **20h**) $20a(PPh_4)_2$ activates dioxygen in dichloromethane or in other weakly coordinating solvents (**Scheme 11**).⁹⁹ This high yield reaction was quick with a color change from orange to black. This species is stable for month in weakly coordinating solvent, but it will convert to the starting material when it is dissolved in methanol or ethanol.⁹⁹



Scheme 11. The formation of diiron(IV) μ -oxo complexes.

The mechanism for the conversion of $Fe^{III}(OH_2)$ to the μ -oxo dimer $Fe^{IV}OFe^{IV}$ is supposed to be similar to the μ -oxo diiron porphyrins formation from ferrous porphyrins and dioxygen, but the oxidation states are one unit higher.⁹² The μ -oxo diiron(TAML), is first formed from the diferric species $LFe^{IV}-O_2-Fe^{IV}L$ ($L = TAML$) through peroxo bridge, followed by O-O cleavage to $LFe^V=O$ species. Next this active species reacts with $[LFe^{III}]^-$ to produce $[LFe^{IV}-O_2-Fe^{IV}L]^{2-}$, as shown in **Scheme 12**.^{92,99} The dimer was characterized by X-ray crystallography, UV/Vis, Mössbauer and so on.⁹⁹ The UV-Vis showed that the peak of $20a(PPh_4)_2$ at 431 nm decreased and the new bands at 542 nm and 856 nm were formed when the solution was exposed to O_2 . X-ray diffraction⁹⁹ showed that each Fe(IV) was coordinated with four amide-N and the axial bridging oxygen atom. The Fe(IV)-O bond was longer than the $Fe^{IV}=O$ bond in various protein and synthetic $Fe^{IV}=O$ species. The angle of $Fe^{IV}-O-Fe^{IV}$ was around $151.5(2)$ - $153.8(2)^\circ$, which indicated that the two TAML faces were not parallel. There were intramolecular hydrogen bonds between the bridging oxygen and the hydrogen on the

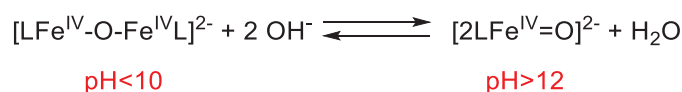
“tail” methyl.



Scheme 12. Proposed mechanism for the formation of the μ -oxo dimer.⁹⁹

Cyclic voltammetry of the μ -oxo dimer from **20a** showed three couples reversible redox potentials, with potentials at $E_{1/2} = -0.23$ ($\Delta E = 77$ mV), 0.37 (68 mV) and 0.72 V (74 mV) versus Fc/Fc^+ and one irreversible reduction at $E_{p, red} = -1.30$ V.⁹⁹

The $Fe^{IV}O$ and μ -oxo dimer $Fe^{IV}OFe^{IV}$ species are related by a pH-control at room temperature.^{92,101} $Fe^{IV}O$ of **20a** dominates at $pH > 12$ while the μ -oxo dimer $Fe^{IV}OFe^{IV}$ dominates at $pH < 10$. It is balanced according to the equilibrium below (**Equation 2**).⁹²



Equation 2. Conversion between $Fe^{IV}OFe^{IV}$ and $Fe^{IV}O$.⁹²

The diiron(IV) μ -oxo complex $Fe^{IV}OFe^{IV}$ from **20a** was proven to catalytically oxidize PPh_3 rapidly to $OPPh_3$ at room temperature through an oxygen transfer reaction.⁹⁹ Moreover, it can oxidize benzylic alcohols such as benzyl alcohol, 4-chlorobenzyl alcohol, 4-nitrobenzyl alcohol, 4-methoxybenzyl alcohol and cinnamyl alcohol to the corresponding aldehydes in the presence of O_2 .⁹⁹ For example, 60 equiv. of benzyl alcohol were converted to benzaldehyde per equivalent of $Fe^{IV}OFe^{IV}$ within 1 h without producing the corresponding acid (**Figure 26**).

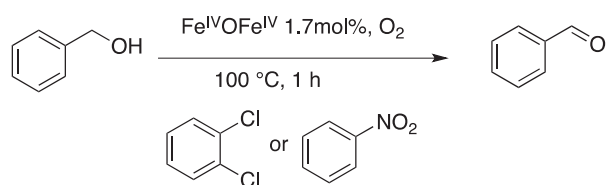
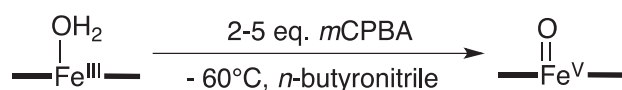


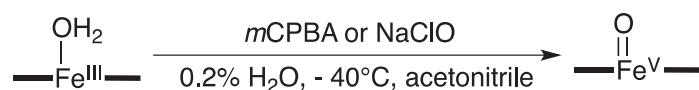
Figure 26. Oxidation of benzyl alcohol to benzaldehyde in the presence of oxygen.⁹⁹

2.4.2 Preparation and properties of Fe^V species

Fe^VO(TAML) complexes are very active species in catalytic oxidation. They are mimics of the active sites of peroxidase and cytochrome P450 enzymes.¹⁰¹ The first Fe^VO(**15**) was produced by reaction of Fe^{III}(**15**) with peracid in *n*-butyronitrile at -60 °C. The highly oxidized species could persist for hours under these conditions (**Scheme 13**).^{101,104} At -60 °C, it would decompose by 10% in 90 min, while it could remain stable for at least one month at -196 °C (77 K).¹⁰⁴ The Fe^VO(TAML) was also produced by oxidation of Fe^{III}(TAML) with *m*-chloroperbenzoic acid or NaClO at -40 °C in acetonitrile in two steps through the intermediate Fe(IV) μ-oxo dimer Fe^{IV}(O)Fe^{IV} (**Scheme 14**).^{102,104,105} Ghosh M. *et al.* reported that Fe^V(O) species were formed at room temperature in wet acetonitrile in the presence of *m*CPBA, while using **27a**_{Cl} from the fifth generation Fe(TAML-N-CH₃) (**Figure 27**). None of the organic oxidants could convert the iron(III) to iron(V) regardless the amount of oxidants. Furthermore, it was characterized by UV-Vis analysis (**Figure 28**), EPR, Mössbauer as well as DFT calculation.¹⁰⁴ The UV-Vis showed that the Fe^V(O) from **20a** oxidized by *m*CPBA in *n*-butyronitrile at -60 °C had two characteristic absorption transitions at 445 nm and 630 nm. The DFT calculations favored the low spin S = 1/2 configuration.



Scheme 13. The first time formation of Fe^V(O) species.



Scheme 14. The formation of Fe^V(O) species with different oxidants.¹⁰²

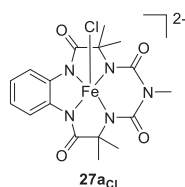


Figure 27. Structure of the complex from the fifth generation Fe(TAML) **27aCl**.

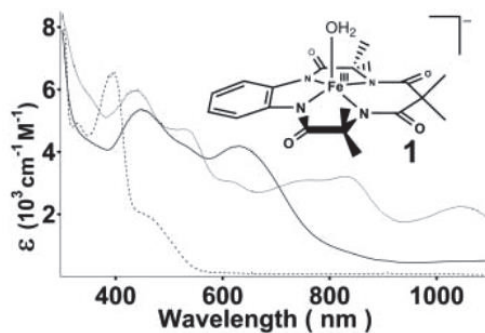


Figure 28. UV-Vis spectrum of Fe^VO(**19**). The dashed line represents Fe^{III}(TAML) **7a**, the dotted line μ-oxo diiron(IV)(**19**) complex and the solid line Fe^VO(**19**).

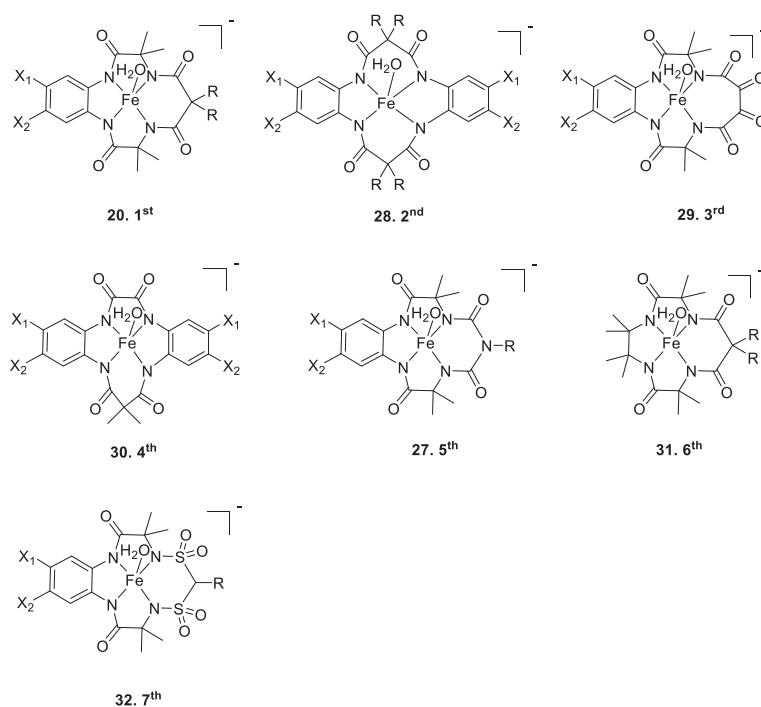
As Fe^{III} can be transformed to Fe^{IV} and further to Fe^V, and Fe^{IV}Fe^{IV} to Fe^V, Fe^V can be also reduced to Fe^{IV}. Hence, in a freshly synthesized Fe^V(O)(**20a**) was added an equal equivalent of Fe^{III} at -40 °C in acetonitrile and Fe^{IV}(O)Fe^{IV} was produced by

comproportionation.⁹² Besides, the comproportionation is strongly controlled by steric factors, so the reaction of the complexes with a methyl group in the “tail” is faster than the comproportionation of complexes bearing ethyl groups.^{92,105} The Fe^V(O) complex could transform to Fe^{IV}Fe^{IV} without any reducing agent because Fe^V(O) is so oxidizing that it spontaneously evolves to a lower oxidation state in nitrile solution at low temperature.^{92,103,105,106}

2.5 Functionalization of Fe(TAML) complexes

In order to design fully functional peroxidase and peroxide models able to activate hydrogen peroxide for better applied processes, up to 7 generations of TAMLs have been developed so far (**Figure 29**).^{92,107} From the 2nd generation, modifications not only occurred on the “head” and “tail”, but also on the cavity. In order to purify water from chemical and biological contamination, generations 1 to 5 were developed progressively. The 2nd and 3rd generations were not used for applications but as synthetic intermediates for the 4th generation. The 2nd generation is similar to the 4th at the exception of the extra -C(CH₃)₂- unit, which makes the later easier to demetallate in water.⁹¹ The 2nd generation presents a larger cavity than the first generation. This large cavity is too large for iron, resulting in a non-planar amido-N ligand. Consequently, the 2nd generation is not stable in neutral water.⁹¹ The 4th generation exhibits a higher reactivity and stability than the first three generations.¹⁰⁸ The 5th generation displays a N-R tail instead of the CR₂ tail typical of the first generation. Introduction of the π -electron pair favors the planarity in the six-membered ring. This increased planarity was proven to induce a higher stability of the catalyst compared to the 1st generation.¹⁰⁷ Nearly all the ligands contain an aromatic ring with substituents except for the 6th generation. The totally aliphatic TAML **31** displays an important steric bulkiness and was proven resistant to acid-induced demetallation at any pH in water.¹⁰⁹ The new 7th generation is very different from the former generation. Indeed, it contains sulfone

connections that were not reported for the other generations. The 7th generation shows a better performance than the former generations in the global reduction of



micropollutants in water, with low-cost, biosafety-scrutinized solutions.¹¹⁰ Different TAMLs, varied from structures, differ in properties and applications. However, within the frame of our studies, we will only discuss about the first generation as it is the prototype and has been the most intensively investigated.

	X₁	X₂	R
a	H	H	Me
f	NO ₂	H	F
i	H	H	Et
d	Cl	Cl	F
e	NO ₂	H	Me

Figure 29. Structures of the 7 generations of TAML.

2.6 Application of Fe(TAML)

2.6.1 General oxidation mechanism using Fe(TAML) and a peroxide

In Nature, there are two kinds of enzyme that are able to activate peroxide, the peroxidases and catalases. While the former activates H_2O_2 for substrate reductions,¹¹⁰ the latter disproportionates H_2O_2 to H_2O and O_2 .¹¹¹⁻¹¹³ The two reactions normally occur in one enzyme. For peroxidase enzyme mimics, the catalyst should have high activity, hence maintaining the catalase activity at a minimum. Numerous iron complexes mimicking peroxidases or catalases display elusive performance.¹¹³⁻¹¹⁵ Conversely, iron TAML complexes as “green” catalysts activate H_2O_2 and mimic peroxidases in the sense that they display high reactivity. The general catalytic cycle of Fe(TAML) activating H_2O_2 is disclosed in the **Figure 30**.

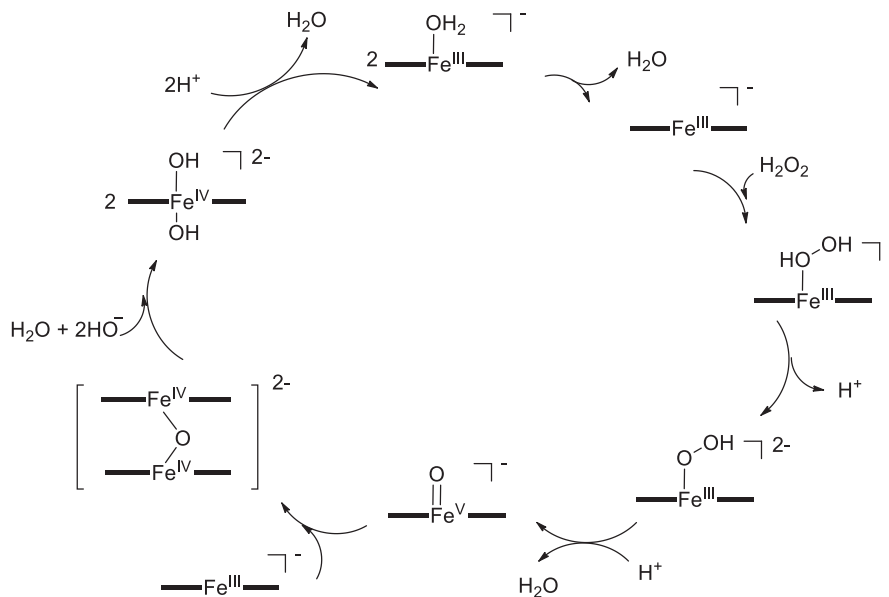
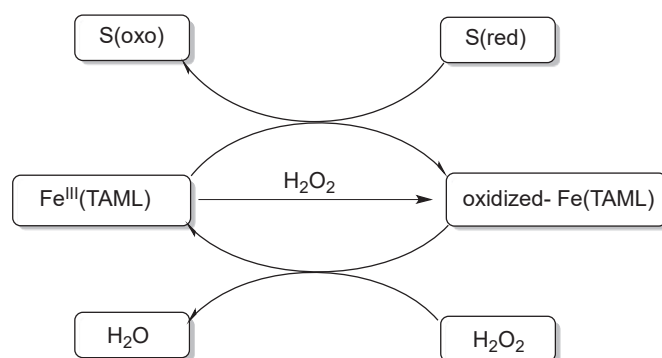


Figure 30. General mechanism of Fe(TAML) activating H_2O_2 .

As shown in **Figure 30**, the $\text{Fe}^{\text{III}}(\text{H}_2\text{O})^-$ species first loses a water molecule and

coordinates an oxygen from H_2O_2 molecule to form a $\text{Fe}^{\text{III}}(\text{H}_2\text{O}_2)^-$ species. Next, the coordinated oxygen loses H^+ to form a $\text{Fe}^{\text{III}}(\text{OOH})^{2-}$ intermediate, which then reacts with a H^+ to lose a water molecule, forming a $\text{Fe}^{\text{V}}(\text{O})^-$ at the same time. The $\text{Fe}^{\text{V}}(\text{O})^-$ reacts with $\text{Fe}^{\text{III}}(\text{TAML})^-$ by comproportionation to form μ -oxo dimer $[\text{Fe}^{\text{IV}}\text{OFe}^{\text{IV}}]$. The dimer turns to $[\text{Fe}^{\text{IV}}(\text{OH})_2]^{2-}$ when reacted with OH^- . Finally, the $[\text{Fe}^{\text{IV}}(\text{OH})_2]^{2-}$ species loses a water molecule, reduced to $[\text{Fe}^{\text{III}}(\text{H}_2\text{O})]^-$.

Generally, Fe^{III} in $\text{Fe}(\text{TAML})$ cannot oxidize substrates directly. However, in the presence of hydrogen peroxide or an organic peroxide, the metallo-complex is oxidized to high valent iron species such as $\text{Fe}^{\text{V}}(\text{O})$ or $\text{Fe}^{\text{IV}}(\text{O})$, which have powerful oxidation capacities. Next, the reactive species react with the substrate to produce the oxidized substrate, and the reduced Fe^{III} form at the same time, as shown in **Scheme 15**.¹¹⁶



Scheme 15. General mechanism of catalysis with $\text{Fe}(\text{TAML})$ and H_2O_2 .¹¹⁶

2.6.2 Homogeneous catalysis application with $\text{Fe}(\text{TAML})$

Organophosphorus(OP) triesters (**Figure 31, 33-35**) are widely used for crop protection, which may also cause cholinergic toxicity, delayed neuropathy and even endocrine disruption.¹¹⁷ Hence, finding ways to degrade OP pesticides is important. An ideal method should be efficient, inexpensive, technically flexible and nontoxic. The Collins group used $\text{Fe}(\text{TAML})$ complexes **20g** and **20d** (**Figure 31**), in order to activate H_2O_2 ,

for the degradation of fenitrothion **33** with complete conversion. At pH 10 (best conditions) and in the presence of 10% of *t*-BuOH in H₂O, fenitrothion is totally converted to the major product of 3-methyl-4-nitrophenol and minor fenitrooxon, while after 2h, the 95%-98% of the former product degrade to small aliphatic acids with hydrolysis of the later, as shown in **Scheme 16**.¹¹⁷ It is also used for other OP pesticides such as parathion and chlorpyrifos methyl, with maleic acid and chloromaleic acid, respectively. This method is promising for safe and environmentally friendly disposal of OP pesticides and their hydrolysis products.

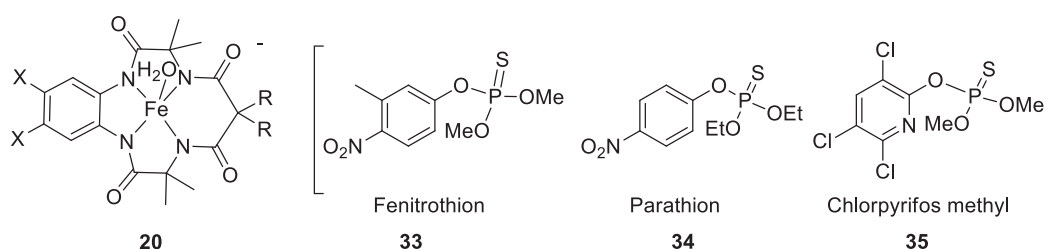
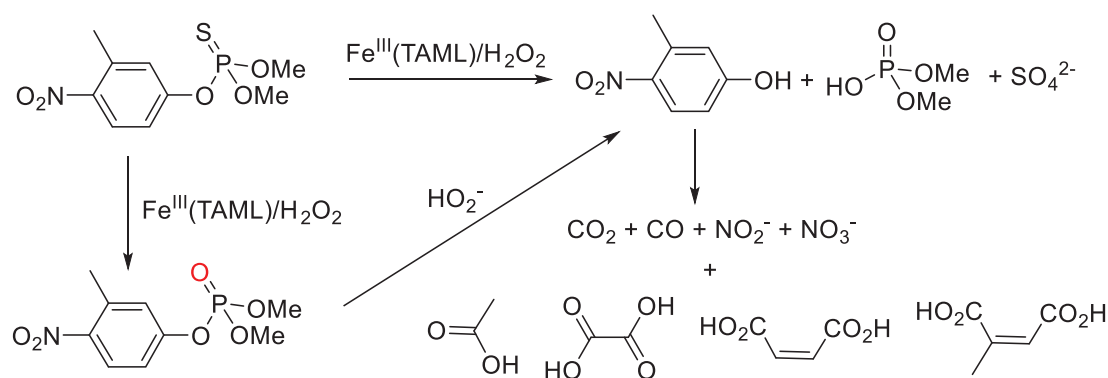


Figure 31. Structures of Fe(TAML) and organophosphorus triesters. **20**: **g**, X = H, R = F; **d**, X = Cl, R = F.



Scheme 16. Degradation of fenitrothion using **20g/20d** with H₂O₂.

It has been reported that the Fe(TAML)/ peroxide systems could rapidly deactivate bacteria spores with relatively nontoxic products.¹¹⁸ Fe(Cl₂-TAML-F₂) **20d** activating H₂O₂, or *tert*-butyl hydroperoxide at pH 10 in aqueous solution in the presence of CTAB

(cetyltrimethylammonium bromide), killed more than 99.9% of *Bacillus atrophaeus* bacteria in less than 1h (**Figure 32**), and similar results were also obtained with TBHP and CTAB at pH 8 within 5 h. This research provides a promising decontamination technology from biological pollution.

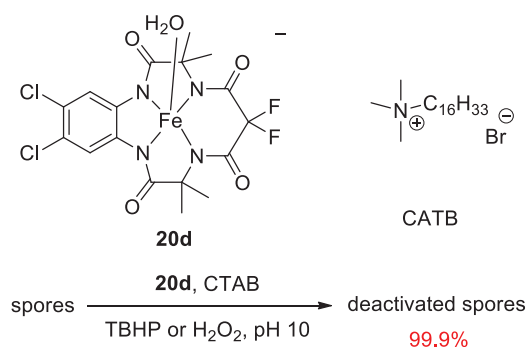


Figure 32. Structures of $[\text{Fe}(\text{Cl}_2\text{-TAML-F}_2)]$, CTAB and deactivation process of spores.

Water oxidation was also investigated with $\text{Fe}(\text{TAML})$ systems by the Collins' group.¹¹⁹ They reported that complexes **20a/d/f/g/j** (**Figure 33**) could activate ceric ammonium nitrate (CAN) at pH 7 to afford oxygen releasing from water. Among those, **20d** displayed the highest reactivity, with a large TOF (turnover frequency, $\text{TOF} = \text{reaction time}/\text{TON}$, $\text{TON} = \text{moles of product}/\text{moles of catalyst}$) of 1.3 s^{-1} , and also can release oxygen for hours, which is competitive with the previous reported iridium catalysts.¹¹¹

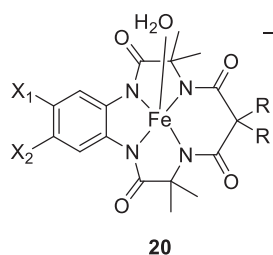


Figure 33. **20a**, $X_1 = X_2 = \text{H}$, $R = \text{CH}_3$; **20j**, $X_1 = X_2 = \text{H}$, $R = \text{CH}_2\text{CH}_2$; **20g**, $X_1 = X_2 = \text{H}$, $R = \text{F}$; **20f**, $X_1 = \text{NO}_2$, $X_2 = \text{H}$, $R = \text{F}$; **20d**, $X_1 = X_2 = \text{Cl}$, $R = \text{F}$.

The Collins' group also reported that $\text{Fe}^{\text{III}}(\text{TAML})$ systems could activate H_2O_2 for bleaching dyes like orange II, pinacyanol chloride, and safranin-O (**Figure 34**) to nontoxic products.^{91,116,120,121} H_2O_2 can be used for decolorization, but is not as efficient as with $\text{Fe}(\text{TAML})$ catalyst. The **20a**/ H_2O_2 system is pH-dependent and at pH 11, the efficiency is the highest. Conversely, **20g**/ H_2O_2 is pH-independent and showed the same high activity at pH 9-11. Kinetic study of **20**/peroxide with orange II also highlighted the reactivity of different kinds of peroxide in the series benzoyl peroxide > hydrogen peroxide > *t*-BuOH > cumyl hydroperoxide.

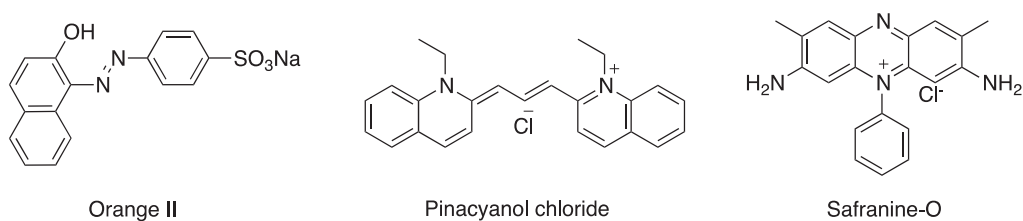


Figure 34. Structures of the three dyes evaluated with **20** H_2O_2 .

In 2011, Collins *et al.* applied **20a**/ H_2O_2 to decompose completely concentrated azo dye tartrazine (**Figure 35**), which was hard to oxidize by only H_2O_2 .¹²² With this method, only very low concentration (7.5×10^{-5} M) of catalyst is needed for concentrated tartrazine (3.09×10^{-2} M), with the major biodegraded products, such as 4-phenolsulfonic acid (4-PSA), formic acid, maleic acid and so on as biodegradable products, which shows a promising commercial application.

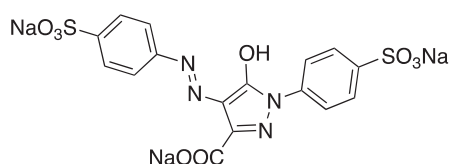


Figure 35. Structure of tartrazine.

Chlorophenols such as pentachlorophenol (PCP) 2,4,6-trichlorophenol (TCP) are priority pollutants for the environment. It was found that the $\text{Fe}^{\text{III}}(\text{TAML})/\text{H}_2\text{O}_2$ system could rapidly biodegrade completely microscale of both PCP and TCP with substantial mineralization under ambient conditions in water.¹²³ $\text{Fe}(\text{TAML})$ complexes, **20c** and **21a** (**Figure 36**) work at high pH (pH 10 buffer, 0.1 M NaHCO_3 , 0.1 M Na_2CO_3) could degrade PCP and TCP with a catalyst/ratio substrate 1: 715 and 1: 2000, respectively, within 9 min. At neutral condition, **20g** (**Figure 36**) is the most reactive catalyst among the three, and it can degrade chloromaleic acid completely (more than 99%) within 12 hours under ambient conditions (pH 7, $\text{KH}_2\text{PO}_4/\text{KHPO}_4$ buffer), whereas **20c** and **21a** could also work under these conditions, with 65% of the degradation. Products were detected by HPLC and NMR and mineralization was quantified by TOC (total organic carbon: it is the amount of carbon found in organic compound). Nontoxic products were detected, with only organic acids and CO_2 , CO , and HCl as final products (**Figure 37**). $\text{Fe}^{\text{III}}(\text{TAML})/\text{H}_2\text{O}_2$ system is far more efficient than biological and other chemical systems reported so-far, provided a promising technology for scale-up applications.

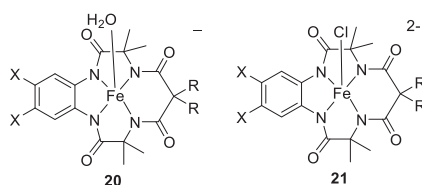


Figure 36. The structures of $\text{Fe}(\text{TAML})$. **20c**: $\text{X} = \text{Cl}$, $\text{Y} = \text{H}_2\text{O}$, $\text{R} = \text{CH}_3$; **21a**: $\text{X} = \text{H}$, $\text{Y} = \text{Cl}$, $\text{R} = \text{CH}_3$; **20g**: $\text{X} = \text{H}$, $\text{Y} = \text{H}_2\text{O}$, $\text{R} = \text{F}$.

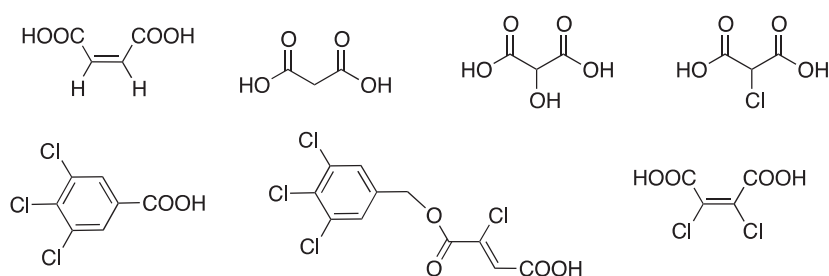


Figure 37. Products detected after degradation of TCP and PCP.

Our group also carried research on the catalytic oxidation with $\text{Fe}^{\text{III}}(\text{TAML})$.^{61,78} First, the catalytic oxidation of alcohols and lignin model compounds with **20a** and (diacetoxyiodo)-benzene (DAIB) as the oxidant was investigated in acetone at 25 °C. It was found that there is a good selectivity for the oxidation of primary alcohol to the corresponding aldehyde or acid depending on the amount of water present in the reaction medium. Besides, the **20a**/DAIB system displayed a good ability for cleaving linkages in lignin model compounds (**Figure 38**). In addition, the oxidation of benzylic C-H bond with $\text{Fe}^{\text{III}}(\text{TAML})$ (**20a**) was also investigated. The authors found that 4-ethylanisole reacted with **20a**/TBHP in acetone and water (buffer: KCl/NaOH, pH 12) at -10 °C, with 96% of conversion affording 4-methoxyacetophenone in 94% yield of in 3 h. A series of benzylic compounds was also tested and most of them were converted with high yield and/or selectivity.

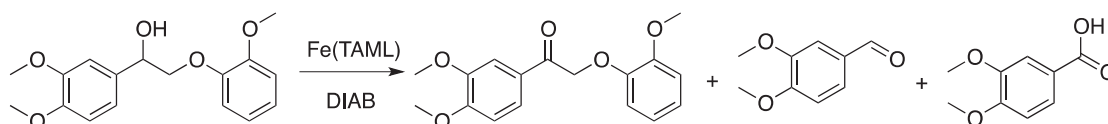
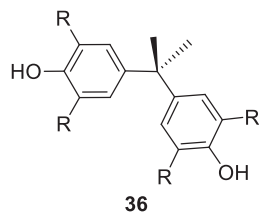


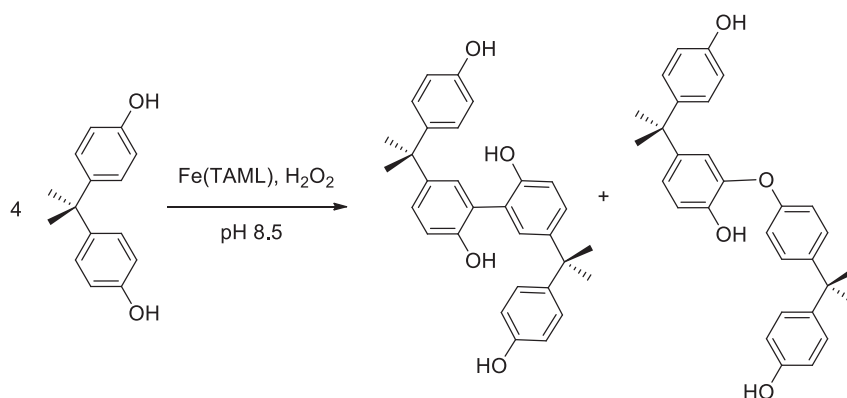
Figure 38. Lignin model compound and corresponding products.

Bisphenol A (2,2-bis(4-hydroxyphenyl)propane, BPA) **36a** in **Figure 39** is considered toxic for human reproduction. In addition, a low concentration of phenolic compounds results in the contamination of eluent streams due to incomplete removal by physical, chemical and biological processes. Collins *et al.* reported that $\text{Fe}(\text{TAML})$ (**20a**) and H_2O_2 can converted bisphenol A to controllable oxidative oligomers at pH 8.5 (**Scheme 17**).¹²⁴ While at pH 11, the catalytic system could also oxidize **36a** (**Figure 39**) to mainly CO_2 , CO with acetone and formic acid (**Scheme 18**). The process was proven very efficient.¹²⁴

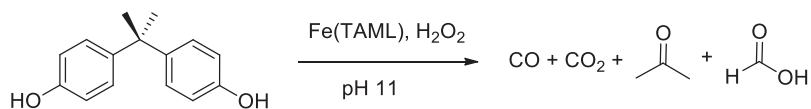


R= H (**36a**); CH₃ (**36b**); Cl (**36c**); Br (**36d**).

Figure 39. Structures of bisphenol A and its derivatives.¹²⁴



Scheme 17. Conversion of bisphenol A at pH 8.5.



Scheme 18. Conversion of bisphenol A at pH 11.

2.6.3 Heterogeneous catalysis applications with Fe(TAML)

Until now, most of the research on Fe^{III}(TAML) were carried out in homogenous media.

Only a few of them dealt with heterogeneous catalysis. In the later cases, Fe^{III}(TAML) catalysts were grafted on different kinds of supports.

Hence, the first and the second generations of Fe^{III}(TAML) were supported on activated charcoal in the Collins' group for the degradation of the orange II dye.¹²⁵ Using this strategy, the catalysts retain the performance they displayed in homogeneous media, but were much more resistant than the homogeneous one. The stability of the catalysts was also evaluated in a phosphate buffer and very little demetallation of the catalyst was observed. The carbon supported oxidation system was applied for treatment of low level waste water stream.¹²⁵

Kumari, S. *et al.* developed a method to use Fe^{III}(TAML) supported on mesoporous silica nanoparticles (MSN) to make peroxidase mimic for femtomolar protein detection.^{126,127} Fe(TAML) was developed to mimic peroxidase enzyme horseradish peroxidase (HRP), combined with antibodies, and used for protein detection.¹²⁶ They used the 5th generation of TAMLs, the modified [Fe^{III}(biuret-amide)] **37**, according to the structure shown in **Figure 40**. The strategy for synthesizing a heterogeneous catalyst, modified [Fe^{III}(biuret-amide)]- MSN, is as following: first, synthesis of the functionalized azido MSN particles (N₃-MSN); next, grafting of the amino propyl group on the MSN support followed by attachment of the modified [Fe^{III}(biuret-amide)] to N₃-MSN by Cu(I) catalyzed azide-alkyne click chemistry, which was already presented in the **Scheme 19**.¹²⁷ With this method, around 25000 alkyne-tagged modified [Fe^{III}(biuret-amide)] were attached inside a 40 nm MSN support. This catalyst was the best small molecule mimic of the HRP enzyme. In addition, it displayed reaction rates similar to the natural enzyme, but with a much better operational stability. The catalytic activity of this material was almost 1000 times that of the natural HRP enzyme.

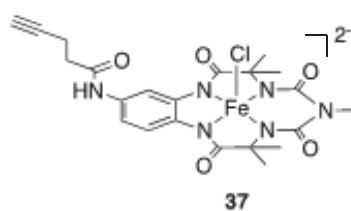
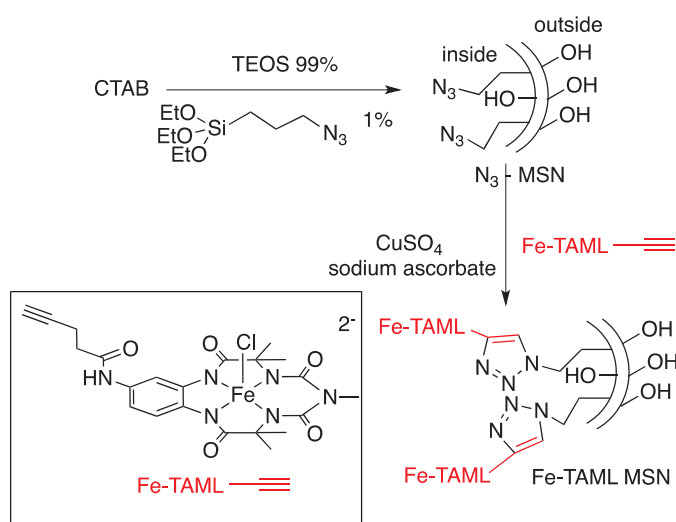


Figure 40. The structure of modified $[\text{Fe}^{\text{III}}(\text{biuret-amide})]$.¹²⁶



Scheme 19. Strategy for the synthesis of modified $[\text{Fe}^{\text{III}}(\text{TAML})]$ -MSN.¹⁹

The $\text{Fe}(\text{TAML})$ -mediated catalytic oxidation of water for oxygen release has been investigated in homogeneous media as discussed above. The Kitchin's group also carried out research on water oxidation with TAML in heterogeneous electrochemistry.¹²⁸ Indeed, **20a** was used as the homogeneous catalyst for water oxidation, but it turned out to be inactive. However, after supporting **20a** on an electrode as an electrocatalyst, it turned out to be effective for oxygen evolution reaction (OER). The control experiment with $\text{FeCl}(\text{OEP})$ ($\text{OEP} = 2,3,7,8,12,13,17,18$ -octaethyl-21H, 23H-porphine) on the support did not release any oxygen. This result evidenced that **20a** was an active electrocatalyst for OER.

The Fe(TAML) complex was also stabilized on pyrolytic graphite (PG) electrode, which could still retain its native electrochemistry property with nearly reversible for a redox couple.¹²⁹ The iron complex exhibited a good electrocatalytic behavior for the decomposition of hydrogen peroxide, which can be used as the potential hydrogen peroxide sensor.

Iron is a common and useful metal in chemical and biological catalysis, while manganese shares the realm of catalytic oxidation with iron in nature. Manganese also plays an important role in industry and biology. It has an indispensable position in catalytic chemistry.

3 State of the art on Mn(Me₂EBC)Cl₂

3.1 Introduction on cyclam

Manganese plays an important role in nature. It dominates with iron and copper over the area of redox catalysis in nature, biomimicry and catalysis.⁸¹ Manganese-based oxidation exists in the active site of natural enzyme systems, such as superoxide dismutase,^{130,131} catalase,¹³² oxygen evolving complex (OEC) in Photosystem II^{133,134} and lipoxygenase.¹⁰ It takes part in many redox species as it reaches high valent states like Mn^{IV} and Mn^V . Accordingly, it is of prime interest to exploit and understand the functions and behaviors of manganese complexes. For a better investigation of the manganese complexes in biomimicry and homogeneous catalysis, many ligands and their corresponding manganese complexes have been synthesized, as mentioned before.

Manganese-based catalytic systems have been the most developed for the asymmetric epoxidation of olefins. In 1992, Mukaiyama *et al.* described the manganese(III) salen complexes (**Figure 41**) for epoxidation of conjugated olefins with molecular oxygen and pivalaldehyde with moderate to good enantioselectivities (43-77% ee) (**Figure 41**).¹³⁵ The proposed mechanism involved the oxidation of aldehyde to the corresponding peroxycarboxylic acid, which was further reacted with manganese catalyst to form the active species.

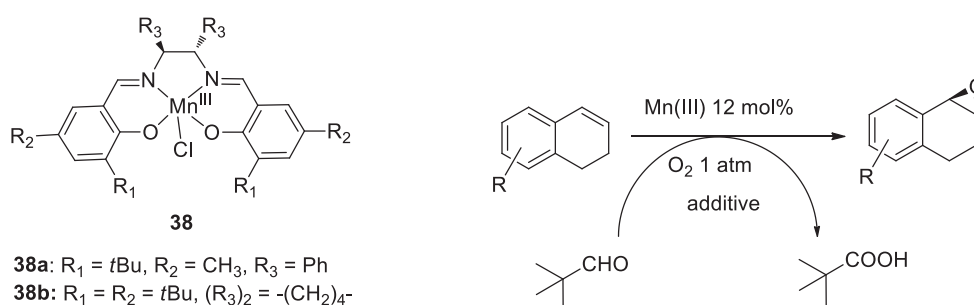


Figure 41. Mukaiyama's catalytic system for the epoxidation of olefins.

Manganese salen complexes have been very popular since then, and have been proven

powerful catalysts for epoxidations. Modifications of the salen ligand have been developed progressively, focusing on the R₁ – R₃ parts (**Figure 41**).¹³⁶

Except for salen ligands, manganese has been used to coordinate to many other ligands, such as C₃-symmetric chiral triazacyclononane-derived chiral ligands by Bolm *et al.* (**Figure 42, 39**),¹²⁵ L-proline-derived triazacyclononane (**Figure 42, 40**),¹²⁹ the aminopyridine family (**Figure 42, 41**)¹¹⁴ and so on. The development of ligands is always a significant issue in developing new and better catalysts. With the large realm of possibilities and within the frame of this PhD work, we have focused on cyclam Mn complexes.

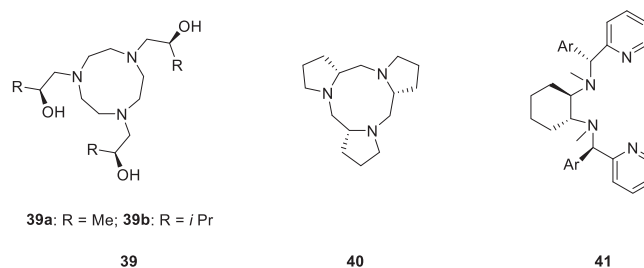


Figure 42. Examples of structures of ligands able to bind manganese.

The cyclam (1,4,8,11-tetraazacyclotetradecane) macrocyclic ligand is a 14-membered tetraamine macrocycle **42** (**Figure 43**). It is one of the polycyclic polyamines which shows a large coordination capacity.¹³⁷ Various modifications on the cyclam macrocycle have been done (**Figure 43. 13, 43-48**),^{80,81,103,138} including bridging of nonadjacent nitrogens (**Figure 43. 13, 44, 48**), addition of pendant arms (**Figure 43. 45, 47**), introducing a pyridine (**Figure 43. 46-47**).

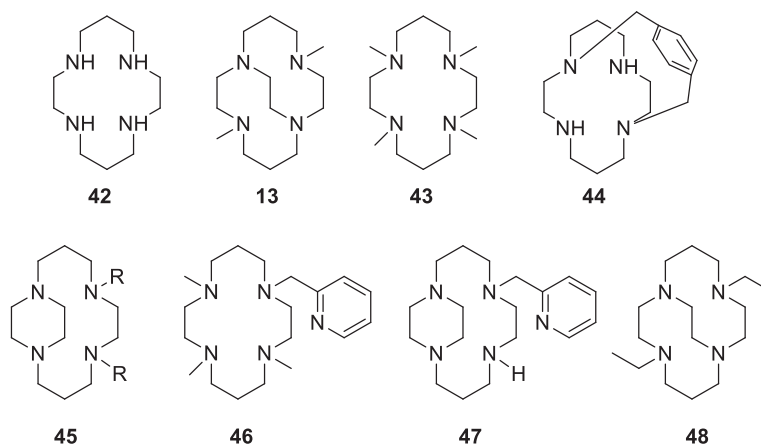


Figure 43. Structures of cyclam and derivatives.

Among all the modifications that have been operated on the cyclam ligand, the structure of the rigid two-carbon cross-bridged tetraazamacrocycle (**Figure 44**) attracted our attention.¹³⁹ Indeed, the additional bridge provides rigidity, configuration and kinetic stability to the complexes.⁸⁰ The modification is on the size of the macrocycle and the nature of the R group. When $n = m = 1$, $R = \text{CH}_3$, we have a cross-bridged cyclam **13** (**Figure 44**), while when $n = m = 0$, we have a cross-bridged cyclen **50** (**Figure 44**). The ligands corresponding to the 12- and 14-membered rings have been used for the synthesis of complexes with a lot of metal cations such as Mn^{II} , Mn^{III} , Fe^{III} , Fe^{II} , Co^{II} , Cu^{II} , Cu^{I} and Zn^{II} .¹³⁹ Cross-bridged cyclen has a smaller internal cavity than the corresponding cross-bridged cyclam. Accordingly, the corresponding complexes are scarce.

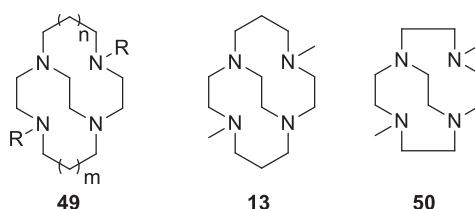
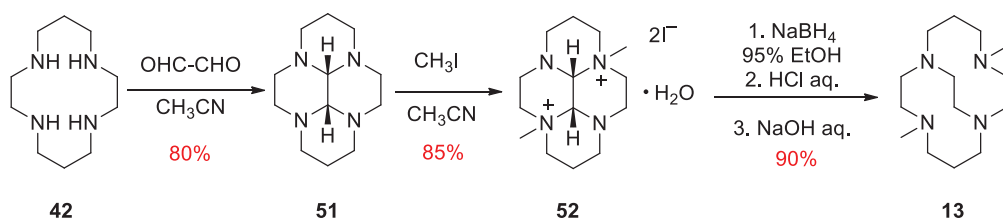


Figure 44. Structures of two-carbon cross-bridged ligands. $m = 0-1$, $n = 0-1$, $R = \text{H}$, Me or Bn.

In this PhD manuscript, we will introduce the cross-bridged cyclam ligand **13**, the first example of cross-bridged ligand (4,11-dimethyl-1,4,7,11-tetraazabicyclo[6.6.2]hexadecane), which is also called Me₂EBC. Me₂EBC contains an ultra-rigid ethylene cross-bridged with two nonadjacent nitrogen atoms from the ligand cyclam.^{81,140} In addition, the ligand has flexible bicycles, which can adopt different conformations with respect with the four nitrogen lone pairs on the cavity for metal complexation. The synthesis protocol is shown in **Scheme 20**.^{81,140} This ligand strongly binds with divalent transition metal ions, such as Mn^{II}, Fe^{II}, Ni^{II}, Cu^{II}.¹⁴¹ Herein, we will focus on Mn^{II}.



Scheme 20. Synthetic access to a cross-bridged cyclam.⁸¹

3.2 Introduction on [Mn^{II}(Me₂EBC)Cl₂]

3.2.1 Structure and the synthesis of [Mn^{II}(Me₂EBC)Cl₂]

The cross-bridged manganese complex [Mn^{II}(Me₂EBC)Cl₂] **14** (**Figure 45**) presents a distorted octahedral structure, where the macrobicyclic ligand occupies two axial nitrogen atoms and two *cis* equatorial ones with another two chloride ligands standing at the remaining *cis* equatorial positions. The manganese(II) coordinates with four nitrogen atoms and two chloride ions. The short cross bridge forces the cyclam ligand to fold. Cyclam **42** coordinates Mn^{II} with the four equatorial nitrogen atoms in a square planar of an octahedral, leaving the two labile sites at the *trans* axial sites,¹⁴² which is quite different from the structure of the cross-bridged cyclam coordinated metal complexes.

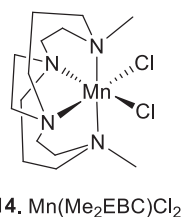
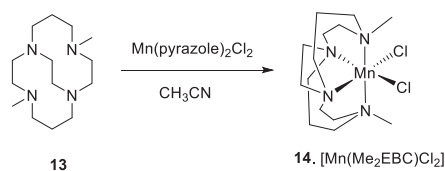


Figure 45. Scheme of manganese complex with a cross-bridged cyclam ligand.

The deprotonated cross-bridged cyclam has a proton-sponge nature, with $pK_{a1} = 9.58$ indicating that at least one nitrogen is protonated, and only the strongest binding metals can compete for the cavity.⁸¹ It has been reported that Cu^{II} and Ni^{II} form the more stable metallo-complexes among the first row of divalent metals. Fe^{II} and Mn^{II} are the strongest competitors for the proton. Therefore, during the synthesis of [Mn(Me₂EBC)Cl₂] complex, a totally dry and inert atmosphere is needed to avoid any trace of protons. The synthetic protocol is described in **Scheme 21**.^{81,143}



Scheme 21. Synthesis of [Mn(Me₂EBC)Cl₂].^{81,143}

3.2.2 Properties of [Mn^{II}(Me₂EBC)Cl₂]

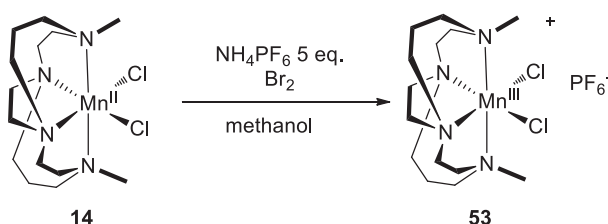
The [Mn^{II}(Me₂EBC)Cl₂] complex does not display any UV-Vis characteristic absorbance but the EPR data revealed a signature with a regular six-line spectrum for the complex as other manganese(II) complex in ethanol at 77 K.⁸¹ When treating [Mn^{II}(Me₂EBC)Cl₂] with a weak monoprotic acid, both chlorides are replaced by water molecules with only one pK_a found (10.87).⁸¹ It is quite similar to [Mn(H₂O)₆]²⁺ (10.9),¹⁴⁴ indicating that the ligand does not influence the ability of Mn^{II} to polarize

water molecule. Electrochemical studies showed that, the manganese complex has two reversible redox couples that are $\text{Mn}^{\text{II}}/\text{Mn}^{\text{III}}$ at 0.585 V (*vs* SHE) and $\text{Mn}^{\text{III}}/\text{Mn}^{\text{IV}}$ at 1.343 V (*vs* SHE).

At last, there is an important property of the manganese complex: the highest oxidation state of Mn in $[\text{Mn}^{\text{II}}(\text{Me}_2\text{EBC})\text{Cl}_2]$ is +4, unlike the manganese catalysts with porphyrin ligands Mn^{III} ,^{145,146} indicating that the complex is a very moderate oxidizing catalyst. In addition, it can tolerate harsh aqueous conditions without decomposition or dimerization.¹⁴⁷

3.3 Introduction on Mn^{III} complexes with Me_2EBC

There are several Mn^{III} complexes synthesized with Me_2EBC with different anions reported.¹⁴⁸ $[\text{Mn}^{\text{III}}(\text{Me}_2\text{EBC})\text{Cl}_2]\text{PF}_6$ **53** was the first complex to be synthesized by oxidizing the corresponding $\text{Mn}^{\text{II}}(\text{Me}_2\text{EBC})\text{Cl}_2$ with Br_2 in the presence of an excess of NH_4PF_6 in methanol under nitrogen (**Scheme 22**). $[\text{Mn}^{\text{III}}(\text{Me}_2\text{EBC})(\text{N}_3)_2]\text{PF}_6$, $[\text{Mn}^{\text{III}}(\text{Me}_2\text{EBC})(\text{OH})(\text{OAc})]\text{PF}_6$, and $[\text{Mn}^{\text{III}}(\text{Me}_2\text{EBC})(\text{OMe})_2]\text{PF}_6$ were also synthesized by ligands substitution from $[\text{Mn}^{\text{III}}(\text{Me}_2\text{EBC})\text{Cl}_2]\text{PF}_6$.¹⁴⁸ These manganese(III) complexes have been characterized by X-ray crystal structure, cyclic voltammetry and magnetic measurements.¹⁴⁸



Scheme 22. Synthesis of manganese(III) complex $[\text{Mn}^{\text{III}}(\text{Me}_2\text{EBC})\text{Cl}_2]^+\text{PF}_6^-$.

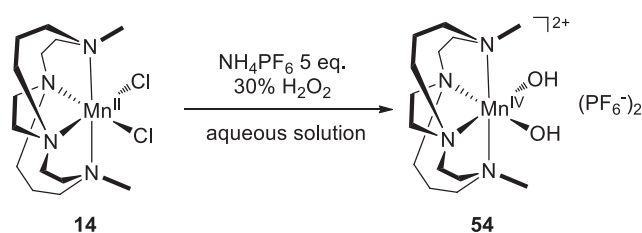
From the crystal structure, the $[\text{Mn}^{\text{III}}(\text{Me}_2\text{EBC})]^{3+}$ complex presents a distorted octahedral geometry, with the metal in the center and the cross-bridged cyclam

occupying two *cis* equatorial and two axial sites, similar to the structure obtained with a manganese(II) complex. The electronic structure indicates that the manganese(III) complexes are high spin d^4 and their X-band EPR spectra are silent for the complexes, as expected for high spin $S = 2$ system. The UV-Vis spectrum of $[\text{Mn}^{\text{III}}(\text{Me}_2\text{EBC})\text{Cl}_2]\text{PF}_6$ displays several charge transfer bands, . Titration measurements for the determination of the acidity of the bound water in aqueous solution indicated that the complex can bind up to two water molecules, with respective dissociation constants: $\text{pK}_{\text{a}1} = 1.6(2)$ and $\text{pK}_{\text{a}2} = 5.87(2)$. The cyclic voltammogram for $[\text{Mn}^{\text{III}}(\text{Me}_2\text{EBC})\text{Cl}_2]\text{PF}_6$ showed that there are two couples of redox potential: $E_{1/2}$ for $\text{Mn}^{\text{III}}/\text{Mn}^{\text{II}}$ and $\text{Mn}^{\text{IV}}/\text{Mn}^{\text{III}}$ 0.582 V and 1.343 V, respectively.

3.4 The corresponding manganese(IV) complexes

3.4.1 Structure and synthesis of $[\text{Mn}^{\text{IV}}(\text{Me}_2\text{EBC})(\text{OH})_2](\text{PF}_6)_2$

The highest oxidation state of Mn in Mn(Me₂EBC) complex is the corresponding $[\text{Mn}^{\text{IV}}(\text{Me}_2\text{EBC})(\text{OH})_2]^{2+}$. It is synthesized by oxidation of $[\text{Mn}^{\text{II}}(\text{Me}_2\text{EBC})\text{Cl}_2]$ complex in aqueous solution with hydrogen peroxide in the presence of NH_4PF_6 (Scheme 23). A pure purple $[\text{Mn}^{\text{IV}}(\text{Me}_2\text{EBC})(\text{OH})_2](\text{PF}_6)_2$ compound **54** was obtained and isolated. It was the first monomeric manganese(IV) complex with two hydroxide ligands.¹⁴⁷



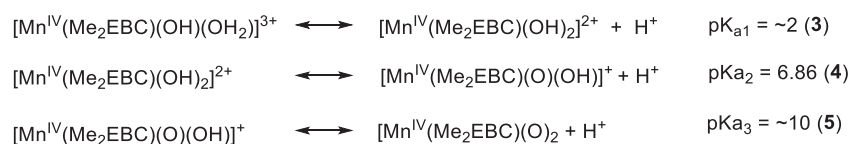
Scheme 23. Synthesis of a manganese(IV) complex.¹⁴⁷

The manganese(IV) complex is a six coordinated complex in the solid state: two axial

nitrogen, two *cis* equatorial nitrogen and two *cis* equatorial hydroxyl are evidenced by the crystal structure. The two methyl groups on the nonbridged nitrogen atoms prevent the complex to dimerize or oligomerize from deprotonation of the $[\text{Mn}^{\text{IV}}(\text{OH})_2]^{2+}$ unit.¹⁴⁹

3.4.2 Properties of $[\text{Mn}^{\text{IV}}(\text{Me}_2\text{EBC})(\text{OH})_2](\text{PF}_6)_2$

From potentiometric titrations, the first proton dissociation constant affording $[\text{Mn}^{\text{IV}}(\text{Me}_2\text{EBC})(\text{O})(\text{OH})]^+$ from $[\text{Mn}^{\text{IV}}(\text{Me}_2\text{EBC})(\text{OH})_2]^{2+}$ was calculated at pK_a 6.86.¹⁵⁰ The other two pK_a are ~ 2 and 10.0. The former values corresponded to the addition of one proton to generate $[\text{Mn}^{\text{IV}}(\text{Me}_2\text{EBC})(\text{OH})(\text{OH}_2)]^{3+}$ and the latter the removal of one proton to form $[\text{Mn}^{\text{IV}}(\text{Me}_2\text{EBC})(\text{O})_2]$. The latter corresponded not only to the second proton deprotonation, but also to the dimerization of the complex. As Mn^{IV} is not stable in basic media, it contributes to the results from high pH not understand. The deprotonation process proceeds as indicated below (**Equations 3 to 5**).¹⁴⁷



Equations 3-5. Deprotonation process of $[\text{Mn}^{\text{IV}}(\text{Me}_2\text{EBC})(\text{OH})(\text{OH}_2)]^{3+}$.¹⁴⁷

The manganese(IV) complex presents two broad resonances in the EPR spectrum of g_{eff} values, 1.96 and 3.41.¹⁴⁷ From the cyclic voltammogram, the complex has three reversible redox couples, which are $\text{Mn}^{\text{V}}/\text{Mn}^{\text{IV}}$, $\text{Mn}^{\text{IV}}/\text{Mn}^{\text{III}}$ and $\text{Mn}^{\text{III}}/\text{Mn}^{\text{II}}$ with potentials of 1.013, 0.756 and -0.696 V (*vs* SHE), respectively.¹⁴⁷ The redox couple of $\text{Mn}^{\text{V}}/\text{Mn}^{\text{IV}}$ has a small amplitude, compared with the other two, which suggested that the manganese(V) species was possibly produced during the electrochemical process. The redox potential of $\text{Mn}^{\text{IV}}/\text{Mn}^{\text{III}}$ also suggested that the manganese(IV) is a mild

oxidant.

The manganese(IV) complex $[\text{Mn}^{\text{IV}}(\text{Me}_2\text{EBC})(\text{OH})_2]^{2+}$ has a limited stability of a few days in the solid state at room temperature. Indeed, the purple solid becomes orange after the solid is exposed in air for a few days. The color change corresponds to the transformation of the manganese(IV) to the manganese(III) complex by disproportionation. In aqueous solution, the complex remains still for a few days in weak acidic and neutral solution, but is unstable in basic media.¹⁵¹ At a pH below 2, it turns to manganese(III) compound, while at very low pH, the complex decomposes affording the free ligand and a divalent manganese compound, with no ligand damage.¹⁴⁷ In basic media, the manganese(IV) complex decomposes irreversibly to $[\text{Mn}^{\text{III}}(\text{Me}_2\text{EBC})(\text{OH})_2]^+$ in 88% yield, with a little quantity of ligand destruction.¹⁴⁷ It is also reported that Mn(III) could disproportionate to Mn(II) and Mn(IV) in acidic media, while in basic media, the reaction reversed (**Equation 6**).¹⁴⁷



Equation 6. Disproportionation of Mn^{III} .

3.4.3 The different existing forms of the manganese(IV) complex

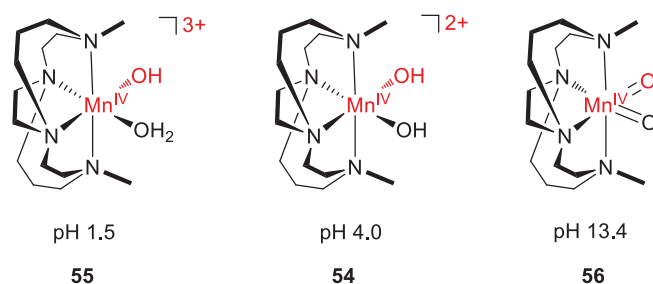


Figure 46. Three different protonation states of manganese(IV) moieties at different pH.

The manganese(IV) complex presents four different dominant species in an aqueous solution depending on the pH. Three dissociation constants, pK_{a1} , pK_{a2} and pK_{a3} are 2, 6.86 and 10, respectively. Therefore, $[\text{Mn}^{\text{IV}}(\text{Me}_2\text{EBC})(\text{OH})(\text{OH}_2)]^{3+}$ having one $[\text{Mn}^{\text{IV}}-\text{OH}]$ functional group dominates at pH 1.5, $[\text{Mn}^{\text{IV}}(\text{Me}_2\text{EBC})(\text{OH})_2]^{2+}$ having two $[\text{Mn}^{\text{IV}}-\text{OH}]$ functional groups dominates at pH 4.0 and $[\text{Mn}^{\text{IV}}(\text{Me}_2\text{EBC})(\text{O})_2]$ having two $[\text{Mn}^{\text{IV}}=\text{O}]$ functional group dominates at 13.4 (**Figure 46**).¹⁵² $[\text{Mn}^{\text{IV}}-\text{OH}]$ in $[\text{Mn}^{\text{IV}}(\text{Me}_2\text{EBC})(\text{OH})(\text{OH}_2)]^{3+}$ and $[\text{Mn}^{\text{IV}}(\text{Me}_2\text{EBC})(\text{OH})_2]^{2+}$ and $[\text{Mn}^{\text{IV}}=\text{O}]$ in $[\text{Mn}^{\text{IV}}(\text{Me}_2\text{EBC})(\text{O})_2]$ show different physicochemical properties and reactivity, listed in **Table 4**.¹⁵⁰

Table 4. The physicochemical properties and oxidative activity of the three species of manganese(IV) complex.¹⁵⁰

Mn ^{IV} moiety	$[\text{LMn}^{\text{IV}}-\text{OH}]^{3+}$	$[\text{LMn}^{\text{IV}}-\text{OH}]^{2+}$	$[\text{LMn}^{\text{IV}}=\text{O}]$
Net charge	3+	2+	0
$E_{1/2}$ (V) ($\text{Mn}^{\text{IV}}/\text{Mn}^{\text{III}}$) vs SCE	+0.54	+0.46	+0.10
$\text{BDE}_{\text{O-H}}$ kcal/mol	77.8	81.9	
Electron transfer rate	$[\text{LMn}^{\text{IV}}-\text{OH}]^{3+} > [\text{LMn}^{\text{IV}}-\text{OH}]^{2+} \gg [\text{LMn}^{\text{IV}}=\text{O}]$		
Hydrogen abstraction rate	$[\text{LMn}^{\text{IV}}-\text{OH}]^{3+} \approx [\text{LMn}^{\text{IV}}-\text{OH}]^{2+} \ll [\text{LMn}^{\text{IV}}=\text{O}]$		

As presented in **Table 4**, the three species $[\text{Mn}^{\text{IV}}(\text{Me}_2\text{EBC})(\text{OH})(\text{OH}_2)]^{3+}$, $[\text{Mn}^{\text{IV}}(\text{Me}_2\text{EBC})(\text{OH})_2]^{2+}$ and $[\text{Mn}^{\text{IV}}(\text{Me}_2\text{EBC})(\text{O})_2]$ obviously have different net charge, +3, +2 and 0. $[\text{LMn}^{\text{IV}}-(\text{OH})(\text{OH}_2)]^{3+}$ and $[\text{LMn}^{\text{IV}}-(\text{OH})_2]^{2+}$ species both have an equatorial group $-\text{OH}$. The other equatorial functional group are H_2O and OH , perpendicular to the $[\text{Mn}^{\text{IV}}-\text{OH}]$ group. However, they have the same axial ligand and ligand, which impact the reactivity of the metal center.¹⁵³ Thus, their different reactivity will be only influenced by the net charge. It evidences the fact that the net charge promotes the reaction.

The $[\text{Mn}^{\text{IV}}\text{-OH}]$ moiety has the ability to induce an electron-transfer reaction while the $[\text{Mn}^{\text{IV}}\text{=O}]$ moiety does not. This is confirmed with the oxidation of 2,2'-azino-bis(3-ethylbenzothiazoline-6-sulphonic acid) (ABTS), a reactively facile electron transfer agent.¹⁵⁴ The UV-Vis analysis of the oxidation reaction showed that the UV-Vis spectra of ABTS changed after adding $\text{Mn}^{\text{IV}}\text{-OH}$ at pH 4.0, while it didn't change after adding $[\text{Mn}^{\text{IV}}\text{=O}]$ at pH 13.4 (**Figure 47**).¹⁵² It is also suggested that the capability of electron-transfer is also related to the net charge of the moieties.^{150,152}

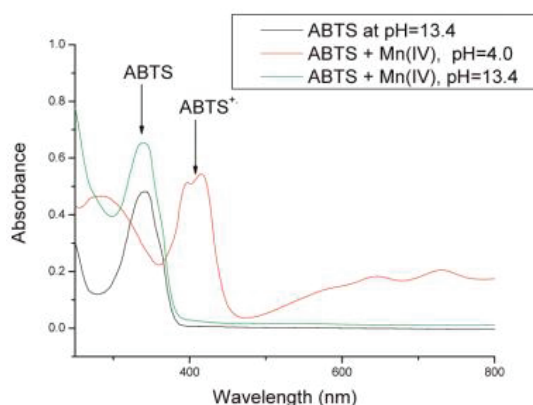


Figure 47. The UV-Vis spectra of the reaction of ABTS by $\text{Mn}^{\text{IV}}\text{-OH}$ at pH 4.0 and $\text{Mn}^{\text{IV}}\text{=O}$ at pH 13.4.

Besides, the redox potentials of the $\text{Mn}^{\text{IV}}/\text{Mn}^{\text{III}}$ couple at pH 1.5, 4.0 and 13.4 are totally different: +0.54, +0.46 and +0.10 V(vs SCE). A large difference of 360 mV between $[\text{Mn}^{\text{IV}}(\text{OH})_2]$ and $[\text{Mn}^{\text{IV}}(\text{O})_2]$ would predict a large difference in electron transfer capacity, which is consistent with the results from hydrogen abstraction from ABTS.

The two species, $[\text{Mn}^{\text{IV}}\text{-OH}]$ in $[\text{Mn}^{\text{IV}}(\text{Me}_2\text{EBC})(\text{OH})_2]^{2+}$ and $[\text{Mn}^{\text{IV}}\text{=O}]$ in $[\text{Mn}^{\text{IV}}(\text{Me}_2\text{EBC})(\text{O})_2]$ have similar hydrogen abstraction ability, which is estimated by the bond dissociation energy (BDE) of O-H. The BDE_{OH} is calculated by Bordwell/Mayer analysis.¹⁵⁵⁻¹⁵⁷ The independent thermodynamic evaluations of the BDE_{OH} for the corresponding reduced species $[\text{Mn}^{\text{III}}\text{-OH}]$ and $[\text{Mn}^{\text{III}}\text{-OH}_2]$ indicate that

the two species $[\text{Mn}^{\text{IV}}=\text{O}]$ and $[\text{Mn}^{\text{IV}}-\text{OH}]$ have similar BDE_{OH} values (BDE_{OH} : 83 vs 84 kcal/mol).¹⁵⁸ It indicates that they have similar ability for hydrogen abstraction. However, they have different reaction rate. The second-order rate constants of $[\text{Mn}^{\text{IV}}-\text{OH}]$ and $[\text{Mn}^{\text{IV}}=\text{O}]$ are 3.53×10^{-4} and $0.01496 \text{ M}^{-1}\text{s}^{-1}$ in hydrogen abstraction from 9,10-dihydroanthracene.¹⁴⁹ Hence the reaction rate for hydrogen abstraction is more than 40-times higher for $[\text{Mn}^{\text{IV}}=\text{O}]$ compared to $[\text{Mn}^{\text{IV}}-\text{OH}]$.

The product distributions can be different after hydrogen abstraction with $[\text{Mn}^{\text{IV}}-\text{OH}]$ and $[\text{Mn}^{\text{IV}}=\text{O}]$. For some substrates, it is proposed that different pathways after hydrogen abstraction by different manganese(IV) species $[\text{Mn}^{\text{IV}}-\text{OH}]$ and $[\text{Mn}^{\text{IV}}=\text{O}]$ occur for the first step: oxygenation and desaturation, for example, in the hydrogen abstraction of 9,10-dihydroanthracene (**Scheme 24**). For $[\text{Mn}^{\text{IV}}-\text{OH}]$ species, it is reduced to $[\text{Mn}^{\text{III}}-\text{OH}_2]$ after hydrogen abstraction. The reduced $[\text{Mn}^{\text{III}}-\text{OH}_2]$ can not rebound the OH_2 group to radical R group. Conversely, the reduced $[\text{Mn}^{\text{III}}-\text{OH}]$ can rebound OH to the substrate radical to generate oxygenation product.

desaturation



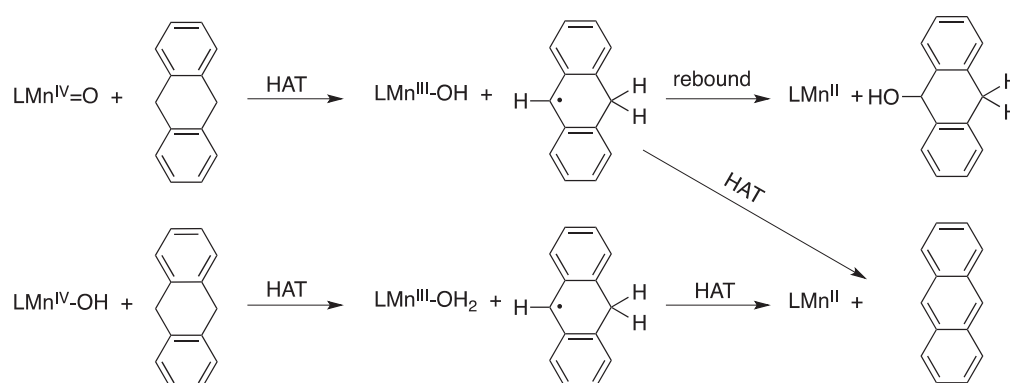
oxygenation



Scheme 24. Two pathways after abstraction of 9,10-dihydroanthracene by two different manganese(IV) species.^{150,152}

In the case of the hydrogen abstraction of 9,10-dihydroanthracene by $[\text{Mn}^{\text{IV}}=\text{O}]$ in $[\text{Mn}^{\text{IV}}(\text{Me}_2\text{EBC})(\text{O})_2]$ and $[\text{Mn}^{\text{IV}}-\text{OH}]$ in $[\text{Mn}^{\text{IV}}(\text{Me}_2\text{EBC})(\text{OH})(\text{OH}_2)]^{3+}$, the $[\text{Mn}^{\text{IV}}=\text{O}]$

reduced and protonated product $[\text{Mn}^{\text{III}}\text{-OH}]$ is capable of electron transfer in addition to hydrogen abstraction from 9,10-dihydroanthracene, affording another product. In contrast, the reduced and protonated product $[\text{Mn}^{\text{III}}\text{-OH}_2]$ can only perform hydrogen abstraction with the same substrate. The structures of these two species oxidizing 9,10-dihydroanthracene are presented in **Scheme 25**. The results were also confirmed by GC-MS.



Scheme 25. Mechanisms of hydrogen abstraction by $[\text{Mn}^{\text{IV}}\text{-OH}]$ and $[\text{Mn}^{\text{IV}}\text{=O}]$ species. HAT: hydrogen abstraction.¹⁵²

It is also reported that the $\text{Mn}^{\text{IV}}\text{-OOH}$ moiety (**Figure 48**) is a much more powerful oxidizing reagent than the corresponding $\text{Mn}^{\text{IV}}\text{-OH}$ and $\text{Mn}^{\text{IV}}\text{=O}$ species in both hydrogen abstraction and oxygen transfer.¹⁵⁹ It is generated by ligand exchange between $\text{Mn}^{\text{IV}}\text{-OH}$ and hydrogen peroxide. It was found that the $\text{Mn}^{\text{IV}}\text{-OOH}$ moiety had a capability in hydrogen abstraction from diphenylmethane ($\text{BDE}_{\text{CH}} = 82 \text{ kcal/mol}$) and ethylbenzene ($\text{BDE}_{\text{CH}} = 85 \text{ kcal/mol}$). Hence, $\text{Mn}^{\text{IV}}\text{-OOH}$ is more powerful than the corresponding $\text{Mn}^{\text{IV}}\text{-OH}$ and $\text{Mn}^{\text{IV}}\text{=O}$ complexes, with a driving force limited to 80 kcal/mol.¹⁵⁰ The $\text{Mn}^{\text{IV}}\text{-OOH}$ moiety can efficiently oxidize methyl phenyl sulfide,

diphenyl sulfide and benzyl phenyl sulfide.¹⁵⁹

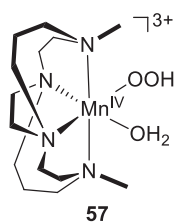
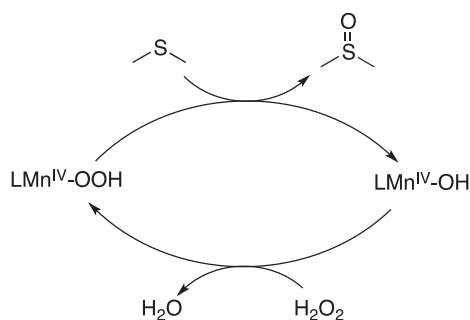


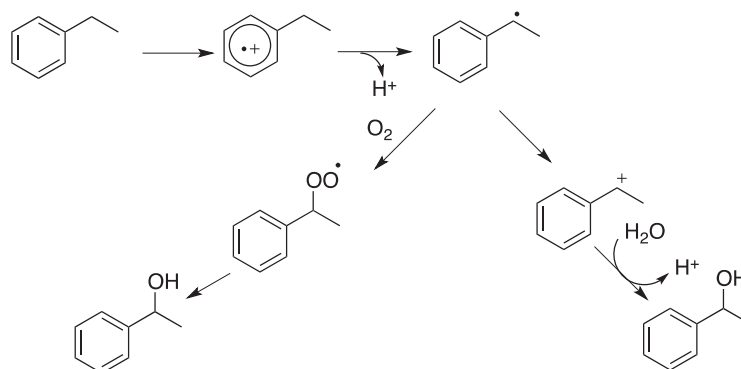
Figure 48. The structure of Mn^{IV}-OOH moiety.

For the oxidation of sulfide, the sulfoxide was produced by concerted oxygen transfer from Mn^{IV}-OOH moiety to the substrate (**Scheme 26**).



Scheme 26. Oxidation of dimethylsulfide.

The oxidation of ethylbenzene to 1-phenylethanol by [Mn^{II}(Me₂EBC)Cl₂] using H₂O₂ at pH 1.5 is also proposed to involve the active intermediate, [Mn^{IV}-OOH], which is generated *in situ*. A plausible mechanism is proposed to take place through an electron transfer and proton transfer process (**Scheme 27**). The substrate radical is generated by electron transfer, followed by two possible routes. The substrate radical either traps dioxygen from the atmosphere leading 1-phenylethanol, or loses one more electron to form a substrate cation, which reacts with water to form the alcohol.



Scheme 27. Example of an electron transfer mechanism.

3.5 Application of $[\text{Mn}^{\text{II}}(\text{Me}_2\text{EBC})\text{Cl}_2]$

Dong L. *et al.* reported that the manganese(II) complex $[\text{Mn}^{\text{II}}(\text{Me}_2\text{EBC})\text{Cl}_2]$ could efficiently catalyze the oxidation of thioanisole to the corresponding sulfoxide with PhIO in the presence of redox-inactive metal ions Lewis co-catalysts such as Na^+ , Mg^{2+} , Ca^{2+} , Al^{3+} , Sc^{3+} and so on (**Figure 49**).⁷⁹ It has been observed that the acceleration effect was related to the positive charge of the Lewis acid: the higher the charge, the higher the efficiency. For example, with only manganese(II) complex, the conversion of thioanisole was 9.8% with 5.1% yield of sulfoxide after 4 hours, while in the presence of Al^{3+} , the conversion increased to 97.1% with 95.4% yield after 4 hours. Besides, using $[\text{Mn}^{\text{IV}}(\text{Me}_2\text{EBC})(\text{OH})_2](\text{PF}_6)_2$ alone or with Al^{3+} as a Lewis acid, the same acceleration as the one observed with Mn(II) and Al^{3+} was evidenced. This observation proved that Mn(IV) was the active species.

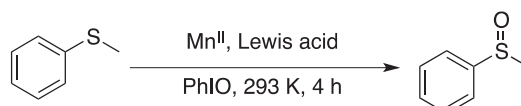


Figure 49. Sulfoxidation by $[\text{Mn}^{\text{II}}(\text{Me}_2\text{EBC})\text{Cl}_2]$ with PhIO in the presence of Lewis acid.

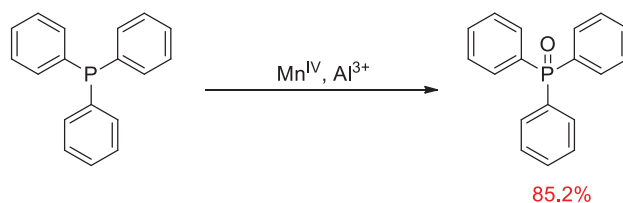


Figure 51. Stoichiometric oxidation of triphenylphosphine with $[\text{Mn}^{\text{IV}}(\text{Me}_2\text{EBC})(\text{OH})_2](\text{PF}_6)_2$ and a Lewis acid.

In the catalytic epoxidation of cyclohexene, the $[\text{Mn}^{\text{II}}(\text{Me}_2\text{EBC})\text{Cl}_2]$ complex with PhIO was tried for a 14 h reaction at 298 K (**Figure 52**).⁷⁹ The yield was only around 5.5%, while it increased to around 12.9% in the presence of Lewis acid Al^{3+} . Although the yield was still poor, it proved that the Lewis acid could accelerate the epoxidation reaction catalyzed by a manganese(II) complex.

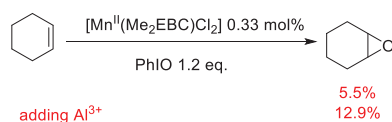


Figure 52. Epoxidation of cyclohexene with $[\text{Mn}^{\text{II}}(\text{Me}_2\text{EBC})\text{Cl}_2]$ in the presence of PhIO.

Epoxidation of various olefins by $[\text{Mn}^{\text{II}}(\text{Me}_2\text{EBC})\text{Cl}_2]$ with 50% of H_2O_2 was also reported (**Figure 53** and **Table 5**).^{161,162} The epoxidation of cyclohexene afforded the corresponding oxide in 18% yield and the cyclohexen-1-one in 13.3% yield, respectively. With styrene, the styrene oxide was isolated in 45.5% with only 2.8% of benzaldehyde co-produced. The oxidation of norbornylene only provided 32% yield of norbornylene oxide, but the epoxidation of *cis*-stilbene provided three products: 17.5% yield of *cis*-stilbene oxide, 2% yield of *trans*-stilbene oxide and 2.6% yield of benzaldehyde. It was proved that the key intermediate for the epoxidation of olefins

was a manganese(IV) hydroperoxide moiety, $[\text{Mn}^{\text{IV}}(\text{Me}_2\text{EBC})(\text{O})(\text{OOH})]^+$, through a Lewis acid pathway, in which the oxygen was transferred from that adduct to the olefin.

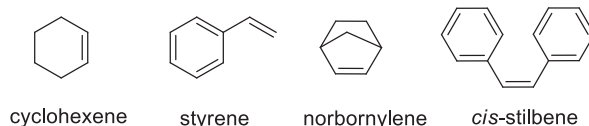


Figure 53. Structure of substrates.

Table 5. Epoxidation of various olefins by $[\text{Mn}^{\text{II}}(\text{Me}_2\text{EBC})\text{Cl}_2]$ with 50% of H_2O_2 in acetone and water media.^{a, 162}

Substrate	Product	Yield %
cyclohexene	cyclohexene oxide	18.0
	cyclohexen-1-one	13.3
styrene	styrene oxide	45.5
	benzaldehyde	2.8
norbornylene	norbornylene oxide	32.0
<i>cis</i> -stilbene	<i>cis</i> -stilbene oxide	17.5
	<i>trans</i> -stilbene oxide	2.0
	benzaldehyde	2.6

^aConditions: acetone/water (4: 1), Mn^{II} 1 mM, olefin 0.1 M, 50% H_2O_2 (1 mL) added stepwise by 0.2 mL/ 0.5 h, room temperature, GC yield.

Hydrogen abstraction reaction was also conducted by $[\text{Mn}^{\text{II}}(\text{Me}_2\text{EBC})\text{Cl}_2]$ from 1,4-cyclohexadiene with H_2O_2 at 30°C, giving 86.2% of conversion and 71.4% yield of benzene in 4 hours (**Figure 54**).⁸⁰ It indicated that $[\text{Mn}^{\text{II}}(\text{Me}_2\text{EBC})\text{Cl}_2]$ had a high efficiency combined with H_2O_2 .

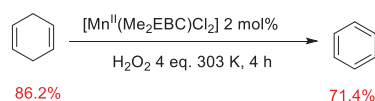


Figure 54. Hydrogen abstraction from 1,4-cyclohexadiene with $[\text{Mn}^{\text{II}}(\text{Me}_2\text{EBC})\text{Cl}_2]$ in the presence of H_2O_2 .

It has been reported that $[\text{Mn}^{\text{II}}(\text{Me}_2\text{EBC})\text{Cl}_2]$ could efficiently decolorize dyes in the presence of H_2O_2 through a wide range of pH from pH 1 to 13.¹⁶⁰ Three common dye materials namely methylene blue (MB, **58**), methyl orange (MO, **60**), Rhodamine B (RhB, **59**) were chosen as model compounds to test the decolorization capability of the catalyst (**Figure 55**). It has been found that in the presence of the manganese complex and H_2O_2 , MO and RhB were completely decolorized in 5 and 14 min, respectively, while for MB, the decolorization needed 300 min for 50% removal in neutral solution.

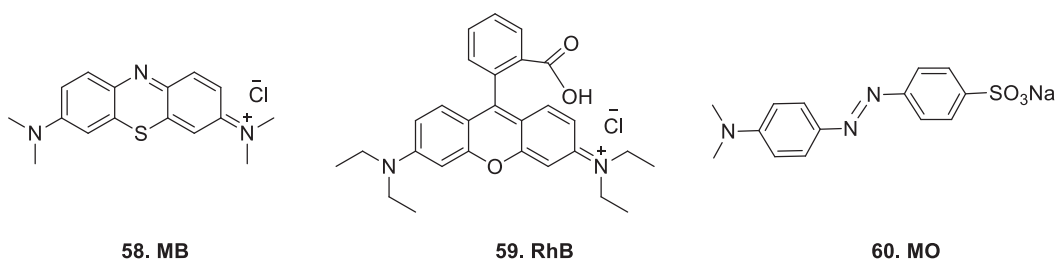


Figure 55. Structures of three dye materials: **58** methylene blue, **60** methyl orange, and **59** Rhodamine B.

Next, different initial pH for the decolorization of the relatively robust substrate **58** were investigated. The manganese complex exhibited a significant activity from acid to basic medium. The highest catalytic activity appeared at the lowest pH 1.3 or at the highest pH 12.7. On the contrary the lowest activity occurred at pH 7 because the catalyst decomposed H_2O_2 . A manganese(IV) hydroperoxide intermediate, $\text{LMn}^{\text{IV}}\text{-OOH}$, was proposed to be the active species, rather than the $\text{HO}\cdot$ radical or manganese(V) oxo species.¹⁶⁰

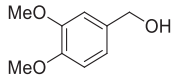
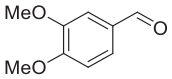
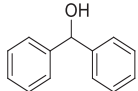
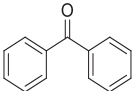
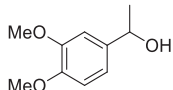
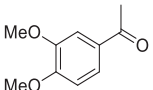
Manganese plays an important role both in industry and biology. Synthesis of high efficient manganese catalysts is still crucial in catalytic chemistry. Moreover, investigation of the possible applications of the synthetic manganese complexes is ongoing.

Part II. Results and discussion on Iron(TAML)

1 Synthesis of functionalized Fe(TAML) for oxidation catalysis

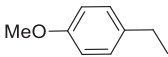
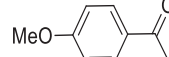
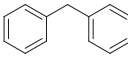
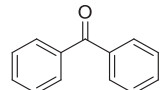
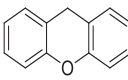
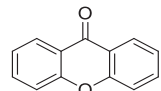
Our Laboratory has carried out a lot of researches on the catalytic oxidation with the simple iron TAML complex **7a**, in particular, to oxidize alcohols with (diacetoxyiodo)benzene (DIAB) (**Table 6**).⁶¹ The combination system was proven very efficient for converting primary and secondary alcohols to aldehydes and ketones, respectively. Moreover, it has been applied to lignin model compounds for oxidative cleavage. In addition, the Fe(TAML) **7a** complex was found to efficiently catalyze the benzylic C-H oxidation with *tert*-butylhydroperoxide (**Table 7**).⁷⁸ Various benzylic compounds were oxidized to the corresponding ketones in good yields.

Table 6. Oxidation of various alcohols by Fe(TAML-Me₂) with DIAB.^{a, 61}

Entry	alcohol	Conversion %	Aldehyde/Ketone	Yield %
1		60		57
2		100		99(99)
3		100		99(97)
4		97		93(91)

^aConditions: acetone, Fe^{III} 1 mol%, DIAB 2 eq., 25 °C, 1 h, GC yield. Isolated yield in parentheses.

Table 7. Oxidation of benzylic C- H by Fe(TAML-Me₂) with TBHP.^{a, 78}

Entry	Substrate	Product	Isolated yield
1			93
2			86
3			97
4			99

^aConditions: acetone/ buffer solution pH 12 (KCl/ NaOH), Fe^{III} 1 mol%, TBHP 6 eq., 10 °C, 3 hours.

On the basis of the aforementioned promising results, we envisioned the functionalization of the Fe(TAML) complex in order to have a better stability or to use the catalyst in heterogeneous catalysis, or for recycling the catalyst. We also aimed at comparing the physical and chemical properties of the catalysts. All the Fe(TAML) complexes we synthesized in the manuscript are coordinated with an axial water molecule. To make the structure of Fe(TAML) complexes short and clear, the axial water molecule on the complexes are omitted. Besides, the counteractions are always Li⁺ if not mentioned specially.

1.1 Strategies of functionalization of Fe(TAML)

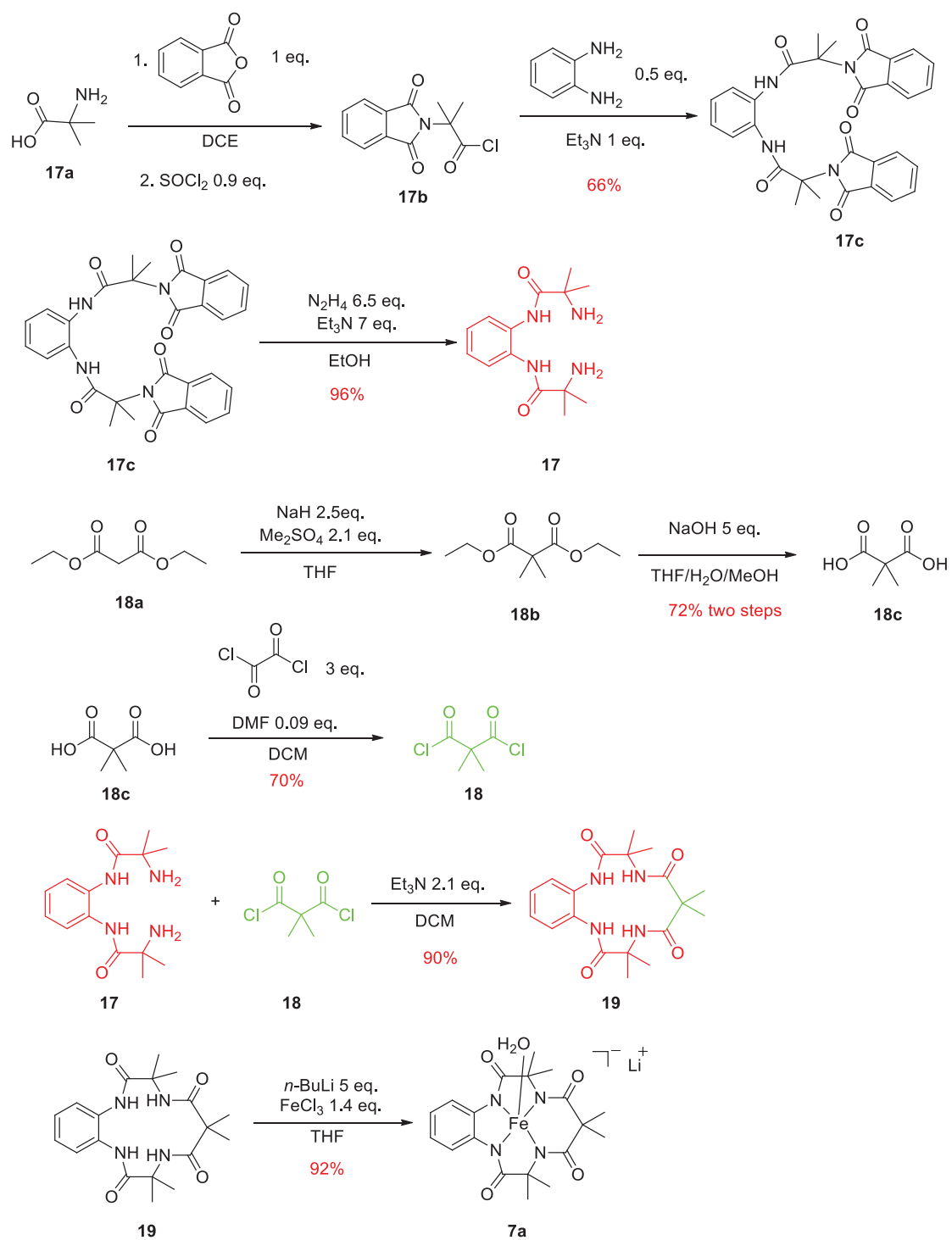
The synthesis of iron TAML has been extensively studied and several synthetic routes have been described. The most recent method of synthesis of the simple Fe(TAML-Me₂) **7a** was developed by Horwitz *et al.* in 2006 (**Scheme 28**).⁸⁸ We decided to follow Horwitz's strategy.

Firstly, as indicated earlier (see p 23) the product **17** was synthesized by the protection of the amino-acid **17a** using a phthalimide, followed by formation of the corresponding acid chloride **17b** using thionyle chloride. Next, the protected “diamide diamine” **17c** was synthesized by reaction between 1,2-phenylenediamine and **17b**. At last, the diamide diamine **17** was obtained by deprotection of **17c** with hydrazine in an almost quantitative yield.

The product **18** was synthesized in 4 steps starting from diethyl malonate **18a**. **18a** was converted to **18b** by reacting with dimethyl sulfate after deprotonation with sodium hydride. The compound **18c** was obtained by saponification of **18b**. The yield for the two steps was 72%. The final dichloride product **18** is obtained in 70% yield using oxalyl chloride as a chlorinating agent.

The TAML ligand **19** was efficiently obtained in 90% yield by reaction between compound **17** and 2,2-dimethylmalonyl dichloride **18**. Finally, the $[\text{Fe}(\text{TAML-Me}_2)]\text{Li}$ **7a** was obtained by deprotonation of the ligand with *n*-butyllithium, before reaction with FeCl_3 . This procedure affords the expected complex in 92% yield after purification by column chromatography.

The key point for the complexation was to keep the whole system anhydrous and oxygen free. So, all the reagents used were dried under argon. Besides, purification was also essential here. After reaction with anhydrous FeCl_3 , there were excess FeCl_3 (excess FeCl_3 made the ligand TAML-Me₂ reacted completely), impurities from TAML-Me₂ accumulated in the final mixture. Purification was conducted by chromatography. A column chromatograph was filled with Al_2O_3 . CH_3OH and CH_2Cl_2 were used as mobile phase. After purification and dried, a shiny red powder was obtained.



Scheme 28. Typical synthesis of $[\text{Fe}(\text{TAML-Me}_2)]\text{Li}$ **7a**.⁸⁸

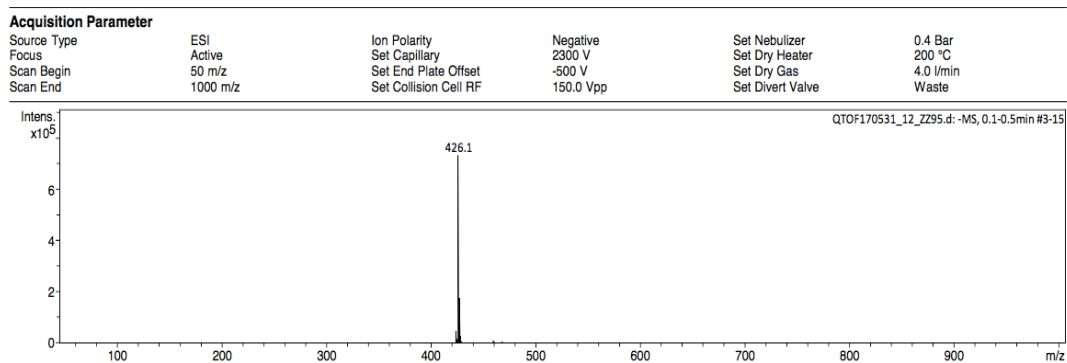


Figure 56. Mass spectra of $[\text{Fe}(\text{TAML-Me}_2)]^+$.

Among other methods, the product was analyzed by ESI-mass spectrometry (**Figure 56**). The ESI-mass spectrum of $[\text{Fe}(\text{TAML-Me}_2)]\text{Li}$ **7a**, evidenced a high degree of purity for the complex and confirmed that the structure is in total agreement with data from the literature.⁸⁸

As discussed in **Part I**, the functionalization of TAML could be envisioned in two ways. Based on the first generation of TAML (**7a**), the functionalization could either take place on the “head” or on the “tail (**Figure 57**). For a functionalization on the head, we first considered inserting a bromide on the aromatic group to tune the reactivity and stability of the complex. For the functionalization of the tail, several strategies were available. On the basis of a preliminary work carried out in the group by Dr. R. Kieffer and co-workers, we decided to use a “click” reaction between an alkyne-functionalized TAML and a simple chain azide to afford a triazole moiety. Within the frame of this PhD work, with investigated a hexyl-substituted triazole following Dr. Kieffer’s work, a silicon-functionalized-triazole or a perfluorinated triazole (*vide infra*).

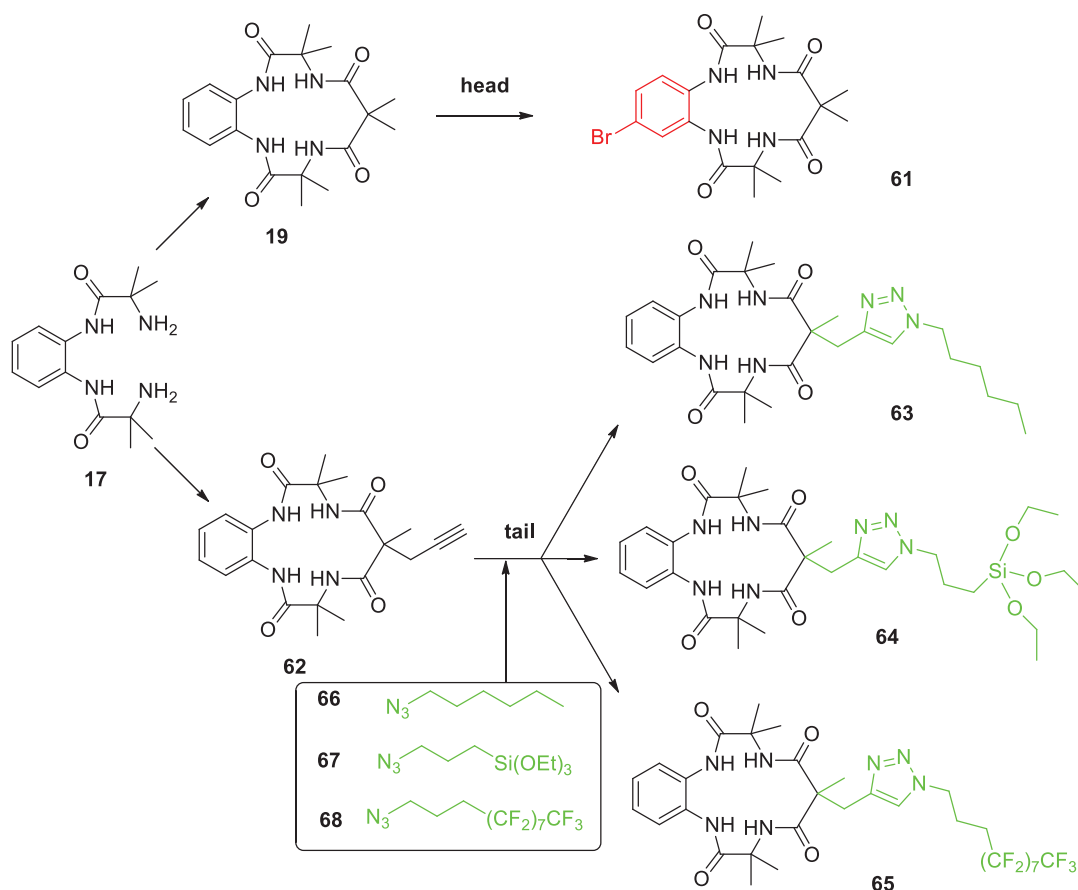


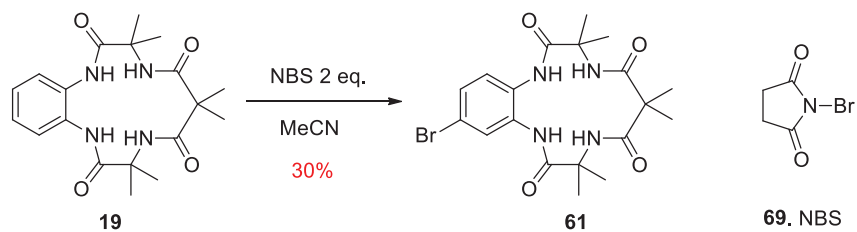
Figure 57. Selected strategies for the functionalization of TAML.

The introduction of a Br atom on the head was to distract the positive charge of the iron in the complex in order to potentially tune the selectivity and lifetime of the catalyst. In addition, Br could be used to further functionalize the TAML complex using cross-coupling reactions for instance. The role of the different tails addressed different issues. Indeed, the long alkyl chain could influence the physicochemical properties of the metal catalysts that could be used in homogeneous catalysis. Conversely the silicon tailed-one is designed to be grafted on an inorganic support for a use in heterogeneous catalysis. At last, the purpose of the fluorinated tail was to increase the solubility of the complex in fluorinated solvents for a potential use in a biphasic mixture that could favor the recyclability of the catalyst.

1.2 Synthesis of functionalized Fe(TAML).

1.2.1 Functionalization of TAML on the head.

For the synthesis of Fe(Br-TAML-Me₂), we first tried to functionalized the TAML-Me₂ ligand directly. Two distinct methods to synthesize Br-TAML-Me₂ **61** were envisioned. We first chose bromine as the brominating agent.¹⁶³ In this reaction, Br₂ was too reactive as only a small amount of mono brominated TAMLs and a large quantity of di-brominated products were obtained. Next, we switched to *N*-bromosuccinimide, NBS, which is a milder brominating agent than Br₂.^{164,165} The optimization of the reaction conditions by changing the amount of NBS from 1 eq. to 4 eq. was carried out. With 2 eq. of NBS, the best compromise was found. The pure target product **61** was isolated in 30% yield after purification by flash column chromatography (**Scheme 29**).



Scheme 29. Synthesis of Br-TAML-Me₂ **61**.

Despite the lengthy optimization, the reaction appeared very difficult to control, and the different region-isomers extremely difficult to separate despite many attempts (**Figure 58**). For this reason, the yield of the target compound **61** never exceeded 30%, and we had to give up with this strategy.

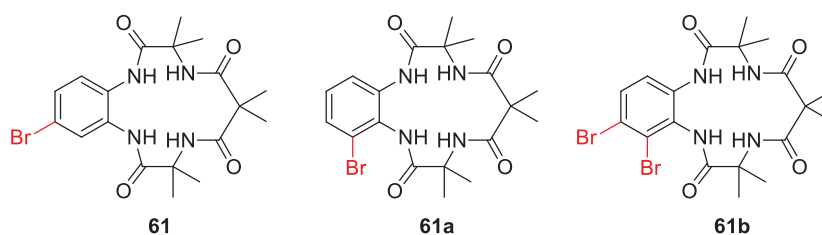
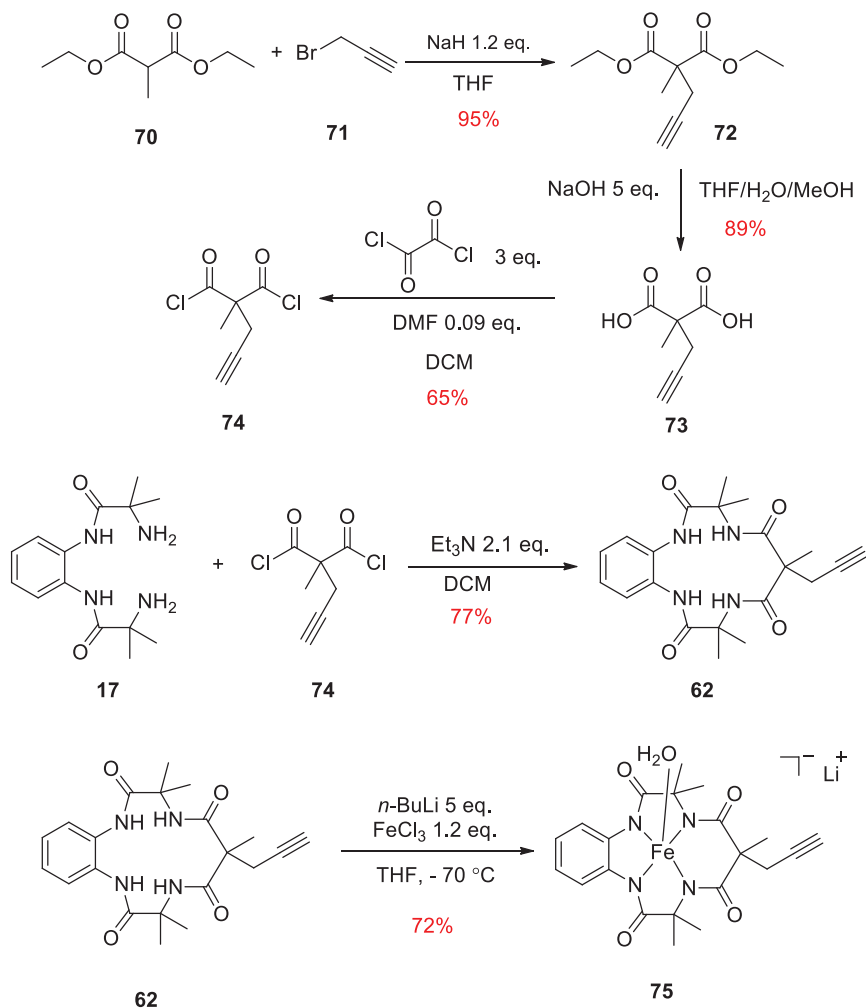


Figure 58. Different products observed after the reaction of TAML-Me₂ with NBS.

1.2.2 Functionalization of TAML on the tail.

The functionalization of TAML-Me₂ on the “tail” did not proceed directly from the reference ligand TAML-Me₂ **19**, but required the synthesis of a TAML with an alkynylated-tail in order to allow the introduction of the triazole moiety by click chemistry. The protocol of synthesis of TAML-(Me)(CH₂CCH) **62** was quite similar to that of TAML-Me₂ but required the use of 2-methyl-2-propargylmalonyl dichloride **74** instead of 2,2-dimethylmalonyl dichloride **18** for the synthesis of the alkynylated-TAML (Scheme 30).



Scheme 30. Synthesis of compound $[\text{Fe}[(\text{OH}_2)\text{-TAML-(Me)(CH}_2\text{CCH)}]]\text{Li}$ **75**.

The synthesis of the iron complex, $[\text{Fe}[(\text{OH}_2)\text{-TAML-(Me)(CH}_2\text{CCH)}]]\text{Li}$ **75**, was similar to the complexation of (TAML-Me₂) with FeCl₃ (**Scheme 30**). However, as the alkyne tail was reactive towards strong bases (the CCH is deprotonated by *n*-BuLi and can easily generate an allene function), we had to use a lower temperature to decrease the reaction rate. Dry ice and acetone were combined to bring the reaction temperature around -70 °C. At this temperature *n*-BuLi was added. The purification was also carried out by column chromatography on alumina using CH₃OH/ CH₂Cl₂ (1:10) as the mobile phase. The iron complex was isolated in 72% yield.

Acquisition Parameter

Source Type	ESI	Ion Polarity	Negative	Set Nebulizer	0.4 Bar
Focus	Active	Set Capillary	2300 V	Set Dry Heater	200 °C
Scan Begin	50 m/z	Set End Plate Offset	-500 V	Set Dry Gas	4.0 l/min
Scan End	1000 m/z	Set Collision Cell RF	400.0 Vpp	Set Divert Valve	Waste

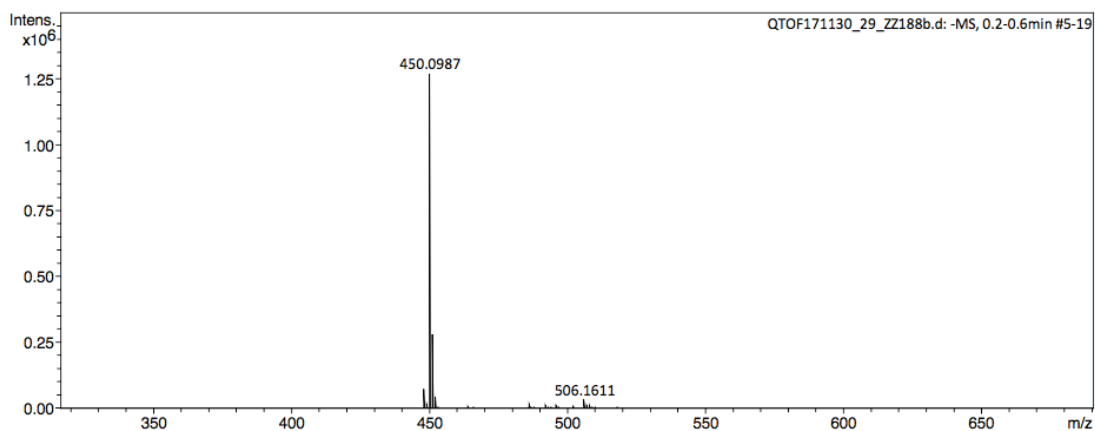
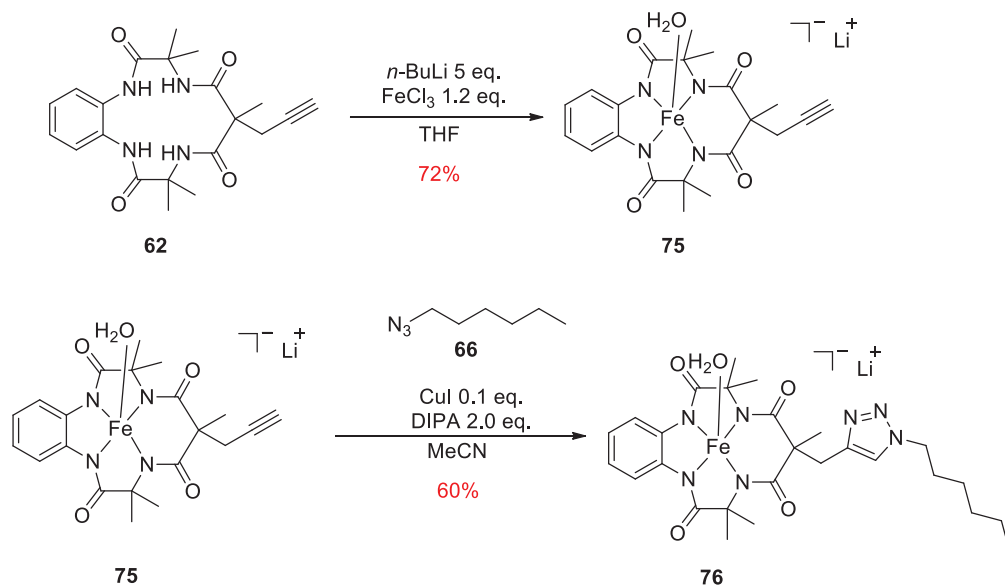


Figure 59. High resolution mass spectrum of $[\text{Fe}(\text{TAML})-(\text{Me})(\text{CH}_2\text{CCH})]^+$.

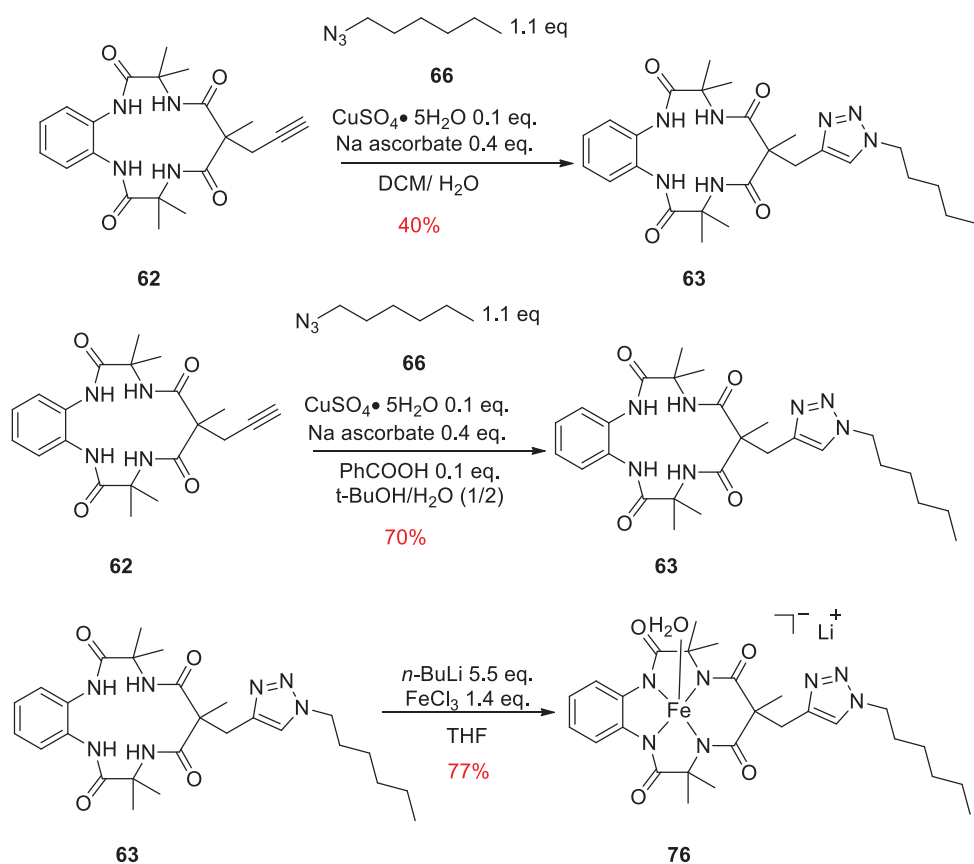
The product was analyzed by mass spectrometry (**Figure 59**). The high resolution mass spectra of $[\text{Fe}[(\text{OH}_2)\text{-TAML}-(\text{Me})(\text{CH}_2\text{CCH})]]\text{Li}$ **75**, acknowledged the purity and the structure of the complex.

$\text{Fe}[(\text{OH}_2)\text{-TAML}-(\text{Me})(\text{triazole})]\text{Li}$ **76** was synthesized using two different synthetic strategies. First, we used the alkynylated-TAML ligand **62** directly with FeCl_3 to afford the $\text{Fe}[(\text{OH}_2)\text{-TAML}-(\text{Me})(\text{CH}_2\text{CCH})]\text{Li}$ **75** complex according to a strategy similar to that used for the preparation $\text{Fe}(\text{TAML}-\text{Me}_2)$ (**Scheme 31**). Next, complex **75** was reacted with 1-azidohexane **66** through a “click” reaction procedure to produce a triazole with a long chain (**Scheme 31**). However, the overall yield (around 42%) for the two steps (complexation + functionalization) was much lower than that obtained for the reference $[\text{Fe}[(\text{OH}_2)\text{-TAML}-\text{Me}_2]]\text{Li}$ **7a**.



Scheme 31. Synthetic protocol for the synthesis of Fe[(OH₂)-TAML-(Me)(triazole)] **76** from Fe[(OH₂)-TAML-(Me)(CH₂CCH)]Li **75**.

The second method we tried involved initially the “click” reaction using TAML-(Me)(CCH) **62** with 1-azidohexane to afford the TAML-(Me)(triazole) ligand (**Scheme 32**). Next, this ligand was reacted with FeCl₃ according to a similar strategy as the one described in the **Scheme 28**. According to literature precedents, several methods to conduct the “click” reaction are available.¹⁶⁶⁻¹⁶⁸ First, we tried to use sodium ascorbate as a reducing agent for copper sulfate in two different solvent systems. In a dichloromethane/water system, the TAML ligand could not dissolve properly and the reaction efficiency was low. After purification, the yield was around 40%. When changing the solvent to *t*-butanol/water, with addition of benzoic acid as the phase transfer catalyst, the yield was much higher, and reached 70%. The complexation with FeCl₃ was similar as before, except that it needed a longer reaction time (24 hours) for completion of the reaction.



Scheme 32. Synthetic protocol for Fe[(OH₂)-TAML-(Me)(triazole)]Li **76** from complexation of TAML-(Me)(triazole) with FeCl₃.

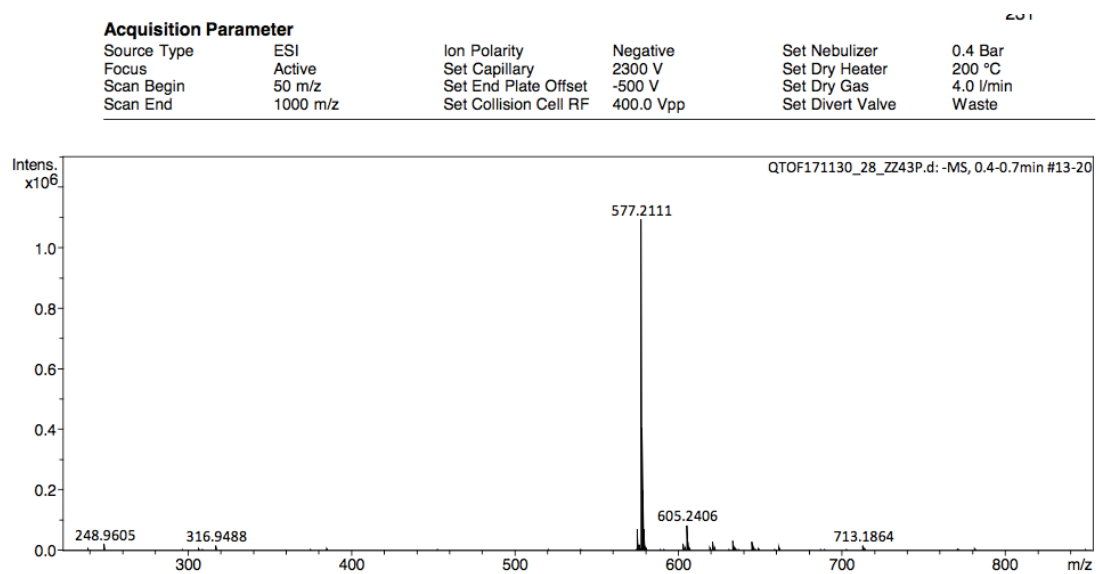
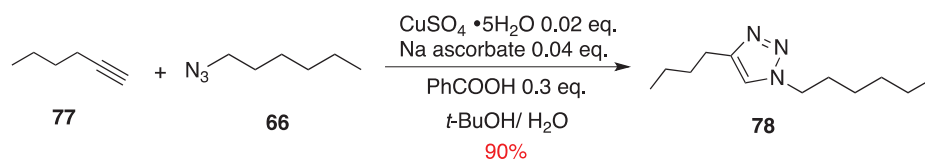


Figure 60. High resolution mass spectrum of Fe[(OH₂)-TAML-(Me)(triazole)]⁺.

The product was analyzed by mass spectrometry (**Figure 60**). From the high resolution mass spectra of Fe[(OH₂)-TAML-(Me)(triazole)]Li **76**, we could see that the molecular weight of the product was identical to the calculated one.

Using this second method, we obtained the pure target products in 70% yield for the first step and 77% of the second step. The “click” reaction was established in a way to afford 4-butyl-1-hexyl-1*H*-1,2,3-triazole **78** (**Scheme 33**).¹⁶⁶ The compound **78** was synthesized first to develop a method to synthesize TAML-(Me)(triazole). Second, the compound **78** had a triazole but without TAML. Thus, when compare the properties of TAML-(Me)(triazole) and **78**, the interaction between TAML and triazole was indicated directly.



Scheme 33. Synthesis of 4-butyl-1-hexyl-1*H*-1, 2, 3-triazole **78**.

As discussed above, in order to envision a grafting of the Fe(TAML) complex on an inorganic material, which could be used in heterogeneous catalysis, we decided to insert a silicon group “tail” (**Figure 61**).^{127,169,170}

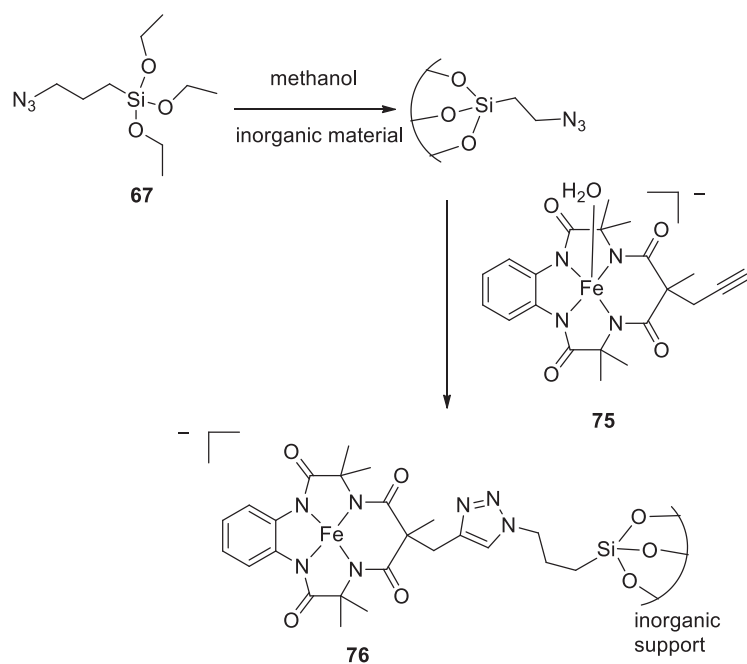


Figure 61. Strategy for grafting the Fe(TAML) on an inorganic material.¹²⁷

The complex Fe[(OH)₂-TAML-(Me)(triazole-(CH₂)₃Si(OEt)₃)]Li **79** was synthesized as follows (**Scheme 34**): The (3-azidopropyl)triethoxysilane **67** was synthesized from (3-chloropropyl)triethoxysilane and sodium azide in 65% yield. Next, the obtained azido **67** was reacted with Fe[TAML-(Me)(CCH)] **75** through a “click” reaction according to the synthetic strategy described in **Scheme 34**. The expected functionalized Fe(TAML) **79** was isolated in 60% yield.

unidentified peak at 486.0.

The long C6-alkyl chain “tail” also brought us to synthesize a Fe(TAML) compound with a long perfluorinated chain containing -CF₂- , which could dissolve in fluorinated solvents. Hence, we could use a bi-phasic solvent system for the reaction and consider recycling the catalyst (**Figure 63**). In **Figure 63**, we illustrate a typical protocol catalyst recycling. First, there are two phases, and the catalyst is in the fluororous phase. The reactants are either in the organic phase or in the fluororous phase. Next, upon heating the system, the two phases become one phase and the catalytic reaction can proceed. After the reaction is over, by cooling down the system, it becomes biphasic again, and the catalyst is in the fluororous phase. After separation, the fluororous phase can be used for the next catalytic reaction.

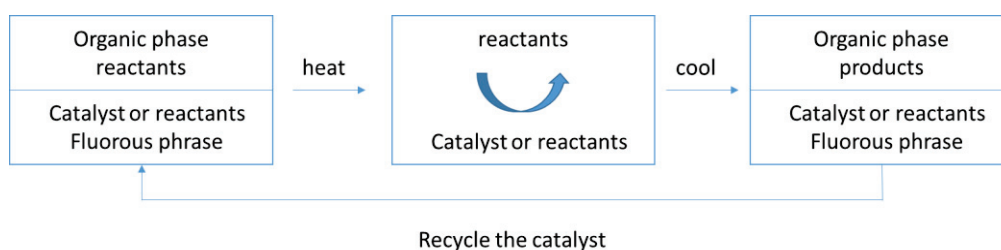
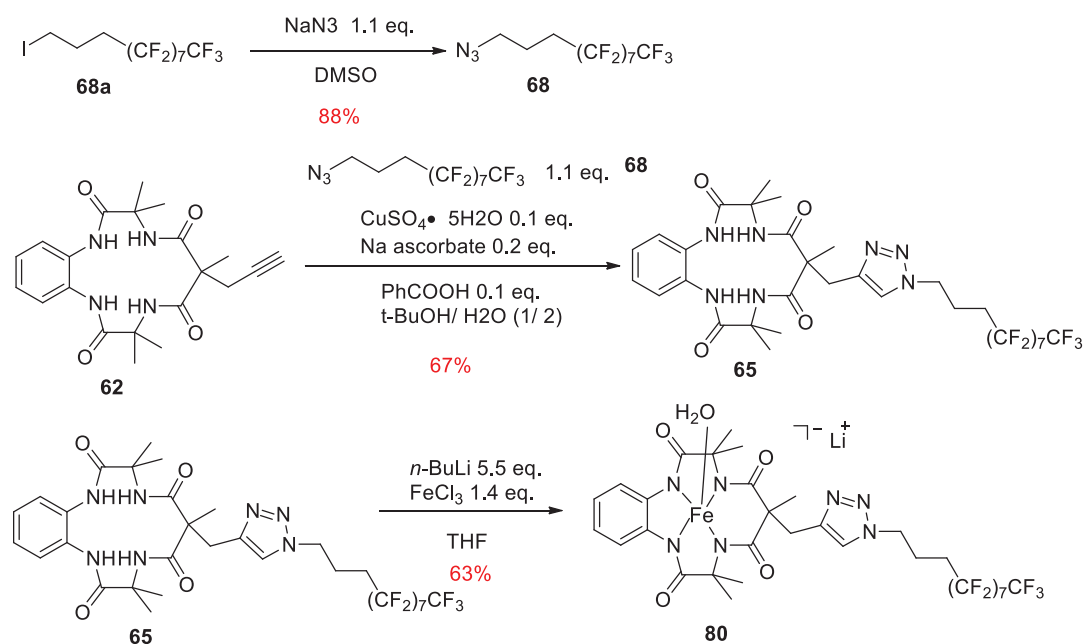


Figure 63. Catalyst recycling process using fluorinated solvents.

According to the idea presented above, we synthesized a Fe(TAML) catalyst with a long perfluorinated tail Fe[(OH₂)-TAML-(Me)(triazole)-(CH₂)₃(CF₂)₇CF₃]]Li **80**. The synthetic protocol for the catalyst is described in the **Scheme 35**. As before, we synthesized an azido-functionalized fluorinated chain compound **68** in 88% by reacting the corresponding iodo derivative **68a** with sodium azide.¹⁷¹ Next, the azido **68** was reacted with the alkyned-TAML **62** through a “click” reaction to afford the fluorinated TAML ligand. The choice of **68a** with three -CH₂- before perfluorinated tail was to create the condition that lead to the “click” reaction. Without CH₂, there were -CF₂- groups, which could attract the electron strongly, and the alkyne could not react with

azido **68**. The fluorinated Fe(TAML) catalyst **80** was next prepared in two steps (deprotonation and complexation) according to the strategy established earlier. The fluorinated Fe(TAML) complex **80** was isolated in 63% overall yield for the last two steps.



Scheme 35. Synthesis of the fluorinated Fe(TAML) **80**.

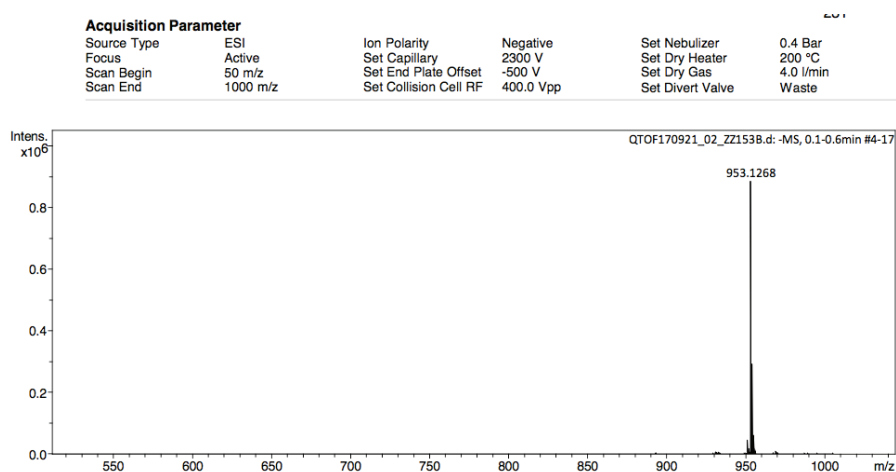


Figure 64. High resolution mass spectrum of the fluorinated TAML **80**.

As previously, the product was analyzed by high resolution mass spectrometry (**Figure 64**). From the high resolution mass spectra of **80**, we could ascertain the purity of the complex.

2 Characterization of Fe(TAML)

During our PhD studies, we concentrated our investigations on the $[\text{Fe}[(\text{OH}_2)\text{-TAML-(Me)(\text{triazole})}]]$ **76** complex. In particular, we aimed at determining whether the triazole moiety could coordinate the Fe metal center in an intramolecular 1:1 manner. Besides, we compared the physical and chemical properties between the simple $\text{Fe}(\text{TAML-Me}_2)$ **7a** and the $[\text{Fe}[(\text{OH}_2)\text{-TAML-(Me)(\text{triazole})}]]\text{Li}$ complexes **76** and how the triazole-substituent could influence these. When needed, we also studied $[\text{Fe}[(\text{OH}_2)\text{-TAML-(Me)(CH}_2\text{CCH)}]]\text{Li}$ **75** (**Figure 65**).

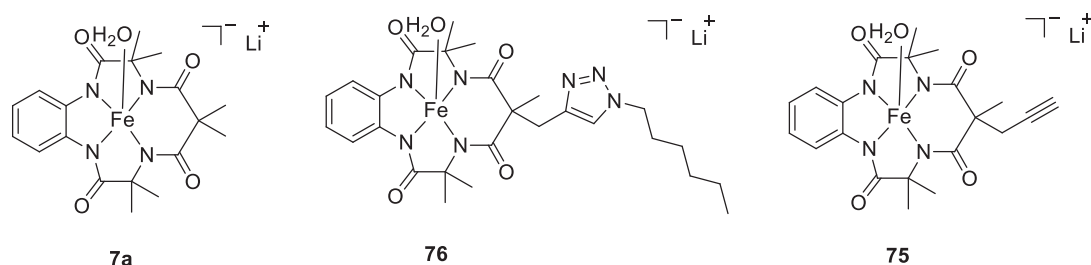


Figure 65. Structures of the TAML complexes studied in this part.

2.1 DFT calculations

DFT calculations on model of the complex **76** (replacing the alkyl chain by a methyl group) was performed. This complexes had a ground spin state of 3/2. Two configurations were investigated in the case of **76** (**Figure 66**). In the first one, the imidazole coordinated the iron center while in the other one it did not. The coordinated one was equally or even more stable than the opened configuration, with a slight impact of the solvent included as a continuum model. It was stabilized by 11 kJ/mol in methanol and 0.4 kJ/mol in acetonitrile. The coordination of the imidazole weakened the N-Fe bonds within the equatorial plane and triggered the metal off the plane of the TAML core as shown in the two optimized structures shown in **Figure 66**. Computer

modelling demonstrated that the intramolecular coordination of the triazole moiety on the Fe metal center was possible.

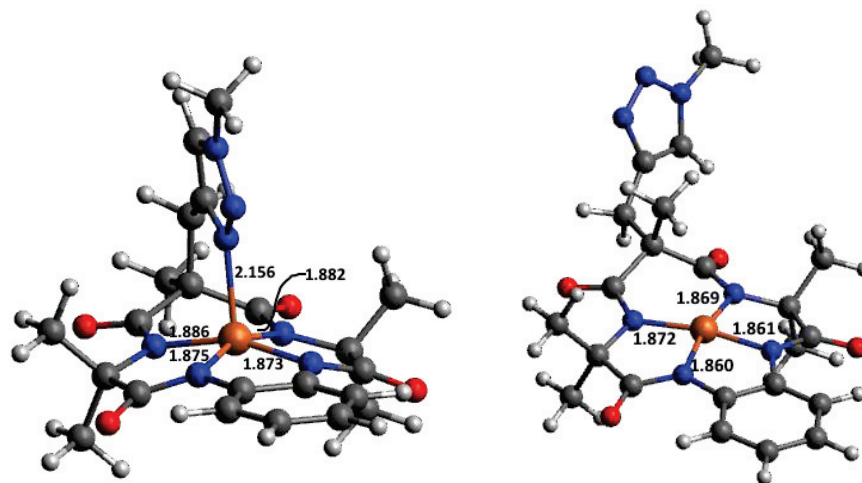


Figure 66. Optimized structures of complex **76** (replacing the alkyl chain by a methyl group) with and without imidazole coordination. Fe-N distances are given in Å. Those structures were optimized with Gaussian09 using the OPBE functional, a cc-pvtz basis for Fe and cc-pvdz basis set of N, C, O and H, and using a polarizable continuum model of MeOH. Fe shown in orange, N in blue, O in red, C in grey, H in white.

2.2 Mossbauer

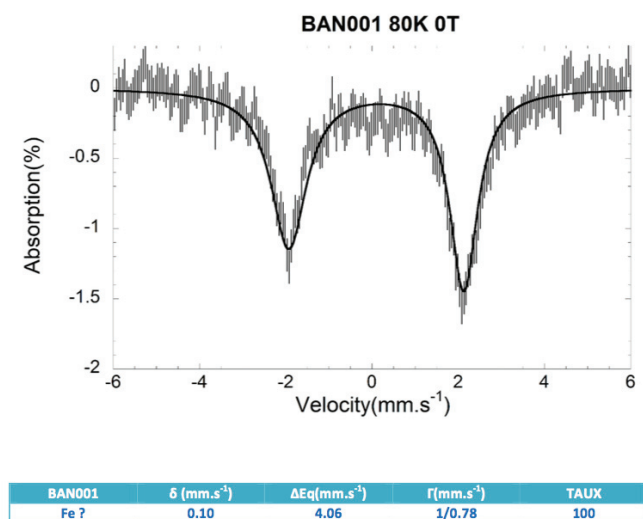


Figure 67. Mossbauer spectrum of compound **76** at 80 K and zero field.

The zero-field Mossbauer spectrum of the solid compound **76** at 80 K and zero field consists of a doublet which can be seen in **Figure 67**. The important parameters are isomer shift and quadrupole splitting, which can determine the spin state of iron in the complex. The parameter values of the complex **76** ($\delta = 0.10 \text{ mm}\cdot\text{s}^{-1}$ and $\Delta E_Q = 4.06 \text{ mm/s}$) are very close to those reported for another compound $\text{Fe}[(\text{MeO})_2\text{-TAML-(Et)}_2]$ ($\delta = 0.14 \text{ mm}\cdot\text{s}^{-1}$ and $\Delta E_Q = 4.19 \text{ mm/s}$).¹⁷² According to this article, the spin of Fe in this complex is $S = 3/2$. We infer that it is the same in our complex **76**, which is consistent with the result from EPR.

2.3 Electrochemical studies

In the literature, it was reported that the $\text{Fe}(\text{TAML})$ **28b** (**Figure 68**) has two oxidation peaks at $E_{1/2} = 0.36 \text{ V}$ and 0.68 V (*vs* SCE) (**Figure 69**).¹⁷³ When the complex **28b** was oxidized to complex **28c** and **28g** by one electron oxidation, respectively, it was proved that the oxidation state of iron didn't change, remaining at iron(III). The oxidation happened on not the iron center but on the ligand. To be more precise, it happened on

both aromatic ring. It was also reported that the complex $\text{Fe}^{\text{III}}(\text{MAC})\text{Cl}^-$ was oxidized by one electron oxidation, the oxidation happened on the iron, from $\text{Fe}^{\text{III}}(\text{MAC})\text{Cl}^-$ to $\text{Fe}^{\text{IV}}(\text{MAC})\text{Cl}^-$ (**Figure 68**).¹⁷² So it indicated that if the TAML ligand without an aromatic ring, the oxidation happened directly on the iron center.

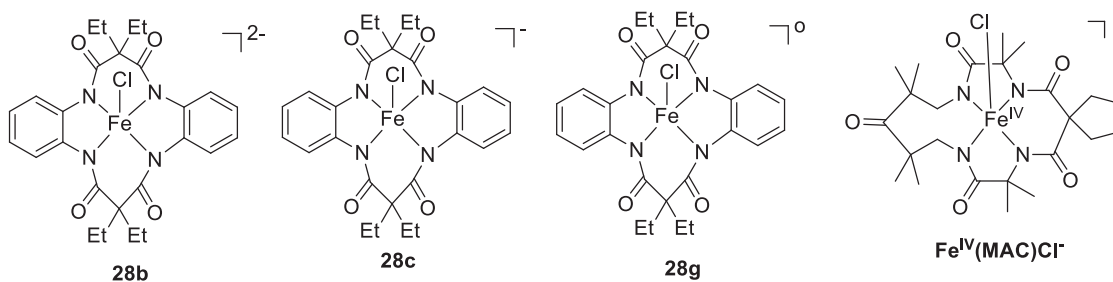


Figure 68. Structures of complexes **28b**, **28c**, **28g** and $[\text{Fe}^{\text{IV}}(\text{MAC})]\text{Cl}^-$.

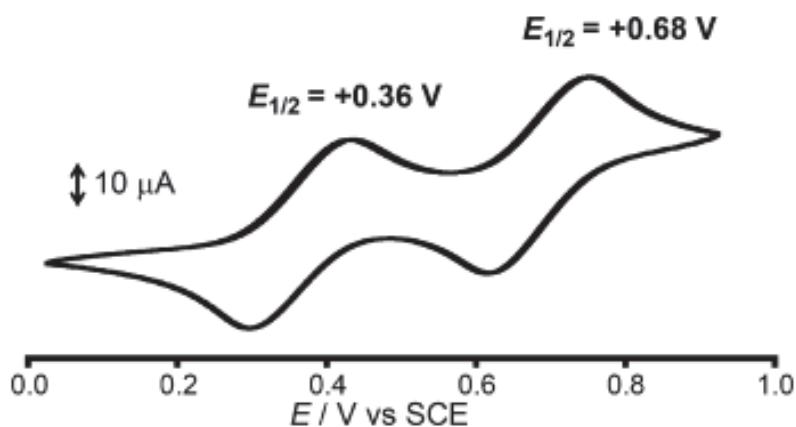


Figure 69. Cyclic voltammogram of complex **28b**.¹⁷³

In order to compare the physical properties of the **7a** and the **76** complexes, we have recorded the electrochemical spectra of these two complexes in different solvents. We carried out these studies in collaboration with Dr. Christophe Bucher from ENS -Lyon. The electrochemical studies were done in different solvents, namely, methanol, and acetonitrile. These solvents covered different polarities (MeOH and MeCN) in the presence of tetrabutylammonium perchlorate (TBAP) or tetrabutylammonium

hexafluorophosphate (TBAH) as the supporting electrolyte in a glove box under nitrogen. We use the cyclic voltammetry method with a carbon electrode as the working electrode. The couple DMFc/DMFc⁺ (DMFc: decamethylferrocene) was used as the internal reference. The main electrochemical features of the two compounds in methanol are summarized in **Table 8** and the CV in **Figure 70**.

Table 8. 1/2 Potential of reduction and oxidation ($E_{1/2}$) for the compounds **7a** and **76** in methanol (electrolyte: 0.1 M TBAP) in a glove box determined by cyclic voltammetry with a carbon working electrode.

Compound	Reduction	Oxidation potential (V)	
	Potential (V)	$E_{ox,1}$	$E_{ox,2}$
7a	-1.178 ^a	0.881	1.155 ^a
76	-1.119 ^a	0.874	1.139 ^a

^a: non-reversible, E_{peak} ; E vs Ag⁺/Ag, internal standard, DMFc⁺/DMFc, $v = 100$ mV/s.

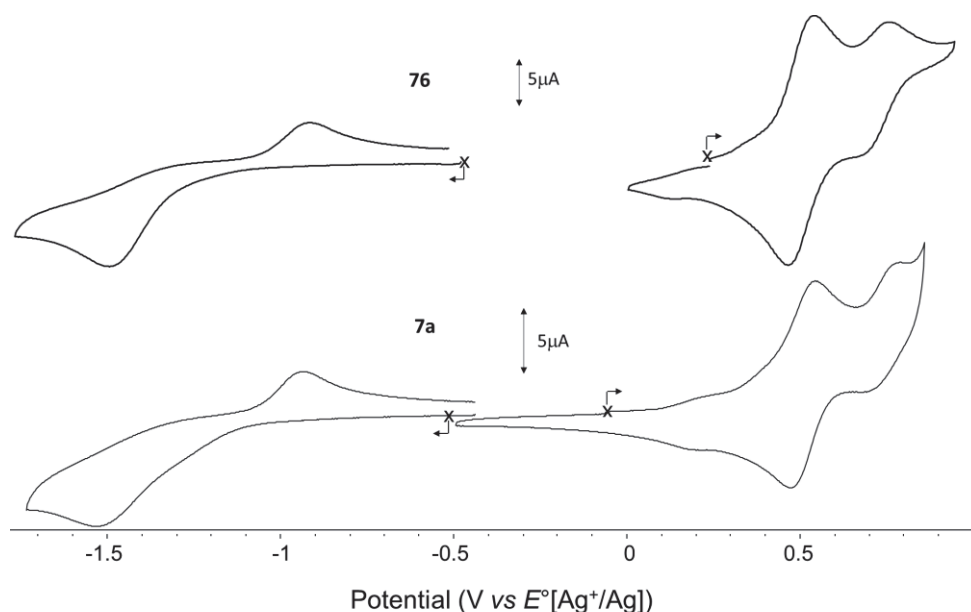


Figure 70. Cyclic voltammograms of compounds **7a** and **76** in methanol. CV curves recorded for **76** and **7a**, TBAP 0.1 M (VC, $\varnothing = 3$ mm, E vs Ag^+/Ag 10^{-2} M, $\nu = 0.1$ V.s $^{-1}$).

In methanol, the cyclic voltammogram (**Figure 70** and **Table 8**) of compound **7a** reveals a couple of reversible oxidation wave at $E_{1/2} = 0.881$ V vs $E(\text{Ag}^+/\text{Ag})$ and one non-reversible reduction wave at $E_p = -1.178$ V vs $E(\text{Ag}^+/\text{Ag})$. For compound **76**, it also has a couple of reversible oxidation wave at $E_{1/2} = 0.874$ V vs $E(\text{Ag}^+/\text{Ag})$ and one non-reversible reduction potential at $E_p = -1.119$ V vs $E(\text{Ag}^+/\text{Ag})$. Those potentials are almost the same to those determined for the compound **7a**. When we compare the spectra with that in the literature, we found that the first redox wave was quite similar. So we infer that the redox happened on the ligand. It is also inferred that these two compounds have the same redox potential in the coordinating solvent methanol. Hence, in this solvent the triazole moiety on compound **76** doesn't influence the redox potential. Possibly, in a coordinating solvent, the solvent coordinates to the metal iron, occupying the axial sites of both compounds. Thus, they have similar electrochemical behavior in a coordinating solvent.

Table 9. $E_{1/2}$ Potential of reduction and oxidation ($E_{1/2}$) for the compounds **7a** and **76** in acetonitrile (electrolyte: 0.1 M TBAH) in a glove box determined by cyclic voltammetry with a carbon electrode.

Compound	Reduction			Oxidation potential (V)	
	Potential (V)				
	$E_{\text{red},1}$		$E_{\text{ox},1}$	$E_{\text{ox},2}$	
7a	-0.853 ^a		0.563	0.812	
76	-1.524 ^a		0.738	1.159	

^a: non-reversible, E_{peak} ; E vs Ag^+/Ag , internal standard, $\text{DMFc}^+/\text{DMFc}$, $\nu = 100 \text{ mV/s}$.

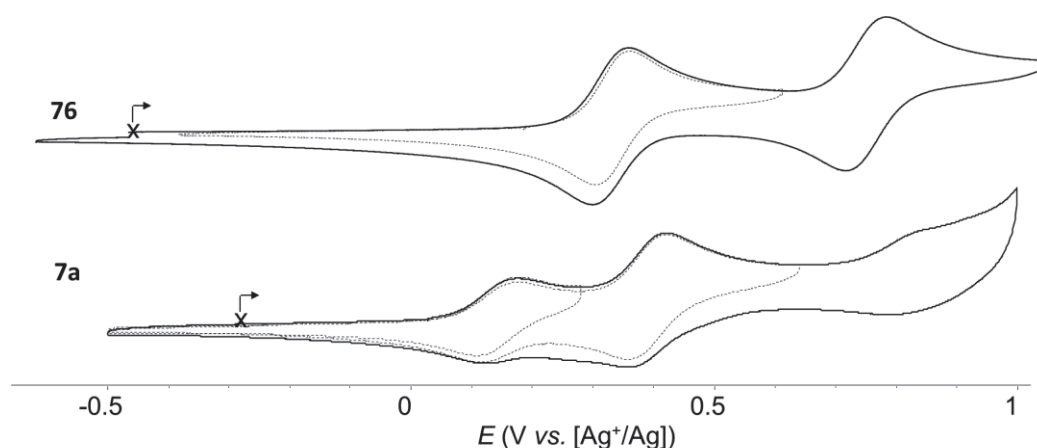


Figure 71. Cyclic voltammogram of compounds **7a** and **76** in acetonitrile. CV curves recorded for **76** and **7a**, TBAH 0.1 M (VC, $\varnothing = 3 \text{ mm}$, E vs Ag^+/Ag , 10^{-2} M , $\nu = 0.1 \text{ V.s}^{-1}$). Arbitrary current scale.

In acetonitrile, the cyclic voltammogram (**Table 9** and **Figure 71**) of compound **7a** reveals two couples of reversible oxidation at $E_{1/2} = 0.563 \text{ V vs } E(\text{Ag}^+/\text{Ag})$ and $E_{1/2} = 0.812 \text{ V vs } E(\text{Ag}^+/\text{Ag})$. Compound **76** also presents two couples of reversible oxidation potential at $E_{1/2} = 0.738 \text{ mV vs } E(\text{Ag}^+/\text{Ag})$ and $E_{1/2} = 1.159 \text{ V vs } E(\text{Ag}^+/\text{Ag})$. We can see that in ACN, the spectra of both complexes are quite similar to that from literature for complex **28b**. So we infer that the first oxidation should happen on the ligand on

the aromatic ring. However, both complex **7a** and **76** are have only one aromatic ring, respectively. It's hard to oxidize the second electron from the same aromatic ring. So the second oxidation should happen on iron center as complex $[\text{Fe}^{\text{III}}(\text{MAC})]\text{Cl}^-$. We also need further experiments to confirm.

The oxidation on ligand was also confirmed in literature by spectrum study.¹⁷³ As shown in **Figure 72**, the absorption peak at 504 nm stands for the complex **28b**, and the new peaks at 610 nm and 900 nm stands for oxidized the complex **28c**. The peaks at 563 nm and 1080 nm stands for the complex **28g**. And as mentioned, all the oxidation happened on ligands.

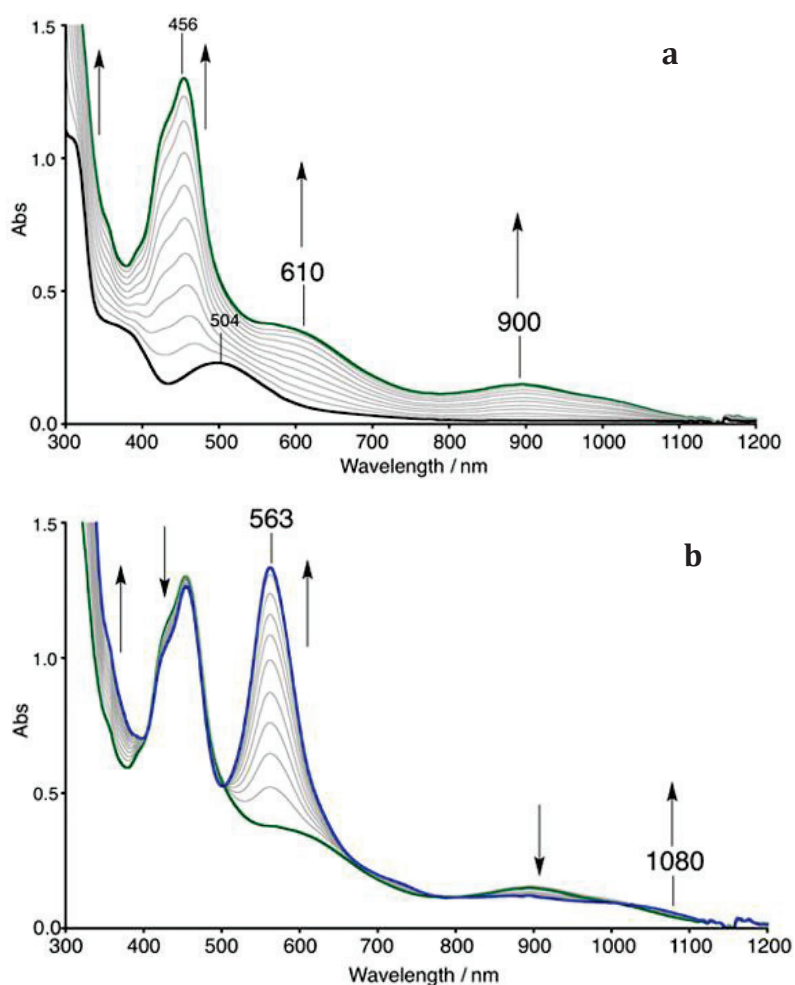


Figure 72. Spectral change of the complex **28b** in the first oxidation and the second oxidation.in acetonitrile.¹⁷³

In order to further confirm our hypotheses that the first oxidation should happen on the ligand, a spectro-electrochemical study has been carried out in order to characterize the species formed of the complex **76** during the oxidation and reduction process (**Figure 73**). It has been measured during the electrolysis of complex **76** in a thin layer of quartz cell in acetonitrile with Pt grid as working electrode.

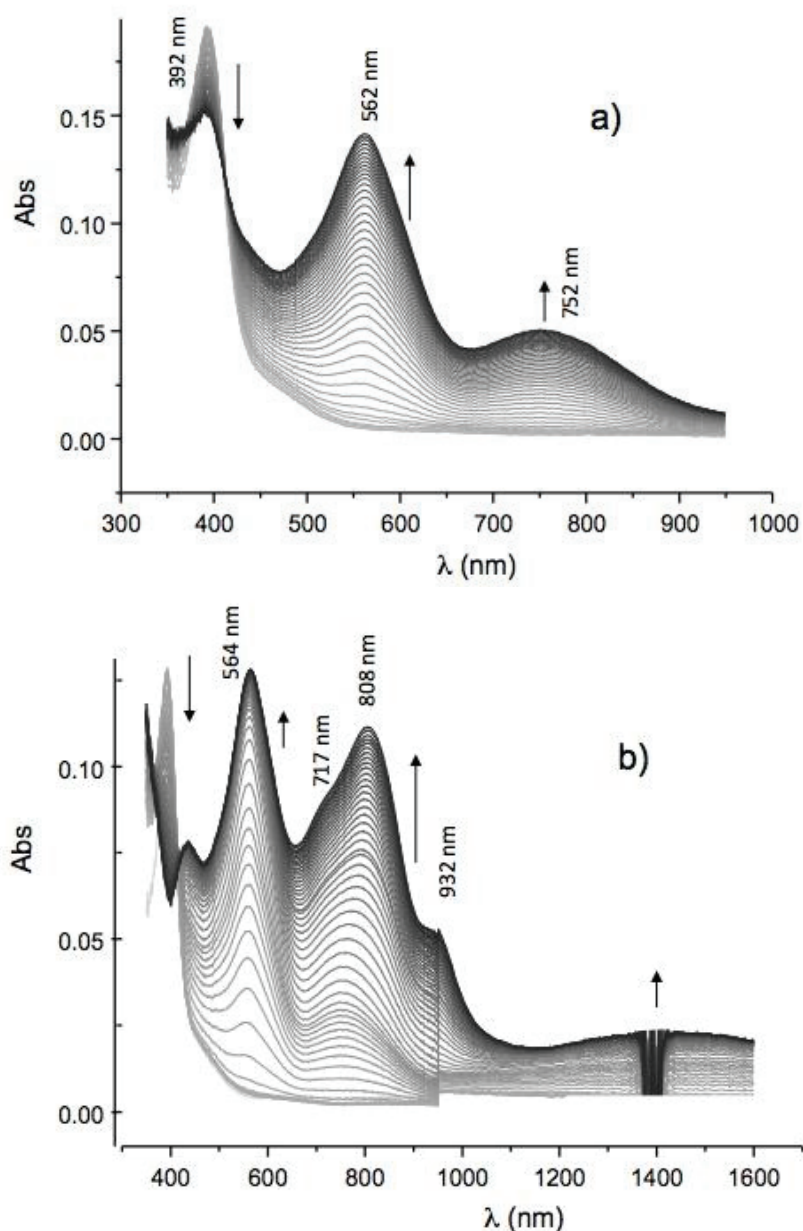


Figure 73. UV-Vis spectra recorded during the electrolysis of **76** in acetonitrile (0.1 M TBAP) with Pt grid. a) $E_{app} = 0.5$ V (Ag⁺/Ag), b) $E_{app} = 1$ V (Ag⁺/Ag), $I = 1$ mm, 5 min.

The spectra presented on **Figure 73, a** revealed the changes of the absorption bands observed during the scans between 0 and 0.5 V (Ag⁺/Ag). The one-electron oxidation of the complex **76** leads to a sharp decrease in the absorption centered at 392 nm as well as the appearance of new bands at 562 nm and at 752 nm. The spectrum was quite similar to the one in **Figure 72, a**, So it was another proof that the first oxidation

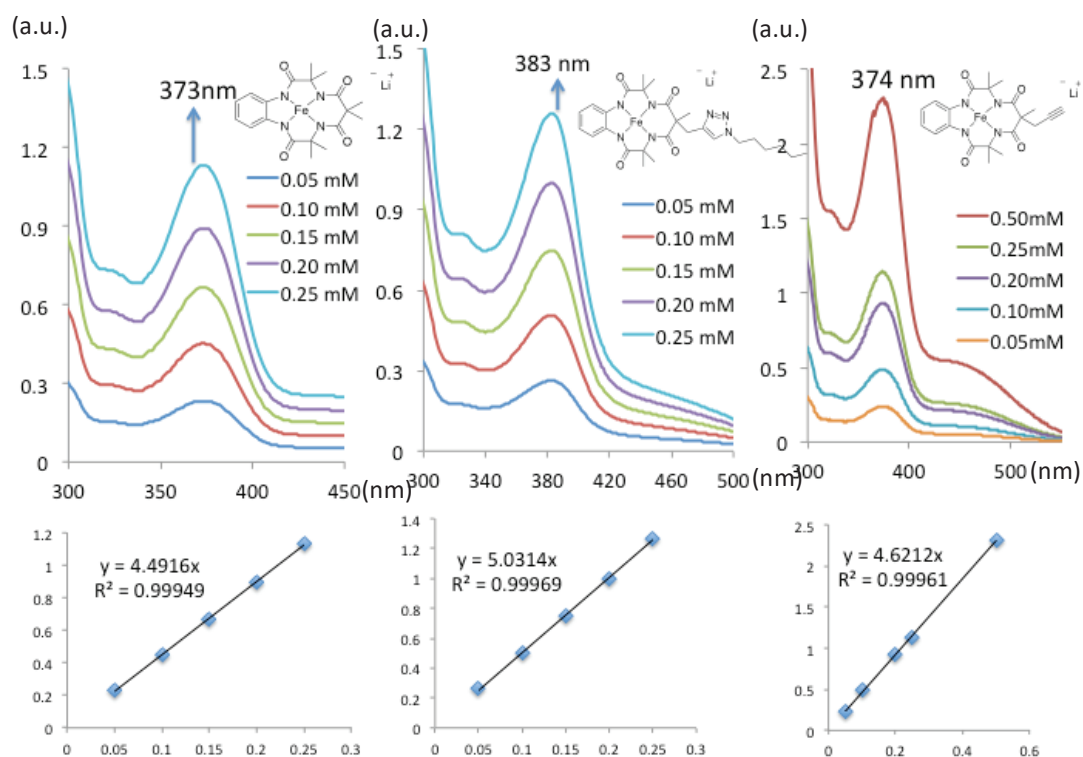
happened on the ligand of the complex **76**.

However, **Figures 73, b** showed the absorption bands observed during the scan between 0 and 1 V. During this scan, we observed two electron oxidation. The decrease of the first band centered at 392 nm leads to the rapid appearance of three new bands at 564, 808 and 932 nm. These were different from the spectra in **Figure 72, b**. The new bands were supposed to be the new species of $\text{Fe}^{\text{IV}}(\text{TAML})(\text{triazole})$, although we need further experiment to confirm.

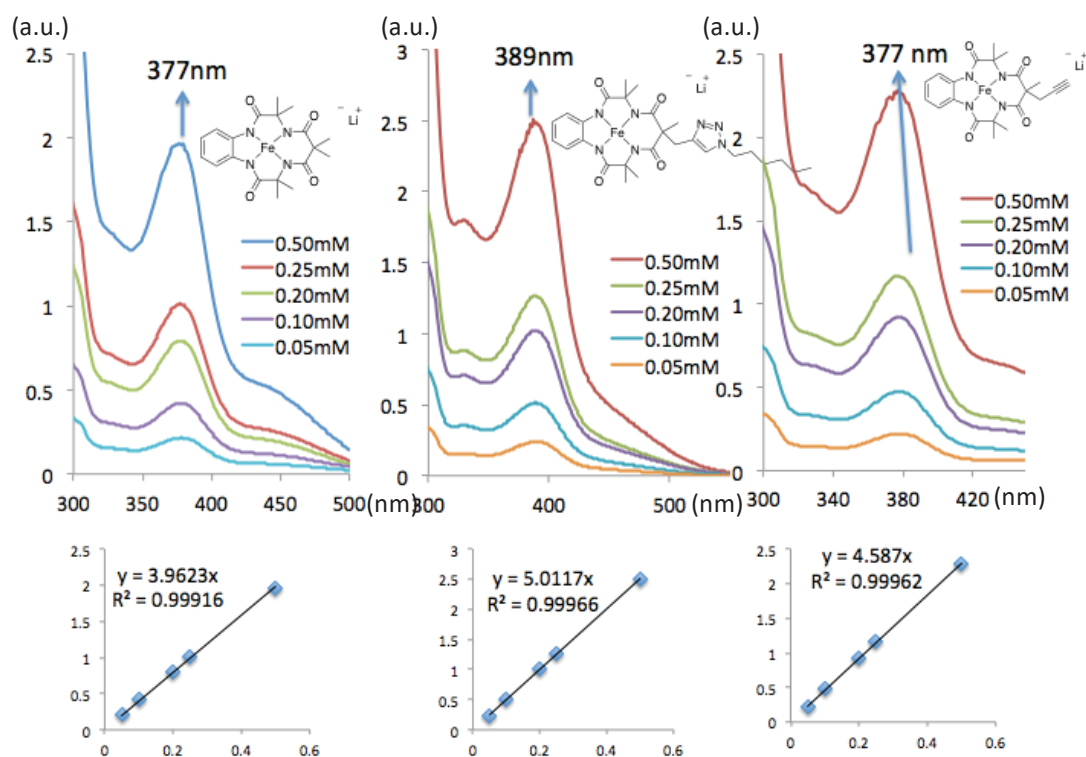
2.4 UV-Vis studies

To further study the influence of the triazole group on the $\text{Fe}(\text{TAML})$ compounds, we have recorded the UV-Vis spectra of the three compounds **7a**, **75** and **76**. Since **75** has an alkynylated-tail and no triazole, we infer that **7a** and **75** may have similar behaviors in different solvents. Like for the electrochemical studies, we used methanol, acetonitrile and DMF for the measurements. The spectra of the three compounds are presented in **Figure 74** and the characteristic features are summarized in **Table 10**.

a. In MeOH



b. In MeCN



c. In DMF

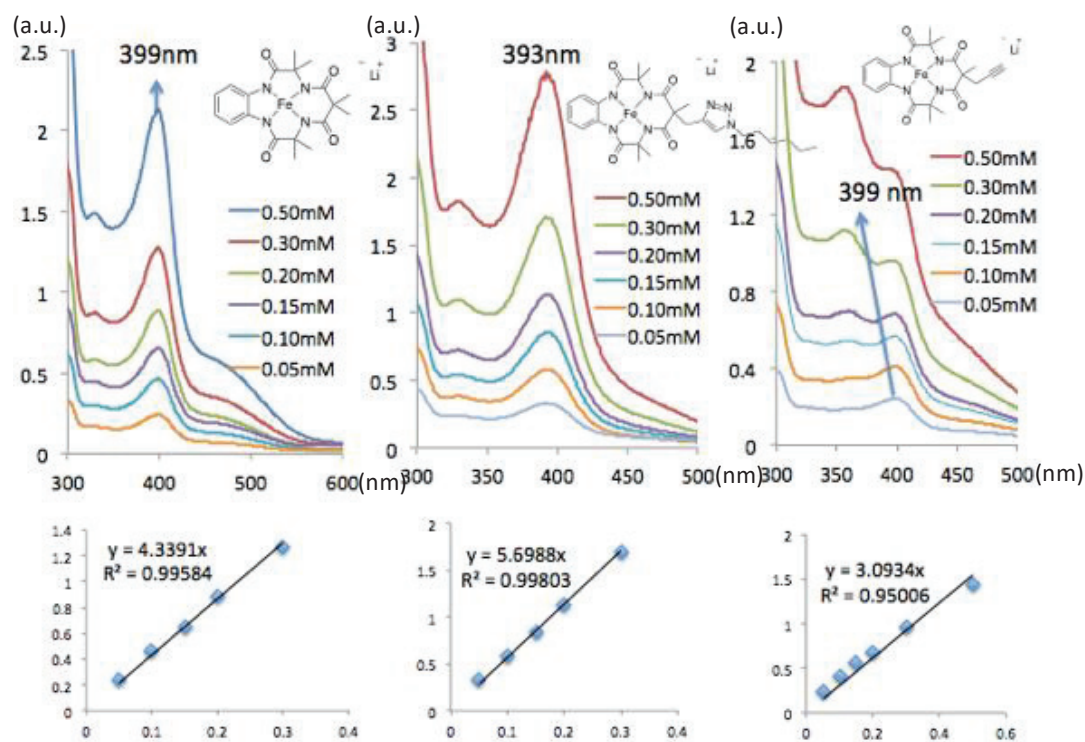


Figure 74. UV-Vis spectra of **7a**, **76** and **75** in three different solvents, λ (nm).

Table 10. Comparison of λ and ϵ for the three Fe(III) complexes in different solvents.

Entry	DMF		MeOH		CH ₃ CN	
	λ nm	ϵ M ⁻¹ cm ⁻¹	λ nm	ϵ M ⁻¹ cm ⁻¹	λ nm	ϵ M ⁻¹ cm ⁻¹
76	389	5012	383	5031	393	5699
7a	377	3962	373	4492	399	4339
75	377	4587	374	4621	399	3093

From the UV-Vis spectra of the three compounds in methanol, we can see that **76** has a characteristic absorption peak at 383 nm with $\epsilon = 5031$ M⁻¹cm⁻¹ while compound **7a** at 373 nm, $\epsilon = 4492$ M⁻¹cm⁻¹, and **75** at 374 nm, $\epsilon = 4621$ M⁻¹cm⁻¹. In acetonitrile, the characteristic absorption peak of compound **76** is at 393 nm ($\epsilon = 5699$ M⁻¹cm⁻¹) while

7a and **75** have the same characteristic absorption peaks at 399 nm, with $\epsilon = 4339 \text{ M}^{-1}\text{cm}^{-1}$ and $\epsilon = 3093 \text{ M}^{-1}\text{cm}^{-1}$, respectively. In DMF, compound **76** has an absorption peak at 389 nm ($\epsilon = 5012 \text{ M}^{-1}\text{cm}^{-1}$), whereas compounds **7a** and **75** are at 377nm ($\epsilon = 3962 \text{ M}^{-1}\text{cm}^{-1}$ and $\epsilon = 4587 \text{ M}^{-1}\text{cm}^{-1}$, respectively). In these three different solvents, we can see that, compounds **7a** and **75** almost have the same characteristic absorption peaks, while compound **76** behaves differently. Contrary to **7a** and **75**, compound **76** has an extra triazole functional group. We can infer that the triazole functional group on the TAML ligand influences the position of absorption of iron(III).

2.5 EPR study

All the spectra shown in **Figure 75** are consistent with the literature data: The complex corresponds to a high spin ($S = 3/2$) Fe(III) complex.^{87,174} The results also confirm the measurements made by Mössbauer. The profile of the spectra of these two complexes depends largely on the solvents. Accordingly, we recorded the EPR spectra of compound **76**, with **7a** as the reference in three different solvents, namely methanol, acetonitrile and DMF.

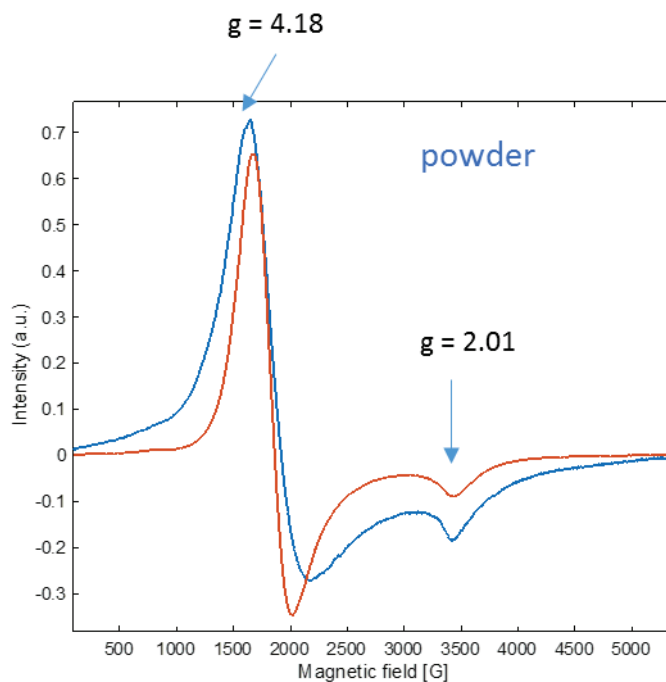


Figure 75. EPR spectra of complexes **7a** (blue) and **76** (red) in solid state at $T = 5-8$ K.

As shown in **Figure 75**, in the solid state, the complexes **7a** and **76** have different spectra at $g_{\text{eff}} = 4.18$, where the red curve is sharper than the blue one. It indicates that the complex **76** is less distorted than the complex **7a**. As the complex **7a** is 5-coordinated with an axial water molecule, the complex **76** may be 6-coordinated with both water molecule and also triazole occupying the axial coordination sites. In this case, the complex **76** would be more axially symmetrical.

The EPR spectra of **7a** and **76** recorded in acetonitrile at $T = 6$ K are identical (**Figure 76, a**). This observation suggests that the two metals are in similar environments in acetonitrile. It reveals that in acetonitrile the two complexes have same coordination state, maybe because in acetonitrile both complexes are coordinated with acetonitrile molecules coordinated in the axial sites.

The spectrum was recorded at 5-8 K in methanol (**Figure 76, b**). Both display signals

at $g_{\text{eff}} = 3.98$ and $g_{\text{eff}} = 2.03$. The blue one is a little sharper than the red one. However, they are quite similar. Accordingly, they may have similar coordination states in methanol. It is proposed that in both cases, two methanol molecules coordinate the metal axially.

Similarly, in DMF, the EPR spectrum of compound **7a** is influenced by the solvent with an extra intense contribution at $g_{\text{eff}} = 5.51$ (**Figure 76, c**, blue curve). The use of DMF leads to rhombic or trigonal defect of the coordination sphere of the complex and a loss of symmetry. These characteristics are reflected on the EPR spectrum by the observation of a third intense contribution at $g_{\text{eff}} = 5.51$. In the case of compound **76**, there is a large signal at $g_{\text{eff}} = 5.80$. This is probably due to the partial coordination of two different ligands in the axis of the Fe(TAML) molecule. The spectra recorded in MeOH (**Figure 76, b**), and DMF (**Figure 76, c**) displays important differences correlated to a deformation of the sphere of coordination around the iron(III).

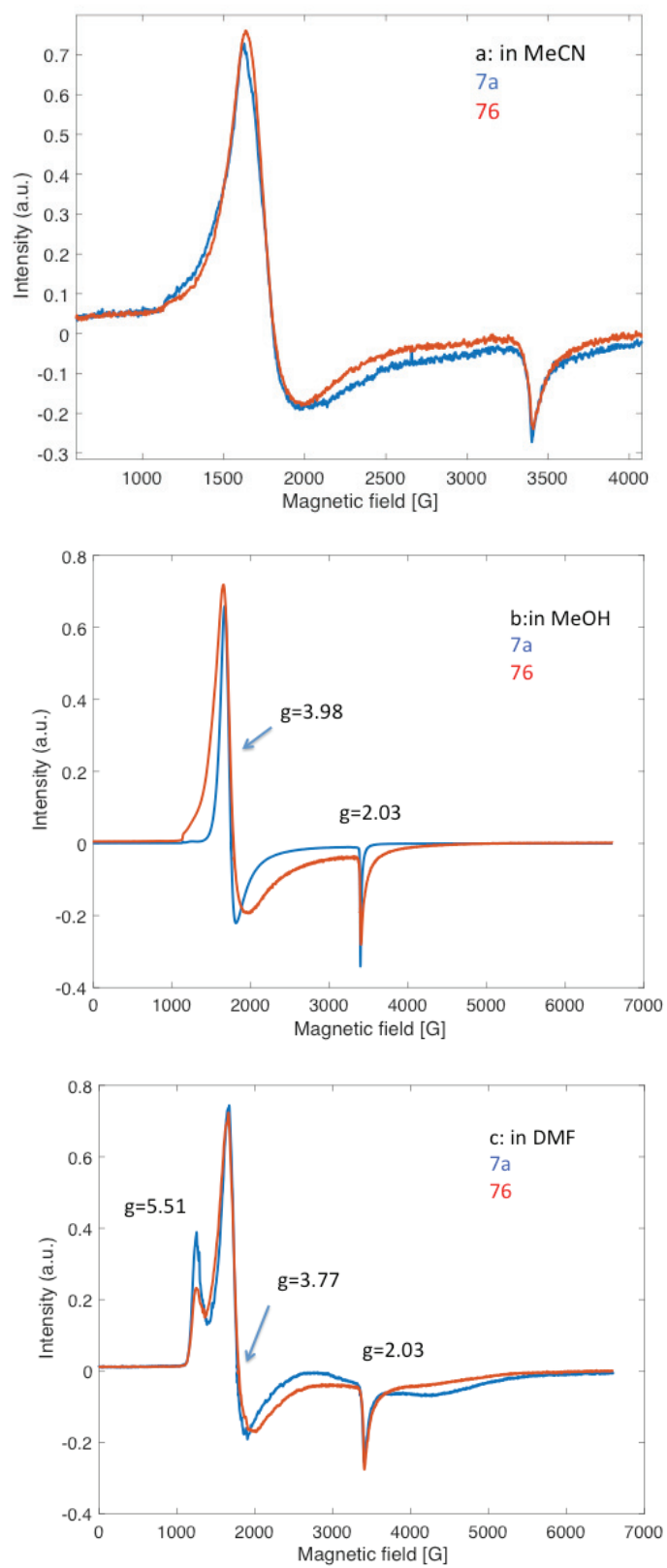


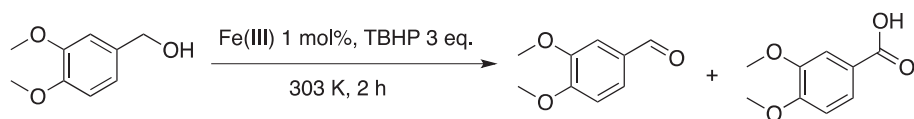
Figure 76. EPR spectra of **7a** and **76** in a, acetonitrile; b, methanol, c, DMF, T = 5-8 K.

3 Catalytic oxidation with Fe(TAML)

Evaluation of the reference complex **7a** has been done on a series of substrates, which were introduced in **Part I**. To compare the catalytic activity of the complexes **7a** and **76**, veratryl alcohol was chosen as the model compound as it had already been used in the group earlier on.⁶¹ However, instead of using DAIB we chose the more environmental friendly oxidant TBHP. As shown in **Table 3**, TBHP has a relatively high oxygen content, 17.8%, which could improve the atom economy of the transformation (atom economy = molecular weight of desired product/ molecular weight of all reactants). In addition, the reduced product from TBHP is *tert*-butanol which is not harmful to the environment.

In the first set of conditions, we used veratryl alcohol as the substrate, 1 mol% of catalysts **7a** and **76** with 3 eq. of 70% of aqueous TBHP in acetonitrile at 30 °C for 2 hours, separately (**Table 11**). Under these conditions, with the reference catalyst **7a**, 95% of substrate was transformed, producing the corresponding aldehyde in 49% and the carboxylic acid in 43%. Interestingly, using **76**, the conversion of the substrate was 85% with 57% and 26% of corresponding aldehyde and carboxylic acid, respectively. Hence, we can infer that the complex **76** is milder than **7a**.

Table 11. Oxidation of veratryl alcohol with two different Fe(III)TAML complexes using TBHP as the oxidant.



Entry	Catalyst	Conversion %	Yield of aldehyde %	Yield of acid %
1	7a	95	49	43
2	76	85	57	26

GC yield. Conditions: solvent CH₃CN 3 mL, Fe^{III} 1mol%, substrate 100 mM, TBHP (70% in water solution) 3 eq. 0.12 mL, 303 K, 2 h.

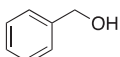
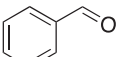
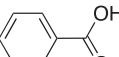
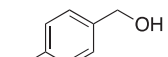
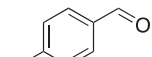
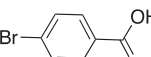
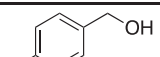
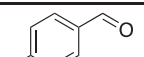
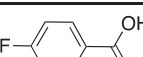
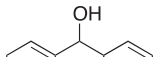
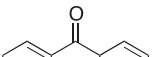
On the basis of these preliminary studies, we investigated the effect of the substituent on the alcohol (**Table 12**). We first tried the catalytic oxidation of the non-substituted benzyl alcohol with the two different catalysts. Using catalyst **7a**, benzyl alcohol was converted into benzaldehyde and benzoic acid with 51% conversion, and 40% yield for the aldehyde and 11% yield for the acid, respectively (**Table 12**, entry 1). With catalyst **76**, the conversion decreased to 40% with only 33% yield of aldehyde and 6% of acid, respectively (**Table 12**, entry 2). Compared to veratryl alcohol, the benzyl alcohol without the electron rich MeO– substituent tended to be less reactive. Similarly, under these conditions, catalyst **76** was less efficient than **7a**.

We also tried the oxidation of electron poor substrates bearing Br or F substituents on the aromatic ring with the two catalysts (**Table 12**, entry 3-6). By comparing entries 3 and 5, using the catalyst **7a**, the two electron-poor substrates were transformed in about 60% yield. This result is quite similar to the one observed with unsubstituted reactants. By comparison between entries 4 and 6, using the same catalyst **76**, one can observe that the conversions were similar, around 50%, with similar proportions of carboxylic products. However, comparing entries 3 and 4, and 5 and 6 separately, we could see

that using catalyst **76**, the conversion is a little lower than with **7a**.

Finally, secondary benzyl alcohols were subjected to oxidation (**Table 12**, entries 7-10). From entries 7 to 8, in the oxidation of 1-phenylethanol, catalysts **7a** and **76** displayed similar efficiencies as the ketone was isolated in similar yields in both cases. When diphenylmethanol was oxidized in the presence of the two catalysts, quantitative yields of ketone were obtained under both conditions within 2 hours. It can be inferred that the two catalysts had similar activities for the oxidation of secondary alcohols under our conditions.

Table 12. Oxidation of different alcohols with Fe(III) complexes using TBHP as the oxidant.

Entry	Catalyst	Substrate	Conv. %	Products and yield %			
1	7a		51		40		11
2	76		40		33		6
3	7a		64		45		17
4	76		52		41		10
5	7a		61		41		18
6	76		50		37		12
7	7a		56		56		
8	76		57		57		
9	7a		100		100		
10	76		100		100		

GC yield. Conditions: solvent CH₃CN 3 mL, Fe^{III} 1mol%, substrate 100 mM, TBHP (70% in water solution) 3 eq., 303 K, 2 h.

In conclusion, in the oxidation of benzylic alcohols, we compared the catalytic activity of the two complexes **7a** and **76**. The oxidation was conducted with 1 mol% of catalyst with TBHP at 30 °C. As for all the benzyl alcohols, the catalytic activity of catalyst **7a**

appeared higher than that of **76**. However, regarding benzylic secondary alcohols, the activities of complexes **76** and **7a** were the same. These observations are in agreement with the fact that **76** has a milder oxidation activity than **7a**, as demonstrated by the electrochemical measurements.

The oxidation of benzylic alcohols have been investigated with different iron(TAML) catalysts in the presence of TBHP. We are curious to know whether manganese complexes also have reactivities towards the oxidation of benzylic alcohols. Thus, we investigated the oxidation of benzylic alcohols with $\text{Mn}^{\text{II}}(\text{MeEBC})\text{Cl}_2$ combined with H_2O_2 .

Part III. Results and discussion on Manganese complex

1 Catalytic oxidation of alcohols

1.1 Choice of the catalyst and the oxidant

Over the past 6 years, our research group has studied the oxidation of alcohols with Fe(TAML)Li in the presence of DAIB. Good yields and selectivity were generally obtained.⁶¹ Within the course of our development of environmental benign catalytic oxidation, we chose a manganese(II) metal complex with a cross-bridged cyclam ligand [Mn^{II}(Me₂EBC)Cl₂] (**Figure 77**), which was kindly provided by Prof. Guochuan Yin, and hydrogen peroxide as a green oxidant. This catalyst had been fully characterized previously and had been used for hydrogen abstraction, oxygen transfer reaction and C-H bond activation and other applications.^{79,80,147,161,162} As shown in **Table 3**, H₂O₂ has a very high oxygen content, up to 47.0%, much higher than the other oxidants such as O₃, NaClO, TBHP and PhIO, which could improve the atom economy greatly. Moreover, the reducing product from H₂O₂ is water, which is really green to the environment. In addition, it has been reported that H₂O₂ can activate [Mn^{II}(Me₂EBC)Cl₂] for a lot of applications, such as oxidation of sulfide,⁸⁰ epoxidation of olefins,^{161,162} and hydrogen abstraction of 1,4-cyclohexadiene.⁸⁰ Herein, we disclose that [Mn^{II}(Me₂EBC)Cl₂] complex can also catalyze the oxidation of a series of benzylic and aliphatic alcohols with H₂O₂.

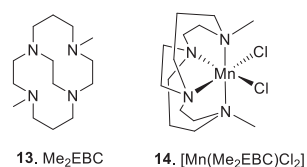


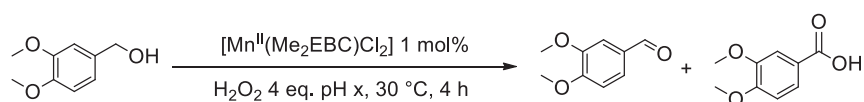
Figure 77. Structures of the cross-bridged cyclam Me₂EBC and the corresponding manganese(II) complex [Mn^{II}(Me₂EBC)Cl₂].

1.2 Optimization the reaction conditions

In the oxidation of alcohols, lots of substrates can be chosen. Our Laboratory has long used veratryl alcohol as a reference substrate, as it is an acknowledged lignin model compound. Accordingly, we decided to carry out our screening on this substrate, using $[\text{Mn}^{\text{II}}(\text{Me}_2\text{EBC})\text{Cl}_2]$ as the catalyst and H_2O_2 as the oxidant for determining the optimal conditions. As previously reported, pH plays a vital role in oxidation reactions with H_2O_2 and it governs the nature of the oxidated form of $[\text{Mn}^{\text{II}}(\text{Me}_2\text{EBC})\text{Cl}_2]$.^{62,66,69}

We first investigated the oxidation of veratryl alcohol at different pH values. We found that at pH 1, 2 or 3, veratryl alcohol was quantitatively converted to the corresponding aldehyde and acid in up and to 80% and 12% yield, respectively, in the presence of 1 mol% of catalyst and 4 eq. of H_2O_2 in 4 hours (**Table 13**, entries 1–3). However, at higher pH (from 4 to 5), the conversion of veratryl alcohol dropped rapidly to 51% at pH 4 and 22% at pH 5 (**Table 13**, entries 4–5). Therefore, we could infer that at $\text{pH} > 3$, the reactivity of the manganese(II) complex decreases. Due to the better selectivity observed and relatively milder conditions at pH 3, we fixed the working conditions at pH 3 using HCl.

Table 13. Oxidation of veratryl alcohol with $[\text{Mn}^{\text{II}}(\text{Me}_2\text{EBC})\text{Cl}_2]$ and H_2O_2 at different pH.



Entry	pH	Conversion (%)	Yield of aldehyde (%) ^[a]	Yield of acid (%) ^[a]
1 ^[b]	1	99	72	11
2	2	98	70	12
3	3	99	80	12
4	4	51	47	0
5	5	22	19	0
6 ^[c]	3	98	83	9
7 ^[d]	3	99	81	11

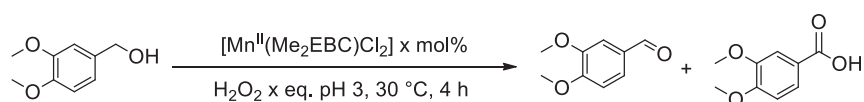
^[a] GC yields. Conditions: solvent $\text{CH}_3\text{CN}/\text{H}_2\text{O}$: 5 mL (4:1), substrate 100 mM, $[\text{Mn}^{\text{II}}(\text{Me}_2\text{EBC})\text{Cl}_2]$ 1 mol%, H_2O_2 0.17 mL 4eq., 303 K, 4 h, pH: adjusted with HCl. ^[b] 3 h; ^[c] pH adjusted with H_2SO_4 ; ^[d] pH adjusted with HNO_3 .

Besides, we investigated the influence of the chloride counter anion in the acid used for lowering the pH. Hence, H_2SO_4 and HNO_3 in replacement of HCl were also investigated for adjusting the working pH at 3. In the presence of H_2SO_4 or HNO_3 , both the conversions and the yields were similar to the results obtained in the presence of HCl (**Table 13**, entry 6 – 7). Accordingly, contrary to former reports from the literature disclosing that the nature of the counter-anion could accelerate the kinetics of the reaction,^{62,67,175} in our conditions, the nature of the counter anion (i.e. Cl^- vs. HSO_4^- or NO_3^-) did not influence significantly the outcome of the reaction.

Next, we investigated the effect of the catalytic charge and the optimal amount of H_2O_2 at pH 3 at 30°C (**Table 14**). Firstly, a control experiment carried out with H_2O_2 only

confirmed that the manganese(II) catalyst was essential for the transformation (**Table 14**, entry 1). Entries 2 to 5 revealed that the conversions increased dramatically from 36% to 99% when increasing the amount of catalyst from 0.1 to 1 mol%. Thus, a minimum catalytic charge of 0.5 mol% appeared necessary for ensuring the efficient transformation of the substrate.

Table 14. Oxidation of veratryl alcohol with different amounts of $[\text{Mn}^{\text{II}}(\text{Me}_2\text{EBC})\text{Cl}_2]$ and oxidant.



Entry	Amount of catalyst /mol%	Amount of H_2O_2 / eq.	Conversion /%	Yield of aldehyde /% ^[a]	Yield of acid /% ^[a]
1	0	4	9	5	0
2	0.1	4	36	28	1
3	0.3	4	75	61	3
4	0.5	4	89	76	7
5	1	4	99	80	12
6	1	1	77	61	1
7	1	2	89	68	3
8	1	3	95	75	9

^[a] GC yields. Conditions: solvent $\text{CH}_3\text{CN}/\text{H}_2\text{O}$: 5 mL (4:1) substrate 100 mM, $\text{Mn}^{\text{II}}(\text{Me}_2\text{EBC})\text{Cl}_2$, H_2O_2 , pH 3, 303 K, 4 h. pH adjusted with HCl.

On this basis, we also investigated the influence of the amount of H_2O_2 (**Table 14**, entries 5–8). With 3 or 4 equivalents of H_2O_2 , conversions were excellent, reaching 99%. By taking into consideration the efficiency, the selectivity and the cost-effectiveness of the transformation, we chose the conditions used in the entry 4, namely

0.5 mol% of manganese(II) catalyst and 4 equivalents of H₂O₂ as the best compromise.

The effect of the reaction time was also investigated (**Figure 78**). When the reaction was run for 6 hours, the conversion reached 99% but at the expense of the selectivity. Indeed, upon running the reaction from 4 to 6 hours, the selectivity dropped down from 9/1 to 5/1, the aldehyde remaining the major product. Hence the quantity of aldehyde reached the maximum after 5 h before slowly decreasing upon oxidation to the corresponding acid.

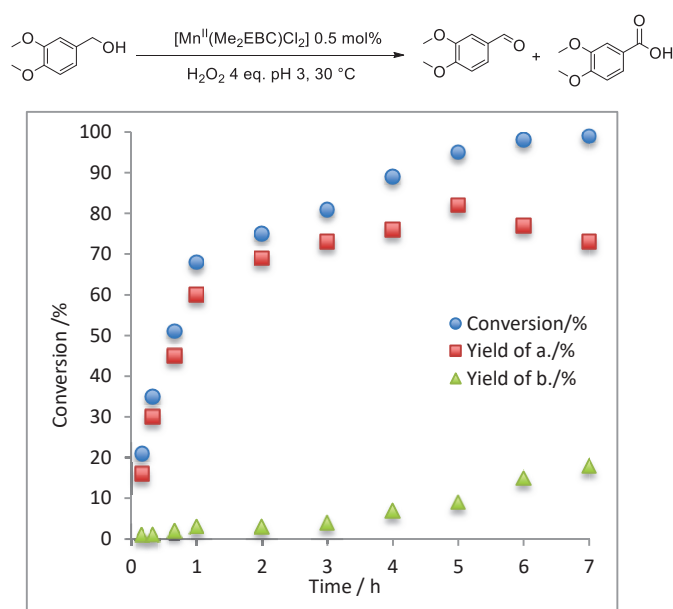


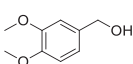
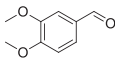
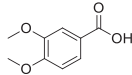
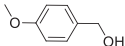
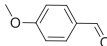
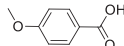
Figure 78. Kinetics of the oxidation of veratryl alcohol with [Mn^{II}(Me₂EBC)Cl₂] in the presence of H₂O₂. Conditions: solvent CH₃CN and H₂O 5 mL (4:1), substrate 100 mM, [Mn^{II}(Me₂EBC)Cl₂] 0.5 mol%, H₂O₂ 0.17 mL, pH 3, 303 K, pH adjusted with HCl.

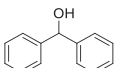
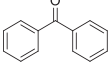
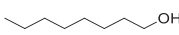
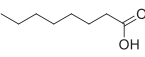
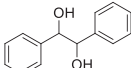
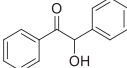
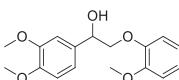
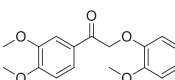
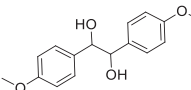
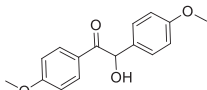
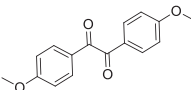
In conclusion, this preliminary study demonstrates that the optimal conditions for oxidizing veratryl alcohol to the corresponding aldehyde involves a catalytic charge of 0.5 mol%, 4 equivalents of H₂O₂ and a 5 h reaction at pH 3 and 30 °C, knowing that the maximum conversion was reached after 6 h.

1.3 Investigation on the scope of substrates

Based on these preliminary studies, we investigated the effect of the substitutions on the alcohol (**Table 16**). As expected, the major effect of the transformation seemed to be the electron richness of the alcohol. Indeed, if the veratryl alcohol was converted to the corresponding aldehyde and acid in 98% in 6 h (**Table 15**, entry 1), the *para*-methoxy benzyl alcohol lacking one -OMe group compared with the parent compound could not be transformed to the corresponding aldehyde or acid in more than 86% conversion even after 18 h (**Table 15**, entry 2). The relative position of the substituent did not influence either, as the *ortho*-methoxy benzyl alcohol analogue was oxidized to the corresponding aldehyde and acid in similar range (**Table 15**, entry 3). The benzyl alcohol (without any substituent) was proven even less reactive as after 6 h the conversion remained in the 40% range and reached 78% after 18 h (**Table 15**, entry 4). However, this decent conversion was obtained at the expense of the selectivity as benzoic acid was generated in substantial amount.

Table 15. Oxidation of different types of alcohols with $[\text{Mn}^{\text{II}}(\text{Me}_2\text{EBC})\text{Cl}_2]$ and H_2O_2 .

Entry	Substrate	Conv. (%)	Aldehyde or ketone		Acid	Yield (%) ^[a]
			Yield (%) ^[a]	Yield (%) ^[a]		
1		98		77		15
2		69 (86)		68 (79)		(6)
3		73 (89)		69 (81)		(6)

4		40 (78)		37 (59)		(11)
5		42 (63)		39 (63)		
6		(32)		(32)		
7		(24)		(11)		(12)
8		(60)		(60)		
9		100/ 100 ^[b]		99/ 99 ^[b]		
10		95/ 95 ^[b]		95/ 95 ^[b]		
11		58/ 96 ^[b,c]		56/ 95 ^[b,c]		
12		98		68		29

^[a] GC yields. Conditions: solvent CH₃CN/ H₂O: 5 mL (4:1) substrate 100 mM, Mn^{II}(Me₂EBC)Cl₂ 0.5 mol%, H₂O₂ 0.17 mL 4eq., pH 3, 303 K, 6 h. ^[b] H₂O₂ 0.34 mL 8 eq.; ^[c] Mn^{II}(Me₂EBC)Cl₂ 1 mol%; Data in brackets: 18 h.

When secondary benzylic alcohols were used in the oxidation (**Table 15**, entries 5–6), the corresponding ketone was isolated in good yield (63%) in the case of the methyl ketone but a relatively long reaction time was proven necessary. However, the diphenylmethanol was more reluctant to oxidation, as the expected ketone was isolated in 32% yield, even after a prolonged reaction time (**Table 15**, entry 6). Similarly, an aliphatic alcohol containing a long alkyl chain such as 1-octanol (**Table 15**, entry 7)

appeared little reactive under our conditions. Interestingly, cyclohexanol was transformed much more efficiently and cyclohexanone was isolated in a decent 60% yield (**Table 15**, entry 8).

On the contrary, very high conversions and selectivities were obtained with 1,2-cyclohexanediol (**Table 15**, entry 9) and 1,2-diphenyl-ethane-1,2-diol (**Table 15**, entry 10). In the latter cases, the corresponding mono-ketones were produced in quantitative yields. Interestingly, the mono-ketones were not further oxidized even in the presence of a larger excess of H₂O₂ (8 equiv. vs. 4 equiv.). This observation was consistent with the former observation regarding the higher reactivity of electron rich alcohols. Hence, an excellent selectivity could be obtained in the case of polyols displaying different environment. For this reason, we investigated the oxidation of lignin model compounds that could be of great interest for understanding the reactivity of lignin. As in lignin, the β -O-4 junctions are the most abundant,^{176,177} we decided to investigate a classical β -O-4 model (**Table 15**, entry 11). In our optimized conditions, the desired ketone was isolated in a moderate 56% yield, but with an excellent selectivity. For this reason, we decided to harden the reaction conditions by doubling the amount of catalyst to 1 mol% and H₂O₂ to 8 equiv. Under these conditions, we were pleased to observe that the conversion went up dramatically and reached 96% while maintaining an excellent selectivity (99%). Using the same conditions, we investigated the reactivity of a β -1 lignin model compound (**Table 15**, entry 12). After 6 h, the transformation of the starting material was almost complete, but a mixture of mono-ketone and dione was obtained. The mono- and diketone were isolated in 68 and 29% yield, respectively. Interestingly though, no C-C bond cleavage was observed. These promising results suggest that the combination of [Mn^{II}(Me₂EBC)Cl₂] with H₂O₂ may constitute an alternative for the valorization of lignin, a bio-source of aromatic compounds.¹⁷⁷

1.4 Mechanistic study

In order to gain some insights on the mechanism of the oxidation reaction, we first investigated the possible existence of radical intermediates. As *t*-BuOH is an acknowledged radical scavenger,¹⁷⁸ we decided to perform the oxidation of veratryl alcohol in the *t*-BuOH/H₂O (4:1) solvent mixture to prevent any radical formation. In these solvent conditions, veratryl alcohol was converted in 67% and afforded veratraldehyde in 65% yield. Hence, this result accounts for a mechanism involving a highly oxidized Mn complex precluding the presence of hydroxyl radicals.^{160,178}

Moreover, we confirmed the absence of hydroxyl radical intermediates using EPR measurements. According to the literature, DMPO (5,5-dimethyl-1-pyrroline-*N*-oxide) trapped radicals affording a DMPO radical adduct that displays a typical four-line EPR spectra^{159,179,180} Consequently, we added DMPO to our experimental conditions and followed the reaction using EPR. As shown in the **Figure 79**, upon adding H₂O₂ to a solution of [Mn(Me₂EBC)Cl₂] and DMPO at pH 3, only the EPR signal of residual Mn(II) ($g \sim 2$, $a_{Mn} \sim 90G$), was observed.¹⁸¹ Hence, this observation confirmed the absence of hydroxyl radicals in our reaction conditions.

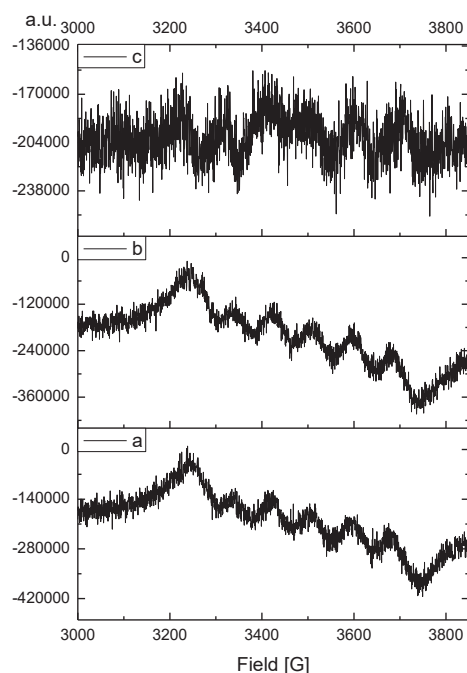


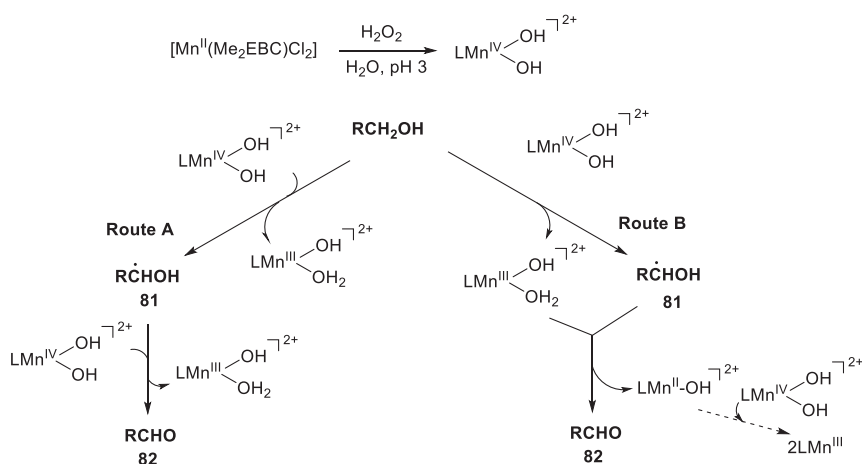
Figure 79. Conditions: solvent acetonitrile and water (ratio 4: 1) at pH 3 at room temperature. The EPR spectrum of 30 mM of $[\text{Mn}^{\text{II}}(\text{Me}_2\text{EBC})\text{Cl}_2]$ catalyst. (a) $[\text{Mn}^{\text{II}}(\text{Me}_2\text{EBC})\text{Cl}_2]$ + solvent, (b) $[\text{Mn}^{\text{II}}(\text{Me}_2\text{EBC})\text{Cl}_2]$ + solvent + 0.2 M of DMPO, (c) $[\text{Mn}^{\text{II}}(\text{Me}_2\text{EBC})\text{Cl}_2]$ + solvent + 0.2 M of DMPO + 0.4 M of 30% H_2O_2 .

To determine the oxidation state of the active Mn species responsible for the catalytic performance (Mn^{IV} or Mn^{V}), we synthesized the $[\text{Mn}^{\text{IV}}(\text{Me}_2\text{EBC})(\text{OH})_2](\text{PF}_6)_2$ complex from $[\text{Mn}(\text{Me}_2\text{EBC})\text{Cl}_2]$ using a known procedure.^{138,147} Without using any oxidant, veratryl alcohol was transformed rather efficiently by a stoichiometric amount of the manganese(IV) complex as the expected aldehyde and acid were isolated in 22 and 7% yield, respectively with a conversion of 40%. This result clearly demonstrates that $[\text{Mn}^{\text{IV}}(\text{Me}_2\text{EBC})(\text{OH})_2]^{2+}$ is capable of oxidizing veratryl alcohol even without any oxidant.

In addition, when $[\text{Mn}(\text{Me}_2\text{EBC})\text{Cl}_2]$ was reacted with an excess of H_2O_2 , only $[\text{Mn}^{\text{IV}}(\text{Me}_2\text{EBC})]^{2+}$ was observed.⁸¹ No higher valent species was generated with this

ligand under these conditions.^{81,147} At last, Prof. Yin *et al.* reported that $[\text{Mn}^{\text{IV}}(\text{Me}_2\text{EBC})(\text{OH})_2]^{2+}$ is the main species observed in acidic media.^{147,150} Consequently, $[\text{Mn}^{\text{IV}}(\text{Me}_2\text{EBC})(\text{OH})_2]^{2+}$ is certainly responsible for the catalytic activity.

Hence, we can propose the following mechanism for explaining the catalytic activity of $[\text{Mn}(\text{Me}_2\text{EBC})\text{Cl}_2]$ at pH 3 in the presence of an excess of H_2O_2 and veratryl alcohol as the substrate (**Scheme 36**). In the presence of H_2O_2 at pH 3, $\text{Mn}(\text{Me}_2\text{EBC})\text{Cl}_2$ is oxidized generating the $[\text{LMn}^{\text{IV}}(\text{OH})_2]^{2+}$ ($\text{L} = \text{Me}_2\text{EBC}$) complex. Next, the Mn^{IV} intermediate can directly oxidize a molecule of alcohol through hydrogen atom abstraction (**Route A**), affording the alcohol radical (**81**) and the reduced $[\text{LMn}^{\text{III}}(\text{OH})(\text{OH}_2)]^{2+}$ complex. **81** can be further oxidized by another $[\text{LMn}^{\text{IV}}(\text{OH})_2]^{2+}$ to afford the expected aldehyde (**82**). Hence, two equivalents of $[\text{LMn}^{\text{IV}}(\text{OH})_2]^{2+}$ are required for producing one equivalent of aldehyde and two equivalents of $[\text{Mn}^{\text{III}}(\text{OH})(\text{OH}_2)]^{2+}$. An alternative route (**Route B**) may involve the transfer of a hydroxyl group to the alcohol radical (**81**) through an oxygen rebound mechanism. Upon losing a water molecule, the acetal produces the expected aldehyde. Meanwhile, the Mn complex is reduced to Mn(II) that further reacts with a Mn(IV) complex producing a Mn(III) upon disproportionation which is favored in acidic media.^{147,149}



Scheme 36. Two possible routes of oxidation of alcohols by manganese complexes in the presence of H_2O_2 .

1.5 Conclusions

In conclusion, we have developed an efficient catalytic system from a bioinspired manganese(II) complex $[\text{Mn}(\text{Me}_2\text{EBC})\text{Cl}_2]$ combined with an environmentally benign oxidant H_2O_2 at pH 3. This new catalytic system has a high efficiency in the oxidation of a range of benzylic alcohols and some aliphatic alcohols. More interestingly, it was proven to be a very powerful method for the oxidation of lignin model compounds. Especially, β -O-4 model molecule was transformed almost quantitatively to the corresponding ketone without C-C bond cleavage. In addition, a mixture of H_2O and MeCN was used instead of acetone and advantageously precluded the possible oxidation of acetone with H_2O_2 . Substrates displaying electron enriched alcohols are proven more reactive and allow for obtaining high selectivities in the oxidation of unsymmetrical diols. At last, we have proven that the oxidation process does not involve any radical and most likely relies on a high valent manganese(IV) complex.

2 Catalytic oxidation of olefins

2.1 Introduction of oxidation of olefins

Catalytic epoxidation is an important transformation in synthesis of organic compounds, and over the last decades, numerous catalytic methods have been developed to generate epoxides.¹⁸² Within the frame of this thesis, we have concentrated on Mn complexes that have been proven the most efficient with H₂O₂ as the oxidant. Various manganese complexes have been developed for the catalytic epoxidation of alkenes, such as manganese-salen,^{182,183} manganese porphyrins,^{184,185} manganese aminopyridine¹⁸⁶ and other manganese complexes.¹⁸⁷ Yin *et al.* have reported that [Mn^{II}(Me₂EBC)Cl₂] can catalytically perform the epoxidation of olefins such as cyclohexene, styrene, norbornylene and *cis*-stilbene in medium yields in the presence of H₂O₂.¹⁶¹ For these reasons, we have decided to evaluate the conditions we have established for the oxidation of alcohols to the epoxidation of alkenes.

2.2 Epoxidation of olefins

We first investigated the epoxidation of cyclohexene with [Mn^{II}(Me₂EBC)Cl₂] and H₂O₂ at pH 3 at 303 K in a mixture of acetonitrile and water for 6 h. It was found that using these conditions, the conversion of cyclohexene reached 97%, and the corresponding epoxide could be isolated in 95% yield. Only traces of cyclohexane-1,2-diol and 2-hydroxycyclohexanone could be detected (**Figure 80**). Hence, the selectivity was up to 98%.

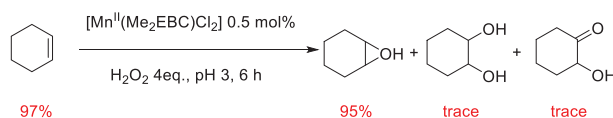
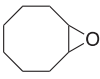
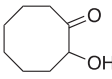
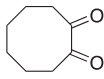
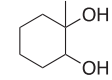
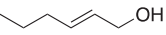
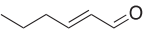
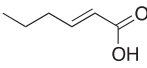
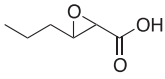


Figure 80. Epoxidation of cyclohexene with [Mn(Me₂EBC)Cl₂] in the presence of H₂O₂.

Next, we investigated other alkenes (**Table 16**) such as cyclooctene, 1-methylcyclohex-1-ene, (*E*)-hex-2-en-1-ol. The corresponding results are gathered in **Table 16**. Cyclooctene has a structure quite similar to that of cyclohexene. Yet the selectivities of the oxidation were quite different. In 18 hours, cyclooctene was fully converted but the amount of 2-hydroxycyclooctanone (58%) was twice that of the epoxide (30%). Cyclooctane-1,2-dione was also detected (11%). Hence, we can conclude that in our conditions, cyclohexene was prone to undergo epoxidation while cyclooctene is more prone to producing alcohol which is further oxidized to the corresponding ketone. 1-methylcyclohex-1-ene was also fully converted in 18 hours but with 74% of identified products including 11% of epoxide, 42% of 2-methylcyclohex-2-enone and 21% of 1-methylcyclohexane-1,2-diol. In the oxidation of (*E*)-hex-2-en-1-ol, with both the alkene and hydroxyl functional groups, the results should be interesting. With 8 eq. of H₂O₂, the substrate was oxidized and produced 30% of aldehyde, 17% of carboxylic acid and 5% of 3-propyloxirane-2-carboxylic acid. From the result, we could infer that the alcohol was easier to oxidize than the alkene under our conditions.

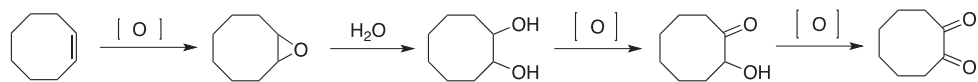
Table 16. Epoxidation of olefins with $[\text{Mn}^{\text{II}}(\text{Me}_2\text{EBC})\text{Cl}_2]$ and H_2O_2 .

Entry	Conv. of		Yield of Products /% ^[a]	
	Substrates /% ^[a]			
1 ^[b]	 97	 95	 trace	 trace
2	 85(99)	 27(30)	 50(58)	 6(11)
3	 57(100)	 17(11)	 16(42)	 12(21)
4	 68	 30	 17	 5

^[a] GC yields. Conditions: solvent $\text{CH}_3\text{CN}/\text{H}_2\text{O}$: 5 mL (4:1) substrate 100 mM, $[\text{Mn}^{\text{II}}(\text{Me}_2\text{EBC})\text{Cl}_2]$ 0.5 mol%, H_2O_2 0.17 mL 4eq., pH 3, 303 K, 6 h.; Data in brackets: 18 h.

2.3 Mechanistic study

The mechanism of epoxidation by $[\text{Mn}(\text{Me}_2\text{EBC})\text{Cl}_2]$ with H_2O_2 was proven to proceed through an oxygen transfer mechanism by a manganese(IV) complex generated *in situ*.¹⁶¹ The oxidation of cyclooctene produced more 2-hydroxycyclooctanone than epoxide, along with cyclooctane-1,2-dione. According to literature precedents (**Scheme 37**), cyclooctene is firstly converted to epoxide according to an oxygen transfer mechanism.¹⁸⁸ With water in the system, the epoxide can next hydrolyze to the corresponding cyclooctane-1,2-diol, which is further oxidized to 2-hydroxycyclooctanone or cyclooctane-1,2-dione.



Scheme 37. Oxidation of cyclooctene.¹⁸⁸

2.4 Conclusions

Under our conditions, the epoxidation of several substrates using $[\text{Mn}(\text{Me}_2\text{EBC})\text{Cl}_2]$ in the presence of H_2O_2 at pH 3 at room temperature is efficient. However, the selectivity strongly depends on the nature of the substrate. Cyclohexene is epoxidized with an excellent selectivity. Conversely, the oxidation of the other substrates was shown more complicated as mixtures of epoxide and other products such as alcohols and ketones was obtained. The presence of H_2O and acid in our conditions tend to ring open the oxirane affording alcohols that can be further oxidized to ketones or acids.

3 Catalytic oxidation of other substrates

3.1 Catalytic oxidation of 5-HMF

Hydroxymethylfurfural (5-HMF, **83**) (**Figure 81**) is an important basic material in fine chemicals. It is a platform molecule produced from C6 sugars that can afford a number of compounds, such as 2,5-furandicarboxylic acid, 2,5-bishydroxymethylfuran, levulinic acid and so on upon oxidation/hydration reactions.¹⁸² 2,5-diformylfuran (DFF, **84**) (**Figure 81**) also has various applications, such as starting material of making drugs, antifungal agents or ligands.¹⁸⁹ As shown in **Figure 81**, 5-HMF has one aldehyde and one alcohol functional groups, while DFF has only aldehyde. Within the frame of our screening, we have decided to investigate the oxidation of 5-HMF to possibly produce DFF.

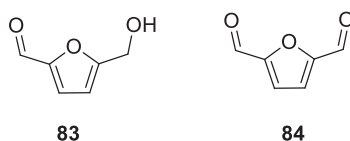


Figure 81. Structure of 5-HMF and DFF.

First, we tried the oxidation of HMF with $[\text{Mn}^{\text{II}}(\text{Me}_2\text{EBC})\text{Cl}_2]$ and H_2O_2 at pH 3 in a mixture of acetonitrile and water (**Figure 82**). After 6 hours, 34% of 5-HMF was converted and 27% of DFF was produced. From a GC-MS analysis, two other products could be identified: 5% of (*E*)-2,5-dioxohex-3-enedial and traces of the corresponding acid. When we doubled the amount of catalyst and oxidant, after 19 hours, the conversion increased to 50% and 37% of DFF and 11% of byproduct were identified.

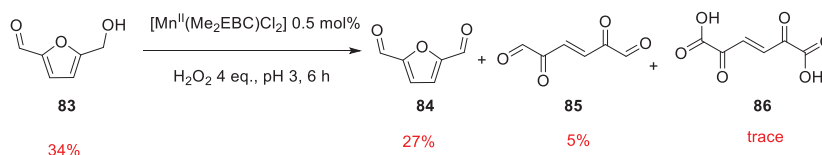


Figure 82. Catalytic oxidation of 5-HMF to DFF.

According to literature reports, acidic conditions are harmful for forming DFF. Accordingly most researchers use bases.^{190,191} For this reason, we tried to perform the oxidation of HMF in neutral solvent, the other parameters remaining unchanged. With 1 mol% of manganese(II) catalyst and 8 eq. of H_2O_2 , after 17 hours, the conversion of HMF was 16% with 14% of DFF, without any byproducts. However, the conversion was too low for presenting any interest. Accordingly, we gave up with this approach.

In conclusion, we try to oxidize 5-HMF to form DFF with $[Mn^{II}(Me_2EBC)Cl_2]$ and H_2O_2 under different conditions. At low pH, the conversion was satisfying but undesirable byproducts were formed. Under neutral conditions, the efficiency was too low. Hence, it appeared that our conditions were not suitable for the oxidation of HMF.

3.2 Catalytic oxidation of lignin model compounds

Lignin is a renewable aromatic polymer, abundant in the lignocellulosic biomass.¹⁹² The valorization of this renewable resource for the production of aromatic chemicals is important for sustainable chemistry. Therefore, the depolymerization of lignin is a key technology for solving this problem. Numerous methods have been developed for the depolymerization of lignin, but it is still troublesome.¹⁹³⁻¹⁹⁵

Our Laboratory also makes efforts in this field by investigating the catalytic oxidation of lignin model compound with $Fe(TAML)Li/DAIB$.⁶¹ We also tried the oxidation of two lignin model compounds with β -O-4 and β -1 linkages by using manganese(II)

catalyst and H₂O₂, with high conversions.⁶¹ Herein we tried other model compounds containing α -O-4, α -1 and β -O-4 (**Figure 83**).

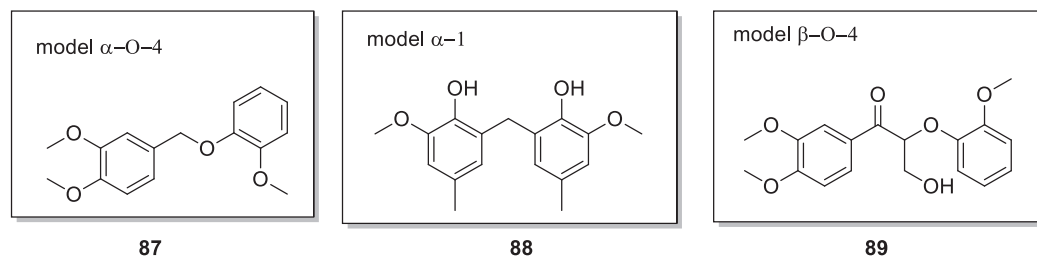


Figure 83. Structures of the lignin model compounds.

Oxidation of lignin model compounds **87**, **88**, **89** (**Figure 83**) was carried out with [Mn^{II}(Me₂EBC)Cl₂] and H₂O₂ at pH 3 in a mixture of acetonitrile and water at 303 K. After 6 hours, from GC-MS analysis, there is no reaction of compound **87** or **88**, and for compound **89**, 5% of GC yield was obtained (**Figure 84**). When we increased the amount of catalyst to 1 mol% and H₂O₂ to 8 eq., after 18 hours, there was no further improvement of this reaction. Compared to the other model compound containing β -O-4, we infer that the hydroxyl in this compound is not as active as the other one (entry 12 in **Table 15**).

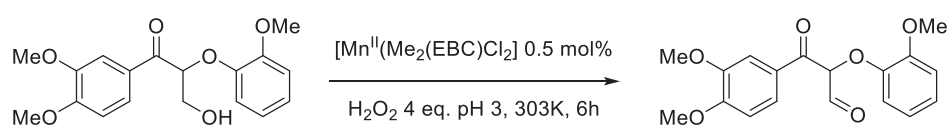


Figure 84. Conversion of model compound **89** to corresponding oxide.

In conclusion, in the oxidation of lignin model compounds containing α -O-4 or α -1 linkages such as compounds **87** and **88**, there were no reaction. For compound **89** containing a β -O-4 linkage, it reacted but the efficiency was low. It could be inferred that our conditions were not suitable for these substrates.

General conclusion and Perspectives

Conclusions

My research mainly focusses on two directions. First, we have synthesized several new iron complexes based on functionalized TAML ligands for different applications. Second, we have developed an efficient catalytic system from a bioinspired manganese(II) complex $[\text{Mn}^{\text{II}}(\text{Me}_2\text{EBC})\text{Cl}_2]$ and an environmentally benign oxidant H_2O_2 at pH 3.

In the synthesis of functionalized Fe(TAML) complexes, after preliminary results obtained in the group by Dr. Kieffer *et al.*, we have successfully synthesized new catalysts by complexation of iron ion with functionalized TAML ligands. The “simple” TAML-Me₂ was first prepared and studied as the “reference” Fe(TAML-Me₂)Li complex. Besides, the functionalization of the TAML ligand was undertaken both on the “head” and the “tail” (**Figure 85**). On the “head”, we added a bromide on the benzene ring to increase the stability towards oxidation and the selectivity. On the “tail”, we envisioned several strategies. We added a long chain on the tail by inserting a triazole between a TAML-(Me)(CH₂CCH) **75** and an azido through a “click” reaction. Alternatively, the long chain was also replaced by shorter system bearing a triethoxysilane Si(OEt)₃ function that could be used to graft the catalyst on an inorganic support and used in heterogeneous catalysis. At last, the purpose of the fluorinated tail was to increase the solubility of the catalyst in fluorinated solvents where a biphasic catalysis could be realized and the catalyst recycled by phase separation.

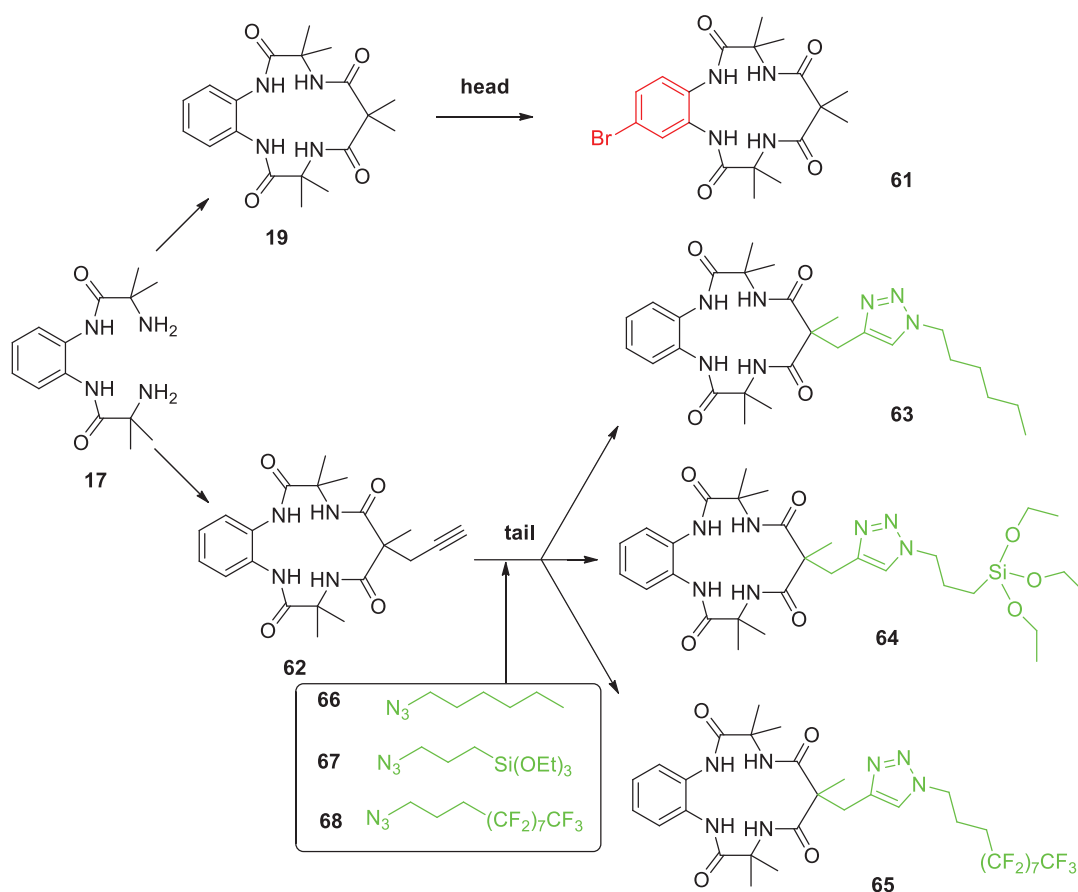


Figure 85. Strategies of functionalization of TAML.

As the Br-TAML-(Me)₂ **61** was proven very difficult to purify and to isolate as a single product the corresponding iron complex was not attempted. Conversely, the other functionalized ligands were successfully converted to the corresponding iron complexes and obtained as pure products (**Figure 86**).

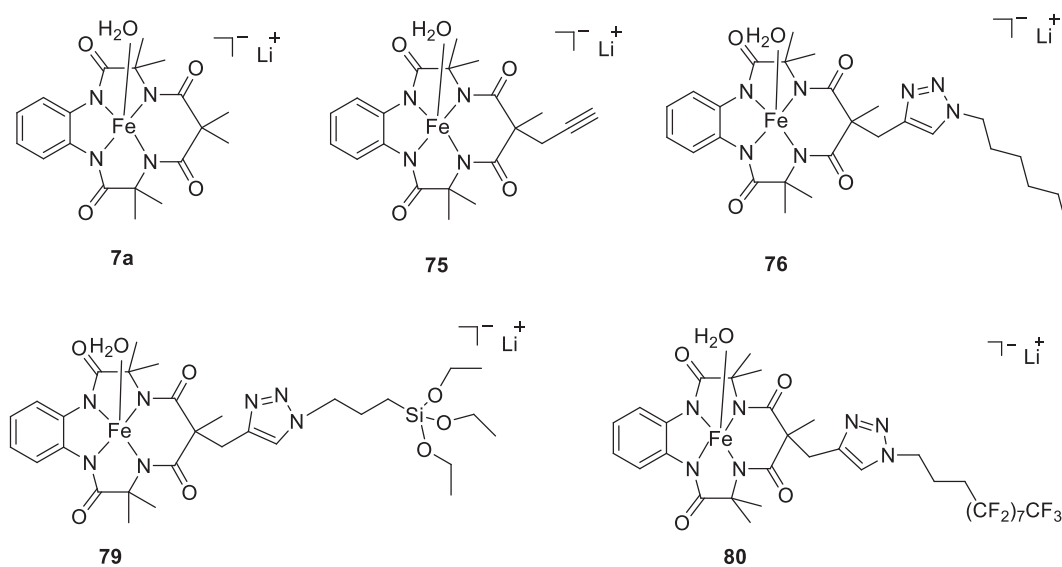


Figure 86. Iron complexes synthesized during this PhD work.

We have also determined and compared the physico-chemical properties of the “reference” complex **7a** Fe(TAML-Me₂)Li and Fe[TAML-(Me)(triazole)]Li **76**. The complete characterization of these two complexes was conducted by electrochemistry, UV-Vis, EPR, and Mössbauer spectroscopies. Regarding electrochemistry, the two complexes presented very different behaviors in three different solvents, namely acetonitrile, methanol and DMF. For example, in acetonitrile, **76** presented a very nice and reversible electrochemical behavior. It was supposed that the first oxidation happened on the ligand, not on the iron center for both complexes. In addition, the UV-Vis spectra of **7a** and **76** display different characteristic absorption peak and absorption coefficient in acetonitrile, methanol and DMF. However, the compound **75** had similar absorption peak with **7a**. It showed that the triazole greatly influenced the absorption of the compounds. As for the EPR analyses of these two compounds, they did not reveal any difference between these two compounds. Accordingly, from these analyses, we concluded that in complex **76**, one nitrogen atom from the triazole tail probably coordinates the center iron in not too strongly coordinating solvents.

Next, we compared the catalytic activity of the two complexes **7a** and **76**. The oxidation of benzylic alcohols was chosen as the prototype reaction, and was conducted with 1 mol% of catalyst, TBHP as oxidant. As for all the benzyl alcohols, the catalytic activity of catalyst **7a** appeared higher than that of **76** under the same conditions. However, regarding benzylic secondary alcohols, the activities of complexes **76** and **7a** were the same. These observations are relevant with the fact that **76** has a milder oxidation activity than **7a**, as demonstrated by the electrochemical measurements.

The second project concentrated on oxidation catalysis using a cross-bridged cyclam coordinated with manganese(II), the $[\text{Mn}^{\text{II}}(\text{Me}_2\text{EBC})\text{Cl}_2]$ complex, which was kindly offered by Prof. Guochuan Yin. We developed an efficient method of catalytic oxidation of benzylic alcohols to the corresponding carboxylic acid with the manganese(II) complex, H_2O_2 as the oxidant at pH 3 and room temperature (**Figure 87**). We found that nearly all the benzylic alcohols were converted with high conversions, except for some aliphatic alcohols. Diols were also transformed with high efficiency and high selectivity to mono ketones. It appeared also powerful for the oxidation of lignin model compounds. In particular, β -O-4 model molecules were converted almost quantitatively to the corresponding ketone without C-C bond cleavage. In addition, a mixture of water and acetonitrile was used at the expense of acetone which is commonly used in oxidation reaction. Advantageously, the MeCN/ H_2O solvent mixture can not undergo oxidation with H_2O_2 , contrary to acetone. A preliminary mechanistic study precluded any trace of hydroxyl radical and proposed that the active species may be a high valent manganese(IV) complex.

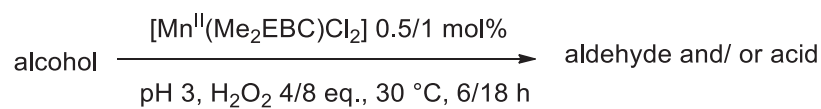


Figure 87. Oxidation of alcohols with $[\text{Mn}(\text{Me}_2\text{EBC})\text{Cl}_2]$ **14** and H_2O_2 .

In the oxidation of other substrates such as olefins and 5-HMF with $[\text{Mn}(\text{Me}_2\text{EBC})\text{Cl}_2]$ and H_2O_2 , only the epoxidation of cyclohexene was proven fruitful both in term of conversion and selectivity. The oxidation of other related substrates afforded too many byproducts to constitute an efficient epoxidation method under these conditions.

Perspectives

During the 3,5 years of PhD work, I have investigated both the synthesis of functionalized Fe(TAML) and homogeneous catalysis with iron and manganese complexes. Both sides have their perspectives.

TAML ligand is a relatively new field compared to porphyrin and salen ligands, especially for uses in synthetic chemistry. Some researches have been reported on different complexes of TAMLs. However, most of the literature concentrated on iron complexes, and their characterization and applications. Other metals such as manganese and copper should also be worth investigating. In addition, the applications of Fe(TAML) mainly focused on homogeneous catalysis. The excellent results we obtained in homogeneous oxidation open new perspectives for a development of heterogeneized Fe(TAML)s. Hence, we have synthesized the $[\text{Fe}(\text{H}_2\text{O})\{\text{TAML}(\text{Me})(\text{triazole}-(\text{CH}_2)_3\text{Si}(\text{OEt})_3)\}] \text{Li}$ complex **79**, which can be supported on inorganic materials (mesoporous silica, for instance) by reacting between $-\text{Si}(\text{OEt})_3$ and hydroxyl groups.

As for the functionalization of Fe(TAML), a lot of progresses have been made. The purpose of functionalization has normally improved the stability. Other functionalizations should also be considered. In our case, the $[\text{Fe}(\text{H}_2\text{O})\{\text{TAML}(\text{Me})(\text{triazole})\}] \text{Li}$ complex **76** we synthesized is the first example of TAML ligands displaying an intramolecularly appended triazole that can coordinate the metal ion. This new system presents special physico-chemical properties, which let us envision new applications besides the oxidation of alcohols that has already been investigated. Besides, an iron TAML complex with a fluorinated tail $[\text{Fe}\{\text{TAML}(\text{Me})(\text{triazole}-(\text{CH}_2)_3(\text{CF}_2)_7\text{CF}_3)\}] \text{Li}$ **80** has been synthesized. This complex with a fluorinated tail can dissolve in fluorinated solvent. We can use it in biphasic reaction, which can turn to one phase at high temperature and phase separate upon cooling. In this way, the catalyst can

be easily separated from product. It would be very useful for catalyst recycling.

In the catalytic oxidation, lignin model compounds are good choices, as the valorization of lignin is a promising field for utilization of biomass. In the oxidation of lignin model compounds, both Fe(TAML) and [Mn(Me₂EBC)Cl₂] were evaluated. However, the products from the oxidation are different. With [Mn(Me₂EBC)Cl₂] as catalyst, the products are only from the oxidation of the hydroxyl group. Conversely, with Fe(TAML), there are products produced from the cleavage of C-C bonds. In addition, with Fe(TAML), lignin model compounds were converted more efficiently than with [Mn(Me₂EBC)Cl₂], but the oxidant combined with manganese catalyst is H₂O₂, which is greener than the DIAB used in combination with Fe(TAML). A greener oxidant with Fe(TAML) needs to be explored. As for [Mn(Me₂EBC)Cl₂], better conditions should be applied in order to transform a larger scope of substrates.

[Mn(Me₂EBC)Cl₂] has been explored for a series of applications, many of which are combined with H₂O₂, which is environmentally friendly. It deserves further applications.

Experimental part

1 General procedures

All the chemical reagents used were commercially available except for lignin model compounds, which were synthesized and characterized previously in our group.⁶ Mn(Me₂EBC)Cl₂ was kindly provided by Prof. Guochuan Yin from Huazhong University of Science and Technology, China. The starting materials were used without further purification except for the following compounds: 1,2-phenylenediamine was recrystallized from ethanol, and *N*-bromosuccinimide was recrystallized from water. *n*-butyl lithium was titrated before being used. The solvents were used without further purification unless stated. Tetrahydrofuran was distilled from sodium/benzophenone under argon, and other anhydrous solvents were purchased from Sigma Aldrich or Carlo Erba. All reactions performed under an argon atmosphere were run in a sealed reaction vials. Reactions were monitored by analytical thin layer chromatography (TLC) using commercial sheets precoated (0.2 mm layer thickness) with silica gel 60F254 (Macherey-Nagel). Column chromatography purifications were carried out either on Macherey-Nagel silica gel or basic aluminum gel.

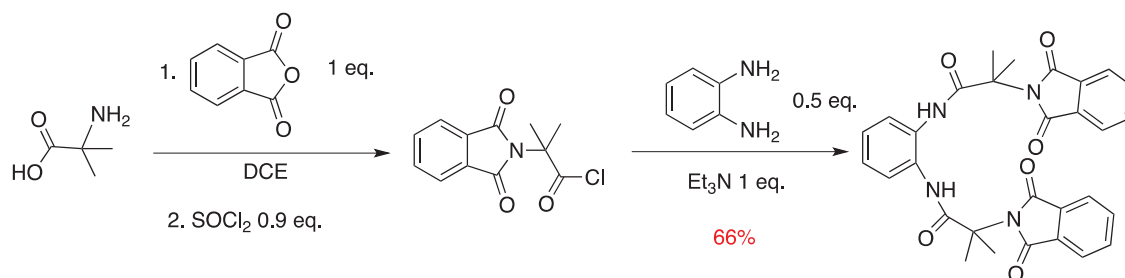
¹H and ¹³C-NMR spectra were obtained on Bruker ALS300, DRX300 or DRX400 spectrometers, and shifts were given relative to the remaining solvent signals (7.26 ppm for CHCl₃). ¹⁹F NMR spectra were recorded at 300 MHz and the chemical shifts are relative to CFCl₃. The following abbreviations were used to explain the multiplicities: s = singlet, d = doublet, t = triplet, q = quartet, m = multiplet, br = broad. High resolution mass spectra (HRMS) were measured by electrospray ionization ion source (ESI-MS), on a mass spectrometer (Micro TOFQ-II, Bruker Daltonics, Bremen). GC-MS analyses were performed on a Shimadzu QP2010 GC/MS apparatus, with a DB-5ms column lined with a mass (EI 0.7 kV) direction system. Electrochemical studies were carried out in a glove box under nitrogen using a carbon electrode, Ag⁺/Ag as reference

electrode, DMFc as internal standard. EPR experiments have been measured using Bruker X-band spectrometer, with standard cavity, at 5-8 K. Microwave power of 6.4mW, modulation amplitude 1G and field modulation 100 kHz were used. Samples were prepared in capillary tubes.

2 Synthetic protocols

2.1 Synthesis of simplest Fe(TAML-Me₂)Li 7a

Synthesis of N,N'-1,2-phenylenebis[2-methyl-2-phthalimidopropanamide] 17c



A 20.2 g of 2-aminoisobutyric acid and 29.1 g phthalic anhydride were mixed in a three neck round bottom flask. The flask was placed in an oil bath and heated to 175 °C. At around 80 °C, phthalic anhydride began to sublime. When 115 °C was reached, the solid began to liquefy and this is complete at around 125 °C. By 155 °C, the mixture was clear. After the water evolution, the reaction was allowed to proceed for 10 minutes.

The solution was removed from the oil bath. The condenser and Argon gas adapter were rapidly connected to the flask. 150 mL of 1,2-dichloroethane was added rapidly. When it cooled down to room temperature, 12.9 mL of thionyl chloride was added, based on the assumption of 10% of the product was the cyclic dimer. The solution was refluxed for 4.5 hrs. Gas evolution appeared to cease after 3 hrs. The solution was cooled to room temperature and filtered to remove the solid.

The orange brown filtrate was transferred to a 3-neck flask. The flask was outfitted with a condenser, Argon adapter, and an addition funnel. 75 mL of 1,2-dichloroethane containing 1,2-phenylenediamine and 10.6 g and triethylamine (27.2 mL) was prepared and placed in the addition funnel. Next, it was added dropwise the funnel under Argon over 30 min. (the 1,2-phenylenediamine was crystallized from ethanol, dried and

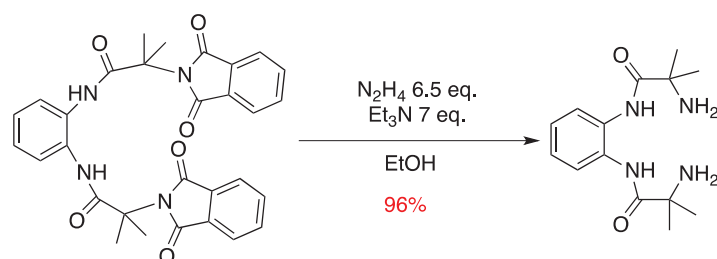
grounded to powder) The solution was refluxed overnight. It was then cooled down to room temperature. 150 mL of water was added to the solution and stirred for 5 minutes. The slurry was filtered, the precipitate was washed with ethanol, which remove the yellow material. The solid was dried then we got white powder (34.6g, yield 66%).

Characterization of N,N'-1,2-phenylenebis[2-methyl-2-phthalimidopropanamide]

¹H NMR (300 MHz, DMSO-d₆): δ (ppm) = 9.41 (br s, 2H, NH), 7.82 (m, 4H, aromatic H), 7.76 (m, 4H, aromatic H), 7.51 (dd, J = 6.0, 3.6 Hz, 2H, aromatic H), 7.16 (dd, J = 6.0, 3.6 Hz, 2H, aromatic H), 1.72 (s, 12H, COC(CH₃)₂).

These results are in agreement with the literature.⁸⁸

Synthesis of N,N'-1,2-phenylenebis[2-methyl-2-methylpropanamide], 17



To a mixture of N,N'-1,2-phenylenebis[2-methyl-2-phthalimidopropanamide] (15.00 g, 27.90 mmol, 1 eq.) and hydrazine hydrate (solution 62%, 9.09 mL, 181.00 mmol, 6.5 eq.) in absolute ethanol (180 mL), triethylamine (Et₃N) (27.15g, 195.30 mmol, 7 eq.) was added dropwise over 30 minutes. Next, the solution was stirred under reflux for 12 hours.

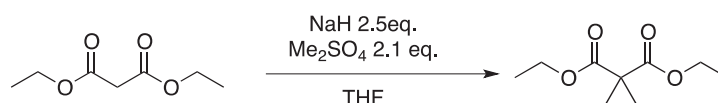
The solution was cooled down to room temperature and concentrated under vacuum. Next, ethyl acetate (350 mL) was added to the yellow powder, the suspension was stirred for 15 minutes and filtered. The filtrate was concentrated under reduced pressure to provide the desired compound as a white powder (7.43 g, yield 96%).

Characterization of N,N'-1,2-phenylenebis[2-methyl-2-methylpropanamide]

¹H NMR (300 MHz, DMSO-d₆): δ (ppm) = 7.61 (dd, J = 6.0, 3.5 Hz, 2H, aromatic H), 7.16 (dd, J = 6.0, 3.5 Hz, 2H, aromatic H), 1.34 (s, 12H, COC(CH₃)₂).

These results are in agreement with the literature.⁸⁸

Synthesis of diethyl 2,2-dimethylmalonate 18b

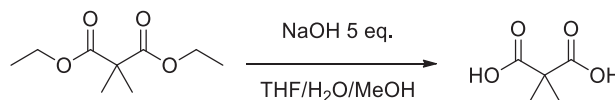


In freshly distilled THF (100 mL) containing sodium hydride (60% in oil, 3.74g, 93.70 mmol, 2.5 eq.) under argon, diethyl malonate (5.72 mL, 37.50 mmol, 1 eq.) was added dropwise at 0 °C over 50 minutes. The solution was kept stirring for 2 h, before cooling down to 0 °C. Dimethylsulfate (7.46 mL, 78.7 mmol, 2.1 eq.) was then added to the cooled solution dropwise over 30 minutes. The solution was kept stirring for 12 hours at room temperature. The solvent was then dried under vacuum, and the resulting oil was diluted with 80 mL of water. The aqueous layer was extracted with dichloromethane 3 times (3*60 mL). The organic layer was dried with MgSO₄, then filtered and dried concentrated under vacuum. The obtained compound was as white oil, directly used in the next step without further purification.

¹H NMR (300 MHz, CDCl₃): δ (ppm) = 4.12 (q, J = 7.1 Hz, 4H, CH₃CH₂CO), 1.39 (s, 6H, C(CH₃)₂), 1.19 (t, J = 7.1 Hz, 4H, CH₃CH₂CO).

These results are in agreement with the literature.⁸⁸

Synthesis of 2,2-dimethylmalonic acid 18c



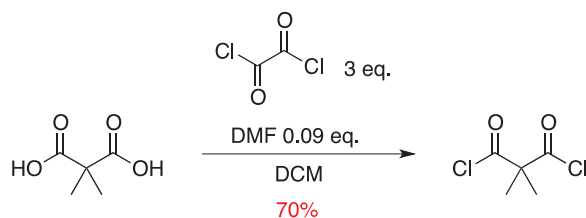
Diethyl 2,2-dimethylmalonate was added to a mixture of THF/methanol/water (75 mL/15 mL/15 mL). Sodium hydroxide (7.50 g, 187.30 mmol, 5 eq.) was added to the solvent progressively under vigorous stirring. The mixture was kept stirring for 24 hours.

After reaction, the solution was evaporated under vacuum, and poured into 80 mL of water. The solution was then washed with dichloromethane (2*40 mL), and the aqueous layer was acidified with hydrochloric acid until pH = 1. The aqueous layer was then extracted with diethyl ether for 3 times (3* 60 mL). The combined organic layers were dried over MgSO₄, followed by filtration and concentration under pressure to obtain the desired compound as white powder (3.54 g, for the first two steps, yield 72%).

¹H NMR (300 MHz, DMSO-d₆): δ (ppm) = 12.61 (br s, 2H, OH), 1.28 (s, 6H, C(CH₃)₂).

These results are in agreement with the literature.⁸⁸

Synthesis of 2,2-dimethylmalonyl dichloride 18.



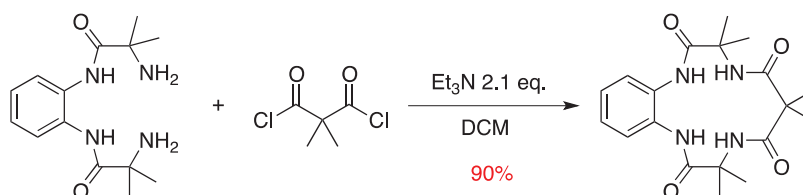
In anhydrous dichloromethane (11 mL) containing 2,2-dimethylmalonic acid (1.00 g, 7.07 mmol, 1 eq.) under argon, dimethylformamide (0.5 mL, 0.68 mmol, 0.09 eq.) was added. Oxalyl chloride (1.95 mL, 22.70 mmol, 3 eq.) was then added over 15 minutes,

and the solution was kept stirring for 12 hours at room temperature. The solvent was evaporated under vacuum. The crude product was purified by distillation under pressure (65-67 °C, 55 mbar). The obtained product was a colorless oil (0.9 g, 70%).

¹H NMR (300 MHz, CDCl₃): δ (ppm) = 1.61 (s, 6H).

These results are in agreement with the literature.⁸⁸

Synthesis of TAML-Me₂ ligand: 3,4,8,9-tetrahydro-3,3,6,6,9,9-hexamethyl-1H-1,4,8,11-benzotetraazocyclotridecane-2,5,7,10(6H,11H)tetrone 19



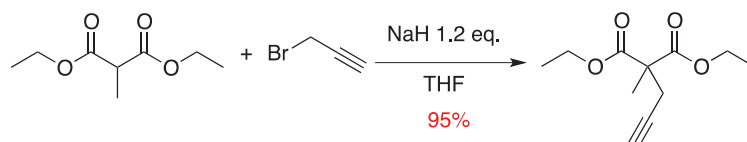
In anhydrous dichloromethane (45 mL) containing 2,2-dimethylmalonyl dichloride (0.6 mL, 4.31 mmol, 1 eq.) under argon atmosphere, a solution of triethylamine (1.25 mL, 9.05 mol, 2.1 eq.) and N,N'-1,2-phenylenebis[2-methyl-2-methylpropanamide] (1.20 g, 4.31 mmol, 1 eq.) in 45 mL anhydrous dichloromethane was added over a period of 6 hours. After the addition, the solution was kept stirring under argon for 12 hours.

After 12 h, the reaction mixture was concentrated under reduced pressure, and the resulting powder was dried under vacuum. It was washed with water for 2 times (2* 10 mL) and then diethyl ether (3* 10 mL) to provide the product as a beige powder (1.49 g, 90%).

¹H NMR (300 MHz, DMSO-d₆): δ (ppm) = 8.29 (br s, 2H, PhNHCO), 7.74 (br s, 2H, C(CH₃)₂NHCO), 7.46 (dd, *J* = 6.0, 3.6 Hz, 2H, aromatic *H*), 7.16 (dd, *J* = 6.0, 3.6 Hz,

2.2 Synthesis of functionalized Fe(TAML)

Synthesis of diethyl 2-methyl-2-propargylmalonate 72

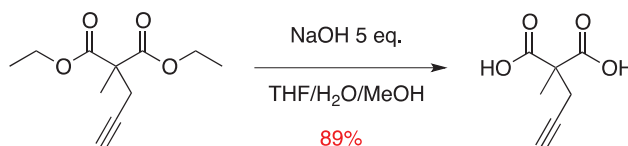


In freshly distilled THF (100 mL) containing sodium hydride (60% in oil, 0.46g, 13.8 mmol, 1.2 eq.) under argon, diethyl methylmalonate (1.96 mL, 11.48 mmol, 1 eq.) was added dropwise at 0 °C over 50 minutes. The solution was kept stirring for 2 h, followed by cooling down to 0 °C. Propargyl bromide (80% in toluene, 1.40 mL, 12.62 mmol, 1.1 eq.) was then added to the cooled solution dropwise over 20 minutes. The solution was kept stirring for 12 hours at room temperature. The solvent was then dried under vacuum, and the resulting oil was diluted into 80 ml of water. The aqueous layer was extracted with diethyl ether 3 times (3*60 mL). The organic layer was dried over MgSO₄, then filtered and concentrated under vacuum. The expected product was isolated as a yellowish oil and was directly used in the next step without further purification (2.30 g, 95%).

¹H NMR (300 MHz, CDCl₃): δ (ppm) = 4.15 (q, J = 7.1 Hz, 4H, CH₃CH₂CO), 2.72 (d, J = 2.6 Hz, 2H, CCH₃CH₂CCH), 2.01 (t, J = 2.6 Hz, H, CCH₃CH₂CCH), 1.48 (s, 3H, C(CH₃)CH₂CCH), 1.20 (t, J = 7.1 Hz, 6H, CH₂CH₃).

These results are in agreement with the literature.¹⁹⁶

Synthesis of 2-methyl-2-propargylmalonic acid 73.



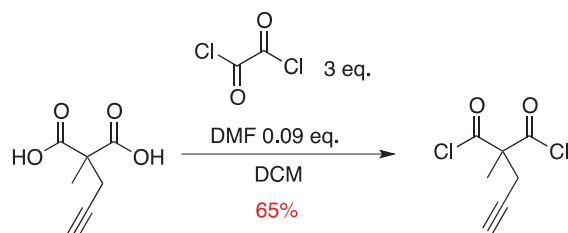
Diethyl 2-methyl-2-propargylmalonate (3.19 g, 15.01 mmol, 1 eq.) was added to a mixture of THF/methanol/water (40 mL/8 mL/8 mL). Sodium hydroxide (3.00 g, 75.03 mmol, 5 eq.) was added to the solvent progressively under vigorous stirring. The mixture was kept stirring for 24 hours.

After the reaction was completed, the solution was evaporated under vacuum, and poured into 40 mL of water. The solution was then washed with dichloromethane (2*20 mL), and the aqueous layer was acidified with hydrochloric acid until pH = 1. The aqueous layer was then extracted with diethyl ether for 3 times (3*30 mL). The combined organic layer were dried over MgSO₄, followed by filtration and concentration under reduced pressure to obtain the desired compound as a yellowish powder (2.09 g, yield 89%).

¹H NMR (300 MHz, DMSO-*d*₆): δ (ppm) = 12.93 (br s, 2H, OH), 2.90 (t, J = 2.7 Hz, 1H, CCH₃CH₂CCH), 2.63 (d, J = 2.7 Hz, 2H, CCH₃CH₂CCH), 1.37 (t, 3H, C(CH₃)(CH₂CCH)).

These results are in agreement with the literature.¹⁹⁶

Synthesis of 2-methyl-2-propargylmalonyl dichloride 74.

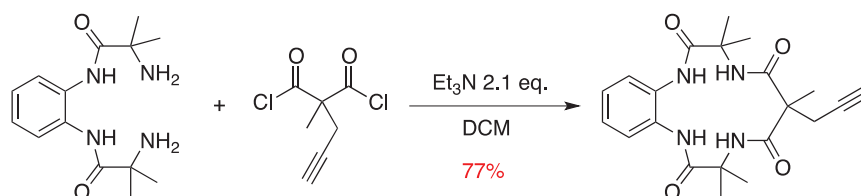


In anhydrous dichloromethane (11 mL) containing 2-methyl-2-propargylmalonic acid (3.52 g, 22.26 mmol, 1 eq.) under argon, dimethylformamide (0.15 mL, 2.00 mmol, 0.09 eq.) was added. Oxalyl chloride (5.73 mL, 66.77 mmol, 3 eq.) was next added over 15 minutes, and the solution was kept stirring for 12 hours at room temperature. The solvent was removed under vacuum. The crude product was purified by distillation under pressure (52-55 °C, 8 mbar). The obtained product was yellowish oil (2.85 g, 65%).

$^1\text{H NMR}$ (300 MHz, CDCl_3): δ (ppm) = 2.97 (d, J = 2.7 Hz, 2H, CH_2CCH), 2.13 (t, J = 2.7 Hz, 1H, CH_2CCH), 1.73 (s, 3H, CH_3).

These results are in agreement with the literature.¹⁹⁶

Synthesis of TAML-(Me)(CH_2CCH) ligand 62.



In anhydrous dichloromethane (45 mL) containing 2-methyl-2-propargylmalonyl dichloride (0.55 g, 2.85 mmol, 1 eq.) under an argon atmosphere, a solution of triethylamine (0.83 mL, 5.99 mmol, 2.1 eq.) and N,N' -1,2-phenylenebis[2-methyl-2-methylpropanamide] (1.20 g, 4.31 mmol, 1 eq.) in 45 mL anhydrous dichloromethane

was added dropwise over a period of 6 hours. After the addition, the solution was kept stirring under argon for 12 hours.

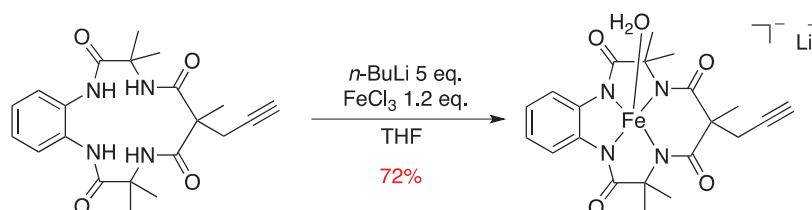
After the reaction, the solvent was evaporated under reduced pressure, and the resulting powder was dried under vacuum. It was dissolved into 120 mL of water and then extracted with ethyl acetate (3*100 mL). The combined organic layers were washed with a saturated NaCl solution (2*100 mL), followed by drying over MgSO₄, filtered and concentrated under vacuum to provide the product as beige powder (0.88 g, yield 77%).

¹H NMR (300 MHz, DMSO-d₆): δ (ppm) = 8.26 (s, 2H, PhNHCO), 7.87 (s, 2H, NH), 7.46 (dd, *J* = 5.9, 3.5 Hz, 2H, aromatic *H*), 7.16 (dd, *J* = 5.9, 3.6 Hz, 2H, aromatic *H*), 2.93-2.92 (m, 3H, C(CH₃)(CH₂CCH)), 1.58 (s, 3H, C(CH₃)(CH₂CCH)), 1.50 (s, 6H, C(CH₃)₂), 1.46 (s, 6H, C(CH₃)₂).

¹³C NMR (75 MHz, DMSO-d₆): δ (ppm) = 173.34 (quaternary CO), 170.85 (quaternary CO), 130.77 (quaternary aromatic C), 126.02 (aromatic CH), 125.56 (aromatic CH), 80.60 (aromatic CH), 73.50 (C(CH₃)(CH₂CCH)), 58.28 (quaternary C(CH₃)₂), 53.90 (quaternary C(CH₃)(CH₂CCH)), 25.52 (C(CH₃)(CH₂CCH)), 25.24 (C(CH₃)₂), 24.80 (C(CH₃)₂), 17.90 (C(CH₃)(CH₂CCH)).

MS spectrum (ESI⁺): [M+H]⁺ calcd. For C₂₁H₂₆N₄O₄: 399.20; found: 399.2;

Synthesis of Fe[TAML-(Me)(CH₂CCH)]Li 75



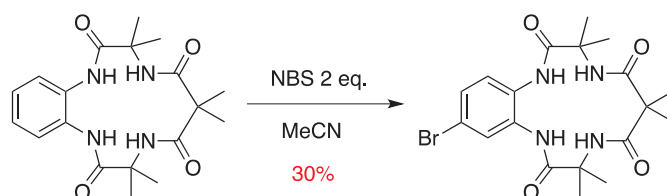
A three-neck round-bottom flask containing a suspension of TAML-(Me)(CH₂CCH)

ligand (0.17 g, 0.427 mmol, 1 eq.) in freshly distilled tetrahydrofuran (10 mL) under argon at -68 °C (dry ice added with acetone) was added a solution of 2.5 M of *n*-butyl lithium (0.85 mL, 2.13 mmol, 5 eq.) over 15 minutes. The solution was then allowed to warm up to room temperature and stirred for 1 hour before adding a solution of dry iron(III) chloride (0.083 g, 0.512 mmol, 1.2 eq.) in fresh distilled THF (3 mL). The suspension was kept stirring for 24 hours.

After the reaction, 40 mL of isopropanol was added to the solution, the suspension was next stirred for 30 minutes and filtered. The filtrate was concentrated under vacuum to provide the crude material. The purification was conducted by column chromatography over a gel of alumina, dichloromethane and methanol (10: 1) as the mobile phase. After purification, a red product was obtained (0.140g, yield 72%).

HR-MS spectrum (ESI): $[M-Li]^+$: calcd. For $C_{21}H_{22}FeN_4O_4$: 450.0990; found: 450.0987.

Synthesis of Br-TAML-Me₂ ligand **61**



In anhydrous acetonitrile (6 mL) containing the TAML-Me₂ ligand (0.3 g, 0.8 mmol, 1 eq.) under argon atmosphere, a solution *N*-bromosuccinimide (0.57 g, 3.20 mmol, 4 eq.) in 3 mL anhydrous acetonitrile was added dropwise. After the addition, the yellow solution was heated to 42 °C and kept stirring under argon for 30 hours.

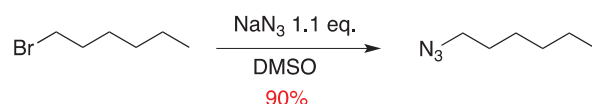
After the reaction, the solution was quenched with 10 mL of water and extracted with dichloromethane (3*10 mL). The combined organic layers were washed with a saturated NaCl solution (20 mL), followed by drying with MgSO₄, filtered and

concentrated under reduced pressure to provide the crude product. A silica gel column chromatography was used for purification, with a mobile phase containing petroleum ether and ethyl acetate (1: 4). After purification, the pure product (0.10 g, yield 30%) was isolated.

¹H NMR (300 MHz, DMSO-d₆): δ (ppm) = 8.40 (s, 2H, PhNHCO), 8.38 (s, 2H, C(CH₃)₂NHCO), 7.77 (s, H, aromatic H), 7.42-7.38 (m, 2H, aromatic H), 1.47 (s, 6H, C(CH₃)₂), 1.47 (s, 6H, C(CH₃)₂), 1.45 (s, 6H, C(CH₃)₂).

HRMS spectrum (ESI⁺): [M + Na]⁺: calcd. For C₁₉H₂₅BrN₄NaO₄⁺: 475.0957; found: 479.0951.

Synthesis of 1-azidohexane 66

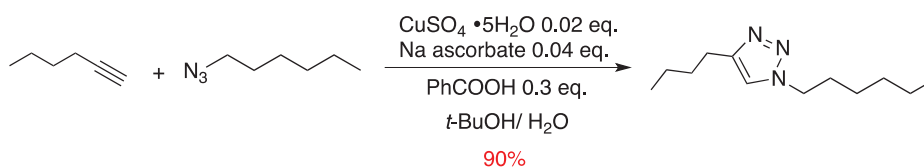


To a solution of 28 mL of dimethylsulfoxide containing 1-bromohexane (1.7 mL, 12.12 mmol, 1 eq), was added sodium azide (0.87 g, 13.33 mmol, 1.1 eq.). The solution was kept stirring for 5 hours, and poured into 50 mL of water. The aqueous layer was extracted with diethyl ether 3 times (3*80 mL). The combined layers were dried with MgSO₄, filtered and dried under vacuum. The obtained product was colorless oil (1.39 g, yield 90%).

¹H NMR (300 MHz, CDCl₃): δ (ppm) = 3.26 (t, *J* = 7.0 Hz, 2H, CH₂N₃), 1.65-1.58 (m, 2H, CH₂CH₃), 1.37-1.33 (m, 6H, CH₂), 0.90-0.95 (t, *J* = 6.8 Hz, 3H, CH₃).

These results are in agreement with the literature.^{197,198}

Synthesis of 4-butyl-hexyl-1*H*-1,2,3-triazole 78



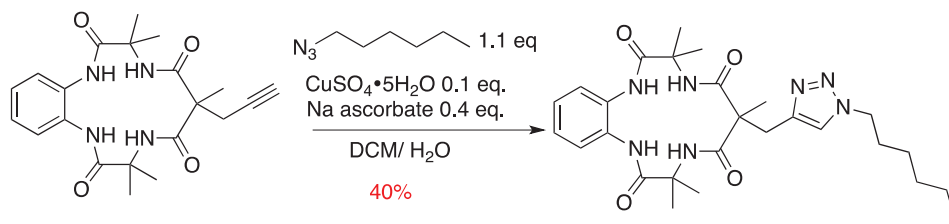
A round-bottom flask was charged with $\text{CuSO}_4 \cdot 5\text{H}_2\text{O}$ (0.01 g, 0.04 mmol, 0.02 eq.), sodium ascorbate (0.016 g, 0.08 mmol, 0.04 eq.) and benzoic acid (PhCOOH) (0.073 g, 0.6 mmol, 0.3 eq.) Next a 2 mL of mixture of *t*-BuOH and water (1:2) was added to the flask. The mixture was kept stirring at room temperature. A mixture of hexyne (0.16 g, 2 mmol, 1 eq.) and 1-azidohexane (0.279 g, 1.1 mmol, 1.1 eq.) was added to the solution. The solution was stirred for 1 hour at 30 °C.

After the reaction, the solvent was evaporated. 3 mL of water was added to dissolve the product, and dichloromethane was added to extract the product for 3 times (3*5 mL). The combined organic layers were dried with MgSO_4 , filtered and dried under vacuum. A silica-gel column chromatography was used for purification, with a mobile phase containing cyclohexane and ethyl acetate (4: 1). After purification, a pure product was obtained (0.45 g, yield 90%).

¹H NMR (300 MHz, CDCl₃): δ (ppm) = 7.26 (s, 1H, CH), 4.35 (t, J = 7.3 Hz, 2H, NCH₂CH₂), 2.76 (t, J = 7.7 Hz, 2H, CH₂CH₂triazole), 1.90-1.88 (m, 2H, CH₂), 1.70-1.65 (m, 4H, CH₂), 1.45-1.31 (m, 6H, CH₂), 0.98 (t, J = 7.3 Hz, 3H, CH₃), 0.88 (t, J = 6.8 Hz, 3H, CH₃).

These results are in agreement with the literature.¹⁶⁸

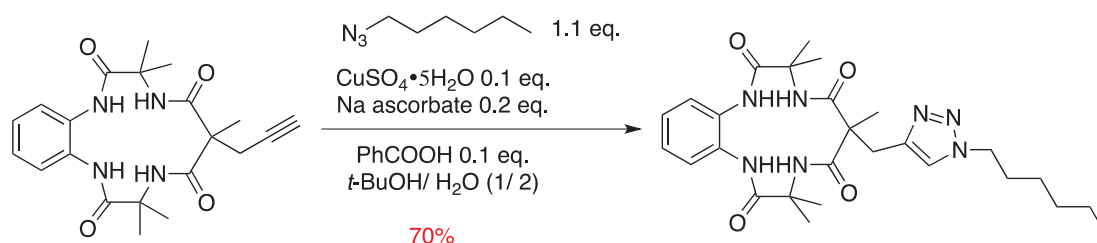
Synthesis of TAML-(Me)(triazole) **63**



To a 5 mL of a mixture of dichloromethane and water (1:1) containing **62** (0.30 g, 0.75 mmol, 1 eq.), 1-azidohexane (0.10 g, 0.83 mmol, 1.1 eq.) and copper(II) sulfate pentahydrate (0.02 g, 0.08 mmol, 0.1 eq.), was added sodium ascorbate (0.06 g, 0.30 mmol, 0.4 eq.). The solution was kept stirring at room temperature for 3 days.

After the reaction, 5 mL of water and dichloromethane were added to the solution to separate the layer. The aqueous layer was extracted with dichloromethane 2 times (2* 10 mL). The organic phases were combined and dried with MgSO_4 and filtered, dried under pressure. The obtained crude product was green. A silicagel column chromatography was used for purification, with a mobile phase containing petroleum ether and ethyl acetate (1: 4). After purification, a pure white product was obtained (0.16 g, yield 40%).

Synthesis of TAML-(Me)(triazole) **63**



A round-bottom flask was charged with $\text{CuSO}_4 \cdot 5\text{H}_2\text{O}$ (0.02 g, 0.08 mmol, 0.1 eq.), sodium ascorbate (0.03 g, 0.16 mmol, 0.2 eq.) and benzoic acid (PhCOOH) (0.098 g,

0.08 mmol, 0.1 eq.). Next, a 3 mL mixture of *t*-BuOH and water (1: 2) was added to the flask. The mixture was kept under stirring at room temperature. A mixture of **62** (0.2 g, 0.5 mmol, 1 eq.) and 1-azidohexane (0.066 g, 0.55 mmol, 1.1 eq.) was added to the solution. The solution was heated to 80 °C and kept stirring for 5 hours.

After the reaction, the solvent was evaporated. 3 mL of water was added to dissolve the product, and dichloromethane was used to extract the product for 3 times (3*5 mL). The combined organic layers were dried with MgSO₄, filtered and dried under vacuum. A silica-gel chromatography was used for purification, with a mobile phase containing cyclohexane and ethyl acetate (1: 4). After purification, the pure product was collected (280 mg, yield 70%).

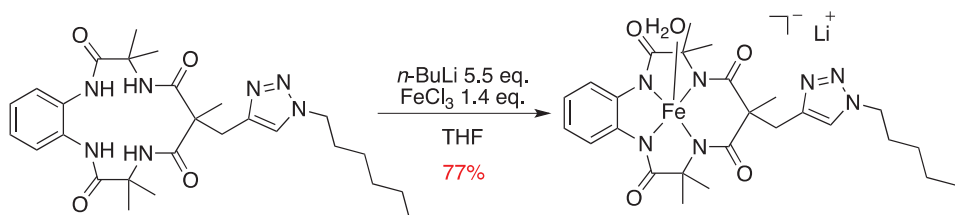
¹H NMR (300 MHz, DMSO-*d*₆): δ (ppm) = 8.31 (br s, 2H, *NH*), 7.88 (br s, 2H, *NH*), 7.71 (s, 1H, triazole *CH*), 7.50-7.47 (dd, *J* = 5.9, 3.6 Hz, 2H, aromatic *H*), 7.19-7.16 (dd, *J* = 5.9, 3.6 Hz, 2H, aromatic *H*), 4.31 (t, *J* = 6.8 Hz, 2H, NCH₂), 1.80-1.77 (m, 2H, C(CH₃)(CH₂triazole)), 1.48 (s, 12H, C(CH₃)₂), 1.40 (s, 3H, C(CH₃)(CH₂triazole)), 1.26-1.18 (m, 8H, NCH₂(CH₂)₄CH₃), 0.85 (t, *J* = 6.8 Hz, 3H, CH₂CH₃).

¹³C NMR (101 MHz, DMSO-*d*₆): δ (ppm) = 173.41 (quaternary CO), 171.65 (quaternary CO), 142.83 (quaternary C(C)(CH)), 130.84 (quaternary aromatic C), 126.03 (aromatic CH), 125.55 (aromatic CH), 123.63 (triazole CH), 58.22 (quaternary C(CH₃)₂), 55.37 (quaternary C(CH₃)(CH₂triazole)), 49.62 (C(CH₃)(CH₂triazole)), 40.55 (NCH₂), 40.27 (NCH₂(CH₂)₄(CH₃)), 39.99 (NCH₂(CH₂)₄(CH₃)), 39.72 (NCH₂(CH₂)₄(CH₃)), 30.23 (C(CH₃)₂), 25.91 (C(CH₃)₂), 25.59 (NCH₂(CH₂)₄(CH₃)), 28.28 (C(CH₃)(CH₂triazole)), 14.29 (NCH₂(CH₂)₄(CH₃)).

MS spectrum (ESI⁺): [M+H]⁺ calcd. for C₂₇H₃₉N₇O₄⁺: 526.31; found: 526.3;

[M+Na]⁺ calcd. for C₂₇H₃₈N₇O₄Na⁺: 548.31; found: 548.3.

Synthesis of Fe[TAML-(Me)(triazole)]Li 76

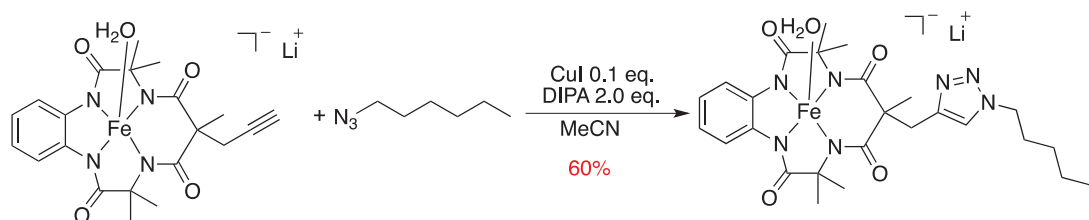


In a three-neck round-bottom flask containing a suspension of TAML-(Me)(triazole) ligand (0.18 g, 0.34 mmol, 1 eq.) in freshly distilled tetrahydrofuran (5 mL) under argon in an ice bath (0 °C) was added a solution of 1.5 M of *n*-butyl lithium (1.25 mL, 1.88 mmol, 5.5 eq.) over 15 minutes. The solution was then allowed to warm up to room temperature and stirred for 40 minutes before adding a solution of dry iron(III) chloride (0.074 g, 0.48 mmol, 1.4 eq.) in fresh distilled THF (3 mL). The suspension was kept stirring for 24 hours at room temperature.

After the reaction, the suspension was filtered off and the resulting filter cake was washed with diethyl ether (3*5 mL). The obtained solid was then added in isopropanol (30 mL), the suspension was then stirred for 30 minutes and filtered. The filtrate was concentrated under vacuum to provide the crude product. Purification was conducted by flash column chromatography over basic alumina. Dichloromethane and methanol (10: 1) was used as the mobile phase. After purification, a red product was obtained (0.168 g, yield 77%).

HRMS spectrum (ESI): $[\text{M-Li}]^-$ calcd. For $\text{C}_{27}\text{N}_{35}\text{FeN}_7\text{O}_4$ $^-$: 577.2100; found: 577.2111.

Synthesis of Fe[TAML-(Me)(triazole)]Li 76

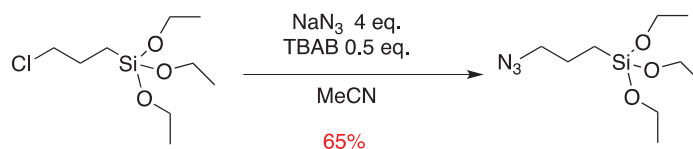


In 4 mL of anhydrous acetonitrile containing $\text{Fe}[\text{TAML}-(\text{Me})(\text{CCH})]\text{Li}$ (0.10 g, 0.22 mmol, 1 eq.) and 1-azidohexane (0.030 g, 0.24 mmol, 1.1 eq.), was added copper iodide (0.0042 g, 0.022 mmol, 0.1 eq.) and diisopropylamine (DIPA) (0.060 g, 0.44 mmol, 2 eq.) under argon. The reaction was heated to 82 °C and kept stirring for 24 hours.

After the reaction, the solvent was evaporated under pressure. The solid was washed with *n*-pentane, dichloromethane. Next, the solid was dissolved in ethanol, and filtered off. The filtrate was concentrated under reduced pressure to afford the desired product (0.077 g, yield 60%).

HRMS spectrum (ESI⁻): $[\text{M}-\text{Li}]^-$ calcd. For $\text{C}_{27}\text{N}_{35}\text{FeN}_7\text{O}_4^-$: 577.2100; found: 577.2111.

Synthesis of (3-azidopropyl)triethylsilane 67



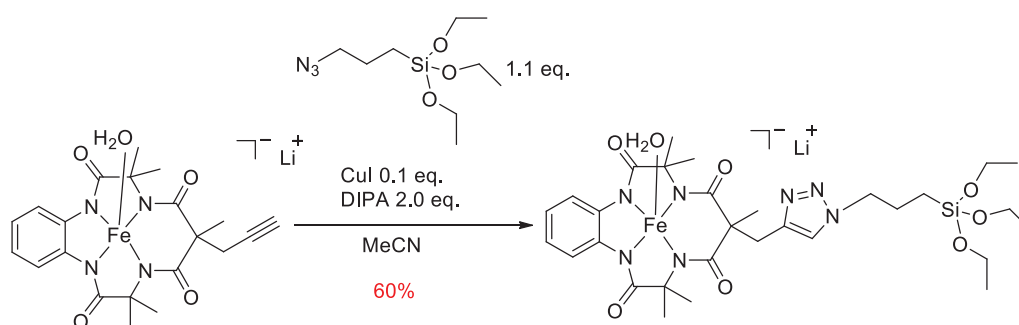
Sodium azide (5.2 g, 80 mmol, 4 eq.) and tetrabutylammonium bromide (TBAB) (3.22 g, 10 mmol, 0.5 eq.) were added to 80 mL of anhydrous acetonitrile. Then (3-chloropropyl)triethylsilane (4.8 g, 20 mmol, 1 eq.) was added to the solution. The

mixture was kept refluxing for 18 hours. After the reaction, the solvent was removed under reduced pressure. The solid was extracted with pentane. The product was obtained in 65% yield (3.20 g).

¹H NMR (300 MHz, CDCl₃): δ (ppm) = 3.84 (q, *J* = 7 Hz, 6H, CH₂), 3.28 (t, *J* = 7 Hz, 2H, CH₂), 1.73 (m, 2H, CH₂), 1.24 (t, *J* = 7 Hz, 9H, CH₃), 0.69 (m, 2H, CH₂).

These results are in agreement with the literature.¹⁷⁰

Synthesis of Fe[TAML-(Me)(triazole-Si(OEt)₃)]Li 79

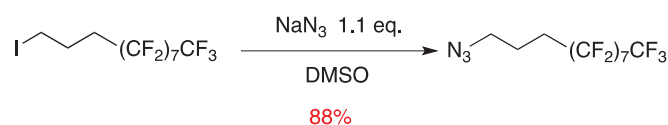


In 4 mL of anhydrous acetonitrile containing Fe[TAML-(Me)(CCH)]Li (0.10 g, 0.22 mmol, 1 eq.) and (3-azidopropyl)triethylsilane (0.061 g, 0.24 mmol, 1.1 eq.), was added copper iodide (0.0042 g, 0.022 mmol, 0.1 eq.) and diisopropylamine (DIPA) (0.060 g, 0.44 mmol, 2 eq.) under argon. The reaction was heated to 82 °C and kept stirring for 24 hours.

After the reaction, the solvent was dried under reduced pressure. The solid was washed with *n*-pentane, dichloromethane. Next, the solid was dissolved in ethanol, and filtered. The filtrate was concentrated under reduced pressure to afford the desired product (90mg, yield 60%).

MS spectrum (ESI): [M-Li]⁺ calcd. For C₃₀N₄₃FeN₇O₇Si: 697.23; found: 697.2.

Synthesis of 11-azido-1,1,1,2,2,3,3,4,4,5,5,6,6,7,7,8,8-heptadecafluoroundecane 68



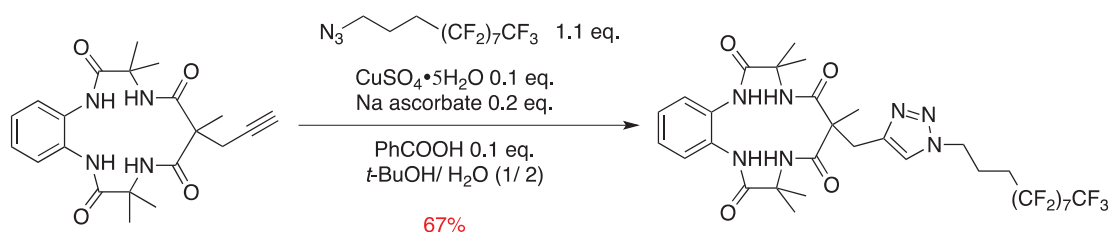
7 mL of dimethylsulfoxide (DMSO) containing sodium azide (0.24 g, 3.73 mmol, 1.1 eq.) and 1,1,1,2,2,3,3,4,4,5,5,6,6,7,7,8,8-heptadecafluoro-11-iodoundecane (2 g, 3.39 mmol, 1 eq.) was kept stirring at room temperature for 5 hours. After the reaction, 20 mL of water was added to the solution. The solution was then extracted with diethyl ether 3 times (3*30 mL), and the combined organic phases were dried over MgSO₄, filtered and dried under reduced pressure. The obtained product was colorless oil (1.5 g, yield 88%).

¹H NMR (300 MHz, CDCl₃): δ (ppm) = 3.43 (t, 2H, *J* = 9.9 Hz CH₂N₃), 2.18 (m, 2H, CH₂CH₂N₃), 1.90 (m, 2H, CH₂CH₂CH₂N₃).

¹⁹F NMR (300 MHz, CDCl₃): δ (ppm) = -81.47 (t, 3F, *J* = 10.1 Hz), -114.77 (m, 2F), -122.18 (m, 2F), -122.40 (m, 2F), -123.23 (m, 2F), -123.93 (m, 2F), -126.69 (m, 2F).

These results are in agreement with the literature.¹⁷¹

Synthesis of TAML-(Me)(triazole-(CH₂)₃(CF₂)₇CF₃) 65.



In a round bottom flask was added CuSO₄ · 5H₂O (0.0125 g, 0.05 mmol, 0.1 eq.), sodium ascorbate (0.0198 g, 0.1 mmol, 0.2 eq.) and benzoic acid (PhCOOH) (0.061 g,

0.05 mmol, 0.1 eq.). Next a 3 mL mixture of *t*-BuOH and water (1: 2) was added to the flask. The mixture was kept stirring at room temperature. A mixture of **62** (0.2 g, 0.5 mmol, 1 eq.) and 11-azido-1,1,1,2,2,3,3,4,4,5,5,6,6,7,7,8,8-heptafluoroundecane (0.278 g, 1.1 mmol, 1.1 eq.) was added to the solution. The solution was heated to 80 °C and kept stirring for 5 hours.

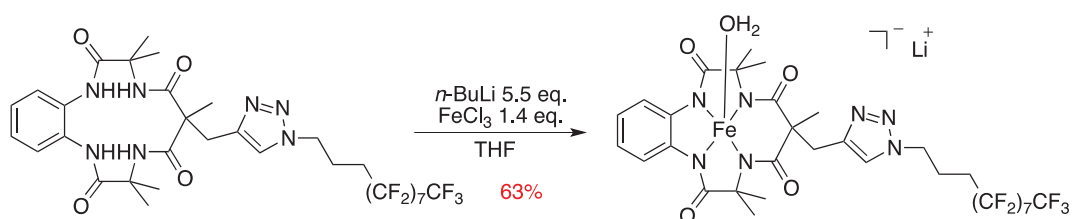
After the reaction, the solvent was evaporated. 3 mL of water was added to dissolve the product, and dichloromethane was added to extract the product 3 times (3*5 mL). The combined organic layers were dried with MgSO₄, filtered and dried under vacuum. A silica-gel chromatography was used for purification, with a mobile phase containing cyclohexane and ethyl acetate (1: 4). After purification, the pure product was collected (120 mg, yield 67%).

¹H NMR (300 MHz, DMSO-*d*₆): δ (ppm) = 8.32 (br s, 2H, NH), 7.87 (br s, 2H, NH), 7.79 (s, 1H, triazole CH), 7.51-7.46 (dd, *J* = 5.9, 3.6 Hz, 2H, aromatic *H*), 7.19-7.16 (dd, *J* = 5.9, 3.6 Hz, 2H, aromatic *H*), 4.48 (t, *J* = 6.8 Hz, 2H, NCH₂), 3.46 (t, *J* = 6.8 Hz, 2H, CH₂), 2.25-2.28 (m, 2H, CH₂(CH₂)₂), 1.46 (s, 12H, C(CH₃)₂), 1.40 (t, *J* = 6.8 Hz, 3H, CH₂CH₃).

MS spectrum (ESI⁺): [M+H]⁺ calcd. For C₃₂H₃₃F₁₇N₇O₄⁺: 902.22; found: 902.2.

[M+Na]⁺ calcd. For C₃₂H₃₂F₁₇N₇O₄Na⁺: 924.22; found: 924.2.

Synthesis of Fe[TAML-(Me)(triazole-(CH₂)₃(CF₂)₇CF₃)] **80**



A schlenk tube containing a suspension of TAML-(Me)(triazole-(CH₂)₃(CF₂)₇CF₃)

ligand **65** (0.30 g, 0.33 mmol, 1 eq.) in freshly distilled tetrahydrofuran (10 mL) under argon in an ice bath (0 °C) was charged with a solution of 2.0 M of *n*-butyl lithium (0.9 mL, 1.82 mmol, 5.5 eq.) over 15 min. The solution was then allowed to warm up to room temperature and stirred for 1 hour before adding a solution of dry iron(III) chloride (0.076 g, 0.46 mmol, 1.4 eq.) in fresh distilled THF (3 mL). The suspension was kept stirring for 24 hours at room temperature.

After cooling down to room temperature, the suspension was filtered and the resulting filter cake was washed with diethyl ether (3*10 mL). The obtained solid was then dissolved in isopropanol (40 mL), the suspension was then stirred for 30 minutes and filtered. The filtrate was concentrated under vacuum to provide crude product. Purification was conducted by chromatography over a gel of alumina. dichloromethane and methanol (10: 1) were used as the mobile phase. After purification, a red product was obtained (0.20g, yield 63%).

HR-MS spectrum (ESI): [M-Li]⁺ calcd. For C₃₂H₂₈F₁₇FeN₇O₄ : 931.1286; found: 931.1268.

3 Catalysis procedures and results

3.1 Catalysis with Mn(Me₂EBC)Cl₂

General procedure for the oxidation of alcohols using Mn(Me₂EBC)Cl₂ in the presence of H₂O₂.

Under Ar, a 25 mL round bottom flask was charged with acetonitrile (4 mL) and water (1 mL) before the pH was adjusted at 3 with HCl. Next, the substrate (100 mM) and 0.5 mol% of Mn(Me₂EBC)Cl₂, 0.17 mL or 0.34 mL of 35% of H₂O₂ aqueous solution (35%) and diphenyl ether as the internal standard were added. The reaction was kept under vigorous stirring for 6 h or 18 h at 303 K in a water bath. Next, the solution was extracted with dichloromethane. After drying, the organic phase was analyzed by GC/MS.

The kinetic follow-up was carried out according to the same protocol, but aliquots were taken every hour.

Experiment protocol for hydroxyl radical trapping with *t*-BuOH.

The protocol for this reaction was the same as the one described above but MeCN (4 mL) was replaced by *t*-BuOH (4 mL).

Stoichiometric oxygenation of veratryl alcohol with manganese(IV) complexes **54.**

A 5 mL a mixture of acetonitrile (4 mL) and water (1 mL) at pH 3 (pH adjusted with HCl) was charged with 1 mM of substrate, 1 mM of Mn(IV) complex **54** and diphenyl ether. The reaction was kept stirring for 6 h at 303 K in a water bath. The conversion and the yields were determined by GC/MS using the internal standard method.

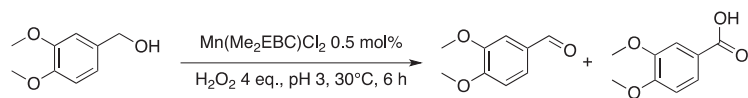
3.2 Catalysis with Fe(TAML) catalysts

Under Ar, a 10 mL round bottom flask was charged with acetonitrile (3 mL). Next, the substrate (100 mM) and 1 mol% of iron catalyst **7a** or **76** were added to the flask. 0.12 mL of 70% of TBHP aqueous solution was added to start the reaction. The reaction was kept under vigorous stirring for 2 h at 303 K in a water bath. After that, diphenyl ether as the internal standard was added. Dried with MgSO₄, the sample was analyzed by GC/MS.

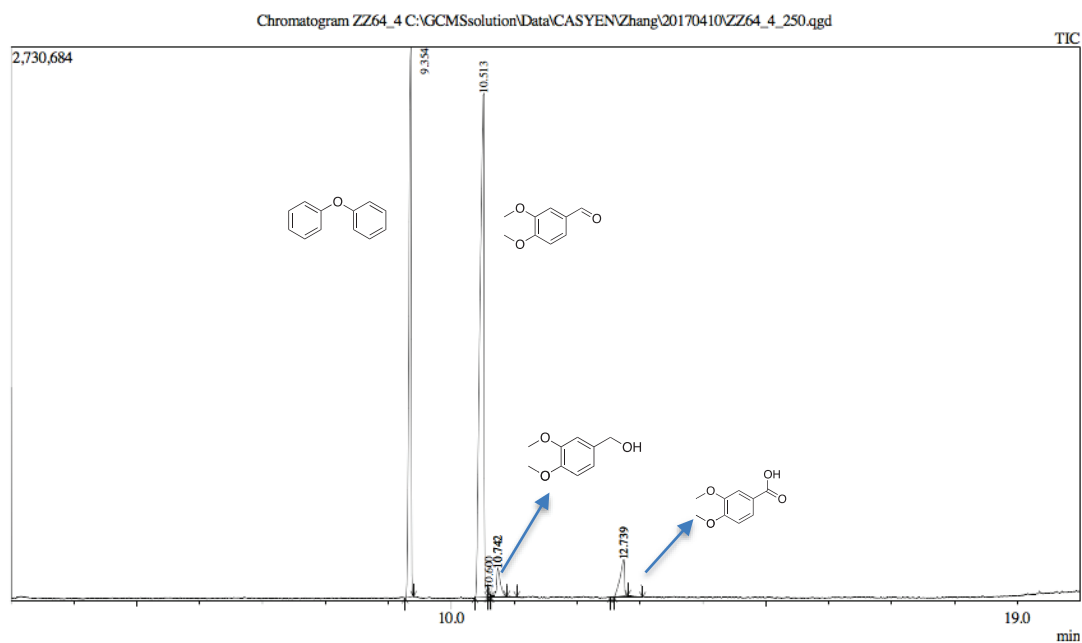
3.3 Results for the oxidation of alcohols

The samples of oxidation of alcohols were analyzed with GC/MS.

Table 15, entry 1



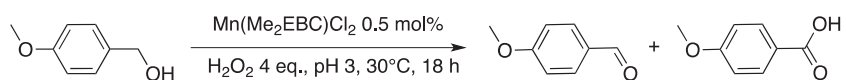
GC/MS analysis with diphenyl ether as an internal standard.



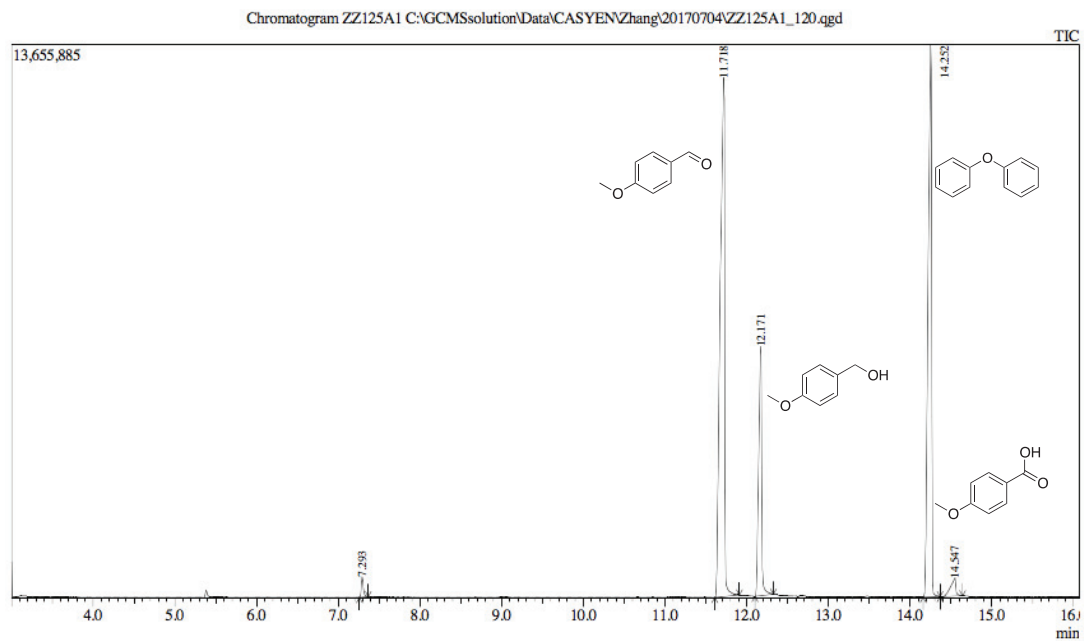
Peak#	R.Time	I.Time	F.Time	Area	Area%	Height	Height%	A/H	Mark	Name
1	9.354	9.267	9.400	7080800	33.27	2710791	45.99	2.61		
2	10.513	10.375	10.575	10931078	51.37	2485993	42.18	4.40		
3	10.600	10.575	10.633	89527	0.42	43240	0.73	2.07	V	
4	10.742	10.633	10.883	615924	2.89	142376	2.42	4.33	V	
5	10.742	10.617	11.042	652663	3.07	143742	2.44	4.54	MI	
6	12.739	12.592	12.808	883139	4.15	180346	3.06	4.90		
7	12.739	12.525	13.042	1027344	4.83	187278	3.18	5.49	MI	
				21280475	100.00	5893766	100.00			

Spectrum

Table 15, entry 2



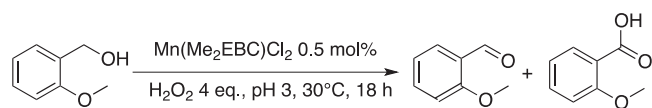
GC/MS analysis with diphenyl ether as an internal standard.



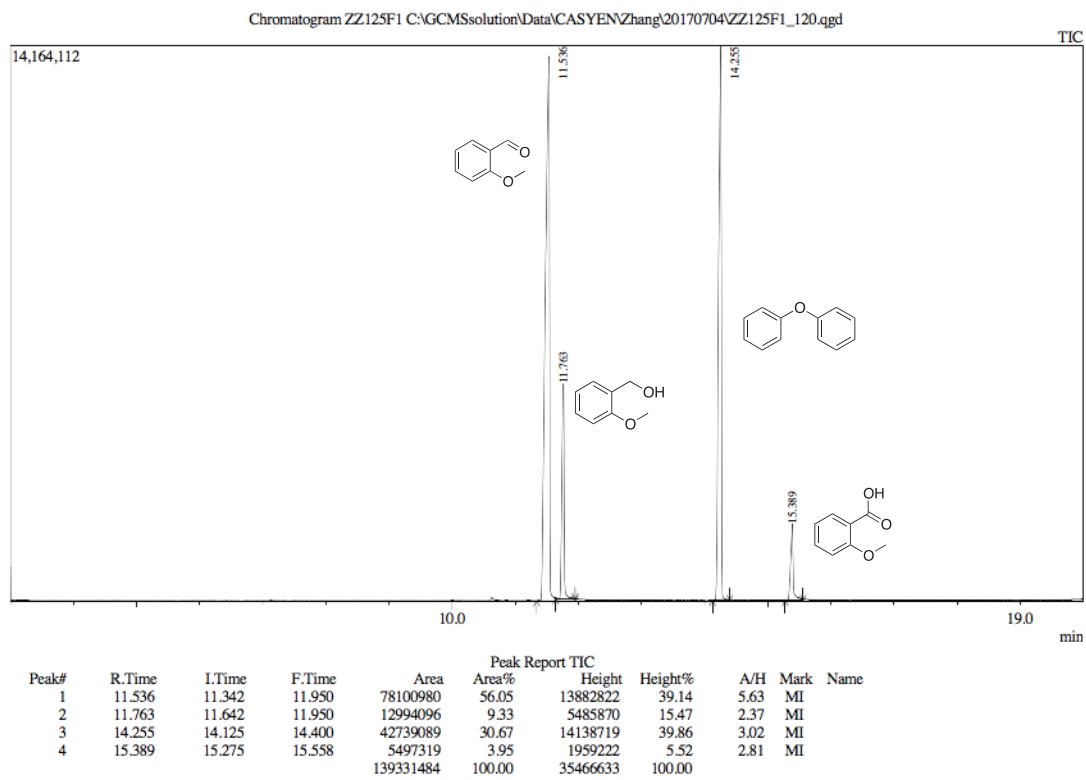
Peak Report TIC										
Peak#	R.Time	I.Time	F.Time	Area	Area%	Height	Height%	A/H	Mark	Name
1	7.293	7.258	7.367	867643	0.81	499156	1.49	1.74		
2	11.718	11.608	11.908	47924313	44.54	12804637	38.18	3.74		
3	12.171	12.100	12.325	15937779	14.81	6156772	18.36	2.59		
4	14.252	14.158	14.367	40878694	37.99	13627200	40.63	3.00		
5	14.547	14.367	14.642	1999645	1.86	449189	1.34	4.45	V	
				107608074	100.00	33536954	100.00			

Spectrum

Table 15, entry 3

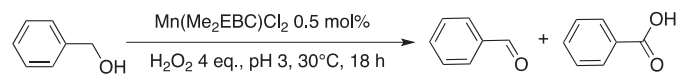


GC/MS analysis with diphenyl ether as an internal standard.

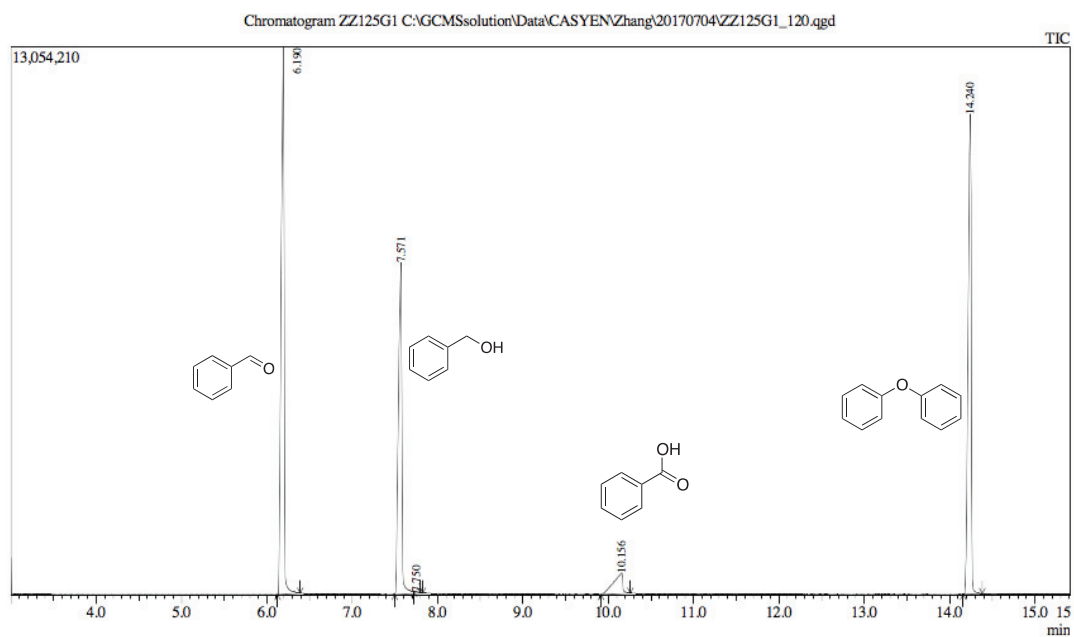


Spectrum

Table 15, entry 4



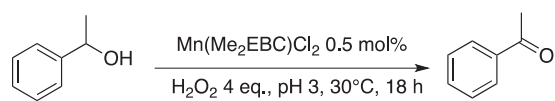
GC/MS analysis with diphenyl ether as an internal standard.



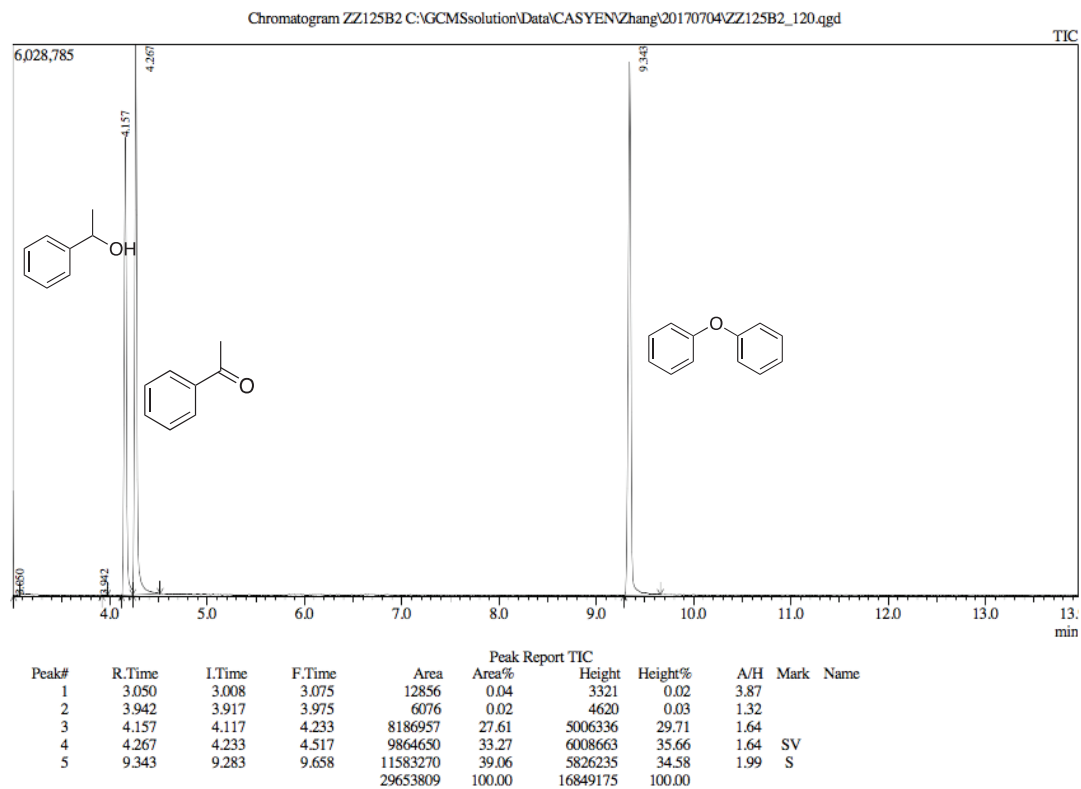
Peak#	R.Time	L.Time	F.Time	Area	Area%	Height	Height%	A/H	Mark	Name
1	6.190	6.125	6.392	32121536	36.78	13030390	39.64	2.47		
2	7.571	7.500	7.825	22439770	25.69	7901961	24.04	2.84	S	
3	7.750	7.725	7.792	22455	0.03	14874	0.05	1.51	T	
4	10.156	9.917	10.258	3694389	4.23	493060	1.50	7.49		
5	14.240	14.158	14.383	29062105	33.27	11431212	34.78	2.54		
				87340255	100.00	32871497	100.00			

Spectrum

Table 15, entry 5

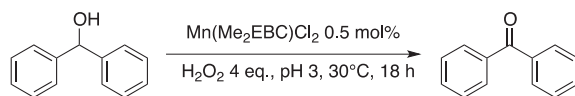


GC/MS analysis with diphenyl ether as an internal standard.

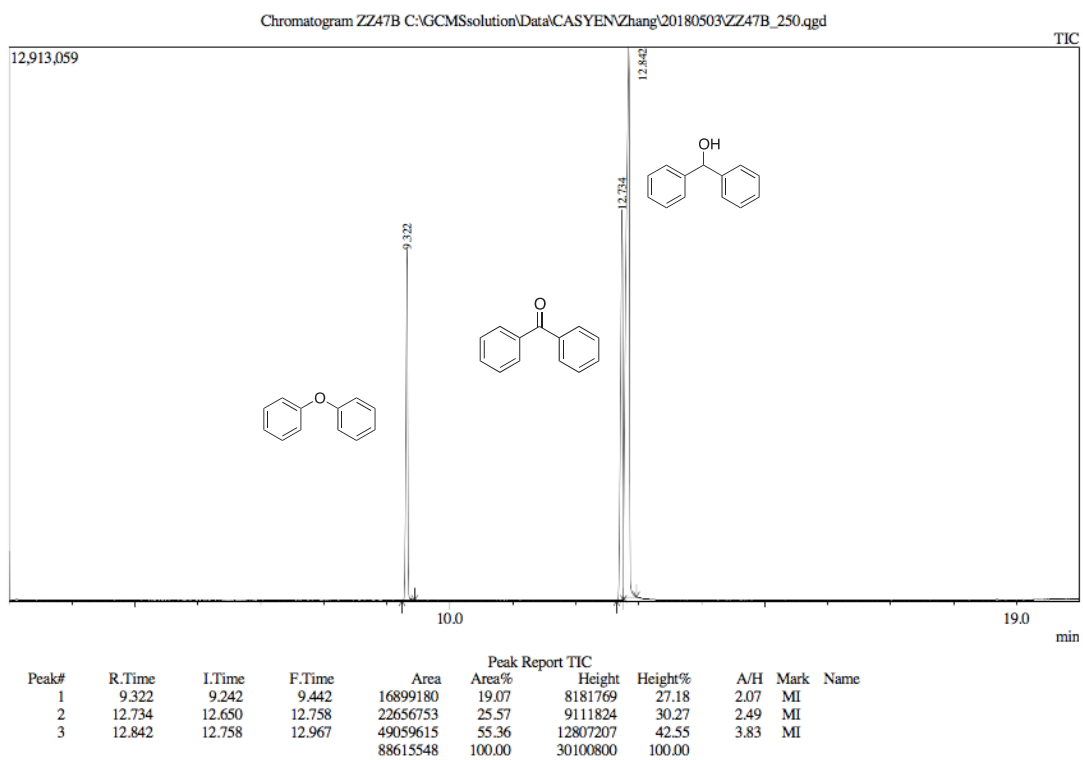


Spectrum

Table 15, entry 6

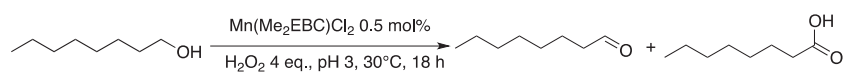


GC/MS analysis with diphenyl ether as an internal standard.

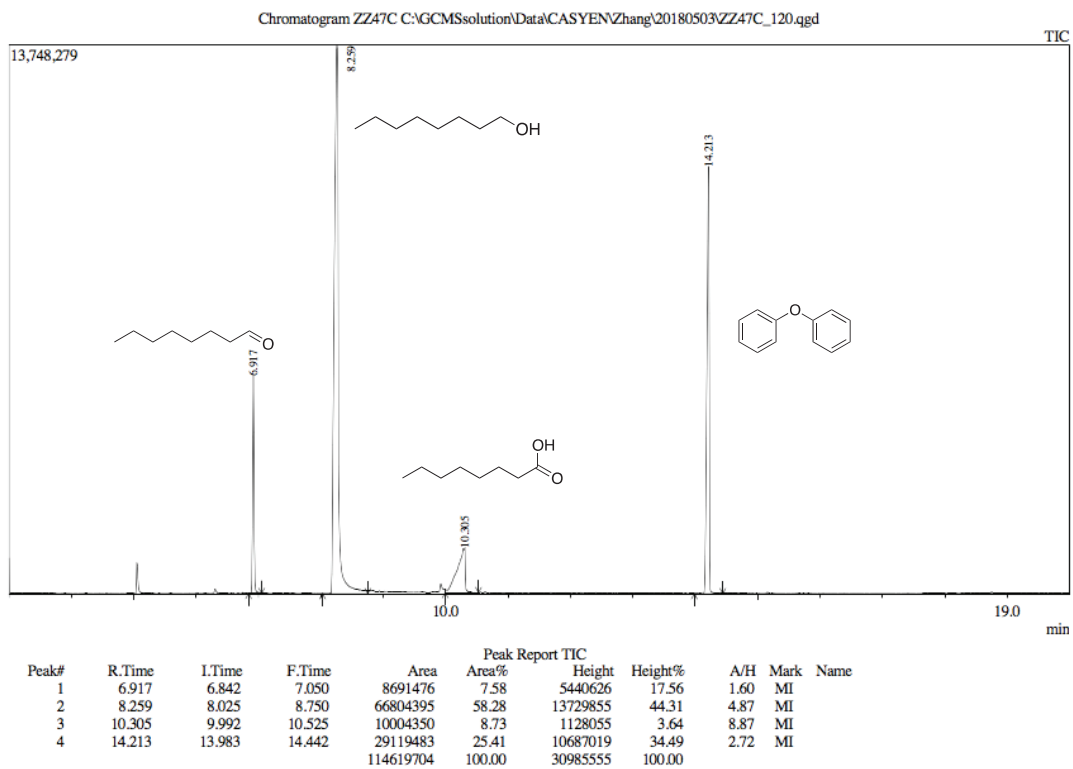


Spectrum

Table 15, entry 7

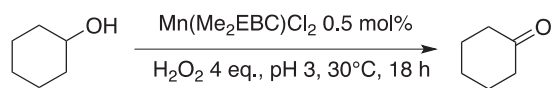


GC/MS analysis with diphenyl ether as an internal standard.

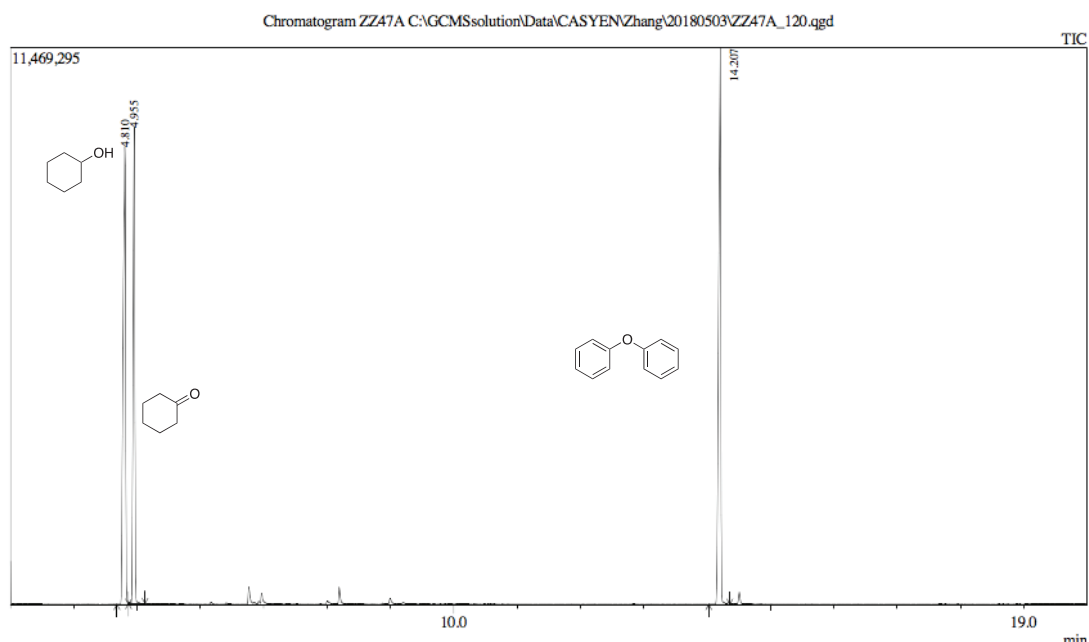


Spectrum

Table 15, entry 8



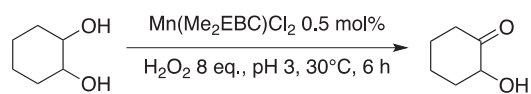
GC/MS analysis with diphenyl ether as an internal standard.



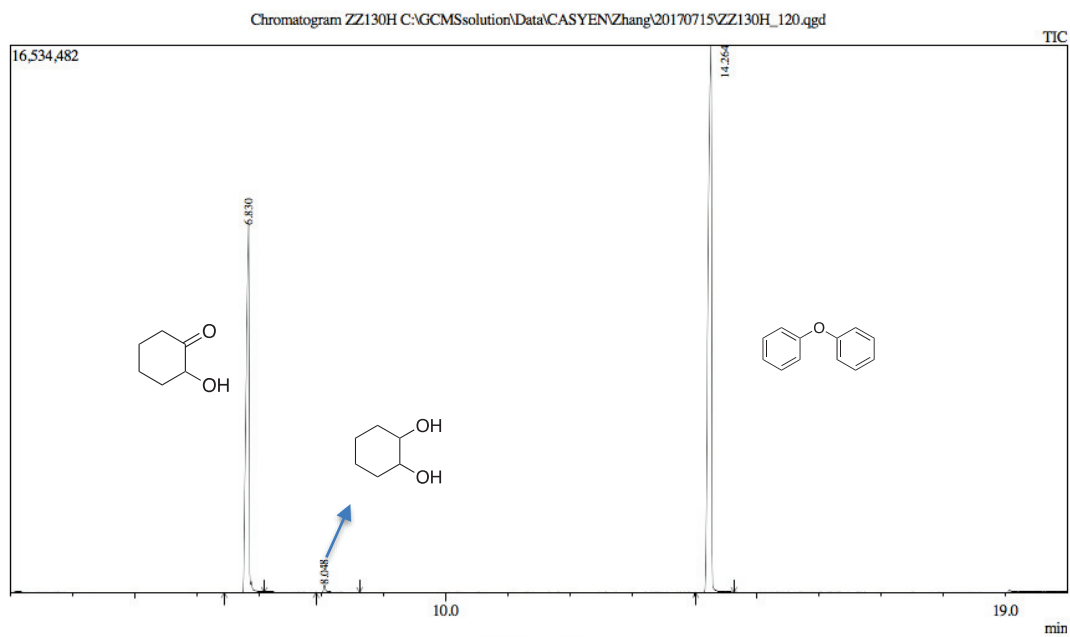
Peak#	R.Time	I.Time	F.Time	Peak Report TIC				A/H	Mark	Name
				Area	Area%	Height	Height%			
1	4.810	4.683	4.867	27835149	36.44	9426636	30.71	2.95	MI	
2	4.955	4.867	5.125	18815946	24.63	9808650	31.96	1.92	MI	
3	14.207	14.025	14.358	29738359	38.93	11457066	37.33	2.60	MI	
				76389454	100.00	30692352	100.00			

Spectrum

Table 15, entry 9



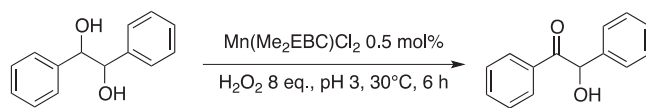
GC/MS analysis with diphenyl ether as an internal standard.



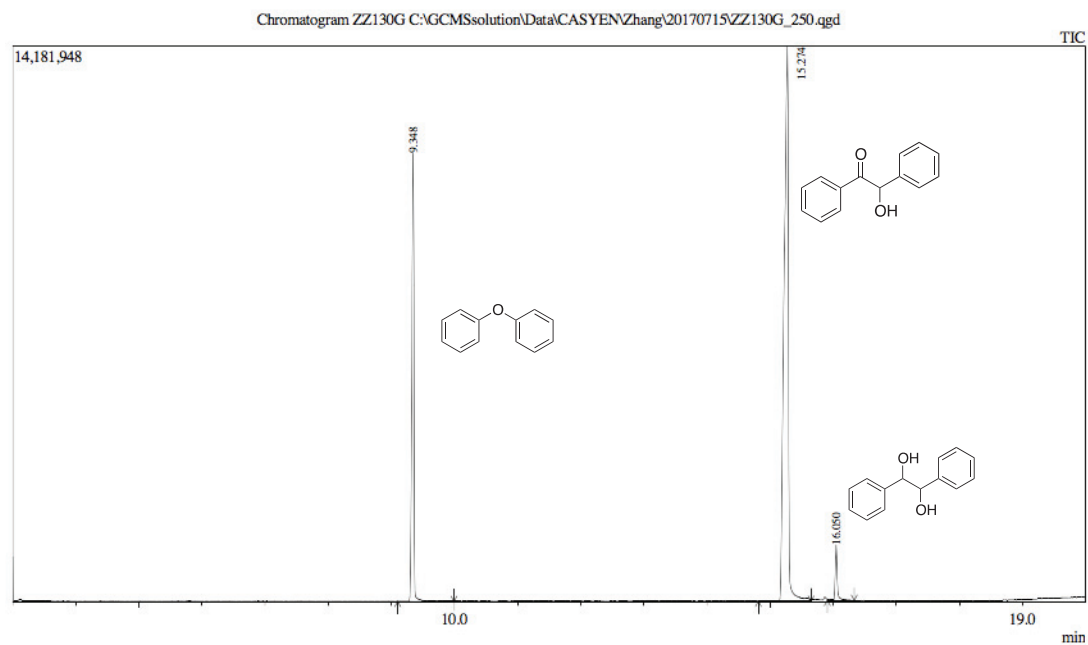
Peak Report TIC										
Peak#	R.Time	I.Time	F.Time	Area	Area%	Height	Height%	A/H	Mark	Name
1	6.830	6.442	7.083	39292626	37.75	11099515	39.84	3.54	MI	
2	8.048	7.917	8.617	562546	0.54	239860	0.86	2.35	MI	
3	14.264	14.017	14.633	64232727	61.71	16518509	59.30	3.89	MI	
				104087899	100.00	27857884	100.00			

Spectrum

Table 15, entry 10



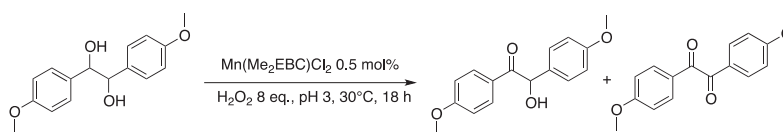
GC/MS analysis with diphenyl ether as an internal standard.



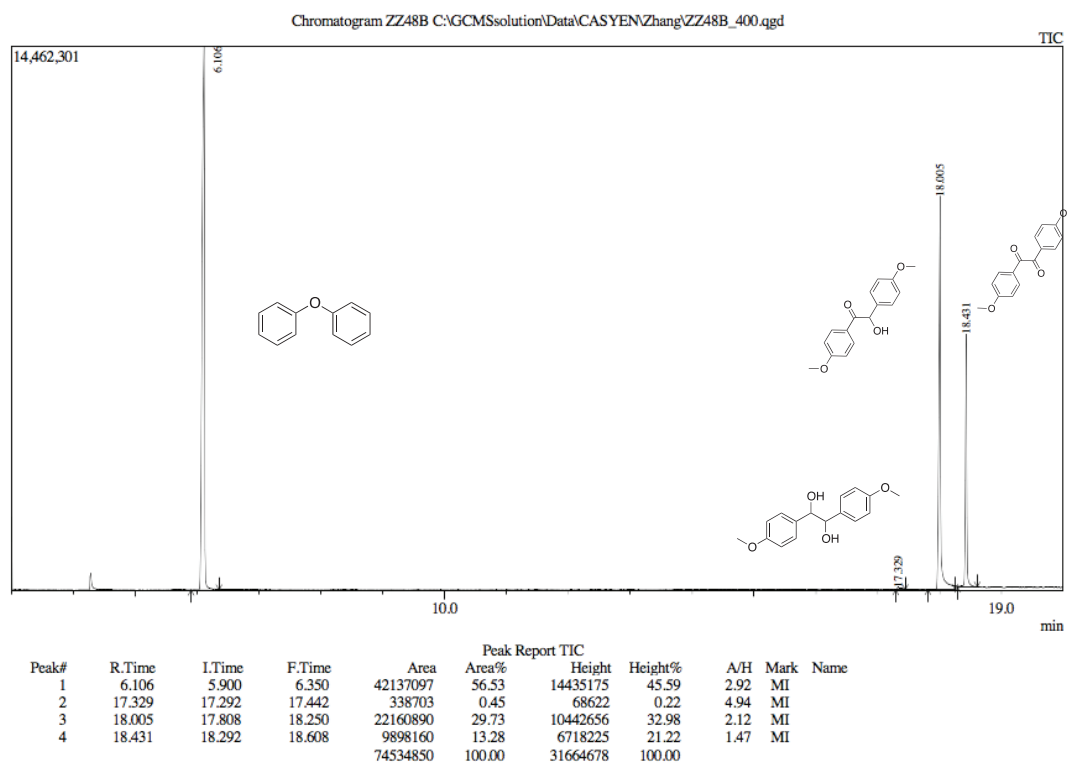
Peak#	R.Time	I.Time	F.Time	Area	Area%	Height	Height%	A/H	Mark	Name
1	9.348	9.100	9.992	27203283	27.77	11433498	42.33	2.38	MI	
2	15.274	14.817	15.650	67614715	69.01	14158187	52.42	4.78	MI	
3	16.050	15.908	16.333	3157079	3.22	1419174	5.25	2.22	MI	
				97975077	100.00	27010859	100.00			

Spectrum

Table 15, entry 11

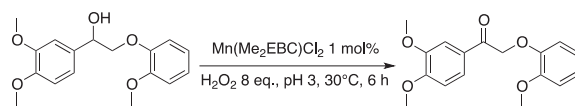


GC/MS analysis with diphenyl ether as an internal standard.

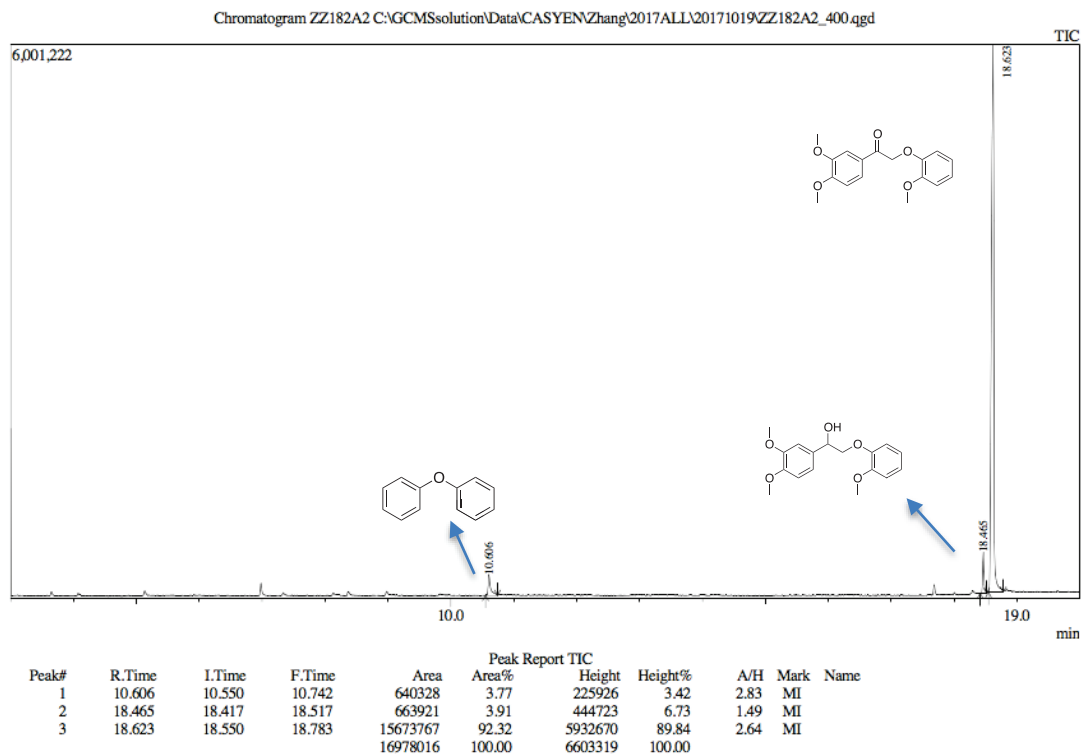


Spectrum

Table 15, entry 12



GC/MS analysis with diphenyl ether as an internal standard.



References

- (1) Guo, Z.; Liu, B.; Zhang, Q.; Deng, W.; Wang, Y.; Yang, Y. *Chemical Society Reviews* **2014**, *43*, 3480.
- (2) Thayer, A. *Chemical & Engineering News* **1992**, *70*, 27.
- (3) Parmeggiani, C.; Matassini, C.; Cardona, F. *Green Chemistry* **2017**, *19*, 2030.
- (4) Lefort, T. *FR* **1931**, *729*, 952.
- (5) Serafin, J.; Liu, A.; Seyedmonir, S. *Journal of Molecular Catalysis A: Chemical* **1998**, *131*, 157.
- (6) Adkins, H.; Peterson, W. R. *Journal of the American Chemical Society* **1931**, *53*, 1512.
- (7) House, M. P.; Carley, A. F.; Bowker, M. *Journal of catalysis* **2007**, *252*, 88.
- (8) Dias, C. R.; Portela, M. F.; Bond, G. *Journal of catalysis* **1995**, *157*, 344.
- (9) Centi, G.; Trifiro, F.; Ebner, J. R.; Franchetti, V. M. *Chemical Reviews* **1988**, *88*, 55.
- (10) Tanase, S.; Bouwman, E. In *Advances in Inorganic Chemistry*; Elsevier: 2006; Vol. 58, p 29.
- (11) Strukul, G. *Catalytic oxidations with hydrogen peroxide as oxidant*; Springer Science & Business Media, 2013; Vol. 9.
- (12) Centi, G.; Perathoner, S. *Catalysis Today* **2003**, *77*, 287.
- (13) Kaneda, K.; Ebitani, K.; Mizugaki, T.; Mori, K. *Bulletin of the Chemical Society of Japan* **2006**, *79*, 981.
- (14) Trost, B. M. *Science* **1991**, *254*, 1471.
- (15) Sheldon, R. *Chem Tech* **1994**, *24*, 38.
- (16) Arakawa, H.; Aresta, M.; Armor, J. N.; Barteau, M. A.; Beckman, E. J.; Bell, A. T.; Bercaw, J. E.; Creutz, C.; Dinjus, E.; Dixon, D. A. *Chemical Reviews* **2001**, *101*, 953.
- (17) Que, L.; Dong, Y. *Accounts of chemical research* **1996**, *29*, 190.
- (18) Han, S.; Eltis, L. D.; Timmis, K. N.; Muchmore, S. W.; Bolin, J. T. *Science*

1995, 270, 976.

(19) Boyington, J. C.; Gaffney, B. J.; Amzel, L. M. *Science* **1993**, 260, 1482.

(20) De Montellano, P. R. O. *Cytochrome P450: structure, mechanism, and biochemistry*; Springer Science & Business Media, 2005.

(21) Ortiz de Montellano, P. R. *Chemical reviews* **2009**, 110, 932.

(22) Sono, M.; Roach, M. P.; Coulter, E. D.; Dawson, J. H. *Chemical Reviews* **1996**, 96, 2841.

(23) Lippard, S. J.; Berg, J. M. *Principles of bioinorganic chemistry*; University Science Books, 1994.

(24) Kendrick, M. J. *Metals in biological systems*; Ellis Horwood Ltd, 1992.

(25) Costas, M.; Mehn, M. P.; Jensen, M. P.; Que, L. *Chemical reviews* **2004**, 104, 939.

(26) Stallings, W. C.; Patridge, K. A.; Strong, R. K.; Ludwig, M. L. *Journal of Biological Chemistry* **1984**, 259, 10695.

(27) Que, L.; Widom, J.; Crawford, R. *Journal of Biological Chemistry* **1981**, 256, 10941.

(28) Beyer Jr, W. F.; Fridovich, I. *Biochemistry* **1985**, 24, 6460.

(29) Hörnsten, L.; Su, C.; Osbourn, A. E.; Hellman, U.; Oliw, E. H. *The FEBS Journal* **2002**, 269, 2690.

(30) Ferreira, K. N.; Iverson, T. M.; Maghlaoui, K.; Barber, J.; Iwata, S. *Science* **2004**, 303, 1831.

(31) Zhang, Z.; Coats, K. L.; Chen, Z.; Hubin, T. J.; Yin, G. *Inorganic chemistry* **2014**, 53, 11937.

(32) Iwata, S.; Barber, J. *Current opinion in structural biology* **2004**, 14, 447.

(33) Mukhopadhyay, S.; Mandal, S. K.; Bhaduri, S.; Armstrong, W. H. *Chemical Reviews* **2004**, 104, 3981.

(34) Umena, Y.; Kawakami, K.; Shen, J.-R.; Kamiya, N. *Nature* **2011**, 473, 55.

(35) Que Jr, L.; Tolman, W. B. *Nature* **2008**, 455, 333.

(36) Arends, I. W.; Sheldon, R. A. *Modern oxidation methods* **2004**, 83.

- (37) Velusamy, S.; Punniyamurthy, T. *Organic letters* **2004**, *6*, 217.
- (38) Mallat, T.; Baiker, A. *Chemical Reviews* **2004**, *104*, 3037.
- (39) Bowden, K.; Heilbron, I.; Jones, E.; Weedon, B. *Journal of the Chemical Society (Resumed)* **1946**, 39.
- (40) Tojo, G.; Fernández, M. I. *Oxidation of alcohols to aldehydes and ketones: a guide to current common practice*; Springer Science & Business Media, 2006.
- (41) Lee, D. G.; Spitzer, U. A. *The Journal of Organic Chemistry* **1970**, *35*, 3589.
- (42) Griffith, W. P.; Ley, S. V.; Whitcombe, G. P.; White, A. D. *Journal of the Chemical Society, Chemical Communications* **1987**, 1625.
- (43) Menger, F. M.; Lee, C. *Tetrahedron Letters* **1981**, *22*, 1655.
- (44) Mancuso, A. J.; Brownfain, D. S.; Swern, D. *The Journal of Organic Chemistry* **1979**, *44*, 4148.
- (45) Ohsugi, S.-i.; Nishide, K.; Oono, K.; Okuyama, K.; Fudesaka, M.; Kodama, S.; Node, M. *Tetrahedron* **2003**, *59*, 8393.
- (46) Tsuchiya, D.; Moriyama, K.; Togo, H. *Synlett* **2011**, *2011*, 2701.
- (47) Mancuso, A. J.; Huang, S.-L.; Swern, D. *The Journal of Organic Chemistry* **1978**, *43*, 2480.
- (48) Collins, T. J. *Accounts of Chemical Research* **2002**, *35*, 782.
- (49) Matsumoto, T.; Ueno, M.; Wang, N.; Kobayashi, S. *Chemistry—An Asian Journal* **2008**, *3*, 196.
- (50) Zhan, B.-Z.; Thompson, A. *Tetrahedron* **2004**, *60*, 2917.
- (51) Punniyamurthy, T.; Velusamy, S.; Iqbal, J. *Chemical Reviews* **2005**, *105*, 2329.
- (52) Nehru, K.; Kim, S. J.; Kim, I. Y.; Seo, M. S.; Kim, Y.; Kim, S.-J.; Kim, J.; Nam, W. *Chemical Communications* **2007**, 4623.
- (53) Schuchardt, U.; Cardoso, D.; Sercheli, R.; Pereira, R.; Da Cruz, R. S.; Guerreiro, M. C.; Mandelli, D.; Spinacé, E. V.; Pires, E. L. *Applied Catalysis A: General* **2001**, *211*, 1.
- (54) Thomas, J. M.; Raja, R.; Sankar, G.; Bell, R. G. *Accounts of chemical research* **2001**, *34*, 191.

- (55) Berkessel, A.; Frauenkron, M.; Schwenkreis, T.; Steinmetz, A. *Journal of Molecular Catalysis A: Chemical* **1997**, *117*, 339.
- (56) Costas, M.; Chen, K.; Que Jr, L. *Coordination Chemistry Reviews* **2000**, *200*, 517.
- (57) Shul'pin, G. B. *Comptes Rendus Chimie* **2003**, *6*, 163.
- (58) Sekino, M.; Furutachi, H.; Tojo, R.; Hishi, A.; Kajikawa, H.; Suzuki, T.; Suzuki, K.; Fujinami, S.; Akine, S.; Sakata, Y. *Chemical Communications* **2017**, *53*, 8838.
- (59) Oh, N. Y.; Suh, Y.; Park, M. J.; Seo, M. S.; Kim, J.; Nam, W. *Angewandte Chemie International Edition* **2005**, *44*, 4235.
- (60) Pestovsky, O.; Bakac, A. *Journal of the American Chemical Society* **2004**, *126*, 13757.
- (61) Napoly, F.; Jean - Gérard, L.; Goux - Henry, C.; Draye, M.; Andrioletti, B. *European Journal of Organic Chemistry* **2014**, *2014*, 781.
- (62) Shen, D.; Miao, C.; Xu, D.; Xia, C.; Sun, W. *Organic letters* **2015**, *17*, 54.
- (63) Aktaş, A.; Acar, İ.; Saka, E. T.; Biyiklioglu, Z. *Journal of Organometallic Chemistry* **2016**, *815*, 1.
- (64) Shi, S.; Liu, M.; Zhao, L.; Wang, M.; Chen, C.; Gao, J.; Xu, J. *Chemistry—An Asian Journal* **2017**.
- (65) Slot, T. K.; Eisenberg, D.; van Noordenne, D.; Jungbacker, P.; Rothenberg, G. *Chemistry—A European Journal* **2016**, *22*, 12307.
- (66) Nam, W. *Accounts of chemical research* **2007**, *40*, 522.
- (67) Miao, C.; Li, X.-X.; Lee, Y.-M.; Xia, C.; Wang, Y.; Nam, W.; Sun, W. *Chemical science* **2017**, *8*, 7476.
- (68) Nguyen, D. H.; Morin, Y.; Zhang, L.; Trivelli, X.; Capet, F.; Paul, S.; Desset, S.; Dumeignil, F.; Gauvin, R. M. *ChemCatChem* **2017**, *9*, 2652.
- (69) Shen, D.; Miao, C.; Wang, S.; Xia, C.; Sun, W. *Organic letters* **2014**, *16*, 1108.
- (70) Chatel, G.; Monnier, C.; Kardos, N.; Voiron, C.; Andrioletti, B.; Draye, M. *Applied Catalysis A: General* **2014**, *478*, 157.

- (71) Rose, E.; Andrioletti, B.; Zrig, S.; Quelquejeu-Ethève, M. *Chemical Society Reviews* **2005**, *34*, 573.
- (72) Jean-Gérard, L.; Kardos, N.; Draye, M.; Andrioletti, B. In *Handbook of Porphyrin Science: with Applications to Chemistry, Physics, Materials Science, Engineering, Biology and Medicine*; World Scientific: 2016, p 1.
- (73) Sorokin, A. B. *Chemical reviews* **2013**, *113*, 8152.
- (74) Meunier, B. *Chemical Reviews* **1992**, *92*, 1411.
- (75) Castro, K. A.; Halma, M.; Machado, G. S.; Ricci, G. P.; Ucoski, G. M.; Ciuffi, K. J.; Nakagaki, S. *Journal of the Brazilian Chemical Society* **2010**, *21*, 1329.
- (76) Ghiaci, M.; Molaie, F.; Sedaghat, M. E.; Dorostkar, N. *Catalysis Communications* **2010**, *11*, 694.
- (77) El Ghachtouli, S.; Wójcik, K.; Copey, L.; Szydło, F.; Framery, E.; Goux-Henry, C.; Billon, L.; Charlot, M.-F.; Guillot, R.; Andrioletti, B. *Dalton Transactions* **2011**, *40*, 9090.
- (78) Napoly, F.; Kieffer, R.; Jean-Gérard, L.; Goux-Henry, C.; Draye, M.; Andrioletti, B. *Tetrahedron Letters* **2015**, *56*, 2517.
- (79) Dong, L.; Wang, Y.; Lv, Y.; Chen, Z.; Mei, F.; Xiong, H.; Yin, G. *Inorganic chemistry* **2013**, *52*, 5418.
- (80) Shircliff, A. D.; Wilson, K. R.; Cannon-Smith, D. J.; Jones, D. G.; Zhang, Z.; Chen, Z.; Yin, G.; Prior, T. J.; Hubin, T. J. *Inorganic chemistry communications* **2015**, *59*, 71.
- (81) Hubin, T. J.; McCormick, J. M.; Collinson, S. R.; Buchalova, M.; Perkins, C. M.; Alcock, N. W.; Kahol, P. K.; Raghunathan, A.; Busch, D. H. *Journal of the American Chemical Society* **2000**, *122*, 2512.
- (82) Anastas, P. T.; Williamson, T. C. *Green chemistry: frontiers in benign chemical syntheses and processes*; Oxford University Press, USA, 1998.
- (83) Bartos, M. J.; Gordon-Wylie, S. W.; Fox, B. G.; Wright, L. J.; Weintraub, S. T.; Kauffmann, K. E.; Münck, E.; Kostka, K. L.; Uffelman, E. S.; Rickard, C. E. *Coordination chemistry reviews* **1998**, *174*, 361.

(84)Collins, T. J.; Kostka, K. L.; Uffelman, E. S.; Weinberger, T. L. *Inorganic Chemistry* **1991**, *30*, 4204.

(85)Popescu, D.-L.; Chanda, A.; Stadler, M.; de Oliveira, F. T.; Ryabov, A. D.; Münck, E.; Bominaar, E. L.; Collins, T. J. *Coordination Chemistry Reviews* **2008**, *252*, 2050.

(86)Chanda, A.; Popescu, D.-L.; de Oliveira, F. T.; Bominaar, E. L.; Ryabov, A. D.; Münck, E.; Collins, T. J. *Journal of inorganic biochemistry* **2006**, *100*, 606.

(87)Ghosh, A.; Ryabov, A. D.; Mayer, S. M.; Horner, D. C.; Prasuhn, D. E.; Sen Gupta, S.; Vuocolo, L.; Culver, C.; Hendrich, M. P.; Rickard, C. E. *Journal of the American Chemical Society* **2003**, *125*, 12378.

(88)Horwitz, C. P.; Ghosh, A.; U.S. Patents No. 7,060,818: 2006.

(89)Collins, T. J. *Accounts of chemical research* **1994**, *27*, 279.

(90)Collins, T. J.; Walter, C. *Scientific American* **2006**, *294*, 82.

(91)Ryabov, A. D.; Collins, T. J. *Advances in Inorganic Chemistry* **2009**, *61*, 471.

(92)Collins, T. J.; Ryabov, A. D. *Chemical reviews* **2017**, *117*, 9140.

(93)Ryabov, A. D. In *Advances in inorganic chemistry*; Elsevier: 2013; Vol. 65, p 117.

(94)Kistenmacher, T. t.; Stucky, G. *Inorganic Chemistry* **1968**, *7*, 2150.

(95)Koenig, D. F. *Acta crystallographica* **1965**, *18*, 663.

(96)Orpen, A. G.; Brammer, L.; Allen, F. H.; Kennard, O.; Watson, D. G.; Taylor, R. *Journal of the Chemical Society, Dalton Transactions* **1989**, S1.

(97)Polshin, V.; Popescu, D.-L.; Fischer, A.; Chanda, A.; Horner, D. C.; Beach, E. S.; Henry, J.; Qian, Y.-L.; Horwitz, C. P.; Lente, G. *Journal of the American Chemical Society* **2008**, *130*, 4497.

(98)Collins, T. J.; Khetan, S. K.; Ryabov, A. D. *Handbook of Green Chemistry: Online* **2010**, 39.

(99)Ghosh, A.; Tiago de Oliveira, F.; Yano, T.; Nishioka, T.; Beach, E. S.; Kinoshita, I.; Münck, E.; Ryabov, A. D.; Horwitz, C. P.; Collins, T. J. *Journal of the American Chemical Society* **2005**, *127*, 2505.

- (100) Groves, J. T. *Journal of inorganic biochemistry* **2006**, *100*, 434.
- (101) Chanda, A.; Shan, X.; Chakrabarti, M.; Ellis, W. C.; Popescu, D. L.; Tiago de Oliveira, F.; Wang, D.; Que Jr, L.; Collins, T. J.; Münck, E. *Inorganic chemistry* **2008**, *47*, 3669.
- (102) Mills, M. R.; Burton, A. E.; Mori, D. I.; Ryabov, A. D.; Collins, T. J. *Journal of Coordination Chemistry* **2015**, *68*, 3046.
- (103) England, J.; Prakash, J.; Cranswick, M. A.; Mandal, D.; Guo, Y.; Münck, E.; Shaik, S.; Que Jr, L. *Inorganic chemistry* **2015**, *54*, 7828.
- (104) Filipe Tiago de oliveira; Arani, C. D. B. *Science* **2007**, *315*, 4.
- (105) Kundu, S.; Thompson, J. V. K.; Ryabov, A. D.; Collins, T. J. *Journal of the American Chemical Society* **2011**, *133*, 18546.
- (106) Ghosh, M.; Singh, K. K.; Panda, C.; Weitz, A.; Hendrich, M. P.; Collins, T. J.; Dhar, B. B.; Sen Gupta, S. *Journal of the American Chemical Society* **2014**, *136*, 9524.
- (107) Warner, G. R.; Mills, M. R.; Enslin, C.; Pattanayak, S.; Panda, C.; Panda, T. K.; Gupta, S. S.; Ryabov, A. D.; Collins, T. J. *Chemistry-A European Journal* **2015**, *21*, 6226.
- (108) Ellis, W. C.; Tran, C. T.; Denardo, M. A.; Fischer, A.; Ryabov, A. D.; Collins, T. J. *Journal of the American Chemical Society* **2009**, *131*, 18052.
- (109) Mills, M. R.; Weitz, A. C.; Zhang, D. Z.; Hendrich, M. P.; Ryabov, A. D.; Collins, T. J. *Inorganic chemistry* **2016**, *55*, 12263.
- (110) Dunford, H. B. *Heme peroxidases*; Wiley-vch, 1999.
- (111) Zámocký, M.; Koller, F. *Progress in biophysics and molecular biology* **1999**, *72*, 19.
- (112) Nicholls, P. *Adv. Inorg. Chem.* **2001**, *51*, 51.
- (113) Marques, H. M. *Dalton Transactions* **2007**, 4371.
- (114) Sigel, H. *Angewandte Chemie International Edition in English* **1969**, *8*, 167.
- (115) Meunier, B. *Biomimetic oxidations catalyzed by transition metal*

complexes; Imperial college press, 2000.

(116) Ghosh, A.; Mitchell, D. A.; Chanda, A.; Ryabov, A. D.; Popescu, D. L.; Upham, E. C.; Collins, G. J.; Collins, T. J. *Journal of the American Chemical Society* **2008**, *130*, 15116.

(117) Chanda, A.; Khetan, S. K.; Banerjee, D.; Ghosh, A.; Collins, T. J. *Journal of the American Chemical Society* **2006**, *128*, 12058.

(118) Banerjee, D.; Markley, A. L.; Yano, T.; Ghosh, A.; Berget, P. B.; Minkley, E. G.; Khetan, S. K.; Collins, T. J. *Angewandte Chemie International Edition* **2006**, *45*, 3974.

(119) Ellis, W. C.; McDaniel, N. D.; Bernhard, S.; Collins, T. J. *Journal of the American Chemical Society* **2010**, *132*, 10990.

(120) Chahbane, N.; Popescu, D.-L.; Mitchell, D. A.; Chanda, A.; Lenoir, D.; Ryabov, A. D.; Schramm, K.-W.; Collins, T. J. *Green Chemistry* **2007**, *9*, 49.

(121) Horwitz, C. P.; Fooksman, D. R.; Vuocolo, L. D.; Gordon-Wylie, S. W.; Cox, N. J.; Collins, T. J. *Journal of the American Chemical Society* **1998**, *120*, 4867.

(122) Beach, E. S.; Malecky, R. T.; Gil, R. R.; Horwitz, C. P.; Collins, T. J. *Catalysis Science & Technology* **2011**, *1*, 437.

(123) Gupta, S. S.; Stadler, M.; Noser, C. A.; Ghosh, A.; Steinhoff, B.; Lenoir, D.; Horwitz, C. P.; Schramm, K.-W.; Collins, T. J. *Science* **2002**, *296*, 326.

(124) Onundi, Y.; Drake, B. A.; Malecky, R. T.; DeNardo, M. A.; Mills, M. R.; Kundu, S.; Ryabov, A. D.; Beach, E. S.; Horwitz, C. P.; Simonich, M. T. *Green Chemistry* **2017**, *19*, 4234.

(125) Collins, T. J.; Horwitz, C. P.; Washburn, N. R.; Ellis, W.; Roy, R.; Google Patents: 2013.

(126) Malvi, B.; Panda, C.; Dhar, B. B.; Gupta, S. S. *Chemical Communications* **2012**, *48*, 5289.

(127) Kumari, S.; Dhar, B. B.; Panda, C.; Meena, A.; Sen Gupta, S. *ACS applied materials & interfaces* **2014**, *6*, 13866.

(128) Demeter, E. L.; Hilburg, S. L.; Washburn, N. R.; Collins, T. J.; Kitchin, J.

- R. *Journal of the American Chemical Society* **2014**, *136*, 5603.
- (129) Wang, J.; Sun, H.; Zhao, X. *Catalysis Today* **2010**, *158*, 263.
- (130) Ludwig, M. L.; Metzger, A. L.; Pattridge, K. A.; Stallings, W. C. *Journal of molecular biology* **1991**, *219*, 335.
- (131) Borgstahl, G. E.; Parge, H. E.; Hickey, M. J.; Beyer Jr, W. F.; Hallewell, R. A.; Tainer, J. A. *Cell* **1992**, *71*, 107.
- (132) Wieghardt, K. *Angewandte Chemie International Edition in English* **1989**, *28*, 1153.
- (133) Proserpio, D. M.; Hoffmann, R.; Dismukes, G. C. *Journal of the American Chemical Society* **1992**, *114*, 4374.
- (134) Ono, T.-a.; Noguchi, T.; Inoue, Y.; Kusunoki, M.; Matsushita, T.; Oyanagi, H. *Science* **1992**, *258*, 1335.
- (135) Yamada, T.; Imagawa, K.; Nagata, T.; Mukaiyama, T. *Chemistry letters* **1992**, *21*, 2231.
- (136) Bryliakov, K. P. *Chemical reviews* **2017**, *117*, 11406.
- (137) Micheloni, M. *Journal of Coordination Chemistry* **1988**, *18*, 3.
- (138) Yin, G.; Danby, A. M.; Day, V.; Roy, S. B.; Carter, J.; Scheper, W. M.; Busch, D. H. *Journal of Coordination Chemistry* **2011**, *64*, 4.
- (139) Hubin, T.; McCormick, J.; Collinson, S.; Busch, D.; Alcock, N. *Chemical communications* **1998**, 1675.
- (140) Weisman, G. R.; Rogers, M. E.; Wong, E. H.; Jasinski, J. P.; Paight, E. S. *Journal of the American Chemical Society* **1990**, *112*, 8604.
- (141) Weisman, G. R.; Wong, E. H.; Hill, D. C.; Rogers, M. E.; Reed, D. P.; Calabrese, J. C. *Chemical Communications* **1996**, 947.
- (142) Martin, L. Y.; DeHayes, L. J.; Zompa, L. J.; Busch, D. H. *Journal of the American Chemical Society* **1974**, *96*, 4046.
- (143) Witteveen, H.; Nieuwenhuijse, B.; Reedijk, J. *Journal of Inorganic and Nuclear Chemistry* **1974**, *36*, 1535.
- (144) Martell, A.; Smith, R.; Motekaitis, R. *NIST standard reference database*

1997, 46.

(145) Groves, J. T.; Lee, J.; Marla, S. S. *Journal of the American Chemical Society* **1997**, *119*, 6269.

(146) Newcomb, M.; Shen, R.; Choi, S.-Y.; Toy, P. H.; Hollenberg, P. F.; Vaz, A. D.; Coon, M. J. *Journal of the American Chemical Society* **2000**, *122*, 2677.

(147) Yin, G.; McCormick, J. M.; Buchalova, M.; Danby, A. M.; Rodgers, K.; Day, V. W.; Smith, K.; Perkins, C. M.; Kitko, D.; Carter, J. D. *Inorganic chemistry* **2006**, *45*, 8052.

(148) Hubin, T. J.; McCormick, J. M.; Alcock, N. W.; Busch, D. H. *Inorganic chemistry* **2001**, *40*, 435.

(149) Yin, G.; Danby, A. M.; Kitko, D.; Carter, J. D.; Scheper, W. M.; Busch, D. H. *Journal of the American Chemical Society* **2008**, *130*, 16245.

(150) Yin, G. *Accounts of chemical research* **2012**, *46*, 483.

(151) Yin, G. *Coordination Chemistry Reviews* **2010**, *254*, 1826.

(152) Shi, S.; Wang, Y.; Xu, A.; Wang, H.; Zhu, D.; Roy, S. B.; Jackson, T. A.; Busch, D. H.; Yin, G. *Angewandte Chemie International Edition* **2011**, *50*, 7321.

(153) Prokop, K. A.; de Visser, S. P.; Goldberg, D. P. *Angewandte Chemie International Edition* **2010**, *49*, 5091.

(154) Scott, S. L.; Chen, W. J.; Bakac, A.; Espenson, J. H. *The Journal of Physical chemistry* **1993**, *97*, 6710.

(155) Bordwell, F.; Cheng, J. P.; Harrelson, J. A. *Journal of the American Chemical Society* **1988**, *110*, 1229.

(156) Mayer, J. M. *Accounts of chemical research* **1998**, *31*, 441.

(157) Cook, G. K.; Mayer, J. M. *Journal of the American Chemical Society* **1994**, *116*, 1855.

(158) Yin, G.; Danby, A. M.; Kitko, D.; Carter, J. D.; Scheper, W. M.; Busch, D. H. *Journal of the American Chemical Society* **2007**, *129*, 1512.

(159) Wang, Y.; Shi, S.; Zhu, D.; Yin, G. *Dalton Transactions* **2012**, *41*, 2612.

(160) Xu, A.; Xiong, H.; Yin, G. *The Journal of Physical Chemistry A* **2009**, *113*,

12243.

(161) Yin, G.; Buchalova, M.; Danby, A. M.; Perkins, C. M.; Kitko, D.; Carter, J. D.; Scheper, W. M.; Busch, D. H. *Journal of the American Chemical Society* **2005**, *127*, 17170.

(162) Yin, G.; Buchalova, M.; Danby, A. M.; Perkins, C. M.; Kitko, D.; Carter, J. D.; Scheper, W. M.; Busch, D. H. *Inorganic chemistry* **2006**, *45*, 3467.

(163) Gervat, S.; Léonel, E.; Barraud, J.-Y.; Ratovelomanana, V. *Tetrahedron letters* **1993**, *34*, 2115.

(164) Zysman-Colman, E.; Arias, K.; Siegel, J. S. *Canadian Journal of Chemistry* **2009**, *87*, 440.

(165) Zhu, H.; Tong, H.; Gong, Y.; Shao, S.; Deng, C.; Yuan, W. Z.; Zhang, Y. *Journal of Polymer Science Part A: Polymer Chemistry* **2012**, *50*, 2172.

(166) Shao, C.; Wang, X.; Xu, J.; Zhao, J.; Zhang, Q.; Hu, Y. *The Journal of organic chemistry* **2010**, *75*, 7002.

(167) Shao, C.; Wang, X.; Zhang, Q.; Luo, S.; Zhao, J.; Hu, Y. *The Journal of organic chemistry* **2011**, *76*, 6832.

(168) Creary, X.; Anderson, A.; Brophy, C.; Crowell, F.; Funk, Z. *The Journal of organic chemistry* **2012**, *77*, 8756.

(169) Ho, K. K.; Chen, R.; Willcox, M. D.; Rice, S. A.; Cole, N.; Iskander, G.; Kumar, N. *Biomaterials* **2014**, *35*, 2336.

(170) Hettegger, H.; Beaumont, M.; Potthast, A.; Rosenau, T. *ChemSusChem* **2016**, *9*, 75.

(171) Berta, M.; Dancsó, A.; Nemes, A.; Pathó, Z.; Szabó, D.; Rábai, J. *Journal of Fluorine Chemistry* **2017**, *196*, 57.

(172) Bartos, M. J.; Kidwell, C.; Kauffmann, K. E.; Gordon - Wylie, S. W.; Collins, T. J.; Clark, G. C.; Münck, E.; Weintraub, S. T. *Angewandte Chemie International Edition in English* **1995**, *34*, 1216.

(173) Kojima, T.; Ogishima, F.; Nishibu, T.; Kotani, H.; Ishizuka, T.; Okajima, T.; Nozawa, S.; Shiota, Y.; Yoshizawa, K.; Ohtsu, H. *Inorganic chemistry* **2018**.

- (174) Pluth, M. D.; Lippard, S. J. *Chemical Communications* **2012**, *48*, 11981.
- (175) Ligtenbarg, A. G.; Oosting, P.; Roelfes, G.; La Crois, R. M.; Lutz, M.; Spek, A. L.; Hage, R.; Feringa, B. L. *Chemical Communications* **2001**, 385.
- (176) Jae, J.; Tompsett, G. A.; Lin, Y.-C.; Carlson, T. R.; Shen, J.; Zhang, T.; Yang, B.; Wyman, C. E.; Conner, W. C.; Huber, G. W. *Energy & Environmental Science* **2010**, *3*, 358.
- (177) Zakzeski, J.; Bruijninx, P. C.; Jongerius, A. L.; Weckhuysen, B. M. *Chemical reviews* **2010**, *110*, 3552.
- (178) Kim, S.; Choi, W. *Environmental science & technology* **2002**, *36*, 2019.
- (179) Luo, W.; Zhu, L.; Wang, N.; Tang, H.; Cao, M.; She, Y. *Environmental science & technology* **2010**, *44*, 1786.
- (180) Xiao, H.; Liu, R.; Zhao, X.; Qu, J. *Journal of Molecular Catalysis A: Chemical* **2008**, *286*, 149.
- (181) Stan, S. D.; Daeschel, M. A. *Journal of agricultural and food chemistry* **2005**, *53*, 4906.
- (182) van Putten, R.-J.; Van Der Waal, J. C.; De Jong, E.; Rasrendra, C. B.; Heeres, H. J.; de Vries, J. G. *Chemical reviews* **2013**, *113*, 1499.
- (183) Saisaha, P.; de Boer, J. W.; Browne, W. R. *Chemical Society Reviews* **2013**, *42*, 2059.
- (184) Groves, J. T.; Stern, M. K. *Journal of the American Chemical Society* **1987**, *109*, 3812.
- (185) Traylor, T. G.; Miksztal, A. R. *Journal of the American Chemical Society* **1989**, *111*, 7443.
- (186) Lyakin, O. Y.; Ottenbacher, R. V.; Bryliakov, K. P.; Talsi, E. P. *Acs Catalysis* **2012**, *2*, 1196.
- (187) Talsi, E. P.; Bryliakov, K. P. *Coordination Chemistry Reviews* **2012**, *256*, 1418.
- (188) Sato, K.; Aoki, M.; Noyori, R. *Science* **1998**, *281*, 1646.
- (189) Halliday, G. A.; Young, R. J.; Grushin, V. V. *Organic letters* **2003**, *5*, 2003.

- (190) Antonyraj, C. A.; Jeong, J.; Kim, B.; Shin, S.; Kim, S.; Lee, K.-Y.; Cho, J. K. *Journal of Industrial and Engineering Chemistry* **2013**, *19*, 1056.
- (191) Amarasekara, A. S.; Green, D.; McMillan, E. *Catalysis Communications* **2008**, *9*, 286.
- (192) Deuss, P. J.; Lancefield, C. S.; Narani, A.; de Vries, J. G.; Westwood, N. J.; Barta, K. *Green Chemistry* **2017**, *19*, 2774.
- (193) Rinaldi, R.; Jastrzebski, R.; Clough, M. T.; Ralph, J.; Kennema, M.; Bruijninx, P. C.; Weckhuysen, B. M. *Angewandte Chemie International Edition* **2016**, *55*, 8164.
- (194) Galkin, M. V.; Samec, J. S. *ChemSusChem* **2016**, *9*, 1544.
- (195) Deuss, P. J.; Barta, K. *Coordination Chemistry Reviews* **2016**, *306*, 510.
- (196) Billiet, L.; Hillewaere, X. K.; Du Prez, F. E. *European Polymer Journal* **2012**, *48*, 2085.
- (197) Liu, W.; Zhu, M.; Xiao, J.; Ling, Y.; Tang, H. *Journal of Polymer Science Part A: Polymer Chemistry* **2016**, *54*, 3425.
- (198) Sinha, J.; Sahoo, R.; Kumar, A. *Macromolecules* **2009**, *42*, 2015.

Abstract

Fe(TAML) complexes have been investigated a lot in recent years. Our group has been investigating the simplest Fe(TAML) catalyst for its oxidation with high efficiency. The purpose of this thesis was to functionalize the complex Fe(TAML-Me₂) for different uses.

One of the functionalizations was to have a hexyl-substituted triazole “tail”, which could influence the physicochemical properties of the iron complex in homogeneous catalysis. Conversely, a silicon tailed-one was designed to be grafted on an inorganic support for a use in heterogeneous catalysis. At last, the purpose of the fluorinated tail was to increase the solubility of the metallocomplex in fluorinated solvents for a potential use in a biphasic mixture that could favor the recyclability of the catalyst.

The other purpose of the thesis was to develop an environmental benign catalytic oxidation with a bioinspired catalyst Mn^{II}(Me₂EBC)Cl₂. we disclosed that Mn^{II}(Me₂EBC)Cl₂ complex could catalyze the oxidation of a series of benzylic and aliphatic alcohols with H₂O₂. Conversions of the alcohols to corresponding carbonyl compounds reached 98% with good to excellent selectivity.

Key-words: TAML, metal complexes, functionalization, catalysis, oxidation,

Résumé

De nombreux complexes de Fe(TAML) ont été décrits au cours des dernières années. Notre groupe a étudié l'utilisation du complexe Fe(TAML-Me₂) pour l'oxydation de liaisons C-H benzyliques. L'un des objectifs de cette thèse était de fonctionnaliser le complexe Fe (TAML-Me₂) à différentes fins.

l'une des fonctionnalisations consistait à utiliser un triazole substitué par une chaîne hexyle, qui pourrait influencer les propriétés physicochimiques du complexe de fer qui pourraient être utilisées en catalyse homogène. Inversement, un silicium à queue a été conçu pour être greffé sur un support inorganique pour une utilisation ultérieure en catalyse hétérogène. Enfin, le but de la queue fluorée était d'augmenter la solubilité du complexe dans les solvants fluorés en vue d'une utilisation potentielle dans un mélange biphasique susceptible de favoriser la recyclabilité du catalyseur.

L'autre objectif de la thèse était de développer une oxydation catalytique bénigne pour l'environnement avec un catalyseur Mn^{II} (Me₂EBC)Cl₂. Nous avons révélé que le complexe pouvait catalyser l'oxydation d'une série d'alcools benzyliques et aliphatiques avec H₂O₂. Les conversions des alcools en composés carbonylés correspondants ont atteint 98% avec une sélectivité bonne à excellente.

Mots-clés: TAML, complexes métalliques, fonctionnalisation, catalyse, oxydation,